Efficient Computational Methods for Structural Reliability and Global Sensitivity Analyses

by

Xufang Zhang

A thesis
presented to the University of Waterloo
in fulfillment of the
thesis requirement for the degree of
Doctor of Philosophy
in
Civil Engineering

Waterloo, Ontario, Canada, 2013

Author's Declaration

I hereby declare that I am the sole author of this thesis. This is a true copy of the thesis, including any required final revisions, as accepted by my examiners.

I understand that my thesis may be made electronically available to the public.

Abstract

Uncertainty analysis of a system response is an important part of engineering probabilistic analysis. Uncertainty analysis includes: (a) to evaluate moments of the response; (b) to evaluate reliability analysis of the system; (c) to assess the complete probability distribution of the response; (d) to conduct the parametric sensitivity analysis of the output. The actual model of system response is usually a high-dimensional function of input variables. Although Monte Carlo simulation is a quite general approach for this purpose, it may require an inordinate amount of resources to achieve an acceptable level of accuracy. Development of a computationally efficient method, hence, is of great importance.

First of all, the study proposed a moment method for uncertainty quantification of structural systems. However, a key departure is the use of fractional moment of response function, as opposed to integer moment used so far in literature. The advantage of using fractional moment over integer moment was illustrated from the relation of one fractional moment with a couple of integer moments. With a small number of samples to compute the fractional moments, a system output distribution was estimated with the principle of maximum entropy (MaxEnt) in conjunction with the constraints specified in terms of fractional moments. Compared to the classical MaxEnt, a novel feature of the proposed method is that fractional exponent of the MaxEnt distribution is determined through the entropy maximization process, instead of assigned by an analyst in prior.

To further minimize the computational cost of the simulation-based entropy method, a multiplicative dimensional reduction method (M-DRM) was proposed to compute the fractional (integer) moments of a generic function with multiple input variables. The M-DRM can accurately approximate a high-dimensional function as the product of a series low-dimensional functions. Together with the principle of maximum entropy, a novel computational approach was proposed to assess the complete probability distribution of a system output. Accuracy and efficiency of the proposed method for structural reliability analysis were verified by crude Monte Carlo simulation of several examples.

Application of M-DRM was further extended to the variance-based global sensitivity analysis of a system. Compared to the local sensitivity analysis, the variance-based sensitivity index can provide significance information about an input random variable. Since each component variance is defined as a conditional expectation with respect to the system model function, the separable

nature of the M-DRM approximation can simplify the high-dimension integrations in sensitivity analysis. Several examples were presented to illustrate the numerical accuracy and efficiency of the proposed method in comparison to the Monte Carlo simulation method.

The last contribution of the proposed study is the development of a computationally efficient method for polynomial chaos expansion (PCE) of a system's response. This PCE model can be later used uncertainty analysis. However, evaluation of coefficients of a PCE meta-model is computational demanding task due to the involved high-dimensional integrations. With the proposed M-DRM, the involved computational cost can be remarkably reduced compared to the classical methods in literature (simulation method or tensor Gauss quadrature method). Accuracy and efficiency of the proposed method for polynomial chaos expansion were verified by considering several practical examples.

Acknowledgements

I especially like to express my sincere appreciation to my supervisor, Professor Mahesh D. Pandey, whose encouragement, guidance, and support from the initial to the final level enabled me to develop an understanding of the subject.

I would like to extend my gratitude to Professor Hanping Hong, Professor Wei-Chau Xie, Professor Liping Fu, Professor Sagar Naik and Professor Scott Walbridge for acting as my thesis committee members, and for their insightful comments and cares for my research.

Appreciation should also go to my master degree supervisor, Professor Yimin Zhang at Northeastern University in China, with whom I started to learn basic concepts in probabilistic mechanics. And I am very grateful to Professor Gordon J. Savage in System Design Engendering, who enlightened me very much on the topic of robust design optimization.

I would like to thank my colleagues and friends: Dr. Tianjin Cheng, Dr. Arun Veeramany, Dr. Dongliang Lu, Dritan Topuzi, Dr. Yusong Xue, Dr. Shun-Hao Ni, Dr. Jian Deng, Yi Zhuang, Ayan Sadhu, Zhaoliang Wang, Deyi Zhang, Bo Li, George Balomenos, Wei Jiang, Zhen Cai, Chao Wu, Sen Long, and other graduate students in the Department of Civil and Environmental Engineering, with whom I shared the unforgettable days in Waterloo.

The consistent financial support by the China Scholarship Council (CSC) is greatly appreciated. The support by the Natural Sciences and Engineering Research Council of Canada (NSERC) and the University Network of Excellence in Nuclear Engineering (UNENE) in the form of a Research Assistantship is greatly appreciated.

Last but not least, without the unflagging love, support, encouragement, and sacrifice from my parents, parents-in-law, my wife and my son, throughout these years, this thesis would not be possible.

TO

My Family

Contents

List of Tables

List of Figures

Chapter 1

Introduction

1.1 Engineering Background

Infrastructure and large engineering systems, such as road and highway networks, power plants and electrical grids, are preconditions of a modern industrial society. Reliable and efficient operation of these systems is crucial to both daily lives of individuals and the prosperity of the whole society. An important characteristic of these engineering systems is that they comprise a vast number of sub-structures and components, which are likely to experience various failure modes during service period of the whole system. Reliability analysis, then, become a significant topic for the design, operation and maintenance of the engineering systems.

Figure 1.1 depicts the Qinshan nuclear power plant (Phase III) constructed in Qinshan Town, Haiyan, Zhejiang, the People's Republic of China. It holds the record for the most nuclear reactors on one site. Qinshan III is the first CANada Deuterium-Uranium (CANDU) project in China to use open-top reactor building construction and the first commercial nuclear power station uses two heavy water reactors. The business contract between China Nuclear Energy (CNE) and Atomic Energy of Canada Limited (AECL) on the project is in the amount of $2.88 billion, which has been the top one business venture between China and Canada up to now.

Figure 1.2 illustrates the general schematic systems of a CANDU reactor, in which one can see that a CANDU nuclear power plant comprises a number of subsystems, i.e., the reactor core system, the heat transfer system, computer control system, the electric generation and transmission systems, etc. Each subsystem comprises a vast number of mechanical equipments, which are connected by the vessels, pressure tubes and switches as a complicated physical network.

Figure 1.1: Qinshan nuclear power plant in Phase III: Unit 1 and Unit 2 (Wikipedia, 2013)

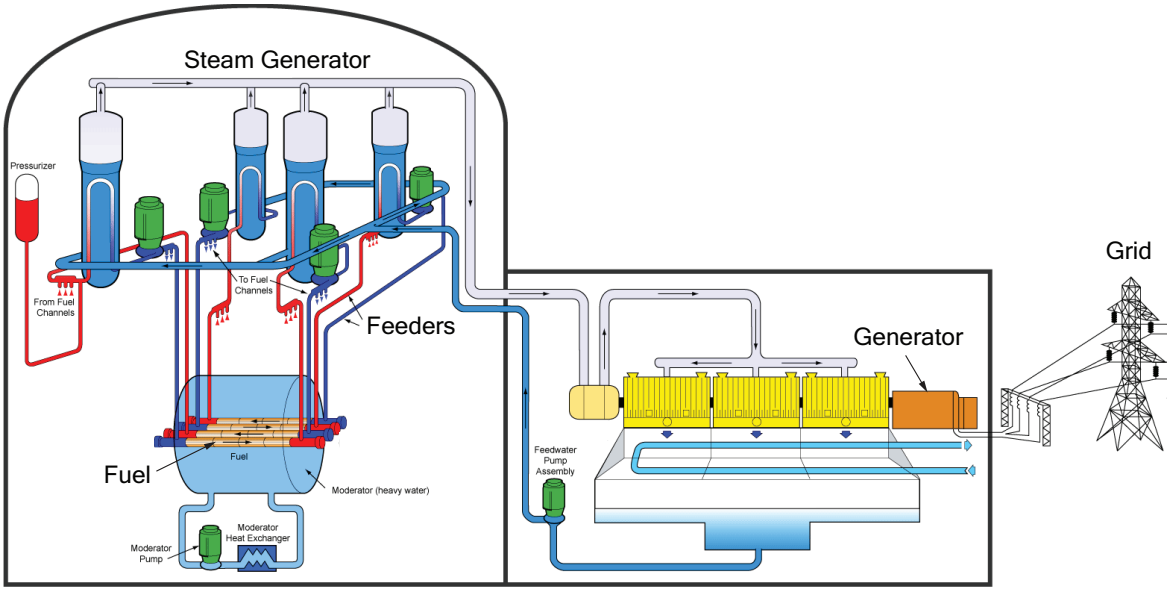

Figure 1.2: Schematic systems of a CANDU nuclear power plant (Cheng, 2011)

Taken the reactor core system as an example, it contains several hundreds pressure tubes, called fuel channels, where the nuclear fuel is stored and the fission reaction takes place. Heavy

water coolant flows over the fuel channels and carries the heat produced by the fission reaction to the steam generators via feeder pipes. The steam generator consists of a large number (3000 to 4000) of thin-wall tubes, in which the heat in the hot coolant is transferred to the secondary side to produce pressurized steam. The steam can drive the turbine and then produces the electricity.

Among the many components and subsystems, the fuel channel inside the reactor core, steam generators, and the feeders are the three key and potentially life-limiting systems. Working in the high-temperature, radiation and high-pressure environment, the reactor components may experience different degradation mechanisms, say the delayed hydride cracking and creep (IAEA, 1998). Similarly, the heat exchanger tubes in the steam generators are also susceptible to different types of degradation such as pitting, denting, fretting, stress corrosion cracking, high load cycle fatigue, and wastage (IAEA, 1997). For the other reactor assemblies (e.g., calandria vessel, end shield, feeder, etc.), the following potential degradation mechanisms have been identified (IAEA, 2005): neutron irradiation embrittlement, stress corrosion cracking, corrosion (i.e., due to pitting, denting, flow-accelerated, etc.), erosion, fatigue, stress relaxation, creep, and mechanical wear.

Safety assessment of the failure sensitive subsystems and components are the significant aspects in design, operating and maintenance of a nuclear facility. Uncertainty is ubiquitous in any subsystem and at any stage during the operation of a nuclear power plant. The uncertainty arises from a vast of sources of variation, such as the usage variation, the manufacturing imprecision, and the knowledge limitation of analyst, etc. Specific examples of the uncertainty in structural engineering include the variations in external loading, material property, and geometrical dimension of a infrastructure. Quantitatively accommodating and managing the uncertainty on an output of the engineering system, hence, are rapidly spreading in both of academia and industry. The success in system development and management depends heavily on how well understanding of the physical mechanisms, how efficiently accounting for the relation mathematically, and how quantifying the uncertainty propagation accurately. An methodology based on the probability theory is sought to conduct the uncertainty quantification in both of component and system levels.

1.2 Motivation and Objective

A mathematic model can be explicitly or implicitly defined to describe a general engineering system. The proposed research is motivated by the following facts:

- Monte Carlo simulation and its variants are expensive to implement in system reliability analysis, especially in the case of a large-scale computer program is employed to represent the complex input-output relation. Typically 10^{k+2} to 10^{k+3} samples are required to estimate a failure probability in the order of 10^{-k}. Hence, a method bearing the accuracy and simplicity, i.e., the uncertainty quantification is only based on a small number of deterministic model evaluations, is desired by industry.

- Uncertainty propagation of input random variables through a complex physical system can be extensively represented by output probability distribution of the system. An effective algorithm for the output distribution is sought by academic community during the development of structural reliability analysis.

- Compared to local sensitivity index in literature, global sensitivity analysis enables engineers to access each input contribution in its entire definition domain. Up to now, simulation-based method is the dominant approach to conduct the analysis. Its low efficiency motivates a modern computational technique for the objective.

Objectives of the document can be summarized as follows:

- Develop a method of using fractional moment for parent distribution estimation of a random variable.

- Develop an efficient simulation-based method for kinematic reliability analysis of mechanism systems.

- Propose a generic multiplicative dimensional reduction method to approximate a complicated input-output relation.

- Develop an efficient method for statistical (fractional and integer) moments computation of a structural response function with multiple input variables, and further to estimate complete output distribution by using the principle of maximum entropy in conjunction with the constrains specified in terms of fractional moment.

- Develop an efficient computational technique to conduct the variance-based global sensitivity analysis.
- Propose an efficient method to perform polynomial chaos expansion (PCE) of a physical model, and further conduct the uncertainty quantification of the system from the aspects of reliability and global sensitivity analyses.

1.3 Proposed Methodology

1.3.1 Approach

A framework proposed in the study for uncertainty propagation of a general engineering system is shown in Figure 1.3. In the methodology, three steps are identified:

- Step A consists in defining the mathematic model (analytic or numeric, implicit or explicit) that will be considered, together with the input and output parameters. One should note that the model defined in the step is purely a deterministic physical model. In addition, it is highly possible that a computational expensive package, e.g., a finite element code, might be employed to express the complicated relation. In summary, the preprocessing step gathers all ingredients used for the deterministic analysis of an engineering system.
- Step B consists in quantifying the sources of uncertainty in the analysis, i.e., using probability distributions to model the input parameters that are not well known. It can be realized by collecting some observations of a parameter at first, and then, employing the available techniques, e.g., the probability paper plot, method of moment, etc., to properly select a distribution or distribution parameters to describe the input variable (Sahoo and Pandey, 2010). The end product of the step is an input random vector with the known probability measures. In some cases, describing the variability of a random variable with respect to time or spatial requires the introduction of random process or random field.
- In Step C, uncertainty propagation of input random variables through a physical model needs to be quantified. This is the kernel step in probabilistic mechanics computation. Postprocessing of the proposed framework needs to evaluate structural reliability at both of component and system levels. In addition, analysts are also interested in the respective impact of input random variables with respect to a system output, which is referred to as

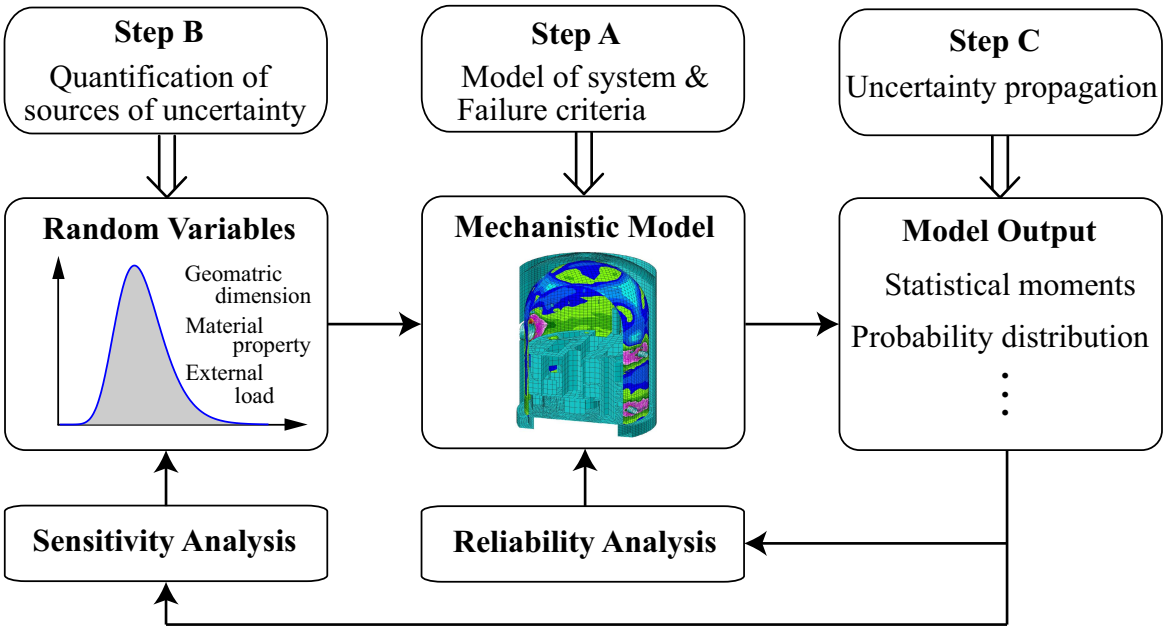

Figure 1.3: Global framework for uncertainty quantification of a system (Sudret, 2007)

the global sensitivity analysis in the study. Therefore, end products of the step include moments, complete probability distribution, result of significant analysis, failure probability and risk, etc., with respect to an output of the system.

The proposed research activities in the document are designed to account for the propagation of input uncertainty through a physical model from the following aspects:

- Estimate probability distribution of a structural response and conduct the associated reliability analysis;
- Estimate extreme event distribution about an array of system responses and conduct the corresponding system reliability analysis;
- Conduct the variance-based global sensitivity analysis to quantify the importance of input random variables with respect to a system output; and
- Conduct the polynomial chaos expansion of a physical model, and further explore the corresponding approach for uncertainty quantification of the system.

The proposed study is built on the theory of high-dimensional model representation. A general multiplicative dimensional reduction method is developed in the thesis to approximate a

generic input-output relation. The model approximation method is further employed to explore the computationally efficient approaches for moment, probability distribution, and global sensitivity analysis of a system output.

1.3.2 Significance

The proposed methodology is significant as it proposes:

- An accurate method of using fractional moments to estimate the parent distribution of a positive random variable;
- An efficient simulation-based method for system reliability analysis of robotic mechanisms;
- A generic multiplicative dimensional reduction method to approximate a complicated input-output relation;
- An efficient method to calculate fractional (integer) moments of a structural response function;
- An efficient method to derive the probability distribution of a model response, or the extreme event of structural responses;
- An efficient computation method to conduct the variance-based global sensitivity analysis of a system;
- An efficient computational method for polynomial chaos expansion of a system, and the corresponding method for uncertainty quantification of the system.

The proposed framework is a non-intrusive method in nature to conduct the uncertainty analysis of an engineering system, which implies it reserves the simplicity of Monte Carlo simulation that the probabilistic computation is only based on a number of deterministic model responses. Compared to the methods in literature, it does not need the response gradients, or set up an extended version of governing equations. The involved deterministic analyses are evaluated at a small number of properly selected "samples" (i.e., integration grids with respect to input variables). From this perspective, the proposed method is easy to be integrated with an available deterministic mechanistic package (e.g., ANSYS©, MSC Nastran©, etc.) to further conduct the

probabilistic analysis. Therefore, it sets the foundation for a computer-based, virtual program that an analyst can perform reliability and global sensitivity analyses of a system.

1.4 Outline of the Dissertation

Literature reviews about methods on moment computation and reliability analysis are provided in Chapter 2, in which the research activities are categorized as statistical moment calculation, structural reliability analysis and the method on global sensitivity analysis.

Chapter 3 is devoted to develop an entropy-based method for parent distribution estimation of a positive random variable. The advantage of using fractional moment over integer moment is illustrated from the relation of one fractional moment with a couple of integer moments. The principle of maximum entropy is employed to construct the distribution from a finite number of fractional moments.

Chapter 4 presents an efficient method for computing kinematic reliability of mechanisms. This problem is equivalent to a series system reliability analysis that can be solved using the extreme value distribution of the positional errors. The principle of maximum entropy is applied to derive this maximal distribution. The fractional moments are obtained from a small, simulated sample of output positional error.

Chapter 5 presents a generic method to derive the probability distribution of a multivariate function of random variables representing the response of a structure. A new multiplicative dimensional reduction method (M-DRM) is proposed to approximate the original input-output relation. An efficient numerical method for fractional (integer) moment calculation is proposed.

Chapter 6 proposes a computationally efficient method for global sensitivity analysis of a system. The development is based on the fact that M-DRM can approximate a general high-dimensional function as the product of a series low-dimensional function. The separative property is employed in the Chapter to simplify the high-dimensional integrations involved in the Sobol' sensitivity index computation.

Chapter 7 presents an efficient method for polynomial chaos expansion (PCE) of a physical model, since that the determined surrogate model can be repeatedly evaluated for uncertainty analysis of the system. However, evaluation of coefficients of a PCE meta-model is computational demanding task due to the involved high-dimensional integrations. The Chapter proposes the use of M-DRM to conduct the polynomial chaos expansion and the associated uncertainty

quantification of the system.

Chapter 8 presents the conclusions and recommendations for future research.

Chapter 2

Literature Review

2.1 Introduction

Uncertainty quantification of a system is a process of determining the effect of input uncertainties on the response metrics of interest. These input uncertainties may be characterized as either aleatory uncertainties, which are irreducible variabilities inherent in nature, or epistemic uncertainties, which are reducible uncertainties resulting from a lack of knowledge. Since sufficient data is generally available for aleatory uncertainties, probabilistic methods are commonly used for computing response distribution based on input probability specifications. Conversely, for epistemic uncertainties, data is generally sparse, making the use of probability distribution assertions questionable and typically leading to non-probabilistic methods based on interval specifications. The proposed study is designed to account for the analysis of aleatory uncertainties using the probabilistic method.

Suppose response of a system is modelled by a generic function, $\mathbf{y} = \eta(\mathbf{x})$, that can be analytically or numerically, explicitly or implicitly. Here, $\mathbf{y}$ is the output vector of the physical model. For sake of simplicity, we can use a scalar y instead of the vector to denote the model response. In some cases, we also have to consider some/all not well-known input parameters as random variables. Then, with the assigned probability distribution to each input random variable, the probabilistic model response can be expressed as

$$Y = \eta(\mathbf{X}) \tag{2.1}$$

where $\mathbf{X} = [X_1, X_2, \cdots, X_n]^{\mathrm{T}}$ is an assembly of input random variables.

The full probabilistic contents of a system response are contained in its probability density function (PDF), $f_Y(y)$, which depends on the input random vector, $\mathbf{X}$, and the mechanistic model, $\eta(\cdot)$. Generally speaking, the distribution is difficult to be analytically determined due to the complexity of $\eta(\cdot)$ and the high-dimensionality of $\mathbf{X}$.

Well-established methods in literature for statistical moment, probability distribution and global sensitivity index are reviewed as shown in Figure 2.1. The approaches for each topic can be classified into sampling and analytical categories. The term "sampling" is designed to indicate a research related to a simulation-based method. In addition, the research activities using non-simulation methods (e.g., the gradient-based method, the orthogonal decomposition method and the weighted integration method, etc.) enter to the "analytical" category.

Therefore, the research activities can be identified from the following aspects:

- When the moments, i.e., mean-value and standard deviation, of a model response are of in-

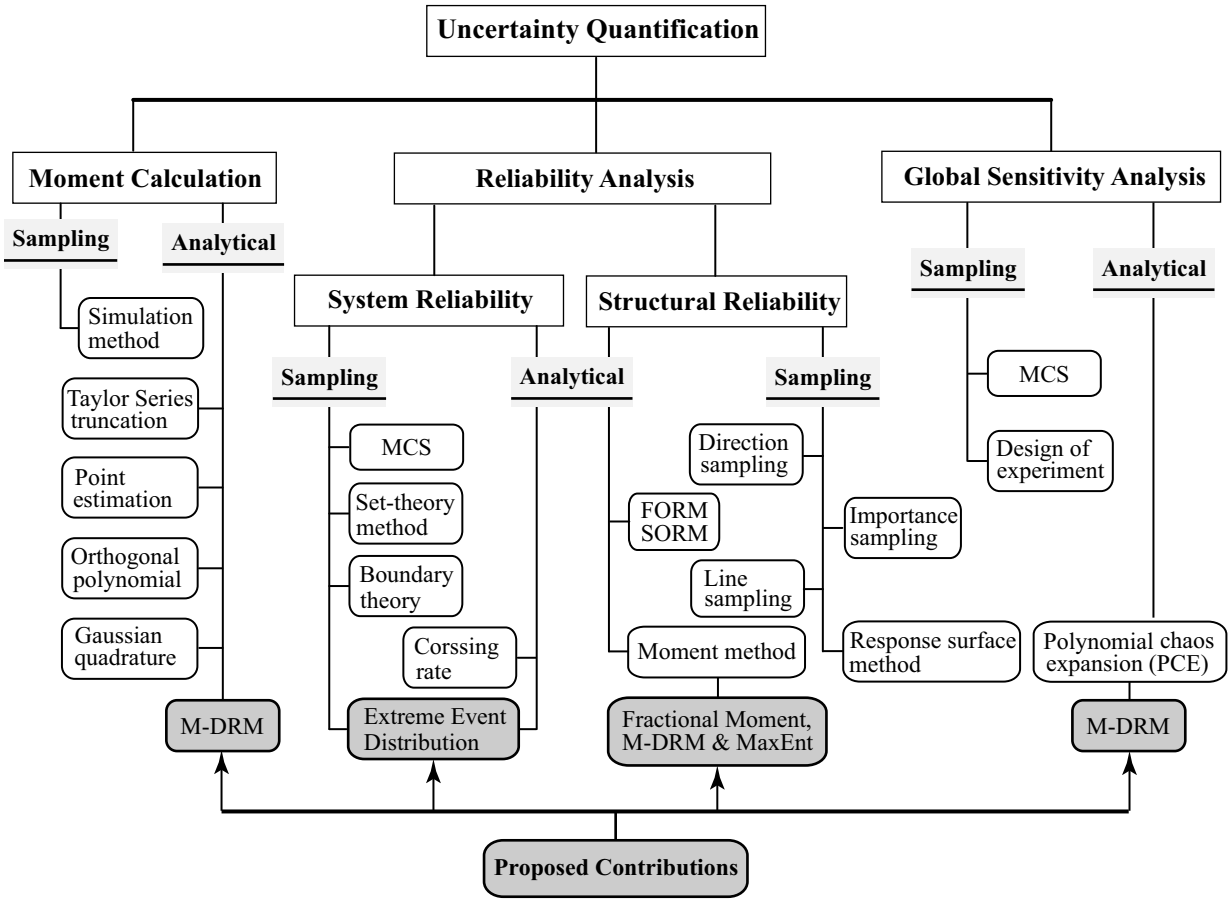

Figure 2.1: Research activities for uncertainty quantification of a system

terest, methods in literature include the truncated Taylor series method, numerical weighted integration, and Monte Carlo simulation. The determined moments can provide the first snapshot on the probabilistic characteristics of a model response.

- When the tail of an output distribution is of interest, the problem can be recast as that of computing the reliability or failure probability of the system. The "failure", here, is defined in a broad sense as a model output "Y is exceeding a prescribed threshold y_0". Methods on structural reliability analysis, such as the first-order second moment (FOSM) method, the first- or second-order reliability method (FORM/SORM), can be used based on the failure criteria (or limit state function). Of course, as summarized in Figure 2.1, the simulation-based method, e.g., crude Monte Carlo simulation and its variants, can be employed to conduct the system reliability analysis.

- When the complete output distribution, instead of a point on the tail, is of interest, crude Monte Carlo simulation is a generic approach to solve the problem. Note that the analysis indirectly encompasses the first-two kinds of problems, since the knowledge of probability density function can be post-processed to obtain moments and a quantile of the distribution.

- Global sensitivity analysis aims to quantify the significance of input variables singly or their combinations within the entire range of variation. The general analysis of variance provides the definition of global sensitivity index, which is related to the conditional variance of model output given an arbitrary group of input random variables. To evaluate the involved high-dimensional integrations, the methods of simulation and tensor Gauss quadrature are mostly employed so far in literature. Therefore, an efficient computational technique to conduct the global sensitivity analysis is sought.

The proposed activities organized in the document are developed to conduct the uncertainty quantification of a complicated physical system from the aspects of: (a) statistical moment calculation; (b) estimation of output probability distribution; and (c) conducting the global sensitivity analysis. Brutal Monte Carlo simulation with 10^6 samples is assumed to provide the benchmark results in verification. Following Sections of the Chapter will briefly review the activities related to each topic in literature.

2.2 Calculation of Moment

In this Section, computational methods for mean-value and standard deviation of a model output, $Y = \eta(\mathbf{X})$, are addressed. Monte Carlo simulation is first presented. Confidence interval on the simulation method is provided. Then the methods of the truncated Taylor series expansion and Gauss quadrature are followed.

2.2.1 Monte Carlo Simulation

Assume that random numbers with respect to input vector, $\mathbf{X}$, with size N have been generated, i.e., $\{\mathbf{x}^{(1)}, \mathbf{x}^{(2)}, \cdots, \mathbf{x}^{(N)}\}$. The estimates of mean-value and standard deviation of model response, respectively, are given as

$$\begin{cases} \widehat{\mu}_Y = \dfrac{1}{N}\displaystyle\sum_{i=1}^{N} \eta\big(\mathbf{x}^{(i)}\big) \\ \widehat{\sigma}_Y^2 = \dfrac{1}{N-1}\displaystyle\sum_{i=1}^{N} \big[\eta\big(\mathbf{x}^{(i)}\big) - \widehat{\mu}_Y\big]^2 \end{cases} \tag{2.2}$$

The estimates of moment are also random variables. It is common to run a single MCS with a large sample size (e.g., $N = 10^5$). However, a rigourous way in using of the simulation method requires to provide the corresponding confidence intervals of the estimates.

Suppose that sample size N is fixed by an analyst. The estimators in Eq.(2.2) are asymptotically Gauss random variables due to central limit theorem. Thus the confidence interval on μ_Y can be determined as

$$\widehat{\mu}_Y - u_{\alpha/2}\frac{\widehat{\sigma}_Y}{\sqrt{N-1}} \leqslant \mu_Y \leqslant \widehat{\mu}_Y + u_{\alpha/2}\frac{\widehat{\sigma}_Y}{\sqrt{N-1}} \tag{2.3}$$

where $u_{\alpha/2} = \Phi^{-1}(1-\alpha/2)$ is a Normal quantile with the two-tailed α significance level. Alternatively, a similar confidence interval can be derived for the estimate of output variance.

Monte Carlo simulation can also be employed to estimate high-order moments. Figure 2.2 depicts the corresponding efficiency of MCS through a simple regression function:

$$\eta(\mathbf{X}) = a_0 + a_1 X_1 + a_2 X_2 + a_3 X_1 X_2 \tag{2.4}$$

where the coefficients $a_0 = 2.5$ and $a_1 = a_2 = a_3 = 1.5$. X_1 and X_2 are the independent Lognormal variables with $\mu_1 = \mu_2 = 2.0$. Coefficients of variation (COVs) are 0.2. MCS

with 10^6 samples is assumed to provide benchmarks of the first-four output moments. Then, the efficiency of Monte Carlo simulation can be assessed as follows.

In each round of simulation, 1000 samples are used to estimate the output moments, i.e., M_Y^k $(k = 1, \cdots, 4)$, and each estimator, $\widehat{M}_Y^k$, is separately stored. The simulation is repeated 1000 times, and thus random samples of moments are obtained. Histograms on the normalized moment, i.e., $\widehat{M}_Y^k / M_Y^k$, are depicted as shown in Figure 2.2. It is clearly to see that the variations of moment estimate are increasing with the order of moment. And accordingly, it has revealed

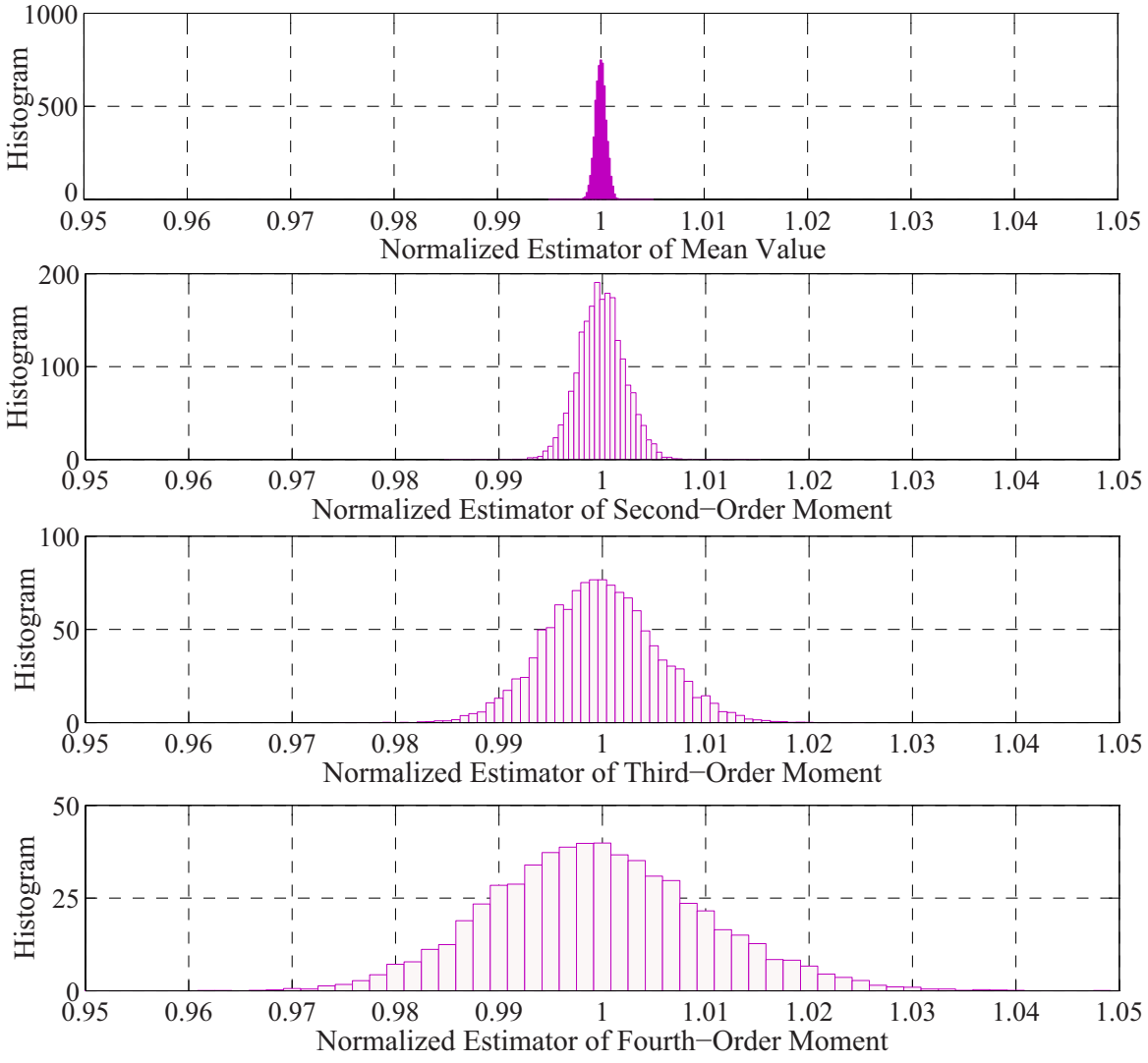

Figure 2.2: Efficiency of crude Monte Carlo simulation in moment estimation

the low efficiency of simulation method for a high-order moment ($k \geqslant 3$) computation.

2.2.2 Method of Taylor Series Expansion

In addition to simulation method, the truncated Taylor series method for moment computation can be traced back to early 1970's. The method needs the expansion of $\eta(\mathbf{x})$ at the mean-values $\boldsymbol{\mu} = [\mu_1, \mu_2, \cdots, \mu_n]^{\mathrm{T}}$ of input vector:

$$\begin{aligned}\eta(\mathbf{X}) = \eta(\boldsymbol{\mu}) + \sum_{i=1}^{n} \left.\frac{\partial \eta(\mathbf{x})}{\partial x_i}\right|_{\mathbf{x}=\boldsymbol{\mu}} (X_i - \mu_i) + \\ \frac{1}{2}\sum_{i=1}^{n}\sum_{j=1}^{n} \left.\frac{\partial^2 \eta(\mathbf{x})}{\partial x_i \partial x_j}\right|_{\mathbf{x}=\boldsymbol{\mu}} (X_i - \mu_i)(X_j - \mu_j) + o\big(\|\mathbf{x} - \boldsymbol{\mu}\|^2\big)\end{aligned} \tag{2.5}$$

Taken expectation of the equation, one can derive that:

$$E[Y] \approx \eta(\boldsymbol{\mu}) + \sum_{i=1}^{n} \left.\frac{\partial \eta(\mathbf{x})}{\partial x_i}\right|_{\mathbf{x}=\boldsymbol{\mu}} E[X_i - \mu_i] + \frac{1}{2}\sum_{i=1}^{n}\sum_{j=1}^{n} \left.\frac{\partial^2 \eta(\mathbf{x})}{\partial x_i \partial x_j}\right|_{\mathbf{x}=\boldsymbol{\mu}} E\big[(X_i - \mu_i)(X_j - \mu_j)\big] \tag{2.6}$$

Since that $E[X_i - \mu_i] = 0$, mean-value of $Y = \eta(\mathbf{X})$, then, can be approximated as

$$E[Y] \approx \eta(\boldsymbol{\mu}) + \frac{1}{2}\sum_{i=1}^{n}\sum_{j=1}^{n} \left.\frac{\partial^2 \eta(\mathbf{x})}{\partial x_i \partial x_j}\right|_{\mathbf{x}=\boldsymbol{\mu}} E\big[(X_i - \mu_i)(X_j - \mu_j)\big] \tag{2.7}$$

where $E\big[(X_i - \mu_i)(X_j - \mu_j)\big]$ is a generic term in the covariance matrix of $\mathbf{X}$.

A particular case of independent input variables implies the covariance matrix is diagonal and contains the variance of each input variable. Then, the mean-value can be reduced as

$$E[Y] \approx \eta(\boldsymbol{\mu}) + \frac{1}{2}\sum_{i=1}^{n} \left(\left.\frac{\partial^2 \eta(\mathbf{x})}{\partial x_i^2}\right|_{\mathbf{x}=\boldsymbol{\mu}} \sigma_i^2 \right) \tag{2.8}$$

Assumed that $E[Y] \approx \eta(\boldsymbol{\mu})$, the variance can be further approximated as

$$\mathrm{Var}[Y] \approx E\left\{ \left[\sum_{i=1}^{n} \left.\frac{\partial \eta(\mathbf{x})}{\partial x_i}\right|_{\mathbf{x}=\boldsymbol{\mu}} (X_i - \mu_i) \right]^2 \right\} \tag{2.9}$$

Thus the first-order approximation of output variance is:

$$\mathrm{Var}[Y] \approx \sum_{i=1}^{n}\sum_{j=1}^{n} \left(\left.\frac{\partial \eta(\mathbf{x})}{\partial x_i}\right|_{\mathbf{x}=\boldsymbol{\mu}} \right) \left(\left.\frac{\partial \eta(\mathbf{x})}{\partial x_j}\right|_{\mathbf{x}=\boldsymbol{\mu}} \right) E\big[(X_i - \mu_i)(X_j - \mu_j)\big] \tag{2.10}$$

With the independent input variables, the approximation results in:

$$\mathrm{Var}[Y] \approx \sum_{i=1}^{n} \left(\left.\frac{\partial \eta(\mathbf{x})}{\partial x_i}\right|_{\mathbf{x}=\boldsymbol{\mu}} \right)^2 \sigma_i^2 \tag{2.11}$$

2.2.3 Method of Gaussian Quadrature

The rule of Gauss quadrature is usually stated as a weighted summation of an integrand evaluated at an array of specific points. It is sufficient to recall a one-dimensional integration can be approximated as

$$I = \int_x h(x)W(x)\mathrm{d}x \approx \sum_{i=1}^{N} w_i h(x_i) \tag{2.12}$$

where the weighting function, $W(x)$, determines the rule of Gauss quadrature. Table 2.1 summarized various rules of Gauss quadrature with different of weigh functions (Davis and Rabinowitz, 1975). And one should note that a rule of Gauss quadrature with N points is constructed to yield the exact integration for a polynomial, $h(x)$, of degree $2N-1$ or less.

Table 2.1: Rules of Gauss quadrature and weight function of orthogonal polynomial

Weight Function $W(x)$	Support Domain	Orthogonal Polynomial	Gauss Quadrature Rule
1	$[-1,1]$	Legendre	Gauss-Legendre
$\exp(-x)$	$[0,\infty)$	Laguerre	Gauss-Laguerre
$\exp(-x^2/2)$	$(-\infty,\infty)$	Hermite	Gauss-Hermite
$1/\sqrt{1-x^2}$	$(-1,1)$	Chebyshev (First kind)	Chebyshev-Gauss
$\sqrt{1-x^2}$	$[-1,1]$	Chebyshev (Second kind)	Chebyshev-Gauss
$(1-x)^a(1+x)^b$	$(-1,1)$	Jacobi	Gauss-Jacobi

A k^{th} order moment of a response function, $Y = \eta(\mathbf{X})$, needs to evaluate a multi-dimensional integration:

$$M_Y^k = E\left\{\left[\eta(\mathbf{x})\right]^k\right\} = \int_{\mathbf{X}} \left[\eta(\mathbf{x})\right]^k f_{\mathbf{X}}(\mathbf{x})\mathrm{d}\mathbf{x} \tag{2.13}$$

With the rules of Gauss quadrature listed in Table 2.1, and supposed that input random variables are independent to each other, a procedure of moment computation with Gauss quadrature can be summarized as follows:

- Given PDF of X_i, one needs to determine the standard Gauss point and weight of the input variable;
- The standard Gauss quadrature needs to be further recast using the distribution parameters of X_i. The tensor product of the Gauss points of each variable determines the global input matrix.

- Evaluate the model responses specified at the global integration grid. Output moment, then, can be numerically evaluated by using the weighted summation of the responses.

Implementation of the tensor Gauss quadrature finally determines a k^{th} moment of $Y = \eta(\mathbf{X})$ with the form of

$$M_Y^k = \int_{\mathbf{X}} [\eta(\mathbf{x})]^k f_{\mathbf{X}}(\mathbf{x}) \mathrm{d}\mathbf{x} \approx \sum_{i_1=1}^{N_1} \sum_{i_2=1}^{N_2} \cdots \sum_{i_n=1}^{N_n} w_{i_1} w_{i_2} \cdots w_{i_n} [\eta(x_{i_1}, x_{i_2}, \cdots x_{i_n})]^k \tag{2.14}$$

where w_{i_l} and x_{i_l} are the Gauss weight and point for an l^{th} random variable, respectively. N_k is the order of Gauss quadrature. It usually is selected as a constant for all random variables, which is referred to as the homogeneous Gauss quadrature method. If input random variables contains the dependent components, an isoprobabilistic transform (Der Kiureghian and Liu, 1986; Rosenblatt, 1952) should be applied.

Main drawback of the Gauss quadrature is the curse of dimensionality. Suppose indeed an N order scheme is retained for each random variable. Then, the nested summation in Eq.(2.14) needs N^n functional evaluations of the mechanistic model $y = \eta(\mathbf{x})$, which is exponentially increasing with respect to the dimensionality of input random vector.

2.3 Methods for Reliability Analysis

Structural reliability analysis aims at computing the failure probability of an engineering system with respect to a prescribed failure criteria by accounting for uncertainties arising in the model description (e.g., geometric dimension, material property, etc.) or the environment (e.g., external load, temperature, humidity, etc.). It is a general theory whose development started in the early of 1950's. The research in this field is still quite active. The reader is referred to textbooks for a comprehensive presentation of the topic (Ditlevsen and Madsen, 1996; Ghanem and Spanos, 1991; Madsen et al., 2006). This Section summarizes some well-established methods to solve the problem.

A system is supposed to fail when some requirements of safety or serviceability are not fulfilled. For each failure mode, a failure mechanism is set up by using a limit state function $g(\mathbf{X})$. One should note that the expression of $g(\mathbf{X})$ is usually defined as a function of system output, $Y = \eta(\mathbf{X})$, and its allowable threshold, y_0. Then, the limit state function is formulated in such a way that:

- $\mathcal{D}_S := \{\mathbf{X} : g(\mathbf{X}) > 0\}$ is the safe domain in the space of input variables;
- $\mathcal{D}_F := \{\mathbf{X} : g(\mathbf{X}) < 0\}$ is the failure domain; and
- $\mathcal{D}_0 := \{\mathbf{X} : g(\mathbf{X}) = 0\}$ is the corresponding limit state surface.

Given the joint PDF of input variables, $\mathbf{X}$, the corresponding probability of failure associated with the limit state function is an integral of

$$P_F = \int_{g(\mathbf{X})\leqslant 0} f_{\mathbf{X}}(\mathbf{x})\mathrm{d}\mathbf{x} \tag{2.15}$$

In all but academic cases, this integral cannot be analytically computed due to the high dimensionality of $\mathbf{X}$ and the complexity of the boundary condition: $\Gamma = \{g(\mathbf{X}) \leqslant 0\}$. Indeed, the failure domain depends on structural response quantities (e.g., displacement, strain, stress, etc.), which are usually computed by means of a computer code (e.g., a finite element package). Hence, the limit state function is implicitly defined and thus a numerical method has to be considered.

2.3.1 Monte Carlo Simulation

Monte Carlo simulation is a universal method for evaluating integrals in Eq.(2.15). Denoting by an indicator function of failure domain, $\mathbf{1}_{\{g(\mathbf{x})\leqslant 0\}}$ (i.e., it takes the value 0 in the safe domain and 1 otherwise), Eq.(2.15), then, can be rewritten as

$$P_F = \int_{\mathbf{X}} \mathbf{1}_{\{g(\mathbf{X})\leqslant 0\}} f_{\mathbf{X}}(\mathbf{x})\mathrm{d}\mathbf{x} = E\left[\mathbf{1}_{\{g(\mathbf{X})\leqslant 0\}}\right] \tag{2.16}$$

where $E[\cdot]$ is the expectation operator. Practically, the above equation can be evaluated by simulating N samples of $\mathbf{X}$, e.g., $\{\mathbf{x}^{(1)}, \mathbf{x}^{(2)}, \cdots, \mathbf{x}^{(N)}\}$. For each sample, one can evaluate the limit state function, $g\left(\mathbf{x}^{(i)}\right)$, through a deterministic code of $y = \eta(\mathbf{x})$. An estimate of P_F, then, can be given as the empirical mean of

$$P_{F,\mathrm{MCS}} = \frac{1}{N}\sum_{i=1}^{N} \mathbf{1}_{\{g(\mathbf{x}^{(i)})\leqslant 0\}} = \frac{N_{\mathrm{fail}}}{N} \tag{2.17}$$

where N_{fail} is the number of samples that are located in the failure domain. According to the large-number law and central limit theorem, it is known that $\widehat{P}_F$ converges to P_F with probability

of one and is asymptotically normally distributed as N goes to infinity. Therefore, the estimate is unbiased $\big($i.e., $E\big[P_{F,\mathrm{MCS}}\big] = P_F\big)$. And the variance of $P_{F,\mathrm{MCS}}$ can be assessed by

$$\mathrm{Var}\big[P_{F,\mathrm{MCS}}\big] = \frac{P_F(1-P_F)}{N} \tag{2.18}$$

Hence, efficiency of the Monte Carlo simulation can be measured by

$$\mathrm{COV} = \frac{\sqrt{\mathrm{Var}[P_{F,\mathrm{MCS}}]}}{E[P_{F,\mathrm{MCS}}]} = \sqrt{\frac{1-P_{F,\mathrm{MCS}}}{N\ P_{F,\mathrm{MCS}}}} \tag{2.19}$$

Practically, the value of failure probability is very small, i.e., $P_F \ll 1$. Therefore, the corresponding number of functional evaluations is:

$$\mathrm{COV} \approx \frac{1}{\sqrt{N\ P_{F,\mathrm{MCS}}}} \quad \Longrightarrow \quad N \approx \frac{1}{\mathrm{COV}^2\ P_{F,\mathrm{MCS}}} \tag{2.20}$$

Suppose that the value of P_F is in the order of 10^{-k} and the required COV is 5%. Using the above equation, one can calculate that the number of required samples is $N \geqslant 4\times 10^{k+2}$, which is a big number when a small value of failure probability (e.g., $P_F = 10^{-4}$) is sought.

2.3.2 First-Order Reliability Method

The first order reliability method (FORM) was introduced to calculate the structural failure probability by means of a limited number of functional evaluations compared to the brutal Monte Carlo simulation.

In FORM, the reliability analysis is recast in the standard Normal space, i.e., one needs to transform the input random variables, $\mathbf{X}$, as the independent standard Normal variables, $\mathbf{U}$. This can be achieved by using an isoprobabilstic transform $\mathbf{U} = T(\mathbf{X})$, such as Rosenblatt transform (Rosenblatt, 1952) or Nataf transform (Der Kiureghian and Liu, 1986). Then, the probability of failure can be evaluated by

$$P_F = \int_{g(\mathbf{X})\leqslant 0} f_{\mathbf{X}}(\mathbf{x})\mathrm{d}\mathbf{x} = \int_{g[T^{-1}(\mathbf{U})]\leqslant 0} \phi_{\mathbf{U}}(\mathbf{u})\mathrm{d}\mathbf{u} \tag{2.21}$$

where $\phi_{\mathbf{U}}(\mathbf{u})$ is the standard independent multi-Normal PDF:

$$\phi_{\mathbf{U}}(\mathbf{u}) = \frac{1}{(2\pi)^{n/2}} \exp\left(-\frac{\mathbf{u}^{\mathrm{T}}\mathbf{u}}{2}\right) \tag{2.22}$$

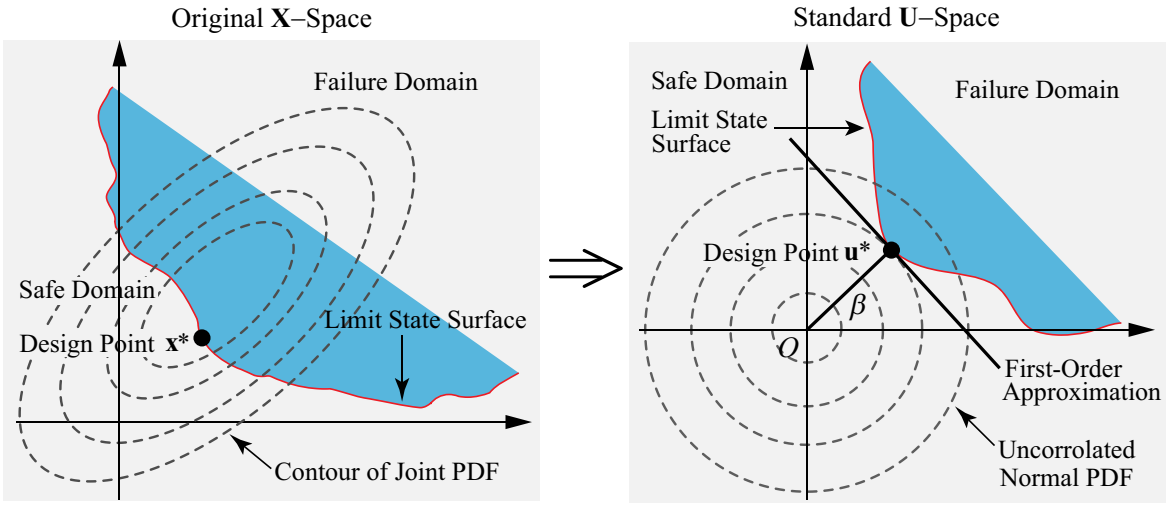

Figure 2.3: Principle of the first-order reliability method (FORM)

Once the transformation to the standard **U**-space has been conducted, the joint multi-Normal PDF is rotationally symmetrical about the origin, and with the maximum density at the origin.

Given the **U**-space as shown in Figure 2.3, the point on the transformed limit state surface that is closest to the origin, hence, has the highest probability density in the failure domain. This is why the point is referred to as the most probable failure point (MPP). The Euclidean distance between the origin and MPP is denoted as the reliability index. And the position of $\mathbf{u}^*$ can be found via a constrained optimization problem:

$$\mathbf{u}^* = \arg\min_{\mathbf{u}} \left\{ \sqrt{\mathbf{u}^{\mathrm{T}}\,\mathbf{u}} : g\left[T^{-1}(\mathbf{u})\right] = 0 \right\} \tag{2.23}$$

Once the design point $\mathbf{u}^*$ in standard Normal space has been identified, it is possible to calculate the reliability index as

$$\beta = \mathrm{sign}\left[g\left(T^{-1}(\mathbf{0})\right)\right] \cdot \|\mathbf{u}^*\| \tag{2.24}$$

which is counted as positive if the origin is in the safe domain, and negative otherwise.

FORM makes the assumption that the failure surface can be fitted exactly with a tangent hyperplan through the design point, $\mathbf{u}^*$, in the standard Normal space as shown in Figure 2.3. Expression of the hyperplane is given as

$$\beta - \boldsymbol{\alpha}^{\mathrm{T}}\,\mathbf{u} = 0 \tag{2.25}$$

where the vector $\boldsymbol{\alpha}$ is the unit outward normal vector at the design point:

$$\alpha_k = -\frac{\nabla g\left[T^{-1}(u_k^*)\right]}{\left\|\nabla g\left[T^{-1}(u_k^*)\right]\right\|} \quad (k = 1, 2, \cdots, n) \tag{2.26}$$

Using the first-order hypeplane to approximate the original limit state surface, the corresponding failure probability can be approximated as

$$P_F = \int_{g[T^{-1}(\mathbf{U})]\leqslant 0} \phi_{\mathbf{U}}(\mathbf{u})\mathrm{d}\mathbf{u} \approx \int_{\beta-\boldsymbol{\alpha}^{\mathrm{T}}\mathbf{U}\leqslant 0} \phi_{\mathbf{U}}(\mathbf{u})\mathrm{d}\mathbf{u} \tag{2.27}$$

As shown in forgoing section, the standard uncorrelated Normal joint PDF is rotationally symmetric. One can rotate the linearized failure surface to any convenient position without changing the probability content on either side of the hyperplane. The most convenient position is such that it is perpendicular to any single axis, since then, the probability calculation becomes an one-dimensional integration. Therefore, the failure probability provided by the first-order approximation can be determined as

$$P_F \approx P_{F,\mathrm{FORM}} = \Phi(-\beta) \tag{2.28}$$

where $\Phi(\cdot)$ is the standard Normal cumulative distribution function (CDF).

One should note that the FORM approaches may provide erroneous results if the optimization problem in Eq.(2.23) is non-convex. Indeed, the following two problems might be happened:

- The adopted optimization scheme might converge to a local minima instead of the global minima of the problem, and then miss the failure region contributed to the structural failure; and
- Even if the global design point is determined, there could be significant contributions to the failure form the vicinity of the local design points in the standard **U**-Space.

To deal with the problems, one can refer to the literature (Der Kiureghian and Dakessian, 1998) for details, in which a method based on the series system reliability analysis was developed to tackle with the problems featuring multiple design points. In addition, by using a higher-order hyperplane to approximate the limit state function can improve the accuracy of FORM in reliability analysis (Dubourg, 2011).

2.3.3 Method of Importance Sampling

FORM allows an analyst to compute a probability of failure with the low computational cost compared to Monte Carlo simulation. However, FORM might reveal its deficiency in the case of a complicated limit state function (e.g., with multiple design points). To bypass the difficulty, a method that integrates FORM and simulation can be employed, namely the importance sampling method (Harbitz, 1983; Shinozuka, 1983).

Consider that the design point $\mathbf{x}^*$ has been identified by FORM. Let us define an auxiliary PDF, denoted it as the importance density:

$$h_{\mathbf{X}}(\mathbf{x}) = f_{\mathbf{X}}(\mathbf{x})\big|_{\boldsymbol{\mu}=\mathbf{x}^*} \tag{2.29}$$

which implies the expression of $h_{\mathbf{X}}(\mathbf{x})$ is identical with the original joint PDF $f_{\mathbf{X}}(\mathbf{x})$, only by changing the mean values of input random variable as the design point $\mathbf{x}^*$. The probability of failure, then, can be recast as(Breitung, 1984; Der Kiureghian et al., 1987)

$$P_F = \int_{g(\mathbf{X})\leqslant 0} \frac{f_{\mathbf{X}}(\mathbf{x})}{h_{\mathbf{X}}(\mathbf{x})} h_{\mathbf{X}}(\mathbf{x})\mathrm{d}\mathbf{x} = E\left[\mathbf{1}_{\{g(\mathbf{X})\leqslant 0\}}(\mathbf{X})\frac{f_{\mathbf{X}}(\mathbf{x})}{h_{\mathbf{X}}(\mathbf{x})}\right] \tag{2.30}$$

An estimate of P_F by the importance sampling is determined by an empirical mean-value of

$$P_{F,\mathrm{IS}} = \frac{1}{N}\sum_{i=1}^{N} \mathbf{1}_{\{g(\mathbf{X})\leqslant 0\}}\left(\mathbf{x}^{(i)}\right)\frac{f_{\mathbf{X}}\left(\mathbf{x}^{(i)}\right)}{h_{\mathbf{X}}\left(\mathbf{x}^{(i)}\right)} \tag{2.31}$$

where $\mathbf{x}^{(i)}$ is an i^{th} sample of random vector $\mathbf{X}$ simulated according to $h_{\mathbf{X}}(\mathbf{x})$.

In the standard $\mathbf{U}$-space, importance sampling can be conducted as

$$P_{F,\mathrm{IS}} = \frac{1}{N}\sum_{i=1}^{N} \mathbf{1}_{\{g[T^{-1}(\mathbf{U})]\leqslant 0\}}\left(\mathbf{u}^{(i)}\right)\frac{\phi_{\mathbf{U}}\left(\mathbf{u}^{(i)}\right)}{\widetilde{h}_{\mathbf{U}}\left(\mathbf{u}^{(i)}\right)} \tag{2.32}$$

where $\mathbf{u}^{(i)}$ is now randomly generated from the auxiliary PDF, $\widetilde{h}_{\mathbf{U}}(\mathbf{u})$:

$$\widetilde{h}_{\mathbf{U}}(\mathbf{u}) = \phi_{\mathbf{U}}(\mathbf{u}-\mathbf{u}^*) \tag{2.33}$$

In the case, estimation of the failure probability can be reduced as

$$P_{F,\mathrm{IS}} = \frac{\exp(\beta^2/2)}{N}\sum_{i=1}^{N} \mathbf{1}_{\{g[T^{-1}(\mathbf{U})]\leqslant 0\}}\left(\mathbf{u}^{(i)}\right)\exp\left(-\mathbf{u}^{(i)}\cdot\mathbf{u}^*\right) \tag{2.34}$$

where β is the reliability index determined by FORM.

To compare the efficiency of importance sampling with crude Monte Carlo simulation, an experiment is designed as follows. At first, 5000 samples of input random vector $\mathbf{X}$ are generated to estimate the failure probability by using importance sampling and Monte Carlo simulation, respectively. The estimates of $P_{F,\mathrm{MCS}}$ and $P_{F,\mathrm{IS}}$ are separately stored. Repeat the procedure 1000 times. One can use the estimates to calculate the corresponding COVs of the methods. Normalizing the estimates by the benchmark of P_F provided by 10^6 simulations, histograms of the normalized failure probabilities, i.e., $P_{F,\mathrm{IS}}/P_F$ and $P_{F,\mathrm{MCS}}/P_F$, are depicted as shown in Figure 2.4, respectively.

According to the histograms of the normalized estimates, it is clear to see that importance sampling is much more efficient than crude Monte carlo simulation (i.e., 2.11% COV by importance sampling versus 12.72% COV by crude MCS). Note that if FORM does not converge, the sequence of points computed by the optimization algorithm may help select a relevant sampling density. Furthermore, various improvements of importance sampling method have been proposed, such as adaptive importance sampling (Au and Beck, 1999; Bucher, 1988), radial importance sampling (Melchers, 1990) and others (Neal, 2001).

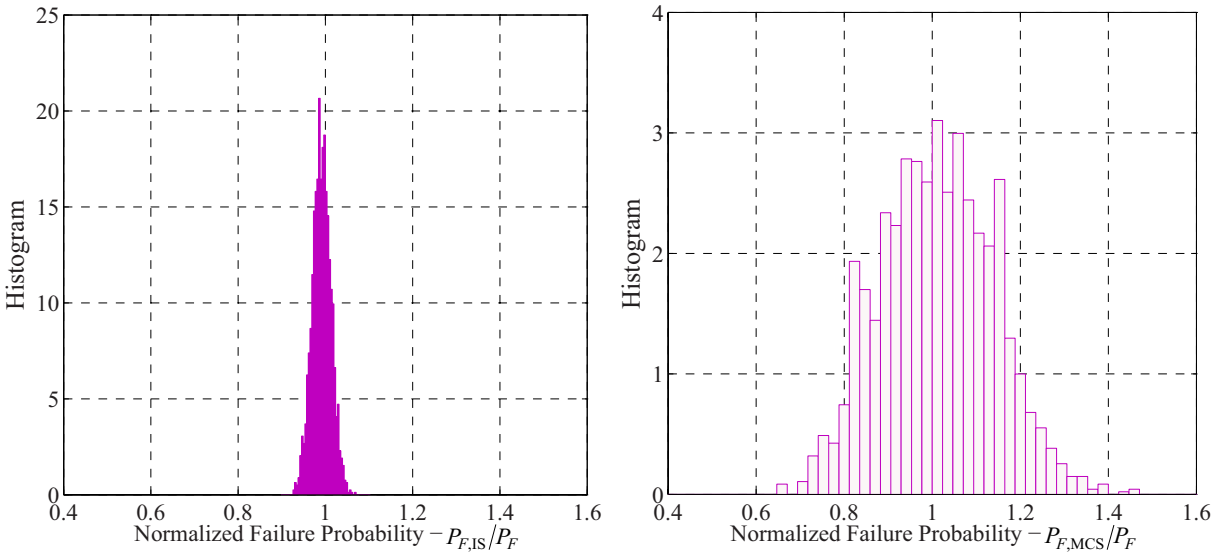

(a) Importance Sampling

(b) Crude Monte Carlo Simulation

Figure 2.4: Histogram of the normalized failure probability ($\widehat{P}_F/P_F$) estimated by Monte Carlo simulation and importance sampling method: $g(\mathbf{X}) = 30 - \left(X_1^2 + X_2^3\right)$, where X_1 and X_2 follow the independent Normal distribution $N(2.0, 0.4)$.

2.3.4 Method of Line Sampling

Line sampling method was developed by Schuëller et al. (2004) to tackle with the reliability analysis with extremely high-dimensional input random variables (e.g., the dimensionality of $\mathbf{X} \geqslant 1000$), in which the lines are employed instead of points to probe the failure domain of interest. The method was applied in literatures (Koutsourelakis et al., 2004; Pradlwarter et al., 2007; Schuëller and Pradlwarter, 2007) to conduct the reliability analysis of liner and non-linear random vibration system excited by a random process. Recently, combined with the artificial neural network, Zio and Pedroni (2009) employed the line sampling method to estimate the functional failure of a passive decay heat removal system in a gas-cooled fast nuclear reactor.

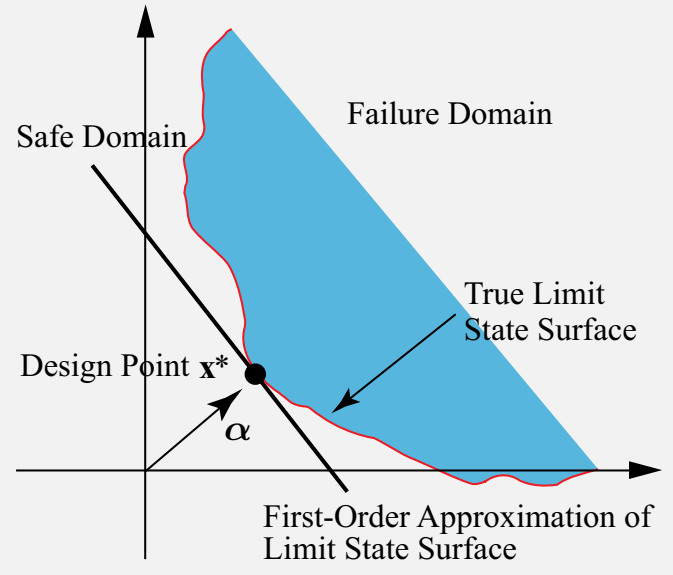

Figure 2.5: Important direction $\boldsymbol{\alpha}$ in line sampling method

Figure 2.5 has illustrated the importance direction in the line sampling method. The direction can be determined from the origin to the design point $\mathbf{x}^*$, since that the way along the direction ($\boldsymbol{\alpha}$) is the shortest one among all possible routes reaching the failure domain. In addition, each element of $\boldsymbol{\alpha}$ measures the relative importance of a particular random variable with respect to the failure probability in the vicinity the design point. Given a specified step along the direction, limit state function should change the most. Therefore, the samples collected along the direction would be more efficient than other manners to obtain the successful "failure shots". The idea is very similar to the axis orthogonal sampling method (Hohenbichler and Rackwitz, 1988) and directional sampling method (Bjerager, 1988).

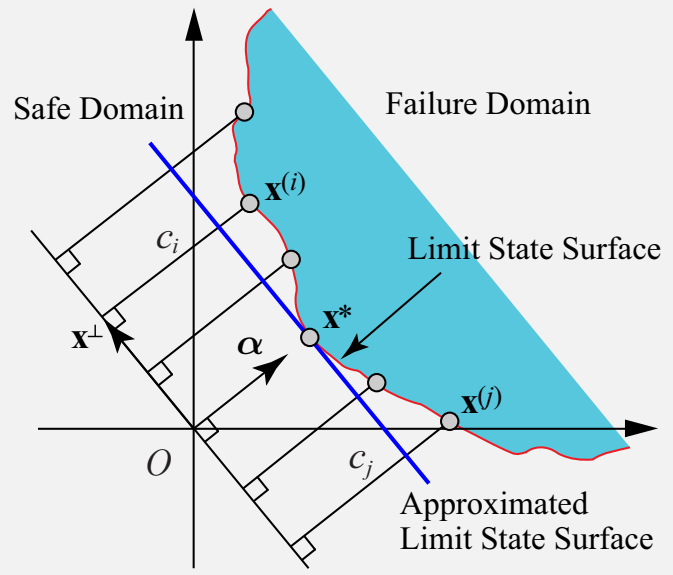

Figure 2.6: Schematic sketch of line sampling procedure

Conceptually, the line sampling is implemented as a sample $\mathbf{x}^{(i)}$ randomly varies parallel to the importance direction $\boldsymbol{\alpha}$ as shown in Figure 2.6. To conduct the simulation, one can generate a sample in the space of $\mathbf{x}^{\perp}$ at first, which is orthogonal to the selected importance direction. Then, the required sample, $\mathbf{x}^{(i)}$, can be defined as the summation of vector $\boldsymbol{\alpha}$ and $\mathbf{x}^{\perp}$. Therefore, use a standardized vector $\mathbf{e} = \boldsymbol{\alpha}/\|\boldsymbol{\alpha}\|$, the sample $\mathbf{x}^{(i)}$ can be expressed as

$$\mathbf{x}^{(i)} = c_i\,\mathbf{e} + \mathbf{x}^{\perp} \tag{2.35}$$

where,

$$\mathbf{x}^{\perp} = \mathbf{x}^{(i)} - \left\langle \mathbf{e}, \mathbf{x}^{(i)} \right\rangle \mathbf{e} \tag{2.36}$$

where, $\langle \cdot, \cdot \rangle$ is the product operator of a vector.

Since the sample $\mathbf{x}^{(i)}$ is on the limit state surface, i.e., it should satisfy $g\left(\mathbf{x}^{(i)}\right) = 0$. The distance c_i, hence, can be determined by solving the following one-dimensional equation:

$$g\left(\mathbf{x}^{(i)}\right) = g\left(c_i\,\mathbf{e} + \mathbf{x}^{\perp}\right) = 0 \tag{2.37}$$

in which, one can see that Eq.(2.37) is a non-linear function in terms of c_i. Numerical Newton-based iteration method is efficient to solve the problem. However, in order to reduce the number of functional evaluations, the interpolation scheme is usually employed to estimate the value of c_i.

In summarize, the line sampling method can be implemented as follows: (a) Generate an i^{th} sample of input variables, $\mathbf{x}^{(i)}$; (b) Calculate the corresponding perpendicular vector $\mathbf{x}^{\perp}$ with respect to the importance direction, $\mathbf{e}$; (c) Estimate the distance c_i by solving Eq.(2.37). An estimate of failure probability, then, can be calculated by $P_F^{(i)} = \Phi(-c_i)$.

Given N samples in line sampling, the estimate of P_F can be determined by mean-value of $P_F^{(i)}$ $(i = 1, 2, \cdots, N)$:

$$P_{F,\text{LS}} = \frac{1}{N}\sum_{i=1}^{N}\Phi(-c_i) \tag{2.38}$$

Line sampling method can be further employed to deal with the system reliability analysis with multiple failure modes. Assumed that a system contains m failure modes, one can use the notations $g_{[i]}(\mathbf{X})$, $\mathbf{e}_{[i]}$ and $D_{[i]} := \{\mathbf{X} : g_{[i]}(\mathbf{X}) \leqslant 0\}$ to denote the corresponding limit state function, importance direction and failure domain of each failure mode, respectively.

In case of the failure domains are independent (has non-overlapped region), the system failure probability can be directly determined by the summation of each failure probability, $P_F^{[i]}$ $(i = 1, 2, \cdots, m)$

$$P_{F,\text{LS}} = \sum_{i=1}^{m} P_F^{[i]} = \frac{1}{N}\sum_{i=1}^{m}\sum_{j=1}^{N}\Phi\big(-c_j^{[i]}\big) \tag{2.39}$$

However, considering the overlapped failure domains, a modification is required to eliminate the interaction effect of failure modes. For the sake of configuration, two failure modes with the overlapped failure domains are demonstrated in Figure 2.7.

Assume that $D_{[i]} := \{\mathbf{X} : g_{[i]}(\mathbf{X}) \leqslant 0\}$ and $D_{[j]} := \{\mathbf{X} : g_{[j]}(\mathbf{X}) \leqslant 0\}$ are two failure domains. Bisector of the angle shaped by $\boldsymbol{\alpha}_{[i]}$ and $\boldsymbol{\alpha}_{[j]}$ can separate the whole failure domain into two independent parts, i.e., $\overline{D}_{[i]}$ and $\overline{D}_{[j]}$, respectively.

Considering a random sample $\mathbf{x}^{(p)}$ simulated for the modified limit state function $\overline{g}_{[i]}(\mathbf{X})$, it falls into $\overline{D}_{[i]}$ as shown in Figure 2.7. The corresponding distance $c_p^{[i]}$ can be determined as the usual case of single failure mode in previous section.

However, as shown in Figure 2.8, the vector $\mathbf{x}^{(k)}$ is simulated for $\overline{D}_{[j]}$. The distances of $\mathbf{x}^{(k)}$ to importance directions $\boldsymbol{\alpha}_{[i]}$ and $\boldsymbol{\alpha}_{[j]}$ are determined as $d_k^{[i]}$ and $d_k^{[j]}$, respectively, which can be numerically calculated as

$$d_k^{[l]} = \left\|\mathbf{x}^{(k)} - \left\langle \mathbf{e}_{[l]}, \mathbf{x}^{(k)}\right\rangle \mathbf{e}_{[l]}\right\| \quad (l = i, j) \tag{2.40}$$

If $d_k^{[j]} \leqslant d_k^{[i]}$, it implies $\mathbf{x}^{(k)} \in \overline{D}_{[j]}$. And the failure probability is:

$$P_{Fk}^{[j]} = \Phi\Big(-c_k^{[j]}\Big) \tag{2.41}$$

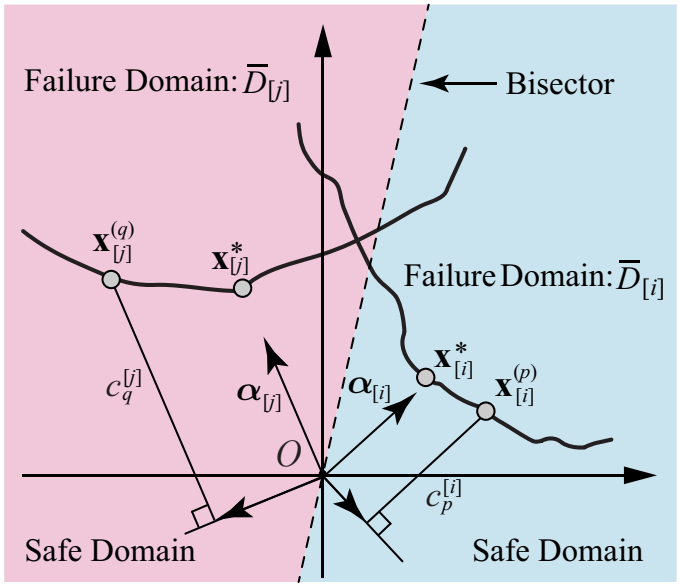

Figure 2.7: Line sampling method in system reliability analysis

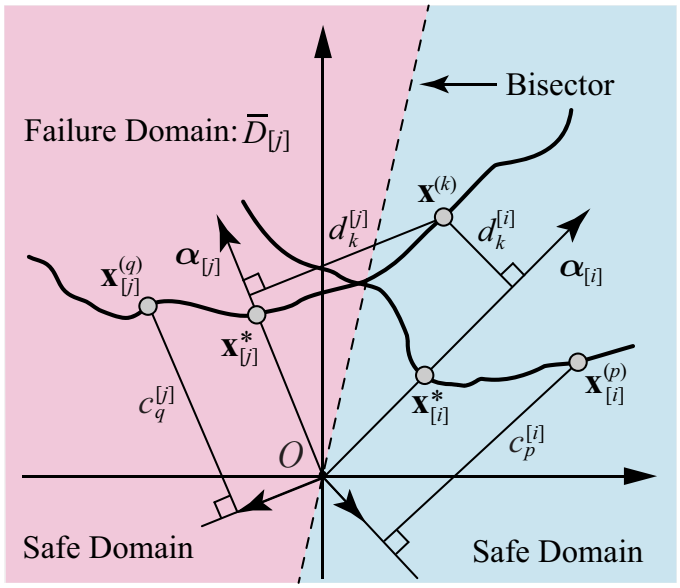

Figure 2.8: Method of line sampling with overlapped failure domains

However, in Figure 2.8, one can see that $d_k^{[j]} > d_k^{[i]}$. It implies the sample $\mathbf{x}^{(k)}$, actually, falls into the failure domain of $\overline{D}_{[i]}$. The corresponding distance, $\overline{c}_k^{[j]}$, can be determined as (Kout-

sourelakis et al., 2004; Schuëller and Pradlwarter, 2007):

$$\overline{c}_k^{[j]} = c_k^{[j]} + \text{sign}\Big(c_k^{[j]}\Big)\frac{d_k^{[j]} - d_k^{[i]}}{\sqrt{1 - \big\langle \mathbf{e}_{[i]}, \mathbf{e}_{[j]} \big\rangle^2}} \tag{2.42}$$

In summary, as the system failure is represented by more than two failure modes, the importance directions $\boldsymbol{\alpha}_{[i]}$ (for $i = 1, 2, \cdots, m$) need be determined at first. Then, utilize the bisectors of importance directions to tailor the overlapped failure domain as m independent regions. Given a random sample simulated for an i^{th} failure domain, $D_{[i]}$, compute the distance of $\mathbf{x}^{(k)}$ to all importance directions. Employe the following criteria to determine whether or not the sample belong to $D_{[i]}$:

$$\mathbf{x}^{(k)} \in D_{[i]} \Longleftrightarrow d_k^{[i]} = \min\Big\{d_k^{[1]}, d_k^{[2]}, \cdots, d_k^{[m]}\Big\} \tag{2.43}$$

If not, use Eq.(2.42) to determine the modified coefficient $\overline{c}_k^{[i]}$.

Finally, the system failure probability can be estimated as

$$P_{F,\text{LS}} = \sum_{i=1}^{m} P_F^{[i]} = \frac{1}{N}\sum_{i=1}^{m}\sum_{k=1}^{N} \Phi\big(-\overline{c}_k^{[i]}\big) \tag{2.44}$$

A structure with six failure modes is considered to illustrate the line sampling method for system reliability analysis. Limit state function of each failure mode is given as (Bennett and Ang, 1983)

$$\begin{cases} g_1(\mathbf{X}) = M_1 + 3M_2 + 2M_3 - 15S_1 - 10S_2; & g_2(\mathbf{X}) = 2M_1 + 2M_2 - 15S_1 \\ g_3(\mathbf{X}) = M_1 + M_2 + 4M_3 - 15S_1 - 10S_2; & g_4(\mathbf{X}) = 2M_1 + M_2 + M_3 - 15S_1 \\ g_5(\mathbf{X}) = M_1 + M_2 + 2M_3 - 15S_1; & g_6(\mathbf{X}) = M_1 + 2M_2 + M_3 - 15S_1 \end{cases} \tag{2.45}$$

Since failure of system can be triggered by the fail of any mode, the system failure event, hence, is recast to as a series system:

$$E_{\text{System}} := \big\{E_1 \cup E_2 \cup E_3 \cup E_4 \cup E_5 \cup E_6\big\} \tag{2.46}$$

where an i^{th} component failure event $E_i := \{g_i(\mathbf{X}) \leqslant 0\}\,(i = 1, \cdots, 6)$. And the random variables $\mathbf{X}$ are defined in Table 2.2.

Assume that random variables are following the distributions of Normal and Lognormal, respectively. System failure probabilities are estimated using the line sampling method. Given

Table 2.2: Random variables of the serial structure

Random Variable	S_1	S_2	M_1	M_2	M_3
Mean Value	50	100	500	500	667
Standard Deviation	10	10	75	75	100

Table 2.3: Example of system reliability analysis using the line sampling method

Distribution	Normal		Lognormal	
Method	Line Sampling	MCS	Line Sampling	MCS
Number of samples	1500	10^6	1500	10^6
Failure Probability	6.69×10^{-5}	7.78×10^{-5}	5.93×10^{-4}	6.10×10^{-4}
COV of $P_{F,\mathrm{LS}}$	3.17%	––	2.43%	––

the benchmarks provided by brutal Monte Carlo simulation, the comparisons are summarized in Table 2.3.

Given the results in Table 2.3, one can see that the line sampling method can determine the system failure probability with a fairly small number of function evaluations. In addition, the values of COV estimated by 100 rounds Monte Carlo experiment are very small. Therefore, compared to brutal Monte Carlo simulation, the line sample method reserves the both of accuracy and efficiency in system reliability analysis.

2.4 Methods for Global Sensitivity Analysis

As stated by Grierson (1983), "The essential objective of sensitivity analysis of any system is to establish a measure of the way of response quantity varies with the change of input parameters that define the system." Therefore, the sensitivity analysis is very useful to (Castillo et al., 2008):

- a designer, who can know which input parameter is most influential to a structural output;
- a builder, who can know how changes in component prices influence the total cost of the project being undertaken; and
- a code maker, who can know safety implications associated with changes in a design format.

In uncertainty quantification, sensitivity analysis is the study of how the uncertainty of an output can be apportioned to different sources of uncertainties in input variables. Methods for the probabilistic sensitivity analysis are usually classified into the following two categories:

- Local sensitivity analysis concentrates on the sensitivity of distribution parameters of an input random variable on a model output. It employs the gradient of response with respect to each parameter around a nominal value. Moment sensitivity factor and the reliability-based sensitivity factor are of two popular indices of the local sensitivity analysis.

- Global sensitivity analysis focuses on the output uncertainty over the whole definition domain of input variables. It takes into account the entire variation of input variables and aims to apportion the output uncertainty to each input factor. Therefore, global sensitivity analysis helps analyst identify the key parameters whose uncertainty affect the most of model output, which in turn can be used to establish experimental research priorities, eventually leading to a better definition of the model function (Saltelli, 2002; Saltelli and Sobol', 1995; Sudret, 2008b).

In local sensitive analysis, the contribution of each parameter (e.g., mean value, standard deviation, etc.) of a random variable with respect to output moment or failure probability is of interest. With the local sensitivity index, critical parameters can be identified. Therefore, it provides the gradient information needed by an optimization procedure to update the distribution parameter in a risk-based design framework (Frangopol, 1985).

However, the local sensitivity index is only validated in the vicinity of a nominal value of distribution parameter. The first-order derivative, hence, is only useful to assess the sensitivity information near a predefined reference point, instead of the entire definition domain of input variable. Due to the limitation, the study is primary focused on the method of global sensitivity analysis.

A good state-of-the-art of the methods for global sensitivity analysis is available in literature (Saltelli et al., 2000, 2008), which gathers the methodology into two groups:

- Regression-based method: the standardized regression coefficients are determined based on a linear regression of the output on the input vector. The input-output correlation coefficients measure the effect of each input variable by the correlation it has with the model output. The partial correlation coefficients are based on results of regressions of the model on all input variables except one. These coefficients are useful to measure the effect of

the input variables if the model is linear, i.e., if the coefficient of determination, R^2, of the regression is close to one. In case of nonlinearity, they fail to represent properly the response sensitivities (Saltelli and Sobol', 1995), which also can be found in the method of design of experiment.

- Variance-based method: The method aims at decomposing the output variance as a summation of variance contributions of each input variable, and the combinations. The method of "General ANalysis Of VArance" (G-ANOVA) enters the category. Each conditional variance is described as a multi-dimensional integration. The simulation methods, such as Monte Carlo simulation and Latin Hypercube sampling, are the dominant approaches for global sensitivity analysis (Sobol', 2001).

2.4.1 Taylor Series Expansion

Method of the truncated Taylor series for moment calculation was reviewed in Section 2.2.2. An approximated expression of output variance was derived as

$$\mathrm{Var}[Y] = \sigma_Y^2 \approx \sum_{i=1}^{n} \left(\left. \frac{\partial \eta(\mathbf{x})}{\partial x_i} \right|_{\mathbf{x}=\boldsymbol{\mu}} \times \sigma_i \right)^2 \tag{2.47}$$

From this expression, it is clear to see that the response variance is a summation of variances related to each input variable. By normalizing each component, one can define a relative importance factor as

$$S_i = \left. \frac{\partial \eta(\mathbf{x})}{\partial x_i} \right|_{\mathbf{x}=\boldsymbol{\mu}} \times \frac{\sigma_i}{\sigma_Y} \tag{2.48}$$

in which, the summation of S_i is up to one. The so-called decomposition of variance is carried out in a linearized context since the variance calculation is based on the first-order Taylor series expansion.

2.4.2 FORM Analysis

The first-order reliability method (FORM) was reviewed in Section 2.3.2. As shown in Eq.(2.25), an approximation on $g(\mathbf{X})$ can be represented as a hyperplane through the design point in the standard $\mathbf{U}$-space:

$$g\left[T^{-1}(\mathbf{U})\right] \approx \beta - \boldsymbol{\alpha}^{\mathrm{T}} \mathbf{U} \tag{2.49}$$

where β is the FORM reliability index; $\boldsymbol{\alpha}$ is the direction from origin to design point $\mathbf{u}^*$, and $T(\cdot)$ is an isoprobabilistic transformation (Der Kiureghian and Liu, 1986; Rosenblatt, 1952).

Through the approximation, the variance of $g(\mathbf{X})$, then, can be evaluated as

$$\mathrm{Var}\left[g\left(T^{-1}(\mathbf{U})\right)\right] \approx \sum_{i=1}^{n} \alpha_i^2 = 1 \tag{2.50}$$

This results is due to the elements of $\mathbf{U}$ are the independent standard Normal variables and $\boldsymbol{\alpha}$ is a unit vector:

$$\alpha_i = -\frac{\nabla g\left[T^{-1}(u_i^*)\right]}{\left\|\nabla g\left[T^{-1}(u_i^*)\right]\right\|} \quad (i = 1, 2, \cdots, n) \tag{2.51}$$

in which, the coefficient α_i^2 $(i = 1, 2, \cdots, n)$ is known as FORM importance factor correspond to the portion of the variance of the linearized limit state function (Ditlevsen and Madsen, 1996). Thus, α_i^2 is interpreted as the importance factor of the i^{th} input variable.

Approximation of $g(\mathbf{X})$ using the FORM-based hyperplane is only exact at the design point $\mathbf{x}^*$. The approximated variance of $g(\mathbf{X})$, hence, is only decomposed exactly at the referenced point. The corresponding important factor α_i^2 $(i = 1, 2, \cdots, n)$ reveals its characteristic as a local sensitivity index. A similar conclusion can be made for the moment-based sensitivity factors as shown in last Section, in which one can see that the reference points are the mean values of input variable.

2.4.3 Global Sensitivity Index

A general decomposition of the input-output function, $Y = \eta(\mathbf{X})$, can be derived as a summand of a series of component functions with an increasing dimensionality (Cox, 1982; Efron and Stein, 1981):

$$\eta(\mathbf{X}) = \eta_0 + \sum_{i=1}^{n} \eta_i(X_i) + \sum_{1 \leqslant i < j \leqslant n} \eta_{ij}(X_i, X_j) + \cdots + \eta_{12\cdots n}(\mathbf{X}) \tag{2.52}$$

in which, one can see that the total terms in the decomposition is 2^n. And each component function is defined as follows.

First of all, the constant η_0 is given as

$$\eta_0 = \int_{\mathbf{X}} \eta(\mathbf{x}) f_{\mathbf{X}}(\mathbf{x}) \mathrm{d}\mathbf{x} \tag{2.53}$$

The univariate component functions are

$$\eta_i(X_i) = \int_{\mathbf{X}_{-i}} \eta(\mathbf{x}) f_{\mathbf{X}}(\mathbf{x}) \mathrm{d}\mathbf{x}_{-i} - \eta_0 \quad (1 \leqslant i \leqslant n) \tag{2.54}$$

where the notation $\mathbf{X}_{-i}$ means the integration over all variables except X_i. Furthermore, the bivariate component functions are defined as

$$\eta_{ij}(\mathbf{X}_{ij}) = \int_{\mathbf{X}_{-ij}} \eta(\mathbf{x}) f_{\mathbf{X}}(\mathbf{x}) \mathrm{d}\mathbf{x}_{-ij} - \eta_i(X_i) - \eta_j(X_j) - \eta_0 \quad (1 \leqslant i < j \leqslant n) \tag{2.55}$$

Here again, $\mathbf{X}_{-ij}$ is the integration over all variables except X_i and X_j.

More generally, we use the symbol "$\mathbf{X}_{-\{\cdot\}}$" denotes "the complementary vector of $\{\cdot\}$" in the study. Following this construction, any member function $\eta_{i_1 i_2 \cdots i_s}(X_{i_1}, X_{i_2}, \cdots, X_{i_s})$ can be expressed by using a serial summation of s-dimensional integrations and lower.

It is interesting to see that an integration over the member function is zero:

$$\int_{\mathbf{X}_s} \eta_{i_1 i_2 \cdots i_s}(x_{i_1}, x_{i_2}, \cdots, x_{i_s}) f_{\mathbf{X}_s}(\mathbf{x}_s) \mathrm{d}\mathbf{x}_s = 0 \tag{2.56}$$

where $\mathbf{X}_s = [X_{i_1}, X_{i_2}, \cdots, X_{i_s}]^{\mathrm{T}}$. This is:

$$E[\eta_{i_1 i_2 \cdots i_s}(X_{i_1}, X_{i_2}, \cdots, X_{i_s})] = 0 \quad \{i_1, i_2, \cdots, i_s\} \subseteq \{1, 2, \cdots, n\} \tag{2.57}$$

Total variance of model output, $Y = \eta(\mathbf{X})$, is defined as

$$V_{\mathrm{Tol}} = \int_{\mathbf{X}} [\eta(\mathbf{x})]^2 f_{\mathbf{X}}(\mathbf{x}) \mathrm{d}\mathbf{x} - \eta_0^2 \tag{2.58}$$

A generic expression of the variance component due to the joint effect of s variables is given as

$$V_{i_1 i_2 \cdots i_s} = \int_{\mathbf{X}_{i_1 i_2 \cdots i_s}} [\eta_{i_1 i_2 \cdots i_s}(x_{i_1}, x_{i_2}, \cdots, x_{i_s})]^2 f_{\mathbf{X}_s}(\mathbf{x}_s) \mathrm{d}\mathbf{x}_s \tag{2.59}$$

By numerical methods to evaluate the integration, it is possible to decompose the total output variance as a series component variances:

$$V_{\mathrm{Tol}} = \sum_{i=1}^{n} V_i + \sum_{1 \leqslant i < j \leqslant n} V_{ij} + \cdots + V_{12 \cdots n} \tag{2.60}$$

The decomposition is referred to as the general ANOVA in global sensitivity analysis, since the model function, $Y = \eta(\mathbf{X})$, is no long limited to a linear model as in the methods of regression or design of experiment.

Based on the general ANOVA, the Sobol' sensitivity index for global sensitivity analysis can be defined as

$$S_{i_1 i_2 \cdots i_s} = V_{i_1 i_2 \cdots i_s} / V_{\text{Tol}} \tag{2.61}$$

And from Eq.(2.60), one can see that:

$$\sum_{i=1}^{n} S_i + \sum_{1 \leqslant i < j \leqslant n} S_{ij} + \cdots + S_{12 \cdots n} = 1 \tag{2.62}$$

Therefore, each index $S_{i_1 i_2 \cdots i_s}$ is a sensitivity measure describing the amount of the total variance that is contributed by the uncertainties contained in a subset of input variables $\{i_1, i_2, \cdots, i_s\}$. The first order index S_i give the influence of each variable taken along, whereas the higher orders indices account for possible mixed influence of various parameters.

2.4.4 Monte Carlo Simulation

Since the variance-based global sensitivity index reviewed in the last section are given as an n-dimensional integration, the method of Monte Carlo simulation is usually employed to estimate the Sobol' index.

To estimate the component variance, one can use the following two-layer simulation method (Ishigami and Homma, 1990; Saltelli and Sobol', 1995). Taken the variance computation of a univariate member function, $\eta_k(X_k)$, as an example, the Monte Carlo simulation can be conducted as

$$\widehat{V}_k = \frac{1}{N} \sum_{i=1}^{N} \left[\eta\left(\mathbf{x}^{(i)}\right) \cdot \eta\left(\mathbf{x}_{-k}^{(i)}\right) \right] - \widehat{\eta}_0^2 \tag{2.63}$$

where $\mathbf{x}_{-k}^{(i)}$ implies all the samples of $\mathbf{X}$ is re-simulated except random variable X_k. Therefore, in an i^{th} round simulation, all random variables are sampled to evaluate $\eta\left(\mathbf{x}^{(i)}\right)$ at first, and then, re-sample $\mathbf{X}$ except X_k to calculate $\eta\left(\mathbf{x}_{-k}^{(i)}\right)$.

The variances of higher orders of member functions can be estimated in a similar manner. Through the methodology, one additional set of sample (with size of N) is needed to compute each $S_{i_1 i_2 \cdots i_s}$ (or $V_{i_1 i_2 \cdots i_s}$) in Eq.(2.62). Given that $2^n - 1$ member functions contained in Eq.(2.52), one should note that it needs $N(2^n - 1)$ model evaluations to compute the variance components in global sensitivity analysis.

The Sobol' index is known to be a good description of the importance of a model output with respect to input variables, since it does not suppose any kind of linearity or monotonicity in the

mechanistic model as compared to the regression method and design of experiment. However, full description of the sensitivity index requires to evaluate $2^n - 1$ n-dimensional integrals, which are not practically feasible unless the dimensionality of $\mathbf{X}$ is low (say $n \leqslant 5$). Therefore, an efficient method for Sobol' sensitivity index computation will be of greatly important.

Chapter 3

Fractional Moment and MaxEnt Distribution

3.1 Introduction

Probability distribution provides the full information contained in a random variable. Given the distribution, e.g., in terms of PDF or CDF, it is easy to calculate the moment, the reliability (i.e., a probability of the random variable exceeding a predefined limit) represented by the random variable. Therefore, method for probability distribution estimation plays the center role in risk analysis of engineering systems. Recently, special attention has been paid on the method of a design quantile estimation corresponding to a small probability of exceedance (POE) (Deng and Pandey, 2008, 2009; Pandey, 2000; Pandey et al., 2001). Such quantile represents a design threshold of load or material property specified in a design code. It is desirable that the estimate be unbiased, i.e., its expected value is equal to the true mean-value. Furthermore, a method should ideally be efficient, i.e., variance of the corresponding estimates is as small as possible. However, the requirements on the accuracy and efficiency are often problematic due to the lack of adequate data.

The key procedure in distribution estimation is fitting an analytical expression to adequately represent the sampled observations. To achieve this, a prior distribution is judged empirically from the available information using the probability paper plot. Then, distribution parameters can suitably estimated with a statistical technique, such as the maximum likelihood, the method of least square, and the method of moment, etc. However, the bias and variation of the estimate

remain sensitive to the assumed prior distribution.

An alternative approach to reconstruct the unknown distribution originates from the modern information theory, the principle of maximum entropy (MaxEnt), has been developed. Jaynes (1957) presented MaxEnt as a rational approach to choose the most unbiased probability distribution amongst all possible candidates. The determined distribution will be consistent with available data and contains minimum spurious information. When only moment constraints are specified, Shore and Johnson (1980) proved that the MaxEnt is a uniquely correct method of probabilistic inference that satisfies all consistency axioms. More information on MaxEnt, one can refer to literature (Kapur and Kesavan, 1992) for details.

Despite the conceptual elegance, practical difficulties with the MaxEnt approach began to emerge. The first issue is that a relatively large number of integer moments (order $\geqslant 4$) are required to achieve a reasonable accuracy in the modeling of the distribution tail. If moments are analytically calculated, such as in random vibration literature (Pandey and Ariaratnam, 1996; Sobezyk and Trebicki, 1990), it is not a major issue. However, the entropy maximization algorithm experiences numerical instability as the number of moment constraints become large (Tagliani, 1994, 1999). Another thorny issue is that the tail of MaxEnt distribution becomes an oscillatory function due to non-monotonic nature of the polynomial embedded in the density function. Instead of a calculation procedure, if sample data are used to estimate the higher moments for MaxEnt analysis, then it poses an additional problem. The sample moment estimates are known to have large statistical error (i.e., bias and standard error), which would creep into the MaxEnt procedure as well. Because of these practical limitations, the interest in engineering application of MaxEnt diminished over time. And the difficulty in obtaining accurate quantile estimates from small samples has been the main impediment to the application of MaxEnt in risk analysis.

Recently, interest in MaxEnt has highlighted with the emergence of use of fractional moments, i.e., real numbers (or fractions) of moment order instead of integers (Inverardi et al., 2003; Novi Inverardi et al., 2005; Taufer et al., 2009). The reason for the interest is that the distribution of a positive random variable can be characterized by a finite number of fractional moments (Gzyl and Tagliani, 2010). In addition, a fractional moment embodies information about a large number of central moments as shown later. An optimal set of the fractions can be determined via the MaxEnt instead of assigning values a priori. The values of fractions determined are typically less than 2, which can be reliably estimated from a modest sample of data.

To sum up, shortcomings of the traditional MaxEnt method, as stated above, can be overcome by the use of fractional moments as constraints in place of the regular integer order moments.

The Chapter is presented to estimate a probability distribution with the fractional moment through the principle of maximum entropy (MaxEnt), which is essentially an extension of the commonly used integer moment-based MaxEnt. Given a small number of observations (e.g., $N = 100$), the proposed MaxEnt optimization with the constraints in terms of fractional moments (ME-FM) is employed to estimate the distribution function and quantile function corresponding to an array of small failure probabilities. The novelty of use fractional moment in the distribution estimation is highlighted by its ability to accurately extract the probabilistic information from a small number of samples. Therefore, with the fractional moments estimated from a small number of data of material property, live load or wave height, etc., a reliable estimate of the unknown parent distribution can be derived with the proposed method of ME-FM. To assess the accuracy and efficiency of the proposed method, Monte Carlo simulation will be used to calculate the bias and root mean square error (RMSE) of the estimates of quantile function.

The Chapter is organized as follows. Section 3.2 presents the motivations of using fractional moment in MaxEnt. Section 3.3 develops a general method to derive the MaxEnt distribution with the constraints specially in terms of fractional moment. A numerical procedure on the parameters of MaxEnt distribution is proposed. In Sections 3.4 to 3.6, examples of generalized Pareto, Weibull and Lognormal distributions are employed to illustrate the applications of the ME-FM in parent distribution estimation of a random variable. Experiment of Monte Carlo simulation is also conducted in each example to study the accuracy and efficiency of the proposed method. Section 3.7 summarizes the conclusions.

3.2 Fractional Moment

Statistical moment of a random variable usually refers to the *positive integer* moment:

$$E[X^k] = \int_X x^k f_X(x)\mathrm{d}x \tag{3.1}$$

where k is a positively defined integer. Given $k = 1$ and 2, one can calculate the mean-value of and variance of X.

Let X be a *positive* random variable. An α^{th} order fractional moment can be defined as

$$E[X^\alpha] = \int_X x^\alpha f_X(x)\mathrm{d}x \tag{3.2}$$

where α is a real number.

3.2.1 Existence of Fractional Moment

Fractional moment of a positive random variable, $E[X^\alpha]$, with negative valued fraction (i.e., $\alpha < 0$) is referred to as the inverse moment problem in literature (Chao and Strawderman, 1972; Cressie et al., 1981; Khuri and Casella, 2002). Piegorsch and Casella (1985) derived the sufficient condition for the existence of $E[X^\alpha]$ $(-1 \leqslant \alpha \leqslant 1)$ only if the continuous density $f_X(x)$ with the bounded value of $f_X(0)$. This is one of limited references considered the value of α should not be necessarily as a positive integer. To derive the condition of the existence of a fractional moments, one can examine the properties of function x^α at first.

Table 3.1: Property of x^α with varied definitions of x and α

Fraction α	Variable x	Property of Function x^α	
		Monotonicity	Domain
$\alpha > 0$	$x \in [0, 1]$	monotonic decrease	$[0,\ 1]$
	$x \in (1, +\infty)$	monotonic increase	$(1,\ +\infty)$
$\alpha < 0$	$x \in [0, 1)$	monotonic decrease	$(1,\ +\infty)$
	$x \in [1, +\infty)$	monotonic increase	$[0,\ 1]$

To study the integral of fractional moment, the characteristic of x^α is summarized in Table 3.1 with the varied possible combinations of x and α. Given the information, one can see that: (a) x^α is a positive monotonic function with respect to x; (b) Functions of x^α for the positively and negatively valued α are convertible. It is can be seen from the following example. Assumed that $\alpha < 0$, by defining a new variable $z = 1/x$, the negative-valued fractional moment can be transformed as a positive fractional moment as

$$z^\beta = \frac{1}{x^\beta} \equiv x^\alpha \tag{3.3}$$

Here $\beta > 0$ (i.e., $\beta = -\alpha$) and z^β should have the identical characteristics with a positive fractional moment.

Theorem 3.1. *Let $f_X(x)$ be a continuous density function defined on $[0, +\infty)$ and has the converged integer moments up to k^{th} $(k \geqslant 1)$ order. An α^{th} order fractional moment, $E[X^\alpha]$, is said to exist as long as $|\alpha| \leqslant k$.*

Proof. The necessary and sufficient condition for the existence of a k^{th} order integer moments is the convergence of the following integration:

$$\int_0^{\infty} \left|x^k\right| f_X(x)\mathrm{d}x = \int_0^{\infty} x^k f_X(x)\mathrm{d}x < +\infty \tag{3.4}$$

This implies

$$\int_0^{\infty} x^k f_X(x)\mathrm{d}x = \int_0^{1} x^k f_X(x)\mathrm{d}x + \int_1^{\infty} x^k f_X(x)\mathrm{d}x < +\infty \tag{3.5}$$

Define a constant $c = c_1 + c_2$, where c_1 and c_2 are the upper boundaries of

$$c_1 = \max\left\{\int_0^{\tau} x^k f_X(x)\mathrm{d}x : 0 < \tau \leqslant 1\right\} \quad \text{and} \quad c_2 = \max\left\{\int_1^{\tau} x^k f_X(x)\mathrm{d}x : 1 < \tau < +\infty\right\}$$

Given the moment integration in Eq.(3.5), one should note that $E[x^k] \in [0, c]$, where $0 < c < +\infty$.

Fractional moment, $E[X^\alpha]$, can be expressed as

$$E[X^\alpha] = \int_0^{\infty} x^\alpha f_X(x)\mathrm{d}x = \int_0^{1} x^\alpha f_X(x)\mathrm{d}x + \int_1^{\infty} x^\alpha f_X(x)\mathrm{d}x \tag{3.6}$$

Given $0 < \alpha \leqslant k$ and the properties of x^α in Table 3.1, the integrations in the RHS of Eq.(3.6) with the boundaries of

$$0 < \int_0^{1} x^\alpha f_X(x)\mathrm{d}x \leqslant \int_0^{1} x^0 f_X(x)\mathrm{d}x \leqslant 1$$

and

$$0 < \int_1^{\infty} x^\alpha f_X(x)\mathrm{d}x \leqslant \int_1^{\infty} x^k f_X(x)\mathrm{d}x \leqslant c$$

The two inequalities lead to the moment integration in Eq.(3.6) is bounded as $0 < E[X^\alpha] \leqslant c + \varepsilon$, where ε is a small positive quantity. And thus, the α^{th} order fractional moment should exist.

Considering that if the fractional exponent $\alpha < 0$, one can use Eq.(3.3) to equivalently evaluate the fractional moment with a positivity valued fractional exponent. Therefore, the final conclusion for the existence of the real valued fractional moment can be summarized as: The fractional moment integration $E[X^\alpha] = \int_0^{\infty} x^\alpha f_X(x)\mathrm{d}x$ is said to be converged only if it exists a k^{th} order integer moment and the fractional exponent $|\alpha| \leqslant k$. □

3.2.2 Need of Fractional Moment

Recovering the parent distribution, $f_X(x)$, from a finite number of integer moments has been documented extensively in literature. For example, Pearson and Johnson system (Johnson, 1949; Pearson, 1963) or generalized Lambda distribution (Ramberg et al., 1979) have been used. Since the inverse problem of deriving the distribution of a random variable from an array of moments has no unique solution, researchers have resorted to heuristics to assume a parametric distribution as a prior. The assumption of the distribution type is a rather contentious one from both philosophical and practical points of view. The reasons are that the tail probabilities tend to be highly sensitive to a parametric form, and assigning a parametric prior implies adding spurious information to the inference.

The motivation of using fractional moment was inspired by the relationship between fractional moment and integer moment (Gzyl and Tagliani, 2010). The fractional moment of a positively defined random variable can been expressed as the weighted summation of all integer moments as shown below.

At first, consider the Taylor series expansion of x^α around a real constant c:

$$x^\alpha = \sum_{i=0}^{\infty} \binom{\alpha}{i} c^{\alpha-i} (x-c)^i \tag{3.7}$$

One should note that the fractional binomial coefficient, $\binom{\alpha}{i}$, is defined as shown in literature (Graham et al., 1988)

$$\binom{\alpha}{i} = \frac{\alpha(\alpha-1)\cdots(\alpha-i+1)}{i(i-1)\cdots 1} \tag{3.8}$$

in which, the upper index, α, emphasizes the fact that the binomial coefficient makes sense when any real number appears in this position. For instance, we have $\binom{-0.5}{3} = (-0.5)(-1.5)(-2.5)/3! = -0.3125$.

Properly choose c to guarantee the series convergence absolutely (say $c = \mu_X$ in literature), and assume that random variable has all orders of integer moment. Taking expectation on both sides of Eq.(3.7), one can obtain the desired relationship between fractional and the centered moments as

$$E[X^\alpha] = \sum_{k=0}^{\infty} \binom{\alpha}{i} c^{\alpha-i} E\left[(X-c)^k\right] \tag{3.9}$$

where $E\left[(X-c)^k\right]$ is a k^{th} centered moment of X with respect to the constant c. Its value can

be determined with the integer moments as

$$E[(X-c)^k] = \sum_{j=0}^{k} (-1)^{k-j} \binom{k}{j} c^{k-j} E\left[X^j\right] \quad (j = 1, 2, \cdots) \tag{3.10}$$

Given all orders of integer moments of X, and the expansion point c, one can see that an α^{th} order fractional moment can be expressed by using a large number of integer moments. Gzyl and Tagliani (2010) has shown that the required number of integer moments in Eq.(3.9) should be 30 or more to guarantee an accurate estimate of a fractional moment. It is fairly difficult even unpractical to provide so many high-order integer moments of an output represented by a complicated input-output relation.

3.2.3 Fractional Moment of a Random Variable

As defined in previous section, an α^{th} fractional moment of X needs to evaluate the integration:

$$E[X^\alpha] = \int_X x^\alpha f_X(x) \mathrm{d}x \tag{3.11}$$

Given the probability distribution of X, an analytic expression of $E[X^\alpha]$ can be derived. Taken the Lognormal distribution as an example, its PDF is given as

$$f_X(x) = \frac{1}{\sqrt{2\pi}\,\zeta\, x} \exp\left[-\frac{(\log x - \theta)^2}{2\zeta^2}\right] \tag{3.12}$$

where θ (> 0) and ζ (> 0) are the location and scale parameters, respectively. Substituting the PDF into Eq.(3.11), one can determine the analytic expression of an α^{th} fractional moment as

$$E[X^\alpha] = \exp\left[\alpha(2\theta + \alpha\zeta^2)/2\right] \tag{3.13}$$

Therefore, given the distribution of Weibull, Gamma, Chi-Square and Beta random variables, the corresponding expressions of an α^{th} order fractional moments are summarized in Table 3.2.

The low orders of fractional moment (e.g., $|\alpha| \leqslant 2$) can be estimated from experimental data, $\{x_1, x_1, ..., x_N\}$:

$$\widehat{M}_X^\alpha = \frac{1}{N} \sum_{i=1}^{N} x_k^\alpha \tag{3.14}$$

which the estimate is unbiased since $E\left[\widehat{M}_X^\alpha\right] = E[X^\alpha]$. The simulation-based fractional moments will be employed in numerical sections to study the efficiency of the proposed method in estimation of a parent distribution.

Table 3.2: Analytic expressions of fractional moment of various distribution

Distribution	Probability density function	Parameters	Fractional moment
Weibull	$f_X(x) = \frac{\delta}{\theta}(x/\theta)^{\delta-1}\exp\left[-(x/\theta)^{\delta}\right]$	$\delta > 0, \theta > 0$	$\theta^{\alpha}\lvert\Gamma(1+\alpha/\delta)\rvert$
Lognormal	$f_X(x) = \frac{1}{\sqrt{2\pi}\,x\zeta}\exp\left[-\frac{(\log x-\theta)^2}{2\zeta^2}\right]$	$\zeta > 0, \theta > 0$	$\exp\left[\alpha(2\theta+\alpha\zeta^2)/2\right]$
Gamma	$f_X(x) = \frac{1}{\theta^{\delta}\Gamma(\delta)}x^{\delta-1}\exp(-x/\theta)$	$\delta > 0, \theta > 0$	$\theta^{\alpha}\lvert\Gamma(\alpha+\delta)\rvert/\Gamma(\delta)$
Chi-Square	$f_X(x) = x^{\theta/2-1}\exp(-\frac{x}{2})/2^{\frac{\theta}{2}}/\Gamma(\frac{\theta}{2})$	$\theta > 0$	$2^{\alpha}\lvert\Gamma(\alpha+\theta/2)\rvert/\Gamma(\theta/2)$
Beta	$f_X(x) = \frac{1}{\mathrm{B}(\theta,\delta)}x^{\theta-1}(1-x)^{\delta-1}$	$\delta > 0, \theta > 0$	$\frac{\Gamma(\delta)\lvert\Gamma(\alpha+\theta)\rvert}{\mathrm{B}(\delta,\theta)\lvert\Gamma(\alpha+\theta+\delta)\rvert}$

where $\Gamma(z) = \int_0^{\infty}\exp(-t)t^{z-1}\mathrm{d}t$, and $B(a,b) = \int_0^1 t^{a-1}(1-t)^{b-1}\mathrm{d}t$.

3.3 Entropy-Based Probability Distribution

3.3.1 General

Consider a event, which can take one of the different states, $\{X_1, X_2, \cdots, X_k\}$ with the respective probability $\{p_1, p_2, \cdots, p_k\}$ under the constraints of $p_i > 0$ and $\sum_{i=1}^{k} p_i = 1$. The self-information of event X_i is defined as

$$\mathcal{S}(X_i) = \log\left(\frac{1}{p_i}\right) = -\log(p_i) \tag{3.15}$$

The use of a logarithmic measure for information is intuitive in following sense: the information provided by a deterministic event (i.e., $p_i = 1$) is zero, and the rarer of an event (i.e., $p_i \ll 1$), the more information is conveyed by the realization. Therefore, it is clear from Eq.(3.15) that the self-information of an event increases as the associated uncertainty grows, i.e., the probability of occurrence reduces. In this respect, the quantity $\mathcal{S}(\cdot)$ is regarded as a measure of uncertainty (Jones, 1979).

Shannon (1949) defined a measure of uncertainty, referred to as entropy, similar to that used in thermodynamics and statistical mechanics. Considering the definition of self-information from Eq.(3.15), Shannon's entropy can be expressed as mathematical expectation of the self-information:

$$\mathcal{H}[X] = -\sum_{i=1}^{k} p_i \log(p_i) \tag{3.16}$$

The entropy vanishes for completely certain outcome, and is maximum when all outcomes are equiv-probable. The axiomatic characterization of entropy and its other mathematical properties

can be found in literature (Kapur and Kesavan, 1992).

Jaynes (1957) presented the principle of maximum entropy (MaxEnt) as a rational approach for choosing a consistent probability distribution amongst all possible distributions that contains minimum spurious information. The principle states that the probability distribution of a random variate can be obtained by maximizing the entropy subjected to constraints supplied by the available information, e.g., moments of a random variable. The distribution so obtained is referred to as the most unbiased, because its derivation involves a systematic maximization of uncertainty about the unknown information.

3.3.2 MaxEnt with Fractional Moment

Let X denote a continuous positive random variate with the density function $f_X(x)$, its entropy can be given as

$$\mathcal{H}\big[f\big] = -\int_X f_X(x)\log\big[f_X(x)\big]\mathrm{d}x \tag{3.17}$$

Then, a MaxEnt optimization procedure will apply the constrains in terms of integer moments as shown in literature (Ramírez and Carta, 2006). This implies some moments (e.g., the first-four or first-six) should be accurately determined to identify the parent distribution. It is well known that the estimation error is increasing with the order of moment. To overcome the shortcoming of the integer moments, a general entropy method with the constrains specially in terms of fractional moments (ME-FM) has been proposed to estimate the parent distribution.

The Lagrangian function associated with the MaxEnt problem is given as

$$\begin{aligned}\mathcal{L}\big[\boldsymbol{\lambda},\boldsymbol{\alpha};\, f_X(x)\big] = &-\int_X f_X(x)\log\big[f_X(x)\big]\mathrm{d}x - (\lambda_0-1)\bigg[\int_X f_X(x)\mathrm{d}x - 1\bigg] \\ &-\sum_{i=1}^{m}\lambda_i\bigg[\int_X x^{\alpha_i} f_X(x)\mathrm{d}x - M_X^{\alpha_i}\bigg]\end{aligned} \tag{3.18}$$

where $\boldsymbol{\lambda} = [\lambda_0,\lambda_1,\cdots,\lambda_m]^{\mathrm{T}}$ are the Lagrange multipliers and $\boldsymbol{\alpha} = [\alpha_1,\alpha_2,\cdots,\alpha_m]^{\mathrm{T}}$ are the fractional exponents.

A key condition for optimal solution is

$$\frac{\partial\mathcal{L}\big[\boldsymbol{\lambda},\boldsymbol{\alpha};\, f_X(x)\big]}{\partial f_X(x)} = 0 \tag{3.19}$$

which leads to the following estimate, $\widehat{f_X}(x)$, of the true PDF

$$\widehat{f_X}(x) = \exp\bigg(-\sum_{i=0}^{m}\lambda_i x^{\alpha_i}\bigg) \quad (\alpha_0 = 0) \tag{3.20}$$

Note that

$$\lambda_0 = \log\left[\int_X \exp\left(-\sum_{i=1}^{m}\lambda_i x^{\alpha_i}\right)\mathrm{d}x\right] \tag{3.21}$$

It is derived from the normalization condition that the PDF must integrate to one. An interesting point is that the fractions α_i $(i = 1, \cdots, m)$ need not be specified a priori, rather they can be determined as a part of the entropy maximization process (Inverardi and Tagliani, 2003).

3.3.3 Parameter Estimation Algorithm

To implement this idea of MaxEnt with fractional moment (ME-FM), an alternate formulation is developed based on the minimization of the Kullback-Leibler (K-L) divergence between the true PDF, $f_X(x)$, and its estimator, $\widehat{f_X}(x)$, given as

$$\begin{aligned}\mathcal{K}[f, \widehat{f}] &= \int_X f_X(x)\log\left[f_X(x)/\widehat{f_X}(x)\right]\mathrm{d}x \\ &= \int_X f_X(x)\log\left[f_X(x)\right]\mathrm{d}x - \int_X \log\left[\widehat{f_X}(x)\right]f_X(x)\mathrm{d}x\end{aligned} \tag{3.22}$$

Substituting for $\widehat{f}(y)$ from Eq.(3.20), the K-L divergence can be written in a compact form as

$$\mathcal{K}[f, \widehat{f}] = -\mathcal{H}[f] + \lambda_0 + \sum_{i=1}^{m}\lambda_i M_X^{\alpha_i} \tag{3.23}$$

where $\mathcal{H}[f]$ is the entropy of the true PDF $f_X(x)$ that is independent of $\boldsymbol{\lambda}$ and $\boldsymbol{\alpha}$. Therefore, minimization of the K-L divergence implies minimization of the following function

$$\mathcal{I}(\boldsymbol{\lambda}, \boldsymbol{\alpha}) = \mathcal{K}[f, \widehat{f}] + \mathcal{H}[f] = \lambda_0 + \sum_{i=1}^{m}\lambda_i M_X^{\alpha_i} \tag{3.24}$$

Therefore, parameters of the MaxEnt distribution can be obtained by

$$\begin{cases}\text{Find:} & \{\alpha_i\}_{i=1}^{m} \text{ and } \{\lambda_i\}_{i=1}^{m} \\ \text{Minimize:} & \mathcal{I}(\boldsymbol{\lambda}, \boldsymbol{\alpha}) = \log\left[\int_X \exp\left(-\sum_{i=1}^{m}\lambda_i x^{\alpha_i}\right)\mathrm{d}x\right] + \sum_{i=1}^{m}\lambda_i M_X^{\alpha_i}\end{cases} \tag{3.25}$$

This optimization is carried out in MATLAB© with the simplex search method (Lagarias et al., 1998), since it is a direct search method that does not use the gradient information.

3.4 Generalized Pareto Distribution

The example is developed to examine the accuracy of ME-FM in approximating the generalized Pareto distribution.

3.4.1 Parent Distribution

A random variable X distributed as the generalized Pareto distribution if its PDF is given as

$$f_X(x) = \frac{1}{\theta}\left(1 - \frac{\delta}{\theta}x\right)^{1/\delta - 1} \tag{3.26}$$

where θ and δ are the scale and shape parameters of the distribution, respectively. The variable X takes values in the range $0 \leqslant X < +\infty$ for $\delta < 0$ and $0 \leqslant X \leqslant \theta/\delta$ for $\delta > 0$. The special case of δ being zero yields the Exponential distribution. The distribution is a logical choice for modeling flood magnitude that exceed a fixed threshold when the successive floods follow a Poisson process and have independent magnitudes (Rao and Hamed, 2000).

An α^{th} order fractional moment of the distribution, then, is analytically determined as

$$\begin{cases} M_X^\alpha = \dfrac{\theta^\alpha \delta^{-(1+\alpha)}\Gamma(1/\delta)\Gamma(\alpha+1)}{\Gamma(1/\delta+\alpha+1)} & \delta > 0 \\ M_X^\alpha = \theta^\alpha \Gamma(\alpha+1) & \delta = 0 \\ M_X^\alpha = \dfrac{\theta^\alpha (-\delta)^{-(1+\alpha)}\Gamma(-1/\delta-\alpha)\Gamma(\alpha+1)}{\Gamma(-1/\delta+1)} & \delta < 0 \end{cases} \tag{3.27}$$

as well as the entropy:

$$\mathcal{H}[f] = 1 - \delta + \log(\theta) \tag{3.28}$$

If scale parameter $\theta = 1.0$, entropy of the Pareto distribution only depends on the shape parameter $\mathcal{H}[f] = 1 - \delta$.

3.4.2 MaxEnt Distribution

Since the Pareto distribution is known to have a long and heavy tail, it can not be reconstructed form a small number of integer moments. To illustrate this, the COV, skewness, kurtosis and entropy of Pareto distribution are reported in Table 3.4 for various values of shape parameter δ. In the present case of $\delta = -0.2$ and scale parameter $\theta = 1.0$, kurtosis and skewness of the

Table 3.3: Moments of the Pareto distribution: Scale parameter $\theta = 1.0$

Shape Parameter	Entropy	Moments of the Pareto Distribution		
δ	$\mathcal{H}[f]$	COV	Skewness	Kurtosis
0.2	0.8	0.85	1.18	4.20
0.1	0.9	0.91	1.52	5.78
-0.1	1.1	1.12	2.81	17.83
-0.2	1.2	1.29	4.65	73.80

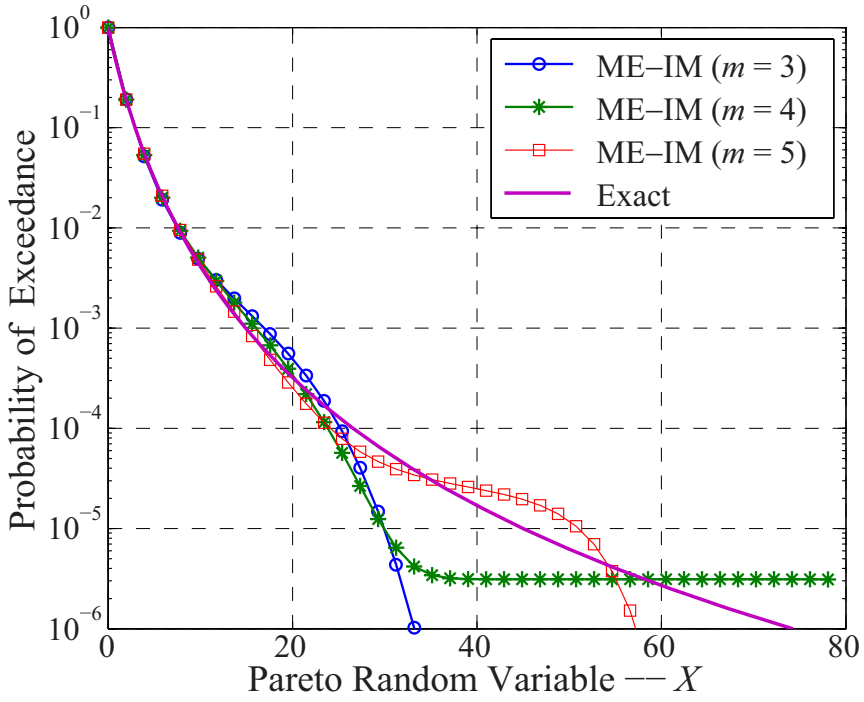

Figure 3.1: Approximation of the generalized Pareto distribution with ME-IM method. (ME-IM: Method of MaxEnt with integer moment; m: The number of integer moment used by the MaxEnt method; Parameters of the Pareto distribution: $\delta = -0.2$, $\theta = 1.0$, and its COV $= 1.29$.)

distribution are 73.80 and 4.65, respectively. The tail heaviness of the distribution is increasing with the decrease of shape parameter δ.

The semi-log plot of POE determined by using various orders of integer moment is presented in Figure 3.1. Although the general shape of the Pareto distribution is will approximated, the attention is focussed on the distribution tail. The MaxEnt distribution obtained with integer moments is reasonable up to POE of 10^{-2}, and beyond this in the far tail region it underestimates

the exceeding probabilities (Pandey, 2000, 2001b; Pandey et al., 2001). To overcome the problem of MaxEnt with integer moment, the proposed method of ME-FM is employed to reconstruct the parent distribution.

Table 3.4: MaxEnt PDF of the generalized Pareto distribution: Scale parameter $\theta = 1.0$

Shape Parameter	$\mathcal{K}[f, \widehat{f}]$	k	0	1	2	3
$\delta = 0.2$	1.03×10^{-6}	λ_k	-1.9673	2.0350	0.8252	0.0023
		α_k	$--$	0.0072	1.1992	4.9025
		$M_X^{\alpha_k}$	$--$	0.9952	0.8682	11.294
$\delta = 0.1$	4.55×10^{-6}	λ_k	0.0066	0.9572	0.2177	-0.2313
		α_k	$--$	1.0576	2.4380	2.3412
		$M_X^{\alpha_k}$	$--$	0.9249	2.1172	1.9573
$\delta = -0.1$	-6.41×10^{-8}	λ_k	0.0025	1.1687	0.1435	-0.2658
		α_k	$--$	1.0299	1.9185	1.8004
		$M_X^{\alpha_k}$	$--$	1.1311	2.5215	2.2054
$\delta = -0.2$	-2.95×10^{-8}	λ_k	-0.0002	5.1283	1.9088	-5.9398
		α_k	$--$	1.2070	1.4603	1.3437
		$M_X^{\alpha_k}$	$--$	1.4967	1.9628	1.7210

Assumed that scale parameter $\theta = 1.0$, and various values of shape parameter are considered. The corresponding MaxEnt parameters, i.e., $\boldsymbol{\alpha}$ and $\boldsymbol{\lambda}$, are summarized in Table 3.4. Comparisons of the MaxEnt distribution with the exact parent distribution are depicted in Figure 3.2.

As expected, the determined distribution with the proposed ME-FM are fairly close to the benchmarks of the Pareto distribution. The tail heaviness, in the present notation, is inversely proportion to the shape parameter. For instance, a distribution with $\delta = -0.2$ has much heavier tail than that of $\delta = 0.2$. As shown in Figure 3.2, it is clear to see that the proposed ME-FM method can accurately model the heavy tail distribution with three-order of fractional moments. Therefore, this approach is robust to the shape parameter of the Pareto distribution.

3.5 Weibull Distribution

The example examines the performance of ME-FM by considering Weibull distribution. Scale parameter of the distribution is fixed as $\theta = 6.0$. If $\delta = 1$, the Weibull distribution denotes as

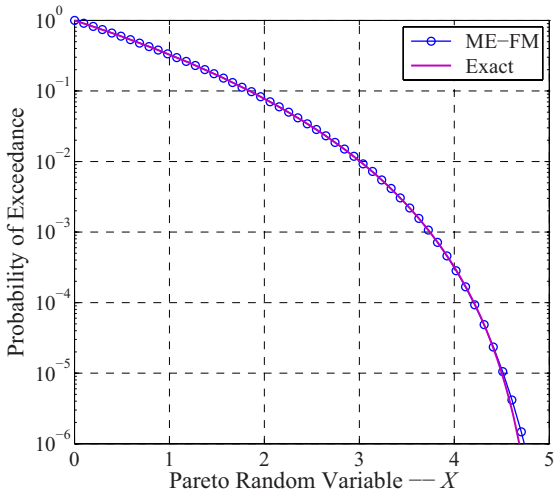

(a) The Generalized Pareto Distribution: $\delta = 0.2$

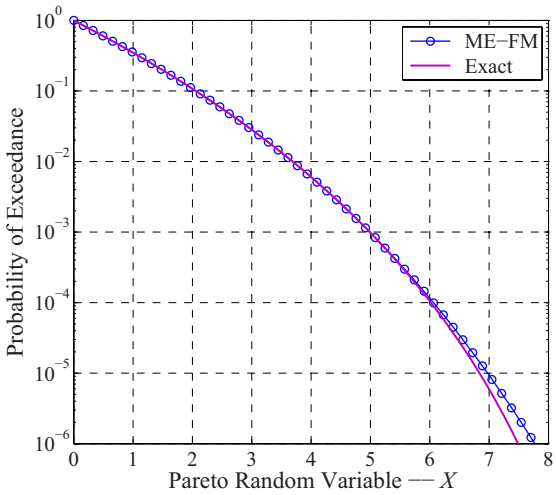

(b) The Generalized Pareto Distribution: $\delta = 0.1$

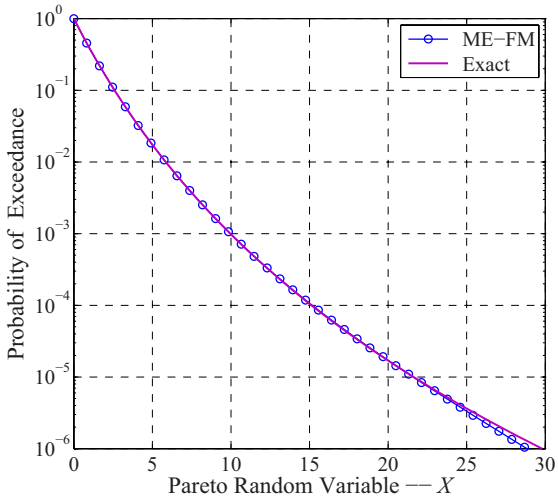

(c) The Generalized Pareto Distribution: $\delta = -0.1$

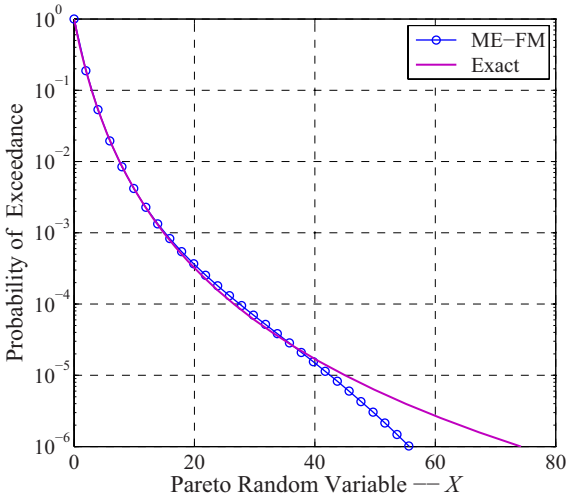

(d) The Generalized Pareto Distribution: $\delta = -0.2$

Figure 3.2: Approximation of the generalized Pareto distribution with ME-FM method (ME-FM: Method of MaxEnt with fractional moments; Scale parameter of the distribution: $\theta = 1.0$.)

the Exponential distribution, and $\delta = 2$, it is corresponding to the Rayleigh distribution.

An α^{th} order fractional moment of the Weibull distribution is given as

$$E[X^\alpha] = \theta^\alpha \left|\Gamma(1+\alpha/\delta)\right| \tag{3.29}$$

together with its entropy:

$$\mathcal{H}[f] = 1 + \gamma(1-1/\delta) + \log(\theta/\delta) \tag{3.30}$$

where γ is the Euler-Mascheroni constant.

3.5.1 MaxEnt Distribution

The Weibull distribution with various shape parameters are reconstructed by using the proposed method of ME-FM. Given one or two orders of fractional moment, parameters of the MaxEnt approximation, namely, the fractional exponents ($\boldsymbol{\alpha}$) and the Lagrange multipliers ($\boldsymbol{\lambda}$) are summarized in Table 3.5. The curves of probability of exceedance (POE) are depicted in Figures 3.3.

According to POE curves in Figure 3.3, one can see that Weibull distributions determined by ME-FM are highly accurate as compared to the analytic results. Especially for $\delta = 1$, in which the case is corresponding to the Exponential distribution, the proposed method of ME-FM with one order of fractional moment can be believed to reconstruct the parent distribution in the entire domain. For other values of shape parameter (i.e., $\delta > 1$), the accuracy of ME-FM with one fractional moment has been deteriorated in terms of tail estimation, i.e., POE $\leqslant 10^{-2}$. However, after using two-order of fractional moments (i.e., $m = 2$) as the constraints in MaxEnt formulation, the close agreement between ME-FM and benchmark result highlights the superiority of using fractional moment in parent distribution construction. In summary, probabilistic information contained in a Weibull variable can be exactly condensed by using two-order fractional moments.

With the determined fractional exponents of the MaxEnt densities, one should note that a Weibull distributed random variable can be accurately represented by using one fractional exponent approximately around its scale parameter, i.e., $\alpha_1 \approx \delta$, as well as a fraction around zero. Therefore, letting the scale parameters δ vary from 1 to 4, the optimized values of $\boldsymbol{\alpha}$ contain 1.0, 2.0016, 3.0133 and 4.0072, respectively. The fractional exponent, which is closed to the corresponding shape parameter, is referred to as the characteristic fraction of the distribution.

Can we represent a Weibull distribution only by using the characteristic fractional exponent? Or alternatively, what is the role of the small fraction as representing the parent distribution? To answer the question, one can recall that a general expression of a MaxEnt PDF associated with two fractional moments is:

$$\widehat{f_X}(x) = \exp\left(-\lambda_0 - \lambda_1 x^{\alpha_1} - \lambda_2 x^{\alpha_2}\right)$$

Take the Rayleigh distribution (i.e., $\delta = 2.0$) as an example, substituted for the optimized $\boldsymbol{\lambda}$

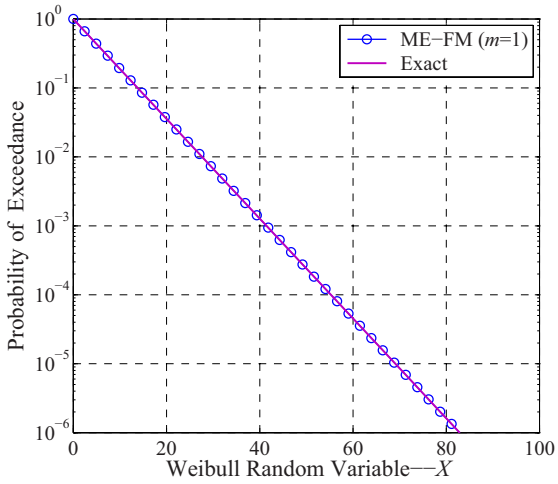

(a) Exponential Distribution: $\delta = 1.0$

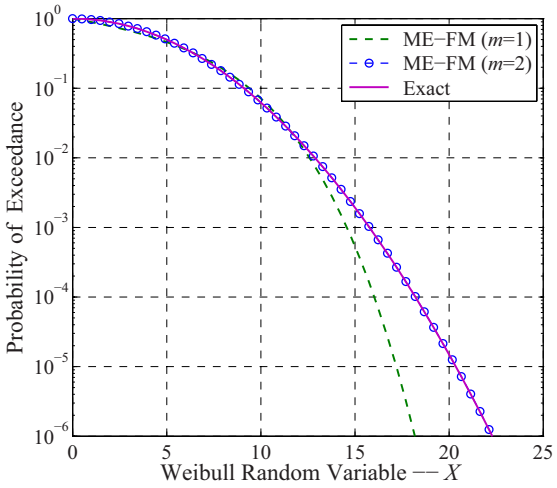

(b) Rayleigh Distribution: $\delta = 2.0$

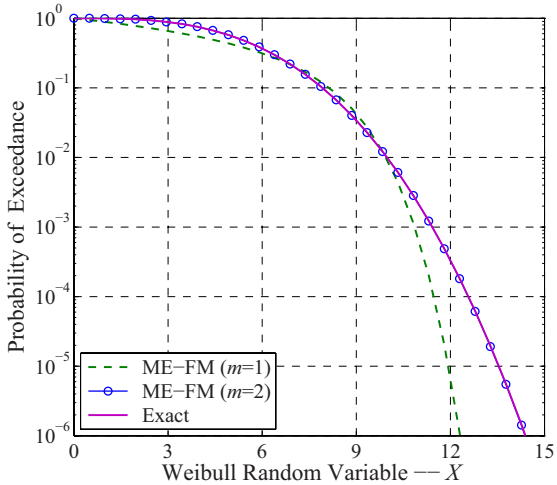

(c) Weibull Distribution: $\delta = 3.0$

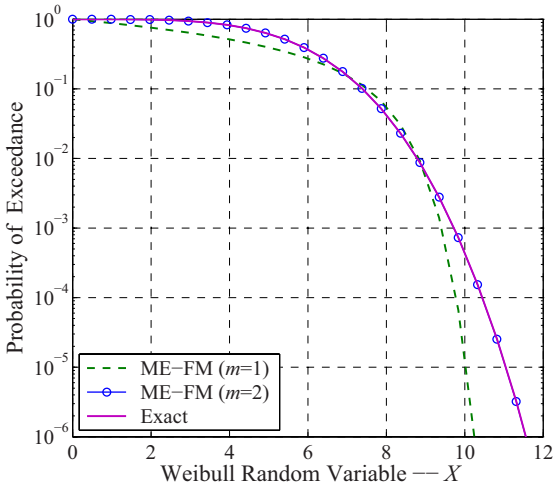

(d) Weibull Distribution: $\delta = 4.0$

Figure 3.3: MaxEnt approximation of the Weibull distribution with various shape parameters: Scale parameter $\theta = 6.0$

and $\boldsymbol{\alpha}$, one can realized the MaxEnt density as

$$\widehat{f}_X(x) = \exp\left(701.91 - 704.80\, x^{-1.4188\times10^{-3}} - 0.0276\, x^{2.0016}\right)$$

The corresponding limit of $x \to 0^+$ (since X is a positive random variable) can determine the value of $f_X(0)$ as

$$\lim_{x\to 0^+} \widehat{f}_X(x) = 0 \tag{3.31}$$

Table 3.5: MaxEnt approximation of Weibull distribution

Distribution	No. of FMs	$\mathcal{K}[f, \widehat{f}]$	k	0	1	2
Exponential	$m = 1$	3.7×10^{-10}	λ_k	1.7918	0.1667	––
($\delta = 1.0$)			α_k	––	1.0	––
			$M_X^{\alpha_k}$	––	6.0	––
Rayleigh	$m = 1$	7.6×10^{-2}	λ_k	2.2151	8.9671×10^{-5}	––
($\delta = 2.0$)			α_k	––	4.0291	––
			$M_X^{\alpha_k}$	––	2767.8	––
	$m = 2$	4.4×10^{-9}	λ_k	−701.91	704.80	0.0276
			α_k	––	-1.4188×10^{-3}	2.0016
			$M_X^{\alpha_k}$	––	0.9979	36.114
Weibull	$m = 1$	2.1×10^{-1}	λ_k	2.1649	1.9660×10^{-8}	––
($\delta = 3.0$)			α_k	––	7.9747	––
			$M_X^{\alpha_k}$	––	6.3783×10^{6}	––
	$m = 2$	4.2×10^{-7}	λ_k	−229.67	233.95	4.4652×10^{-3}
			α_k	––	-8.5894×10^{-3}	3.0133
			$M_X^{\alpha_k}$	––	0.9864	221.64
Weibull	$m = 1$	3.5×10^{-1}	λ_k	2.1083	2.5018×10^{-12}	––
($\delta = 4.0$)			α_k	––	12.427	––
			$M_X^{\alpha_k}$	––	3.2164×10^{10}	––
	$m = 2$	6.9×10^{-8}	λ_k	−722.01	727.79	7.5797×10^{-4}
			α_k	––	-4.1369×10^{-3}	4.0072
			$M_X^{\alpha_k}$	––	0.9932	1313.8

which is due primarily to the small negative-valued fractional exponent $\alpha_1 = -1.4188 \times 10^{-3}$. Together with other two conditions:

$$\lim_{x \to +\infty} \widehat{f}_X(x) = 0 \quad \text{and} \quad \int_X \widehat{f}_X(x) \mathrm{d}x = 1 \tag{3.32}$$

the three expressions are the nominal conditions for a valid MaxEnt density. In addition, Piegorsch and Casella (1985) proved that the bounded value of $f_X(0)$ is the sufficient condition to guarantee the existence of fractional moment of a positive random variable.

In a summary, the small-valued fractional exponent guarantees a close form of a MaxEnt distribution at its LHS tial, i.e., $f_X(0) = 0$. However, a special case can be seen for the Exponential distribution, which $f_X(0) > 0$. Therefore, only one order of fractional moment can precisely

represent the special case of Weibull distribution.

Accuracy of the proposed method on a parent distribution estimation can also be checked by using the Kullback-Leibler divergence as defined in Eq.(3.22). The small values of K-L divergences (i.e., $\mathcal{K}[f, \widehat{f}] \leqslant 10^{-7}$) in Table 3.5 are further validated the proposed ME-FM method in estimation of a parent distribution.

3.5.2 Experiment on Quantile Estimation

Quantile function (QF) of a random variable can be defined as the inverse function of CDF:

$$x(\text{POE}) = F_X^{-1}\big(1 - \text{POE}\big) \tag{3.33}$$

where $F_X^{-1}(x)$ is the inverse CDF of X; and POE is shorted for the probability of exceedance.

The section is designed to estimate QF of Weibull distribution from a small number of samples, since that in engineering reality, one can only collect a small number of observations (e.g., strength property of concrete) of a quantity to be employed for a qantile estimate corresponding to a small failure probability (e.g., POE $\leqslant 10^{-3}$).

In order to quantify that how well an estimate of QF, i.e., $\widehat{X}(\text{POE})$, can approximate its exact counterpart, $X(\text{POE})$, the statistical errors of bias and root mean square error (RMSE) are employed to examine the accuracy and efficiency through a simulation experiment (Pandey, 2001a):

$$\begin{cases} \text{Normalized Bias} = \dfrac{E[\widehat{X} - x]}{x} = \dfrac{1}{N}\displaystyle\sum_{k=1}^{N}\left(\frac{\widehat{x}_k}{x} - 1\right) \\ \text{Normalized RMSE} = \dfrac{1}{x}\sqrt{E[(\widehat{X} - x)^2]} \end{cases} \tag{3.34}$$

The procedure of the Monte Carlo experiment is briefly described as follows. A set of random numbers with size N is simulated from a known distribution, e.g., the Weibull distribution, with preselected parameters. From the sample, fractional moments of order m are estimated and ME-FM can determine an approximate of the parent distribution. The interested quantile value, then, can be computed form the MaxEnt and benchmark distributions, respectively. The simulation is repeated 100 cycles to estimate the corresponding bias and RMSE.

Consider an estimation of quantile with distribution parameters $\theta = 6$ and $\delta = 3$. The sample size (N) in each round of experiment is varied from 20 to 100. MaxEnt with three-order fractional moments (ME-FM) is employed to approximate the parent distribution. Design quantiles corresponding POE $= 10^{-2}, 10^{-3}, 10^{-4}, 10^{-5}$ and 10^{-6} are estimated. The determined

normalized bias versus the sample size (N) are depicted in Figure 3.4, as well as the normalized RMSE in Figure 3.5. To check the performance of ME-FM, results provided by using integer moments (ME-IM) are also provided.

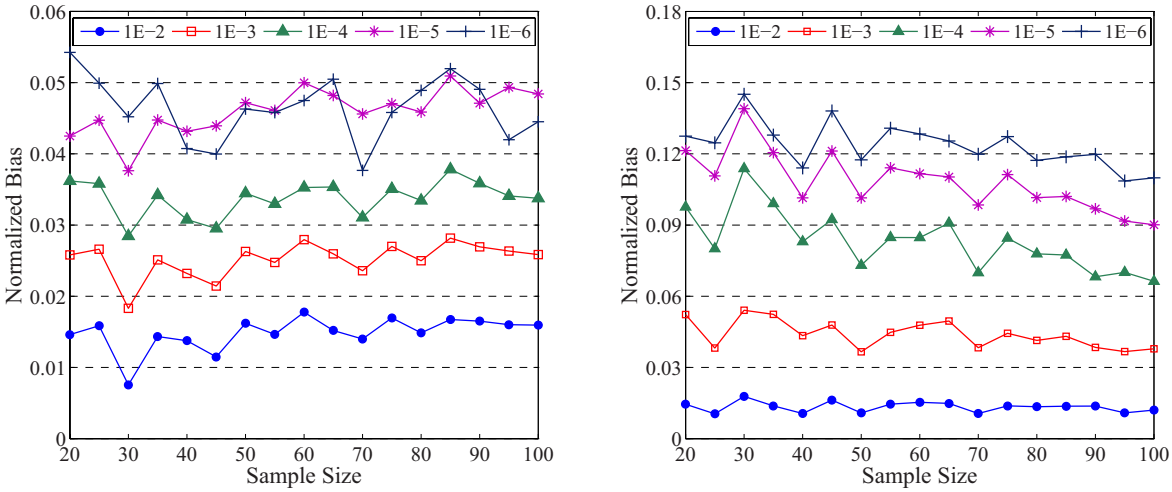

(a) MaxEnt with Three Fractional Moments

(b) MaxEnt with Three Integer Moments

Figure 3.4: Normalized bias of Weibull quantile function for the varied target POEs

Given the normalized bias in Figures 3.4, it is clear to see that ME-FM is far more accurate than ME-IM corresponding to the target failure probabilities. Taken POE $= 10^{-6}$ as an example, the largest bias of the quantile estimates is less than 6% by ME-FM, which is increased to 15% as employing ME-IM. Therefore, it has illustrated the superiority of using fractional moment to extract uncertainty information from a small number of samples.

Figures 3.5 reported the corresponding RMSEs provided by using the ME-FM and ME-IM, respectively. The plot is useful to study the efficiency of each method in the tail estimation. With plots in Figure 3.5, one can see that method of ME-FM is much more efficient than ME-IM. Even for a target POE $= 10^{-6}$, the ME-FM has very small REMS ($\leqslant$ 6%), whereas the REMS of ME-FM is double around 12%. Therefore, the method of ME-FM can be believed to accurately construct a quantile function in an efficient manner.

3.6 Lognormal Distribution

The section evaluates the accuracy of ME-FM for distribution approximation by considering the Lognormal example. One should note that Lognormal distribution cannot be totally characterized

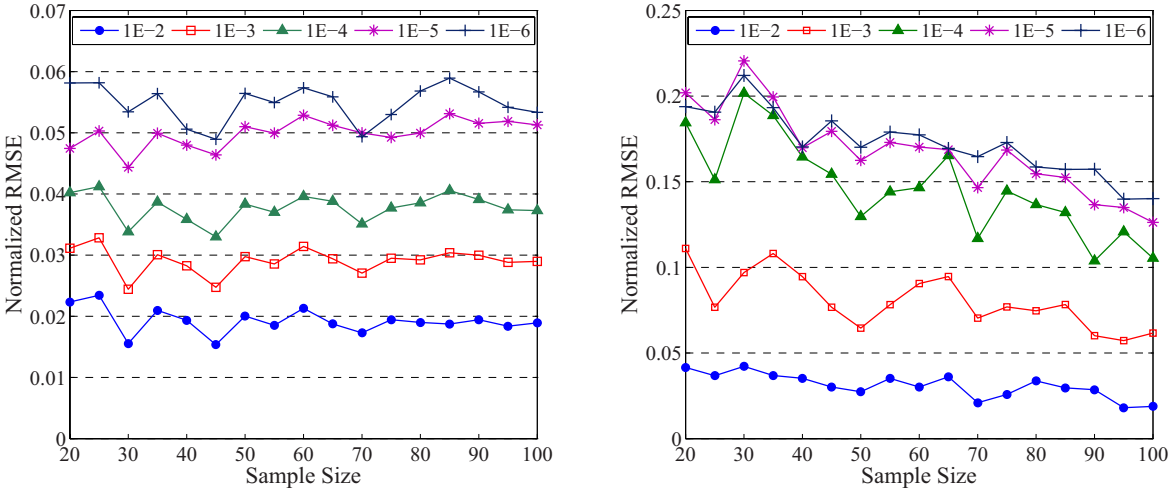

(a) MaxEnt with Three Fractional Moments

(b) MaxEnt with Three Integer Moments

Figure 3.5: Normalized RMSE of Weibull quantile function for the varied target POEs

by using integer moments (Heyde, 1963).

3.6.1 Fractional Moment

Assume that parameters of the Lognormal distribution are $\theta = 0$ and $\zeta = 1.0$, respectively. Using the analytical formula in Eq.(3.13) and a simulation method (e.g., $N = 10^5$ of samples), an α^{th} fractional moment, M_X^α and its estimate $\widehat{M}_X^\alpha$ can be calculated, respectively.

Figure 3.6 depicted the simulated moment of the Lognormal distribution given the fractions $-1 \leqslant \alpha \leqslant 1$. Compared with the benchmarks, it is clear to see the negative and positive fractional moments can be reliably estimated by using the simulation method.

To further study the simulation-based method in calculation of the fractional moments, a Monte Carlo experiment is conducted to estimate the corresponding bias and RMSE. In 100 cycles of the experiment, samples in size of 20 to 100 are simulated. Figure 3.7 reported the corresponding normalized bias and RMSE in the fractional moment calculation.

Given the plot of normalized bias in Figure 3.7(a), one can see that the fractional moment can be reliably estimated by using a small size of samples. The normalized bias is less than 2% as compared to the benchmarks. Furthermore, the RMSE decreases with the decreasing of the absolute value of fractional exponent as shown in Figure 3.7(b).

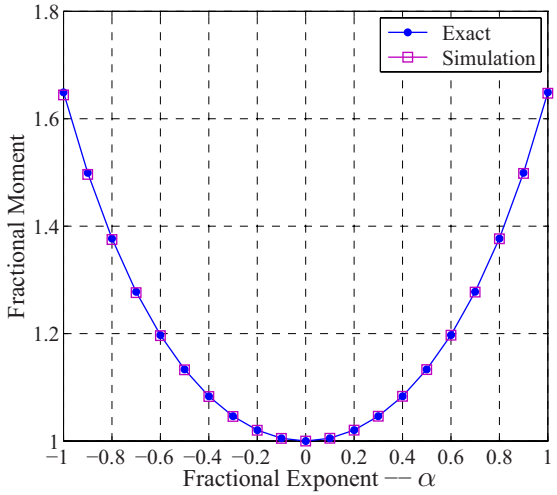

(a) Fractional Moment of Lognormal Variable

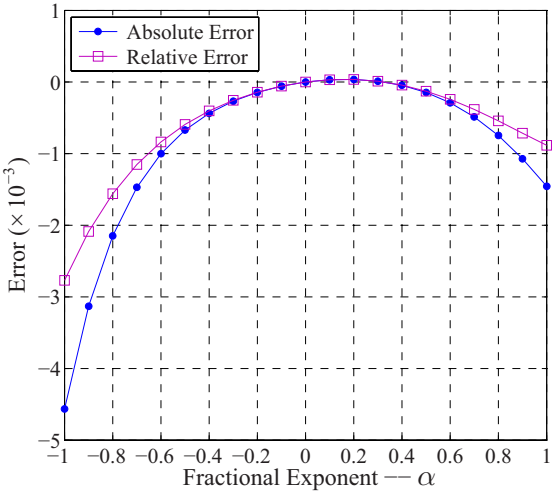

(b) Error of Fractional Moment Calculation

Figure 3.6: Analytical and simulation results of Lognormal fractional moments (Distribution paprameters are $\theta = 0$ and $\zeta = 1$; Exact Moment:= $\exp\left[\alpha(2\theta + \alpha\zeta^2)/2\right]$; Absolute Error:= Exact Moment − Moment by MCS; Relative Error:= (Exact Moment − Moment by MCS)/Exact Moment.)

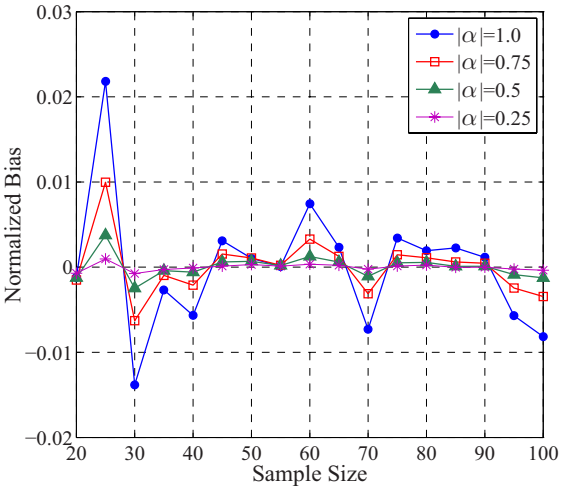

(a) Normalized Bias

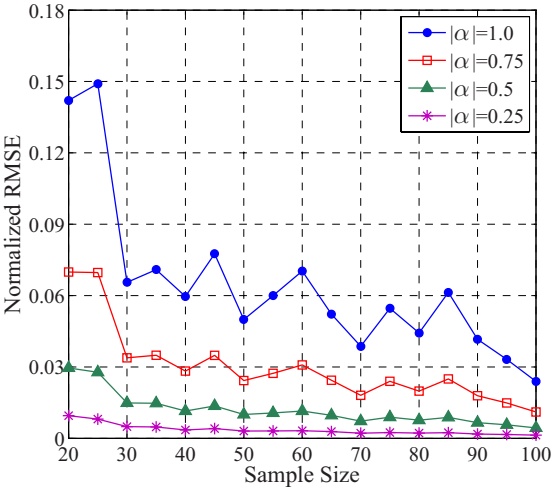

(b) Normalized RMSE

Figure 3.7: Normalized errors of fractional moment with simulation method

3.6.2 MaxEnt Distribution

Given parameters $\theta = 0$ and $\zeta = 1$, entropy of the Lognormal distribution is $\mathcal{H}[f] = 1/2 + \theta + 1/2\log(2\pi\zeta^2) = 1.4189$. Mean and standard deviation of the random variable are $\mu = 1.65$ and $\sigma = 2.16$, respectively, and thus the COV is 1.31. The distribution is highly skewed with a heavy tail, which leads to the problem in approximating its upper quantiles (e.g., POE $\leqslant 10^{-3}$) with integer moments as shown in literature (Heyde, 1963).

ME-FM with various orders of fractional moment (i.e., $m = 1, 2, 3$) is employed to approximate the heavy tail distribution. Comparing with the benchmark, results using the method of MaxEnt with integer moment (ME-IM) are also determined. The optimized parameters of MaxEnt distribution are summarized in Table 3.6. The curves of POE are depicted in Figure 3.8.

Table 3.6: MaxEnt estimates of the Lognormal distribution with ME-FM and ME-IM

Method	# of Moments	$\mathcal{K}[f, \widehat{f}]$	k	0	1	2	3
ME-FM	$m = 1$	7.56×10^{-2}	λ_k	0.3376	0.7963	––	––
			α_k	––	0.8644	––	––
			$M_X^{\alpha_k}$	––	1.4529	––	––
	$m = 2$	6.31×10^{-5}	λ_k	−17.596	12.566	5.9560	––
			α_k	––	0.2073	−0.2691	––
			$M_X^{\alpha_k}$	––	1.0217	1.0369	––
	$m = 3$	2.16×10^{-6}	λ_k	−17.451	18.142	−7.3668	7.5955
			α_k	––	0.3080	0.3893	−0.2265
			$M_X^{\alpha_k}$	––	1.0486	1.0787	1.0260
ME-IM	$m = 3$	6.10×10^{-2}	$\lambda_0 \sim \lambda_3$	0.3623	0.7602	−0.0208	0.0002
			$M_X^1 \sim M_X^3$	––	1.6487	7.3891	90.017
	$m = 5$	6.05×10^{-2}	$\lambda_0 \sim \lambda_3$	0.3565	0.7668	−0.0216	0.0002
			$M_X^1 \sim M_X^3$	––	1.6487	7.3891	90.017
			$\lambda_4 \sim \lambda_5$	––	––	1.55×10^{-6}	-1.65×10^{-8}
			$M_X^4 \sim M_X^5$	––	––	2.98×10^3	2.68×10^5

ME-FM: Method of MaxEnt with fractional moment; ME-IM: Method of MaxEnt with integer moment. In the method of ME-IM, the fractions are integers, i.e., $\boldsymbol{\alpha} = 1, 2, \cdots, m$.

According to K-L divergences listed in Table 3.6, it is clear to see that $\mathcal{K}[f, \widehat{f}]$ decreases very fast with the increase of the employed number of fractional moments in ME-FM. With

three order of fractional moments, an accurate approximation of the heave tail distribution can be obtained in the order of POE $\geqslant 10^{-5}$ (refer to in Figure 3.8 for details). In addition, the value of fractional exponents ($\boldsymbol{\alpha}$) in the process are also decreased. A small value of fraction is helpful if using a small size of samples to estimate the corresponding fractional moment.

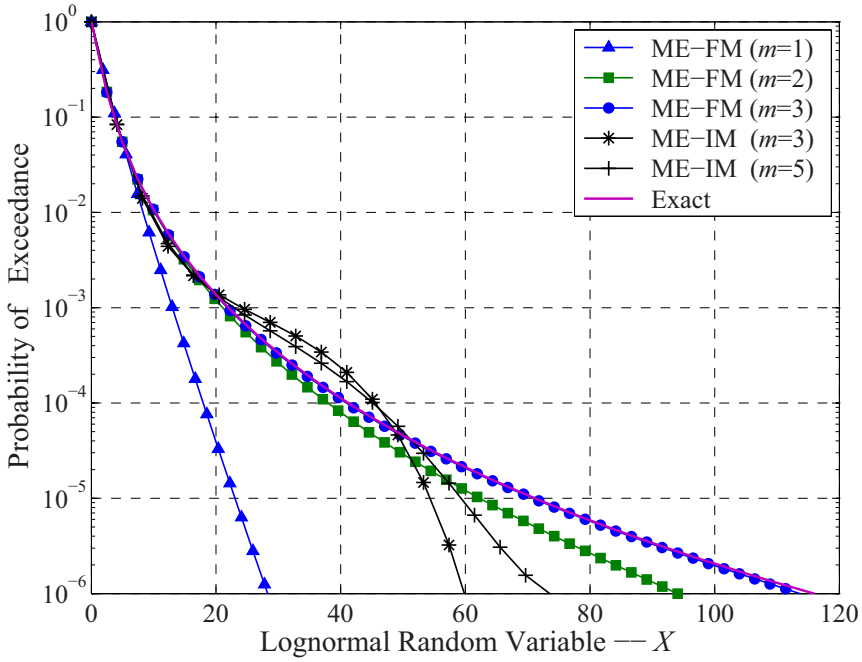

Figure 3.8: Approximation of Lognormal distribution with MaxEnt method (ME-FM: Method of MaxEnt with fractional moment; ME-IM: Method of MaxEnt with integer moment).

Compared to the results determined by ME-FM, ME-IM revealed its inaccuracy in the heavy tail approximation. Given three order of integer moments, ME-IM determines a large $\mathcal{K}[f, \widehat{f}]$, which is nearly identical with ME-FM with only one order of fractional moment, i.e., 6.10×10^{-2} versus 7.56×10^{-2}. In addition, as increase the order of integer moments (m) from three to five, K-L divergences have shown a slow rate of convergence.

3.6.3 Experiment on Quantile Estimation

To examine the accuracy and efficiency of fractional moment in modelling the heavy distribution, the Monte Carlo experiment was also carried out to estimate the upper quantiles with a small sample size. Considering that the values of POE are varying from 10^{-2} to 10^{-6}, the corresponding normalized bias and RMSE are reported as shown in Figures 3.9 and 3.10, respectively.

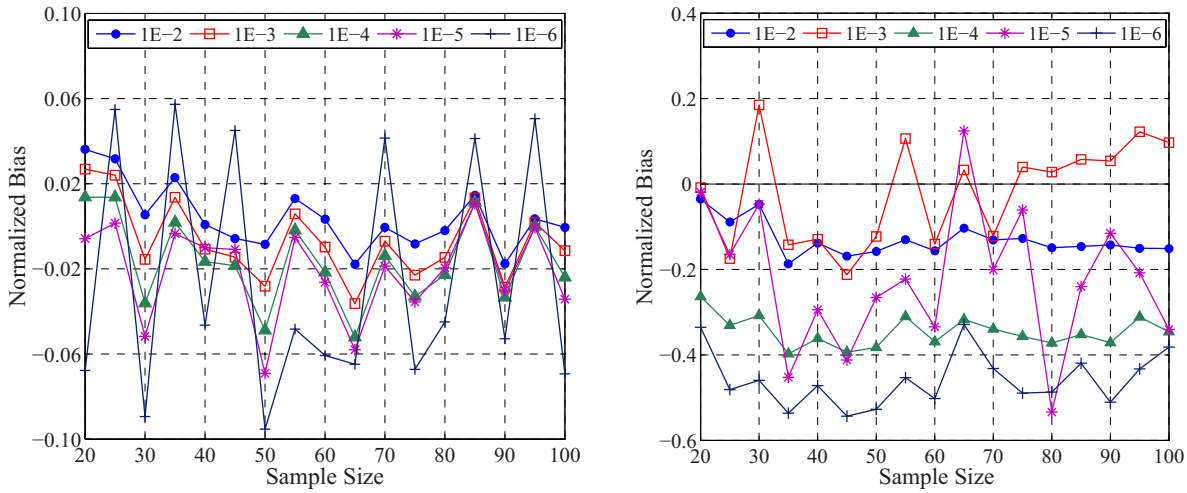

(a) MaxEnt with Three Fractional Moments (b) MaxEnt with Three Integer Moments

Figure 3.9: Normalized bias of the estimates of quantile function with the methods of ME-FM and ME-IM.

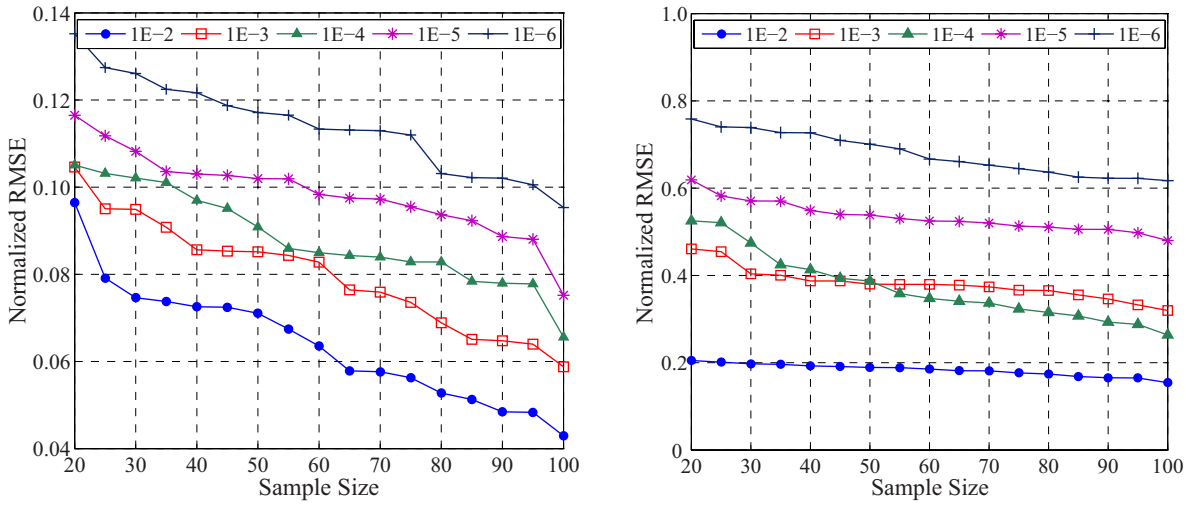

(a) MaxEnt with Three Fractional Moments (b) MaxEnt with Three Integer Moments

Figure 3.10: Normalized RMSE of the Lognormal quantiles for the varied target POEs

The experiment involved 100 cycles simulation, in which the varied sample size (N) was studied. It is interesting to note from Figure 3.9(a) that the quantiles estimated with ME-FM are within 10% error for the entire range of POEs. In addition, the small values of RMSE obtained in Figure 3.10 are further highlighted the efficiency of ME-FM in qunatile estimation. Compared to the results determined by ME-IM method, the use of fractional moment has greatly improved

the accuracy and efficiency of a quantile estimate.

Nominal value of mechanical design load, e.g., live & dead loads, and material property correspond to a POE in the orders of 10^{-3} or less. Therefore, the proposed ME-FM approach can provide reliable estimates of such nominal values form a very small samples that are belong to a general distribution.

3.7 Conclusion

The Chapter presents a distribution free method to model a parent distribution of a random variable. The approach is a moment method, but using the fractional moment instead of integer moment so far in literature. The unknown parent distribution is approximated using the principle of maximum entropy (MaxEnt) subject to the constraints specified in terms of fractional moments of a small observations. Compared to the classical methods based on integer moments, the small values of fractional exponent guarantees the reliable estimates of fractional moment from a small samples.

Efficiency of the proposed method was examined by using a series of simulation experiments. The normalized root mean square error (RMSE) of quantile estimates provided by various sample sizes, i.e., $20 \leqslant N \leqslant 100$, were determined. Compared to the benchmark results, the small RMSEs of quantile values were verified the efficiency of the proposed method.

Chapter 4

System Reliability Analysis of Mechanisms

4.1 Introduction

4.1.1 Background

Mechanisms are widely used to improve the production efficiency and accuracy of repetitive processes in industries, such as automobile and aerospace manufacturing, various types of assembling plants and computer-aided medical surgery.

A mechanism consists of several links and joints to transmit the motion or force from one link to another. The links and the connections at the joints are not perfectly accurate due to the manufacturing tolerances, material deformation and wearing over the service life of the mechanism. The uncertain variations affect the positional and directional control (or kinematics) of the motion performed by the mechanism. As a result, actual motion output of the mechanism deviates from the target output required by the design. This deviation between actual and target performance of the mechanism is referred to as output error in the study.

High precision is often required in mechanism applications (Hirschhorn, 1962). A mechanism consists of several rigid links and joints to transmit the motion or force from one point to another. The connections at the joints are not perfectly accurate due to the manufacturing tolerances, material deformation and wearing over the service life of the robot. The uncertain variations in dimensions of links and joint clearances affect the positional and directional control (or kinematics) of the motion performed by the mechanism.

Randomness in dimensions and clearance in joints will lead to unacceptable performance of mechanism. As a result, actual motion output of the manipulator deviates from the target output

required by the design. This deviation between actual and intended positions of the end-effector is referred to as positional error. Consequently, Dhande and Chakraborty (1973) proposed an optimization procedure to allocate the random tolerances so that the output error is within a specified limit (Faik and Erdman, 1991). In the contributions (Dubowsky et al., 1975; Freudenstein, 1954; Lee and Freudenstein, 1976a,b), an identification procedure was developed to identify the sources of poor mechanism performance due to the random clearance. Choi et al. (1998) employed the clearance vector model to analyze the effectiveness of tolerance on the performance of system output.

The reliability of manipulator kinematics is defined as the probability that the manipulator realizes its required motion path or trajectory within a specified tolerance range (Rao and Bhatti, 2001). The shape and size of specified range (or safety region) depend on the intended use of the manipulator. The reliability can be defined in two ways. The point reliability means that reliability is evaluated with reference to a particular point on the trajectory of the output motion, whereas the system reliability considers the reliability over a range of output motion.

In the point reliability analysis, Kim et al. (2010) applied the first-order reliability method (FORM) to compute the reliability of an open-loop manipulator with six degrees of freedom. Here, all geomantic dimensions and joint angles were considered as normally distributed. By combining the Monte Carlo simulations with Kriging method, Lai and Duan (2011) analyzed the reliability of a turning machine with a random coefficient of friction. Wu and Rao (2007) discussed optimal allocation of tolerances to joint angles by modeling them as interval variables. Huang and Zhang (2010) applied the Taguchi method to determine optimal specifications for a function generation mechanism under the constraints of positional accuracy and assembly cost.

Mechanism system reliability analysis is computationally demanding, because the failure region is represented by multiple performance functions. Literature in this area is rather limited. Zhang et al. (2011a) utilized a stochastic process to describe the positional error along the whole range of mechanism outputs. Considering a mechanism with Normal variables, the linearized limit state function also follows the Gauss distribution. The first-order second moment (FOSM) method, then, can be employed to perform the point reliability analysis. As consider the whole range of outputs, the Poisson process is further assumed to describe the events of output error up-crossing and down-crossing of a design limit. The corresponding counted numbers for the occurrences of failure event in disjoint intervals are independent (Cox and Isham, 1980; Snyder, 1975). Together with the calculated "point" reliability index, calculation of the crossing-rate was

developed in literature by using a general parallel system (Andrieu-Renaud et al., 2004; Rackwitz and Flessler, 1978; Sudret, 2008a). This approach was applied to analyze the system reliability of a four-bar function generator.

4.1.2 Motivation and Approach

Since a mechanism is designed for repetitive work, it may be necessary in most cases that error is controlled in the entire trajectory, instead of a point. This provides motivation for cumulative or system reliability analysis of the mechanism. Approximate methods, such as FORM, is not adequate to analyze a large system reliability problem (Kim et al., 2010). The first-order second moment (FOSM) method is of limited applicability, as it is based on a spurious assumption of the normality of the positional error.

The key objective of this study is to develop a computationally efficient and accurate method for the cumulative (or system) reliability analysis of mechanisms. The developed method should be able to deal with a large number of implicit and correlated performance functions defining the system reliability.

In the study, the cumulative reliability analysis is formulated as a series system reliability problem. The study shows that the series system reliability is equivalent to the probability that the maximum positional error in the entire trajectory is less than a specified limit.

The distribution of maximum positional error is derived using the maximum entropy (MaxEnt) principle, widely used in probabilistic analysis. A novel feature of the study is the use of fractional moments as constraints, instead of integer moments commonly used in the entropy literature. To compute fractional moments of the positional error, a small sample of positional error is simulated based on the model of manipulator kinematics. The Chapter shows that proposed method is highly efficient, and it achieves the same accuracy as that obtained by a large scale Monte Carlo simulation method.

4.1.3 Organization

The Chapter has been organized as follows. Section 4.2 describes the kinematic model and joint clearance analysis of a six degrees of freedom elbow manipulator. Section 4.3 summarizes basic information for the system reliability analysis of a manipulator. A method based on the extreme event distribution is formulated to evaluate the mechanism reliability by using the maximal po-

sitioning error along the entire output trajectory of the end-effector. To estimate the maximal output error distribution, the principle of maximum entropy (MaxEnt) with fractional moment (ME-FM) proposed in Chapter 3 is employed. Numerical result on the system reliability analysis of an elbow manipulator is presented in Section 4.4. Section 4.5 further examines the proposed method by the examples of slider-crank mechanism and a four-bar linkage. And conclusions are summarized in the last Section.

4.2 Model of a Mechanism

A space serial manipulator taken from Kim et al. (2010) is illustrated in Figure 4.1. A similar example was presented by Wu and Rao (2007).

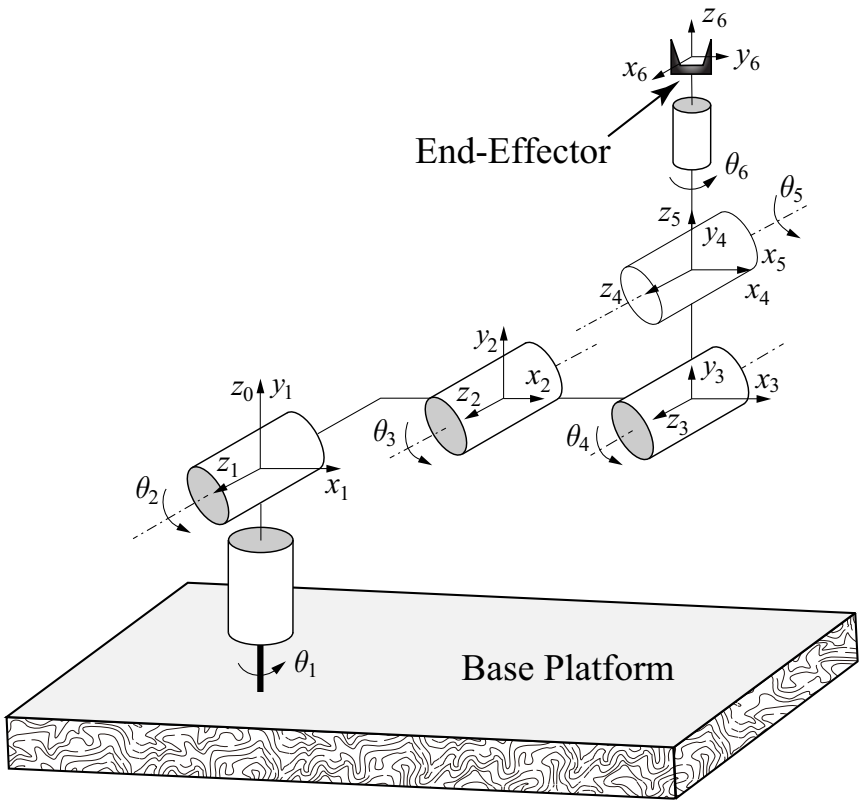

Figure 4.1: A six degree-of-freedom elbow manipulator

4.2.1 Kinematic Analysis

Kinematic equations of an open-chain manipulator are described by the Denavit-Hartenberg (D-H) matrix in terms of position and orientation as (Craig, 2005)

$$\mathbf{T}_{i-1}^{i} = \begin{bmatrix} \cos(\tau_k) & -\cos(\varphi_i)\sin(\tau_k) & \sin(\varphi_i)\cos(\tau_k) & a_i\cos(\tau_k) \\ \sin(\tau_k) & \cos(\varphi_i)\cos(\tau_k) & -\sin(\varphi_i)\cos(\tau_k) & a_i\sin(\tau_k) \\ 0 & \sin(\varphi_i) & \cos(\varphi_i) & d_i \\ 0 & 0 & 0 & 1 \end{bmatrix}_{4\times4} \tag{4.1}$$

where, a_i, d_i, φ_i and θ_i are the D-H parameters. The coordinates of the positions of the end-effector can be written as a product of D-H matrices for all the links:

$$\mathbf{T}_{\text{End}} = \mathbf{T}_0^1 \times \mathbf{T}_1^2 \times \cdots \times \mathbf{T}_{l-1}^{l} = \begin{bmatrix} \mathbf{n} & \mathbf{s} & \mathbf{a} & \mathbf{p} \\ 0 & 0 & 0 & 1 \end{bmatrix} \tag{4.2}$$

where **a**, **n** and **s** denote the vectors of a frame attached to the end-effector as follows. **a** is chosen in the approach direction to object, **s** is normal to **a** in the sliding plane, **n** is normal to **a** and **s**, vector **p** provides the positional coordinates.

Table 4.1: Ranges of rotation angles θ_1 and θ_5

	A→B	B→C	C→D	D→E
θ_1	0°	[0° : 5° : 70°]	70°	[70° : −5° : 50°]
θ_5	[0° : −5° : −45°]	−45°	[−40° : 5° : 30°]	30°

To illustrate a specific example of the trajectory of the end-effector, the following values of the D-H parameters are assumed: $a_1 = a_5 = a_6 = 0\,\text{mm}$, $a_2 = 475\,\text{mm}$, $a_3 = 500\,\text{mm}$, $a_4 = 175\,\text{mm}$, $d_1 = d_3 = d_4 = d_5 = 0\,\text{mm}$, $d_2 = 300\,\text{mm}$, $d_6 = 450\,\text{mm}$, $\varphi_1 = 90°$, $\varphi_5 = -90°$, $\varphi_2 = \varphi_3 = \varphi_4 = \varphi_6 = 0°$, and $\theta_2 = 90°$, $\theta_3 = 0°$, $\theta_4 = -135°$ and $\theta_6 = 0°$. Driven by motors at the 1st and 5th joints (represented by θ_1 and θ_5), the end-effector can realize complicated trajectories of motion.

The position of end effector is changed by varying θ_1 and θ_5 as per the rule described in Table 4.1. The resulting trajectory from A to E has 45 discrete positions, as shown in Figure 4.2. For a specific location, the position of the end-effector can be obtained using data given in Table 4.2. These are basically the design targets for positions of the end effector.

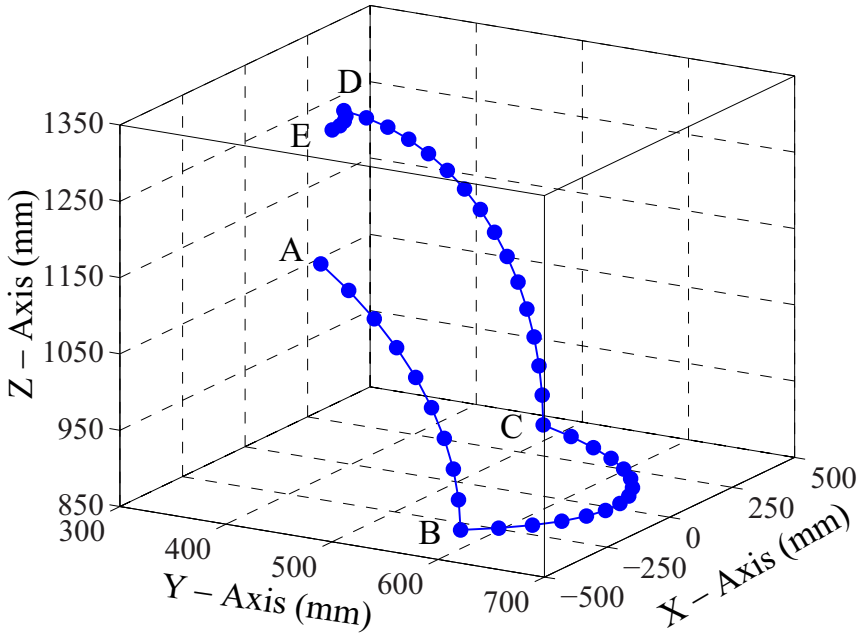

Figure 4.2: Target trajectory of the end-effector of the elbow manipulator

Table 4.2: Coordinates of various positions of the end-effector

Locations	A	B	C	D	E
p_x (mm)	441.94	573.74	478.14	364.07	384.22
p_y (mm)	−300.00	−300.00	436.54	123.12	−8.8230
p_z (mm)	1169.5	851.26	851.26	1285.9	1285.9

4.2.2 Clearance Analysis

The effect of the joint clearance is to introduce variability in the rotation angle. However, the range of this variation is related to the clearance circles, as shown in Figure 4.3(a) for two adjacent joints. Here consider that angle θ_k and dimension a_k are take the values θ'_k and a'_k, respectively, due to the clearance circles at the k^{th} and $(k+1)^{\text{th}}$ joints. For sake of simplicity, first consider in Figure 4.3(b) that, $a'_k = a_k$, i.e., no dimensional variability. Suppose centres of clearance circles, O_k and O_{k+1}, vary between the bounds $O_k^{\min}$, $O_k^{\max}$ and $O_{k+1}^{\min}$, $O_{k+1}^{\max}$. This would cause variation in θ_k between $\theta_k^{\min}$ and $\theta_k^{\max}$, in the following way:

$$\begin{cases} \theta_k^{\min} = \theta_k - \sin^{-1}\left[(R_k + R_{k+1})/a_k\right] \\ \theta_k^{\max} = \theta_k + \sin^{-1}\left[(R_k + R_{k+1})/a_k\right] \end{cases} \tag{4.3}$$

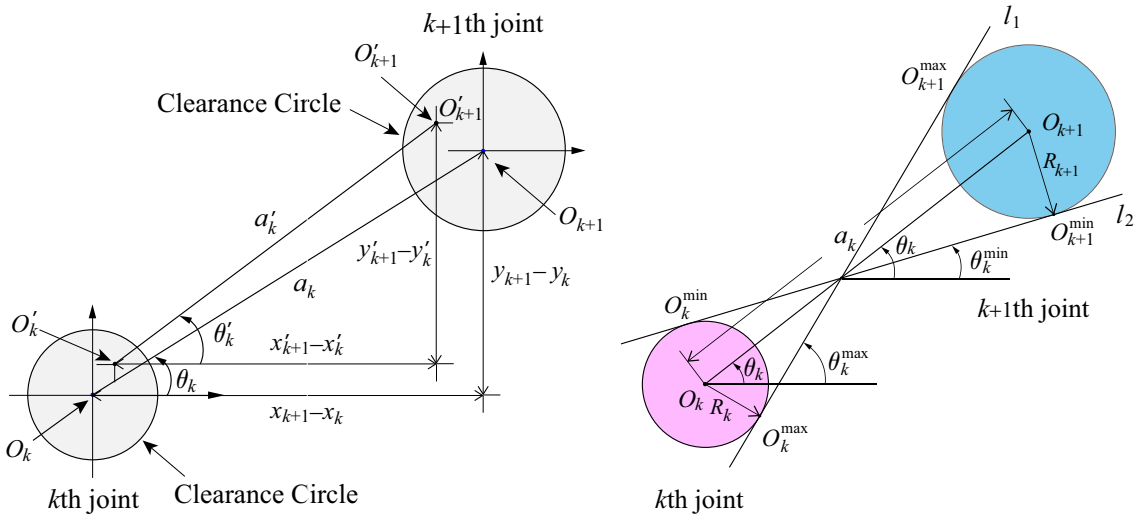

(a) Joint clearance

(b) Variation of θ_k

Figure 4.3: Variation in the rotation angle due to joint clearance

It is reasonable to consider that θ_k is distributed in the interval $\left[\min, \max\left\{\theta_k \pm \sin^{-1}[(R_k + R_{k+1})/a_k]\right\}\right]$. A k^{th} rotation angle can be modeled as $\widetilde{\theta}_k = \theta_k + \varepsilon_{\theta_k}$ (for $k = 1, 5$), where θ_k is the nominal value and ε_{θ_k} is the tolerance. Geometrical dimensions are modeled as normally distributed. All these random variables are summarized in Table 4.3.

Table 4.3: Probability distributions of random variables

Links:	Variable	Distribution	Mean (mm)	Std.D (mm)
	a_2	Normal	475	0.475
	d_2	Normal	300	0.300
	a_3	Normal	500	0.500
	a_4	Normal	175	0.175
	d_6	Normal	450	0.450
Angular Error:	Variable	Distribution	Lower Bound	Upper Bound
	ε_{θ_1}	Uniform	$-0.1°$	$0.1°$
	ε_{θ_5}	Uniform	$-0.1°$	$0.1°$

4.3 System Reliability Analysis

4.3.1 Performance Function

Use a general variable τ_k to represent a k^{th} configuration as shown in Figure 4.2. Then, the target trajectory is discretized by using 45 configurations in total. Suppose the coordinates of the k^{th} position of the end-effector are specified in the design as $\left[p_{\text{x}}^{\text{Ideal}}(\tau_k), p_{\text{y}}^{\text{Ideal}}(\tau_k), p_{\text{z}}^{\text{Ideal}}(\tau_k)\right]$. Because of random tolerance in joint and dimensions of links, actual coordinates of the k^{th} position become random variables, denoted as $[p_{\text{x}}(\mathbf{X}, \tau_k), p_{\text{y}}(\mathbf{X}, \tau_k), p_{\text{z}}(\mathbf{X}, \tau_k)]$. Here, $\mathbf{X}$ denotes a vector of random variables listed in Table 4.3.

The positional error is defined as the difference, $r(\mathbf{X}, \tau_k)$, between the target and actual position of the end-effector. Thus,

$$r(\mathbf{X}, \tau_k) = \sqrt{\left[p_{\text{x}}(\mathbf{X}, \tau_k) - p_{\text{x}}^{\text{Ideal}}(\tau_k)\right]^2 + \left[p_{\text{y}}(\mathbf{X}, \tau_k) - p_{\text{y}}^{\text{Ideal}}(\tau_k)\right]^2 + \left[p_{\text{z}}(\mathbf{X}, \tau_k) - p_{\text{z}}^{\text{Ideal}}(\tau_k)\right]^2} \tag{4.4}$$

Manipulator's performance is considered acceptable, if the positional error is less than a critical limit r_0. With this idea, a performance function in terms of the positional error at a k^{th} position can be defined as

$$g(\mathbf{X}, \tau_k) = r_0 - r(\mathbf{X}, \tau_k) \quad (k = 1, 2, \cdots, 45) \tag{4.5}$$

In this notation, the probability of unacceptable performance or "failure" can be defined as

$$P_F(\tau_k) = \Pr\left[g(\mathbf{X}, \tau_k) \leqslant 0\right] \quad (k = 1, 2, \cdots, 45) \tag{4.6}$$

Note that $P_F(\tau_k)$ is referred to as the "point" probability of failure at the k^{th} configuration of the manipulator.

An example of probability of failure analysis for the point A of the elbow manipulator is shown in Figure 4.4. A vector of random variables, $\mathbf{X}$, is simulated from the distributions specified in Table 4.3, corresponding trajectory of the end effector is calculated from the kinematic model, and positional error at point A, $r(\mathbf{X}, \tau_1)$, is evaluated.

In Figure 4.4, 2000 simulated samples of $r(\mathbf{X}, \tau_1)$ are plotted along with a sphere of radius equal to the critical limit of position error, $r_0 = 2.0$ mm. Thus, all instances of $r(\mathbf{X}, \tau_1) > r_0$ correspond to the failure of the manipulator to meet a specified degree of accuracy.

The system reliability is defined as the probability that the end-effector position lies within a specified limit from the desired target for every point along a specified trajectory, such as that

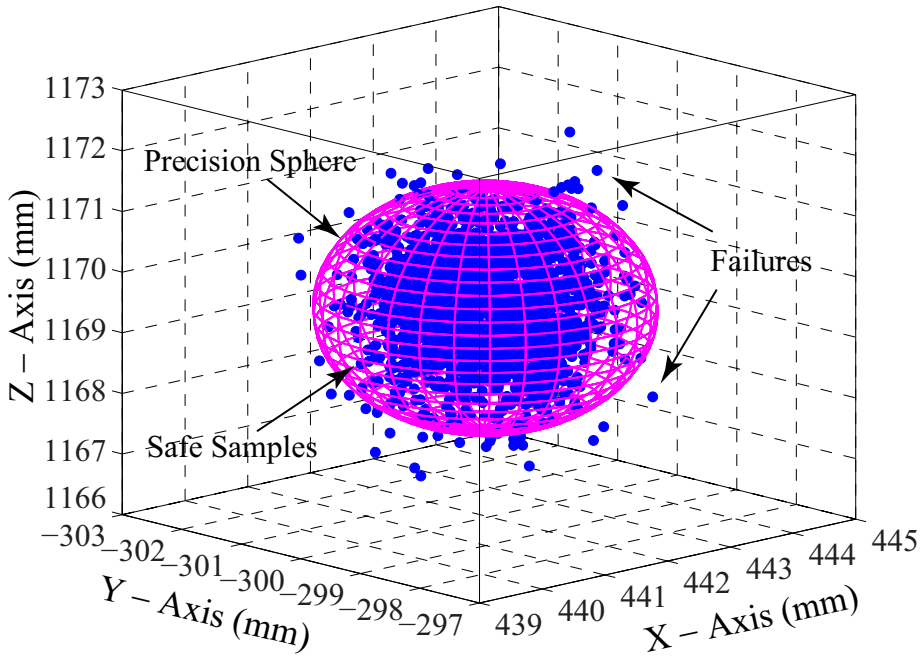

Figure 4.4: Illustration of failure criteria at point A of the trajectory of end-effector

shown in Figure 4.2. Or conversely, failure means that manipulator fails to meet the specified accuracy at any point of its required trajectory. Thus, the probability of failure can be defined similar to that of a series system with b $(= 45)$ components as

$$P_F^S = \Pr\left\{ \bigcup_{k=1}^{b} \left[g(\mathbf{X}, \tau_k) \leqslant 0 \right] \right\} \tag{4.7}$$

Note that $\left\{ g(\mathbf{X}, \tau_1), g(\mathbf{X}, \tau_2), \cdots, g(\mathbf{X}, \tau_b) \right\}$ are performance functions for $b = 45$ points defining the trajectory shown in Figure 4.2.

4.3.2 The Gradient-Based Methods

Considering a k^{th} configuration of positioning output, the performance function can be linearized at the mean-value of random variables as

$$g(\mathbf{X}, \tau_k) \approx g(\boldsymbol{\mu}, \tau_k) + \sum_{i=1}^{n} \frac{\partial g(\mathbf{x}, \tau_k)}{\partial x_i} (X_i - \mu_i) \tag{4.8}$$

When the configuration indicator τ_k is changing from 1 to b, the mean and standard deviation of the k^{th} limit state function $g(\mathbf{X}, \tau_k)$ can be approximated as

$$\begin{cases} \mu_g(\tau_k) \approx g(\boldsymbol{\mu}, \theta_k) \\ \sigma_g(\tau_k) \approx \sqrt{\sum_{i=1}^{n} \left[\left. \frac{\partial g(\mathbf{x}, \tau_k)}{\partial x_i} \right|_{\mathbf{x}=\boldsymbol{\mu}} \sigma_i \right]^2} \end{cases} \tag{4.9}$$

Then, the k^{th} point reliability index determined by the FOSM method is given as $\beta_{\text{FOSM}}(\tau_k) = \mu_g(\tau_k)/\sigma_g(\tau_k)$. And the corresponding point failure probability is:

$$P_F(\tau_k) \approx \Phi\big[-\beta_{\text{FOSM}}(\tau_k)\big] = \Phi\Big[-\frac{\mu_g(\tau_k)}{\sigma_g(\tau_k)}\Big] \tag{4.10}$$

where $\Phi(\cdot)$ is the standard Normal cumulative distribution function.

Limitations of FOSM in the mechanism reliability analysis are two folds. At first, Eq.(4.8) utilized the first-order Taylor series approximating $g(\mathbf{X}, \tau_k)$. The approximation overlooked the distribution properties of random variable. Therefore, one will obtain the same moment values of $g(\mathbf{X}, \tau_k)$ regardless of the change of distribution type of $\mathbf{X}$. Secondly, failure probability estimated by Eq.(4.10) with an assumption that $g(\mathbf{X}, \tau_k)$ follows the Normal distribution. The assumption cannot be guaranteed except $g(\mathbf{X}, \tau_k)$ is a linear function and $\mathbf{X}$ are the Normal variables. However, as shown by later examples, it is too optimistic to model the performance function, $g(\mathbf{X}, \tau_k)$, using a linear function with respect to the input variables.

In addition FOSM, the first-order reliability method (FORM) is an approximate method of reliability analysis that is widely used in civil engineering. One can refer to literature (Ditlevsen and Madsen, 1996) for details. Although this approximation is quite accurate for a small number of performance functions, its accuracy deteriorates as the number of functions exceeds a moderate number (4 or 5). Therefore, FORM is not suitable for system reliability analysis of the manipulator example considered in the study.

4.3.3 Monte Carlo Simulation

It is necessary in most cases that mechanical error of positional output is controlled in the entire trajectory, instead of a few points. Approximate methods, such as FORM, is not adequate to analyze a large system reliability problem. The FOSM method is of limited applicability, as it is based on a spurious assumption of the normality of positional error.

Mont Carlo simulation, however, has been extensively employed in reliability analysis. Implementation of Monte Carlo simulation for mechanism system reliability analysis can be described as follows:

- Kinematic analysis: Determine the close-loop function and ideal output of the mechanism.
- Mechanical error analysis: An i^{th} input parameter is realized by the summation of its nominal value z_i and the error ε_i, i.e., $\widetilde{x}_i = x_i + \varepsilon_i$. One should note that the uncertainty can exist in both of z_i and ε_i. The real input parameters allow to calculate the corresponding actual output trajectory of the mechanism.
- Point reliability analysis: Define an indicator $\mathbf{1}_{\{g_k(\mathbf{X},\tau_k)\leqslant 0\}}\left(\mathbf{x}^{(i)}\right) = 1$ and zero otherwise for an i^{th} sample of random variables. Point failure probability of the k^{th} configuration, then, can be estimated by $\widehat{P}_F(\tau_k) = \sum \mathbf{1}_{\{g_k(\mathbf{X},\tau_k)\leqslant 0\}}(\mathbf{x})/N$.
- System reliability analysis: Indicating function of system failure is $\mathbf{1}_{\left\{\bigcup_{k=1}^{b}[g_k(\mathbf{X},\tau_k)\leqslant 0]\right\}}\left(\mathbf{x}^{(i)}\right) = 1$ and zero otherwise. The indicator is null only for all limit state functions are greater than zero. System failure probability, then, is estimated as $\widehat{P}_F^S = \sum \mathbf{1}_{\bigcup_{k=1}^{b}[g_k(\mathbf{X},\tau_k)\leqslant 0]}(\mathbf{x})/N$.

The procedure of Monte Carlo simulation will be employed to provide the benchmark results in the study.

4.3.4 Proposed Method based on Extreme Event Distribution

Suppose a random variable, Y, denotes the maximum positional error in the entire trajectory of the end effector, i.e.,

$$Y = \max\left\{r(\mathbf{X},\tau_1), r(\mathbf{X},\tau_2), \cdots, r(\mathbf{X},\tau_b)\right\} \tag{4.11}$$

The system reliability analysis can be reformulated as

$$P_F^S = \Pr\left\{\bigcup_{k=1}^{b}\left[g(\mathbf{X},\tau_k)\leqslant 0\right]\right\} \equiv \Pr[Y > r_0] = 1 - F_Y(r_0) \tag{4.12}$$

where, $F_Y(y)$ is the cumulative distribution function (CDF) of Y, which is an extreme event distribution of the positional error.

The proposed method is inspired by the work of Li et al. (2007), who clearly explained the idea that system reliability analysis involving multiple performance functions can be recast in

terms of an equivalent function involving the maximum (or minimum as the case may be) of all performance functions.

Using a simple system involving only two performance functions, the system probability of failure can be evaluated as

$$\begin{aligned} P_F^S &= \Pr\{[g(\mathbf{X}, \tau_i) \leqslant 0] \cup [g(\mathbf{X}, \tau_j) \leqslant 0]\} \\ &= \Pr\{[r(\mathbf{X}, \tau_i) \geqslant r_0] \cup [r(\mathbf{X}, \tau_j) \geqslant r_0]\} \end{aligned} \tag{4.13}$$

Note that $r(\mathbf{X}, \tau_i)$ and $r(\mathbf{X}, \tau_j)$ are correlated as they are the functions of common vector $\mathbf{X}$. Let $f_{ij}(r_i, r_j)$ denote the joint density function of $r(\mathbf{X}, \tau_i)$ and $r(\mathbf{X}, \tau_j)$, such that the system failure probability can be obtained from the following integration:

$$\begin{aligned} P_F^S &= \Pr\{[r(\mathbf{X}, \tau_i) \geqslant r_0] \cup [r(\mathbf{X}, \tau_j) \geqslant r_0]\} \\ &= \int_{r_0}^{\infty} \int_{-\infty}^{\infty} f_{ij}(r_i, r_j) \mathrm{d}r_i \mathrm{d}r_j + \int_{-\infty}^{r_0} \int_{r_0}^{\infty} f_{ij}(r_i, r_j) \mathrm{d}r_i \mathrm{d}r_j \end{aligned} \tag{4.14}$$

See Figure 4.5 for explanation about the integrating domain.

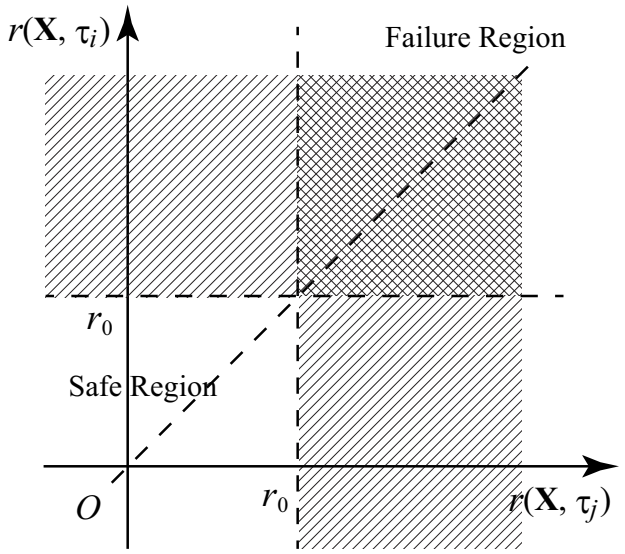

Figure 4.5: Failure region represented by $r(\mathbf{X}, \tau_i)$ and $r(\mathbf{X}, \tau_j)$

Define $r_{\max}(\mathbf{X}) = \max\{r(\mathbf{X}, \tau_i), r(\mathbf{X}, \tau_j)\}$. This is:

$$r_{\max}(\mathbf{X}) = \begin{cases} r(\mathbf{X}, \tau_i) & \text{if } r(\mathbf{X}, \tau_i) \geqslant r(\mathbf{X}, \tau_j) \\ r(\mathbf{X}, \tau_j) & \text{if } r(\mathbf{X}, \tau_i) < r(\mathbf{X}, \tau_j) \end{cases} \tag{4.15}$$

As illustrated in Figure 4.5, the probability of $\Pr\left[r_{\max}(\mathbf{X}) \geqslant r_0\right]$ can be determined as

$$\begin{aligned}\Pr\left[r_{\max}(\mathbf{X}) \geqslant r_0\right] &= \iint_{r_i \geqslant r_j, r_i > r_0} f_{ij}(r_i, r_j)\mathrm{d}r_i\mathrm{d}r_j + \iint_{r_i < r_j, r_j > r_0} f_{ij}(r_i, r_j)\mathrm{d}r_i\mathrm{d}r_j \\ &= \int_{r_0}^{\infty}\int_{-\infty}^{r_i} f_{ij}(r_i, r_j)\mathrm{d}r_j\mathrm{d}r_i + \int_{r_0}^{\infty}\int_{-\infty}^{r_j} f_{ij}(r_i, r_j)\mathrm{d}r_i\mathrm{d}r_j\end{aligned} \tag{4.16}$$

The first term of the equation can be further rewritten as

$$\int_{r_0}^{\infty}\int_{-\infty}^{r_i} f_{ij}(r_i, r_j)\mathrm{d}r_j\mathrm{d}r_i = \int_{-\infty}^{r_0}\int_{r_0}^{\infty} f_{ij}(r_i, r_j)\mathrm{d}r_i\mathrm{d}r_j + \int_{r_0}^{\infty}\int_{r_j}^{\infty} f_{ij}(r_i, r_j)\mathrm{d}r_i\mathrm{d}r_j \tag{4.17}$$

as well as the second term of Eq.(4.16):

$$\int_{r_0}^{\infty}\int_{-\infty}^{r_j} f_{ij}(r_i, r_j)\mathrm{d}r_i\mathrm{d}r_j = \int_{r_0}^{\infty}\int_{-\infty}^{r_0} f_{ij}(r_i, r_j)\mathrm{d}r_i\mathrm{d}r_j + \int_{r_0}^{\infty}\int_{r_0}^{r_j} f_{ij}(r_i, r_j)\mathrm{d}r_i\mathrm{d}r_j \tag{4.18}$$

Then, summation of Eq.(4.18) with the second term of Eq.(4.17), yields

$$\begin{aligned}\int_{r_0}^{\infty}\int_{-\infty}^{r_0} f_{ij}(r_i, r_j)\mathrm{d}r_i\mathrm{d}r_j + \int_{r_0}^{\infty}\int_{r_0}^{r_j} f_{ij}(r_i, r_j)\mathrm{d}r_i\mathrm{d}r_j + \int_{r_0}^{\infty}\int_{r_j}^{\infty} f_{ij}(r_i, r_j)\mathrm{d}r_i\mathrm{d}r_j \\ = \int_{r_0}^{\infty}\int_{-\infty}^{\infty} f_{ij}(r_i, r_j)\mathrm{d}r_i\mathrm{d}r_j\end{aligned} \tag{4.19}$$

Given the first term of Eq.(4.17), finally, it leads to

$$\Pr\left[r_{\max}(\mathbf{X}) \geqslant r_0\right] = \int_{-\infty}^{r_0}\int_{r_0}^{\infty} f_{ij}(r_i, r_j)\mathrm{d}r_i\mathrm{d}r_j + \int_{r_0}^{\infty}\int_{-\infty}^{\infty} f_{ij}(r_i, r_j)\mathrm{d}r_i\mathrm{d}r_j \tag{4.20}$$

which is identical to the results in Eq.(4.14). It is therefore shown that the reliability of a series system can be evaluated in terms of the maximum value distribution.

4.3.5 Implementation Procedure

The Chapter proposes to estimate this extreme event distribution using a small sample of maximum positional error of the mechanism, obtained from the Monte Carlo simulations. A sample-based method with the principle of maximum entropy (MaxEnt) is developed. A novel feature of the study is the use of fractional moments as constraints, instead of integer moments commonly used in the entropy literature. The method is referred to as ME-FM throughout the thesis. To compute fractional moments of the positional error, a small sample of positional error is simulated based on the kinematic model of a mechanism. One can refer to Chapter 3 for the details on the derivation of MaxEnt distribution.

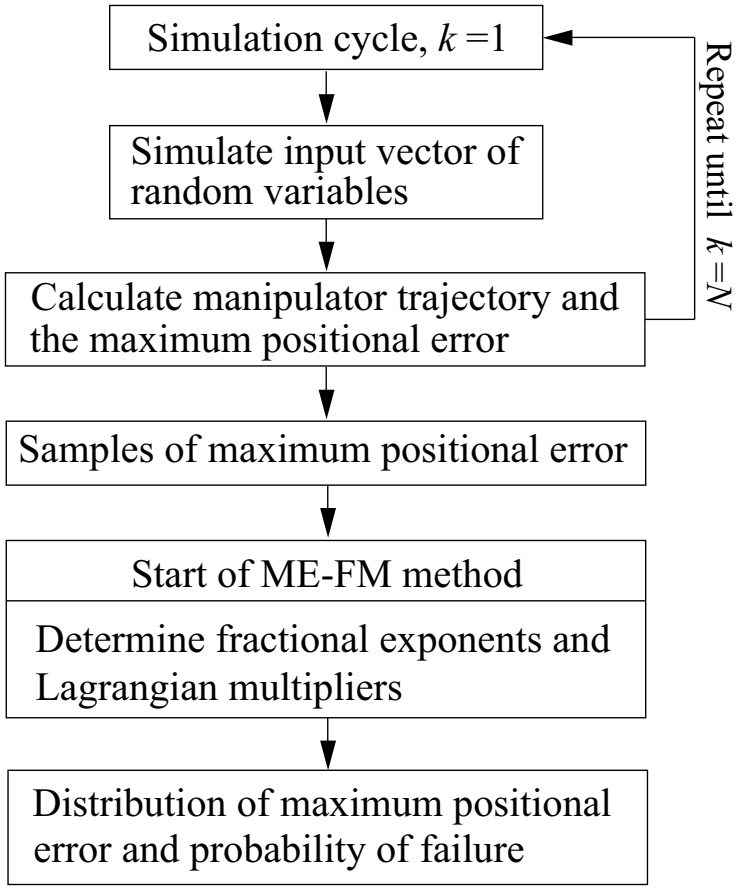

Figure 4.6: Steps in ME-FM method for the estimation of the distribution of maximum positional error

The flow chart of the proposed ME-FM method is shown in Figure 4.6, which is used to derive the distribution of maximum positional error in a complete trajectory of the end-effector.

Firstly an input vector of random variables $\mathbf{X}$ describing the joint clearances and link dimensions (see Table 4.3) is simulated. Given this input, the trajectory shown in Figure 4.2 is computed from the kinematic model of the manipulator. The positional error at each of the 45 positions is evaluated, and maximum error is separately stored. The simulation is repeated $N(= 500)$ times, and thus a random sample of maximum position error is obtained.

Given this sample, the proposed ME-FM method was applied, and the PDF of maximum positional error was estimated similar to Eq.(3.20). Typically three fractional moments were found to be sufficient to achieve convergence in the optimization problem.

4.4 Example of an Elbow Manipulator

In this section, the method of ME-FM for the system reliability analysis of the elbow manipulator in Figure 4.1 is presented.

4.4.1 Observations from Simulation

The positional errors in a sample of five simulated trajectories are plotted in Figure 4.7, which shows that the errors incurred at different points are strongly correlated. Because of this correlation, the cumulative probability of failure at a point can not be calculated as a simple addition of point failure probabilities of all preceding points. A great advantage of the extreme event distribution is that it accounts for this correlation accurately and provides a correct estimate of the failure probability, as shown later in this Section.

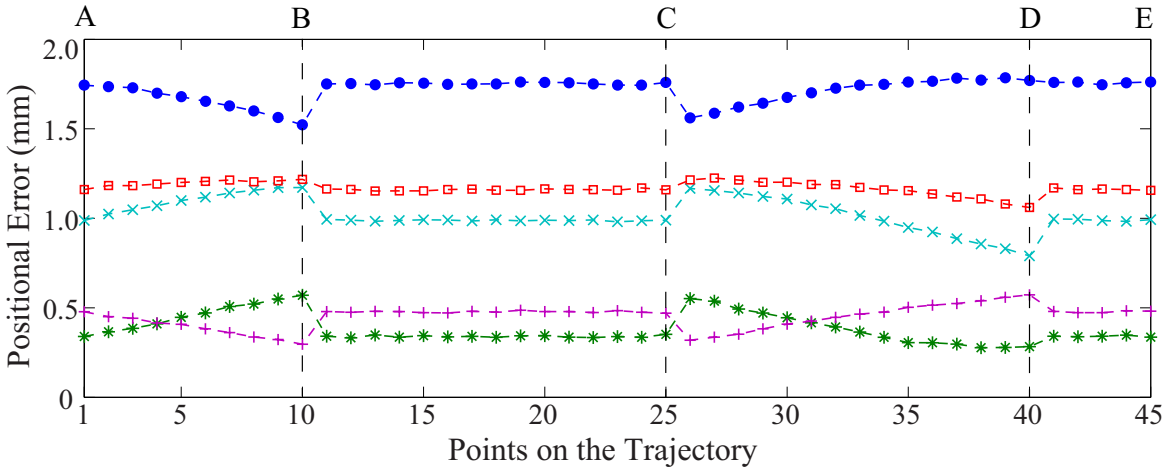

Figure 4.7: A sample of positional errors in five simulated trajectories of the end-effector

Does maximum positional error occur at a fixed point of the trajectory, or could it occur at different points depending on the values of input random variables? This question is answered in Figure 4.8, which shows the relative frequency of the occurrence of maximum positional error at various points along the trajectory of the end-effector. This plot is based on results of 10^5 simulations.

It is interesting to observe that maximum error is most likely to occur at point B (40% times), followed by point D (about 30% times). Having said this, nearly 30% times, the largest positional errors can occur at other points on the trajectory. It means that focusing on the point reliability

at a single point would not ensure achieving the same degree of reliability at other points of the trajectory. Thus, the need for system reliability analysis is justified.

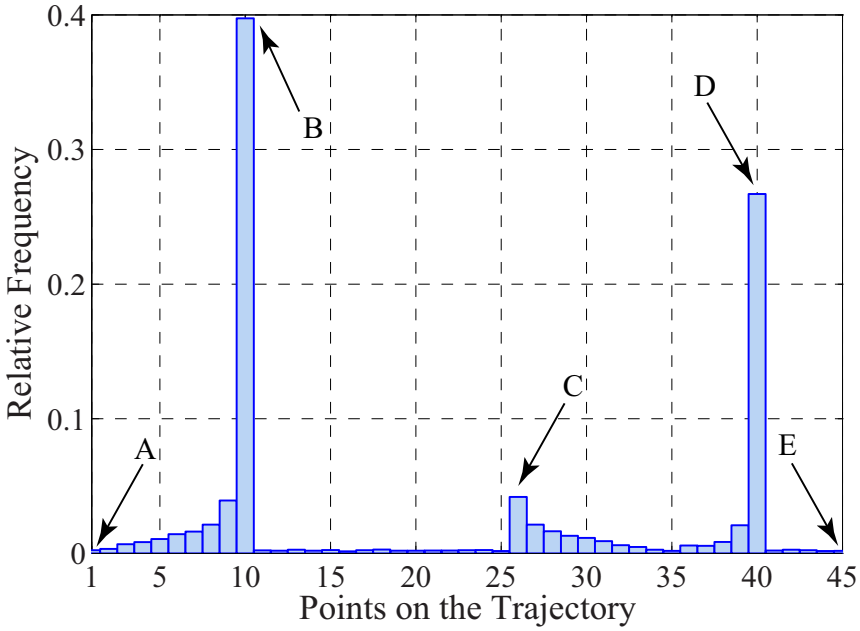

Figure 4.8: Relative frequency of occurrence of maximum positional error at different points of the manipulator trajectory

4.4.2 Results of ME-FM Method

Firstly, the empirical distribution of maximum positional error was obtained from the Monte Carlo simulation in which a large sample of (10^5) trajectories was simulated. This MCS solution is referred to as the benchmark result, which is used to evaluate the accuracy of the proposed ME-FM method.

Table 4.4: Parameters of the MaxEnt distribution

Entropy	k	0	1	2	3
0.5647	λ_k	-36.201	38.990	11.434	-14.152
	α_k		-0.0717	0.9834	0.6201
Moments	$M_Y^{\alpha_k}$		0.9926	1.1966	1.1020

The parameters of the MaxEnt PDF, namely, the fractions (α_i) and the Lagrange multipliers

(λ_i) are given in Table 4.4. These parameters were computed using a sample of $N = 500$ simulated values of the maximum positional error as per the procedure shown in Figure 4.6.

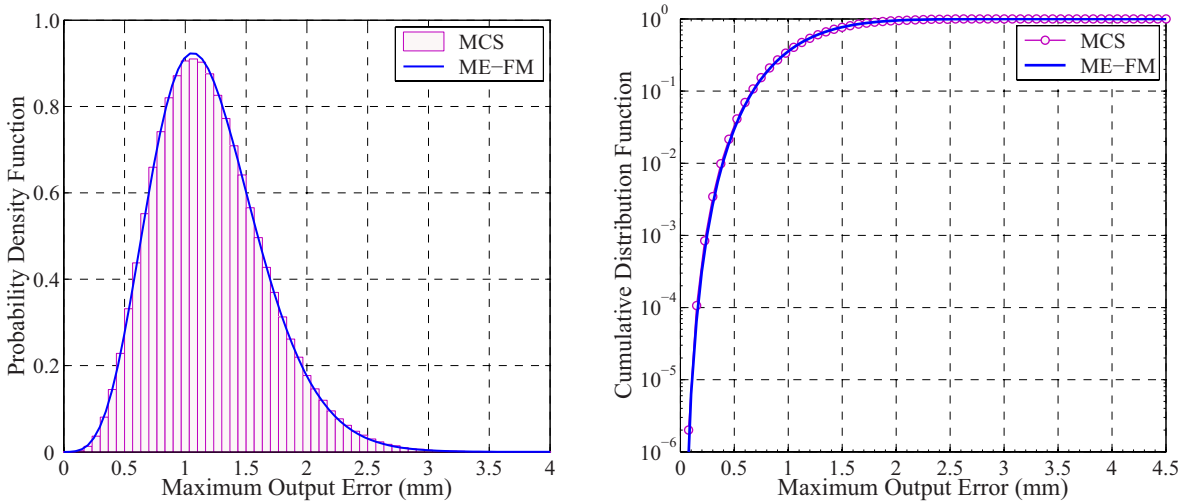

(a) Probability Density Function

(b) Cumulative Distribution Function

Figure 4.9: Distribution of the maximum positional error of the manipulator

The PDF and CDF of the maximum error obtained from ME-FM and MCS methods are compared in Figure 4.9. A close agreement between ME-FM and MCS results confirms the validity of the proposed approach.

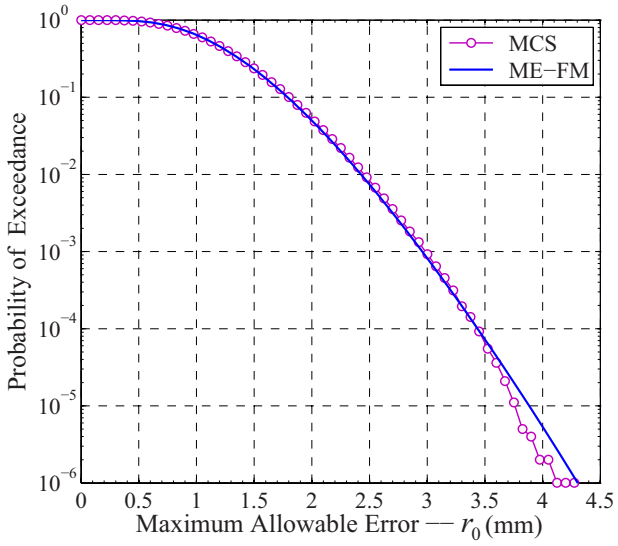

Figure 4.10: System failure probability of the elbow manipulator

The probability of exceedance versus the maximum positional error is shown in Figure 4.10. This plot is useful to calculate the probability of failure of the manipulator for a given threshold (r_0) of the maximum allowable positional error. For example, if $r_0 = 3.0$ mm, the probability of exceeding this value can be obtained from Figure 4.10 as 9.1×10^{-4}, whereas the MCS method provides a close estimate of 8.8×10^{-4}.

4.4.3 Effect of Sample Size

ME-FM method uses a simulated sample of the positional error. Therefore, it is important to investigate the effect of the sample size (N) on the statistical error associated with the probability of failure estimated by this method. In Figure 4.11, probability of failure versus N is plotted for $r_0 = 3.0$ mm.

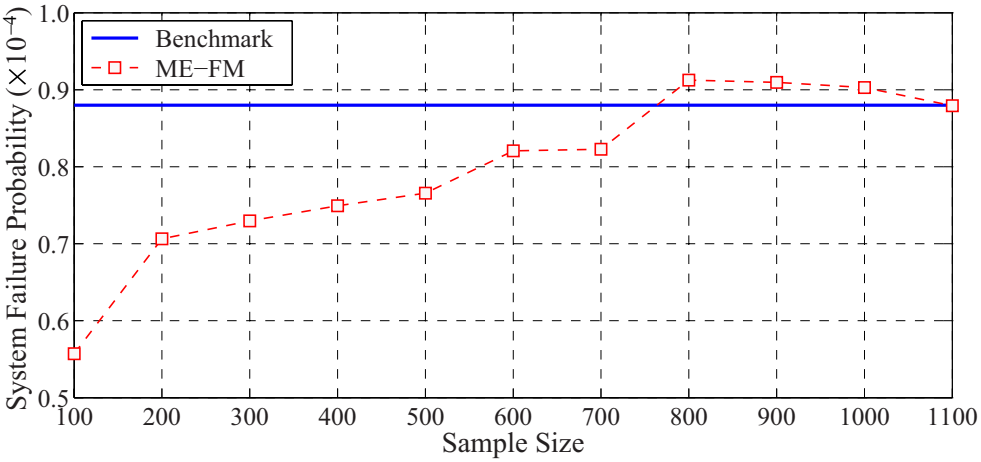

Figure 4.11: Probability of failure versus sample size used in ME-FM estimation

ME-FM estimates obtained from sample size ranging from 100 to 1000 are in fairly close agreement with the MCS benchmark solution. Even for a sample as small as $N = 100$, P_F^S is estimated within the same order of magnitude as the benchmark result.

To understand this matter better, the bias associated with ME-FM result is formally evaluated as a function of N. The normalized bias associated with an ME-FM estimate is defined as follows:

$$\text{Normalized Bias: } = \frac{1}{N_b} \sum_{i=1}^{N_b} \left(\frac{\hat{P}_{Fi}^S}{P_F^S} - 1 \right) \tag{4.21}$$

where, P_F^S denotes the MCS benchmark, $\widehat{P}_F^S$ is an ME-FM estimate, and $N_b = 500$ is the number of simulations used for the evaluation of bias.

Figures 4.12 shows the variation of the normalized bias with the sample size varying from $N = 100$ to 1000. It is rather remarkable that bias associated with ME-FM estimates is within 4% of the benchmark result. Based on this plot, $N = 500$ is quite reasonable sample to be used as input to ME-FM method.

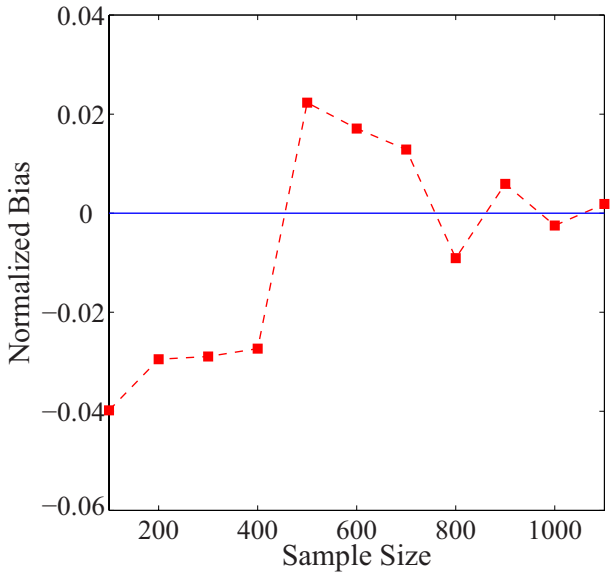

Figure 4.12: Normalized bias associated with ME-FM estimate versus sample size

4.4.4 Number of Fractional Moments

Another important question is that how many fractional moments should be used in the ME-FM method. This can be answered based on the convergence of the entropy of the estimated PDF with respect to the number of moments. Figure 4.13 shows typical, rapid convergence of the entropy as the number (m) of fractional moments exceeds 2. Since the entropy is practically constant for $m \geqslant 3$, it is sufficient to use three fractional moments in the ME-FM method.

4.4.5 Computational Efficiency

The evaluation of the system reliability by MC simulation method is a time consuming task. For example, MCS benchmark requires 884.5 seconds of CPU time. In contrast, ME-FM method

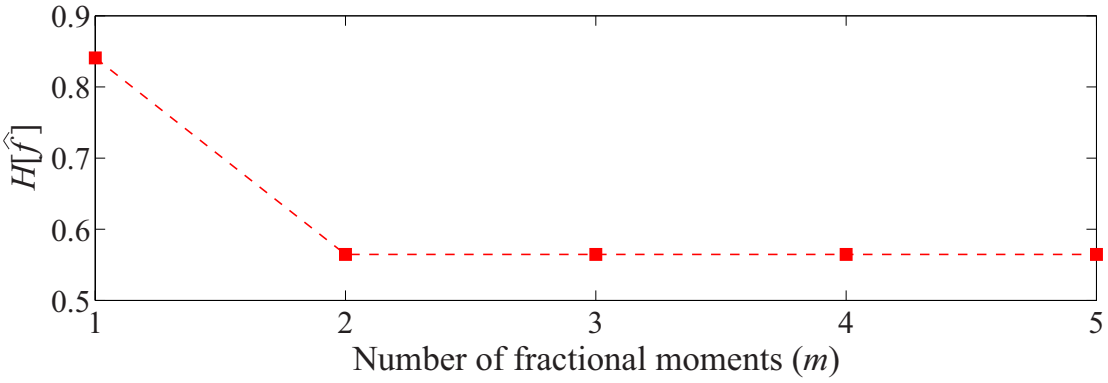

Figure 4.13: Estimated entropy versus the number of fractional moment

with 500 samples takes a very small fraction of CPU time, 5.8 seconds or 0.65%.

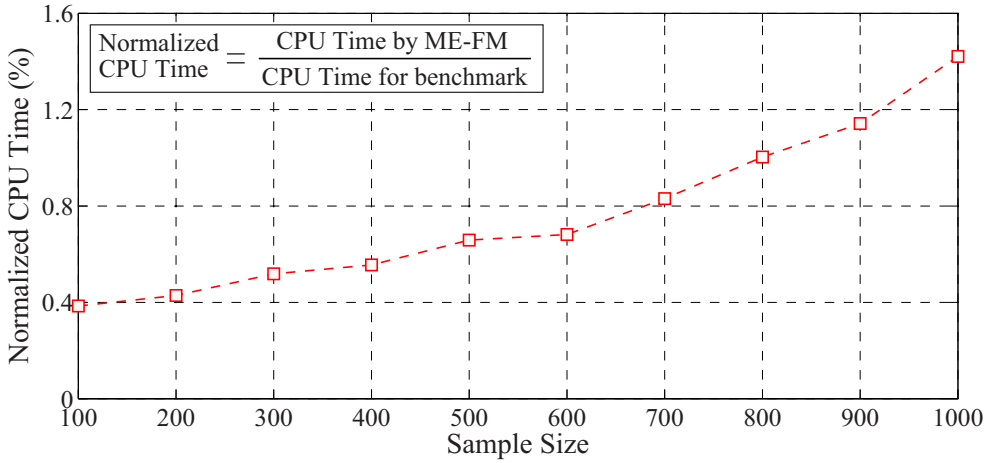

Figure 4.14: Normalized CPU time used by ME-FM Method

CPU time required by ME-FM method as a fraction of benchmark result is plotted in Figure 4.14 for different sample sizes. This plot substantiates extremely high computational efficiency of the proposed ME-FM method for system reliability computation.

4.5 Example of Planar Mechanisms

The section considers the using the ME-FM for the system reliability analysis of planar mechanisms, which are includes a slider-crank mechanism and a four-bar linkage. Objective of the section is further study the accuracy of ME-FM in reliability analysis of mechanism kinematics

as comparing with the methods of FOSM and FORM.

4.5.1 A Slider-Crank Mechanism

Background

The example of a slider-crank mechanism in Figure 4.15 is taken from Wang et al. (2011).

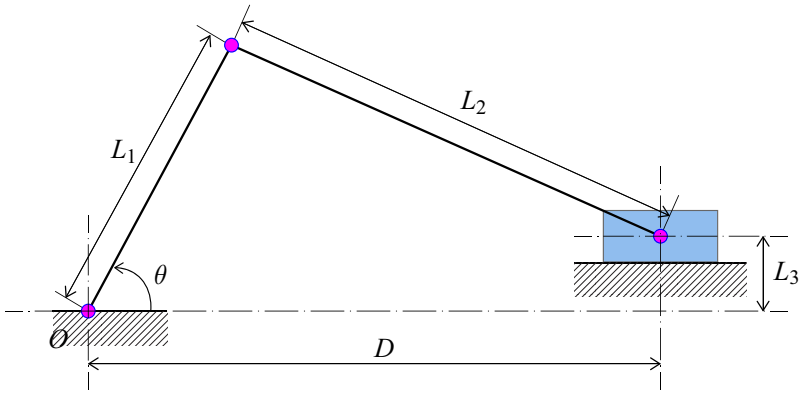

Figure 4.15: Kinematic model of a slider-crank mechanism

Governing equation for the displacement of slider can be defined as:

$$D^{\text{Ideal}}(\theta) = L_1\cos(\theta) + \sqrt{L_2^2 - [L_3 - L_1\sin(\theta)]^2} \tag{4.22}$$

To illustrate a specific example of the displacement of the slider, the following dimensional values are assumed: $L_1 = 80$ mm, $L_2 = 160$ mm and $L_3 = 50$ mm. The rotation angle θ was changed by varying from 0° to 360° with the step of 3.6°. The resulting displacement including 101 discrete points as shown in Figure 4.16.

Given a specific input angle, the displacement of the slider are basically the output targets for the functional consideration of the mechanism.

As presence of joint clearance, the radii of the bearing and journal are different as shown in Figure 4.17. Therefore, the actual displacement of slider with crank rotation angle θ_k will be

$$D(\mathbf{X},\theta_k) = P_1 + P_2 - P_3 + L_1\cos(\theta_k) + \sqrt{L_2^2 - [L_3 - L_1\sin(\theta_k) - Q_1 - Q_2 + Q_3]^2} \tag{4.23}$$

Limit state function for reliability analysis in terms of output error can be defined as

$$g(\mathbf{X},\theta_k) = r_0 - \text{abs}\big[D(\mathbf{X},\theta_k) - D^{\text{Ideal}}(\mathbf{X},\theta_k)\big] \quad (k = 1,2,\cdots,101) \tag{4.24}$$

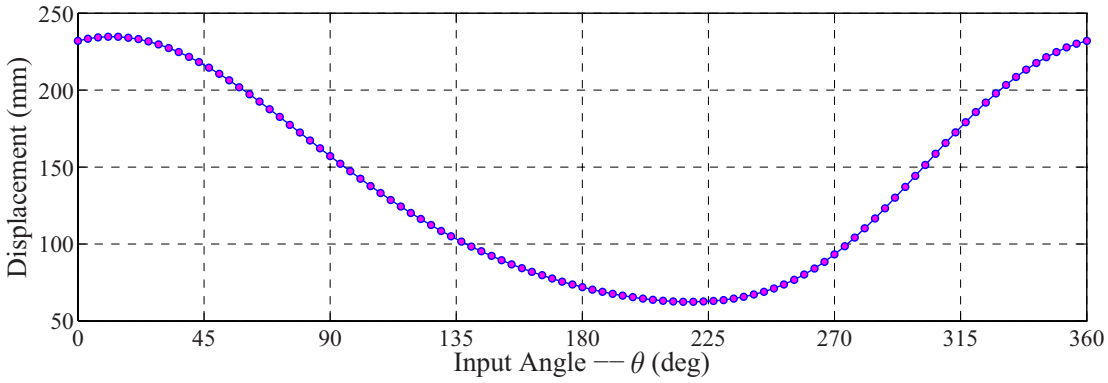

Figure 4.16: Target output of the slider-crank mechanism

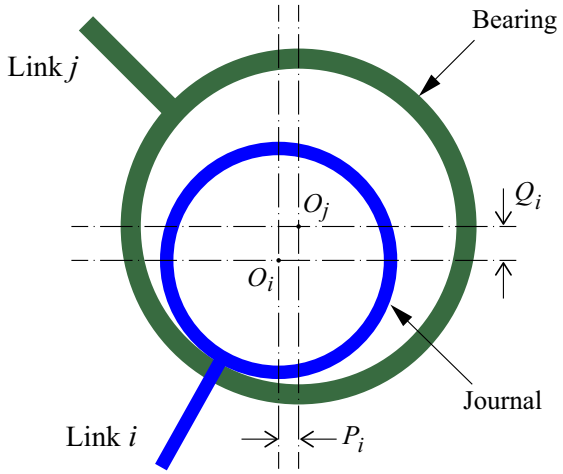

Figure 4.17: Joint clearance model of the slider-crank mechanism

where the probabilistic properties of random variable, $\mathbf{X}$, are summarized in Table 4.5.

In Table 4.5, random variable ε_θ indicates the uniform random error associated the crank rotation angle, θ, with the range of $\varepsilon_\theta \in [-0.1°, 0.1°]$. Therefore, the real input of the system will be $\widetilde{\theta} = \theta + \varepsilon_\theta$ due to the randomness in rotation angle of motor.

Figure 4.18 directs the scatter plot of the system maximum output error versus the corresponding input angle indicating the position of slider. This plot is based on results of $10,000$ simulations. It is interesting to observe that the occurrences of input angle for the system maximal output error has nearly covered the whole range of $[0°,\ 360°]$, with the modes of $\theta = 0°$ (or $360°$) and $\theta = 270°$, respectively. It means that focusing on the point reliability at a single point would not ensure achieving the same degree of reliability at other points of the trajectory. The need for system reliability analysis considering the dependency of failure events is justified.

Table 4.5: Probability distributions of random variables

Description	Variable	Distribution	Mean	Std.D	COV
Geometrical Dimension:	L_1 (mm)	Normal	80	0.8	0.01
	L_2 (mm)	Normal	160	1.6	0.01
	L_3 (mm)	Normal	50	0.5	0.01
Joint Clearance:	P_1 (mm)	Normal	0.1	0.001	0.01
	P_2 (mm)	Normal	0.1	0.001	0.01
	P_3 (mm)	Normal	0.1	0.001	0.01
	Q_1 (mm)	Normal	0.1	0.001	0.01
	Q_2 (mm)	Normal	0.1	0.001	0.01
	Q_3 (mm)	Normal	0.1	0.001	0.01
Angular Error:	ε_θ (deg)	Uniform	0	0.058	—

MaxEnt Distribution

Firstly, the empirical distribution of maximum displacement error was obtained from the Monte Carlo method in which a large sample of (10^6) displacement errors was simulated. This solution is referred to as the benchmark result, which is used to evaluate the accuracy of the proposed ME-FM method.

The parameters of the MaxEnt distribution, namely, the fractional exponents (α_k) and the Lagrange multipliers (λ_k) are given in Table 4.6. These parameters were computed using a sample of $N = 500$ simulated values of the maximum displacement error as per the procedure

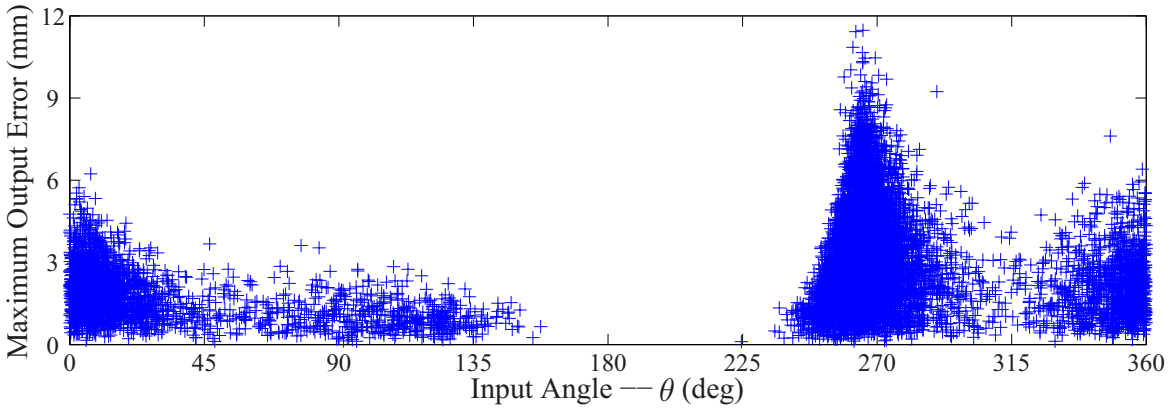

Figure 4.18: Scatter plot of system maximum error versus the occurrence input angle

shown in Figure 4.6.

Table 4.6: MaxEnt PDF of the maximum displacement error

Entropy	k	0	1	2	3
1.8160	λ_k	9.9071	−18.498	6.7936	3.3358
	α_k	−−	0.3552	0.6362	0.4199
Moments	$\widehat{M}_Y^{\alpha_k}$	−−	1.3744	1.8311	1.4645

Probability distribution of the maximum displacement error obtained from ME-FM and MCS methods are compared in Figures 4.19. A close agreement between ME-FM and MCS results confirms the validity of the proposed approach.

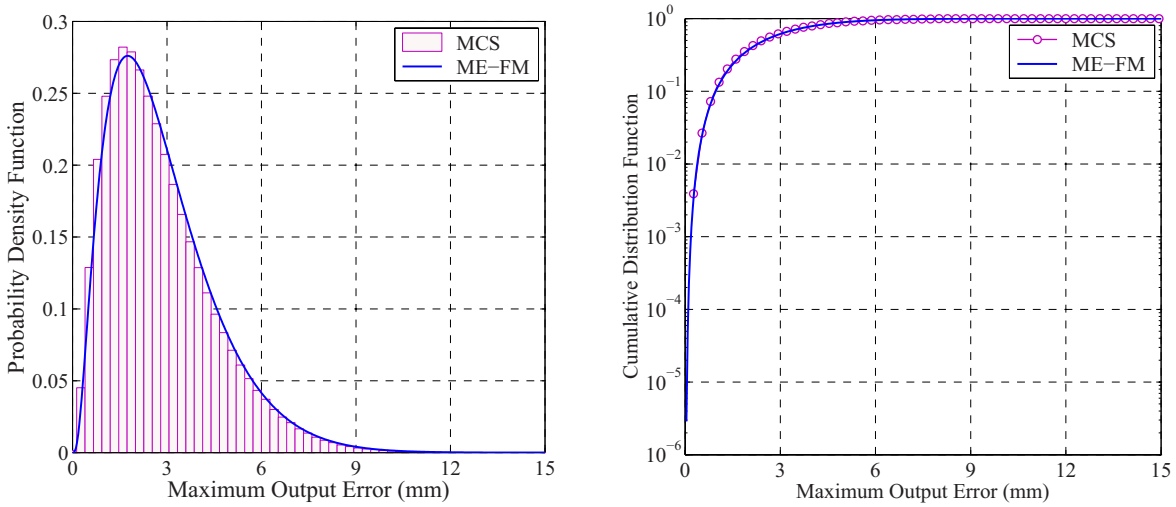

(a) Probability Density Function

(b) Cumulative Distribution Function

Figure 4.19: Distribution of the maximum displacement error of the slider-crank mechanism

System failure probability of the slider-crank mechanism can be easily estimated from the distribution of the maximum displacement error. First-order second moment (FOSM) method and the first-order reliability method (FORM) as used in literature, here, are employed to compare the accuracy. Together with the benchmark provided from crude Monte Carlo simulation (MCS), the estimated system failure probabilities of the planar mechanism are depicted in Figure 4.20. Functional evaluations of each method are listed in Table 4.7.

As depicted in Figure 4.20, it is seen that the distribution of maximum error determined by ME-FM is closed to the benchmark results of Monte Carlo simulation. Given the error threshold

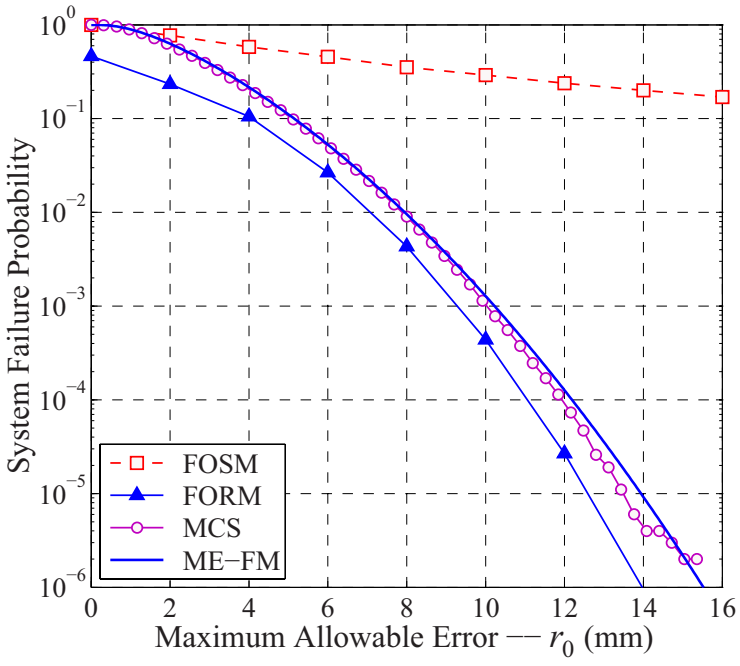

Figure 4.20: System failure probability of the slider-crank mechanism

Table 4.7: Number of functional calls of each method

Method	FOSM	FORM	ME-FM	Monte Carlo simulation
Number of Functional Calls	10	5719	500	10^6

$r_0 = 9.0$ mm, the probability of output error of the mechanism exceeding the value is determined as 3.256×10^{-3} by ME-FM, whereas the MCS method provides a close estimate of 3.359×10^{-3}. Furthermore, the inaccuracy associated with FOSM and FORM is further confirmed the limitations of gradient-based methods in system reliability analysis. ME-FM used 500 samples to calculate the distribution of the system maximum error. Compared with the crude MCS and other techniques, the proposed approach is reliably to estimate the mechanism system reliability analysis with the moderated computational cost.

4.5.2 A Four-Bar Linkage Mechanism

Background

The example consider a four-bar linkage as shown in Figure 4.21. Given the lengths of linkage $\mathbf{L} = [L_1, L_2, L_3, L_4]^{\mathrm{T}}$ and input angle θ, the analytical expression of $\varphi(\theta)$ can be determined as

(Myszka, 2012; Sandor and Erdman, 1984) :

$$\varphi(\theta) = \begin{cases} \pi - \phi(\theta) - \gamma(\theta) & \text{if } 0 \leqslant \theta \leqslant \pi \\ \pi - \phi(\theta) + \gamma(\theta) & \text{if } \pi \leqslant \theta \leqslant 2\pi \end{cases} \tag{4.25}$$

where $S = \sqrt{L_1^2 + L_2^2 - 2L_1L_2\cos(\theta)}$, $\phi(\theta) = \cos^{-1}\left(\frac{L_4^2+S^2-L_3^2}{2L_4S}\right)$, $\gamma(\theta) = \cos^{-1}\left(\frac{L_1^2+S^2-L_2^2}{2L_1S}\right)$.

In the example, the operating angle θ is discretized as $\theta = [97° : 1° : 217°]$. The system reliability analysis involves 121 limit state functions. Random variables, $\mathbf{X}$, are given in Table 4.8. The limit state function for the system reliability analysis is

$$g(\mathbf{X}) = r_0 - \max\left\{r(\mathbf{X},\theta_1), r(\mathbf{X},\theta_2), \cdots, r(\mathbf{X},\theta_b)\right\} \quad (b = 121) \tag{4.26}$$

where $r(\mathbf{X},\theta_k) = \text{abs}\left[\varphi(\mathbf{X},\theta_k) - \varphi^{\text{Ideal}}(\theta_k)\right]$. Parameters of the MaxEnt PDF, namely, the frac-

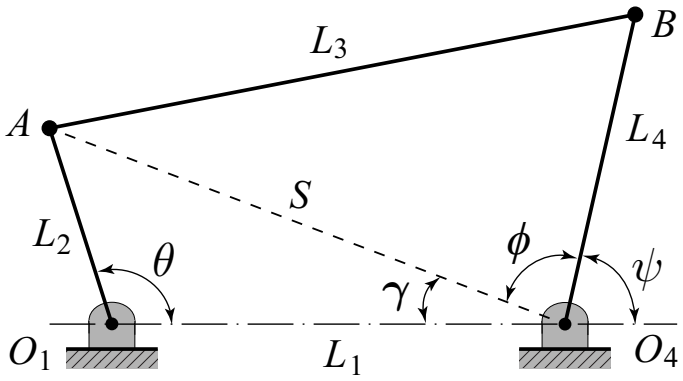

Figure 4.21: Model of a four-bar linkage (Zhang and Du, 2011)

Table 4.8: Statistical distributions of random variable

Description	Variable	Distribution	Mean	Std.D
Geometric Dimensions:	L_1 (mm)	Normal	100	0.10
	L_2 (mm)	Normal	55.5	0.0555
	L_3 (mm)	Normal	144	0.144
	L_4 (mm)	Normal	72.5	0.0725
Angular Error:	ε_θ (deg)	Uniform	0	$1/\sqrt{3}$

tions (α_k) and the Lagrange multipliers (λ_k) are given in Table 4.9. Distribution for the maximum

Table 4.9: MaxEnt PDF of maximum output error in the four-bar linkage

Number of FMs	Entropy	k	0	1	2	3	4
$m = 3$	0.0572	λ_k	12.514	0.9191	−12.744	0.3175	−−
		α_k	−−	5.6594	−0.0457	−0.6800	−−
	Moments	$\widehat{M}_Y^{\alpha_k}$	−−	0.16103	1.0452	2.2395	−−
$m = 4$	−0.0554	λ_k	−94.797	73.446	−37.297	35.210	24.466
		α_k	−−	−0.0490	2.5373	2.7592	0.2937
	Moments	$\widehat{M}_Y^{\alpha_k}$	−−	1.0486	0.2636	0.2484	0.7732

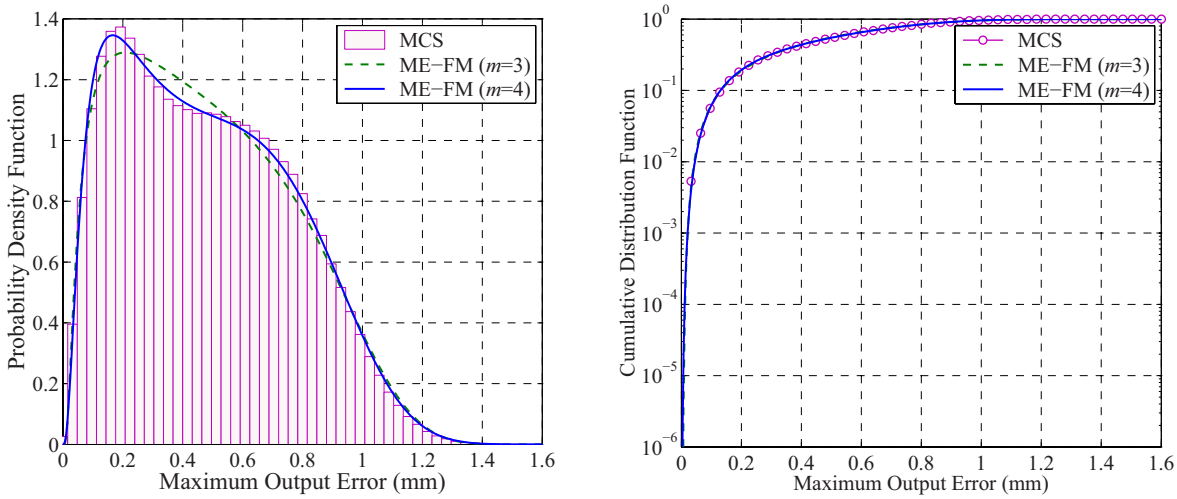

(a) Probability Density Function

(b) Cumulative Distribution Function

Figure 4.22: Distribution of the maximum error for the output angle $\varphi(\mathbf{X})$

output error obtained from MaxEnt and MCS methods are compared in Figures 4.22. A close agreement between MaxEnt and MCS results confirms the validity of the proposed approach.

System reliability of the four-bar function generator was depicted in Figure 4.23 by using the methods of ME-FM, FOSM and FORM, together with the benchmark estimated by crude simulation with 10^6 samples. It is clear to see the proposed method of ME-FM with four fractional moments has shown its advantage in the calculation of system failure probability. Linear scale graph on the estimated probability of exceedance versus the allowable threshold of output errors is shown in Figure 4.23(a), which has shown the results determined by FOSM and FORM are strongly deviated from benchmark. Comparatively, the close agreement between ME-FM and MCS further validates the accuracy of the proposed method in mechanism system reliability

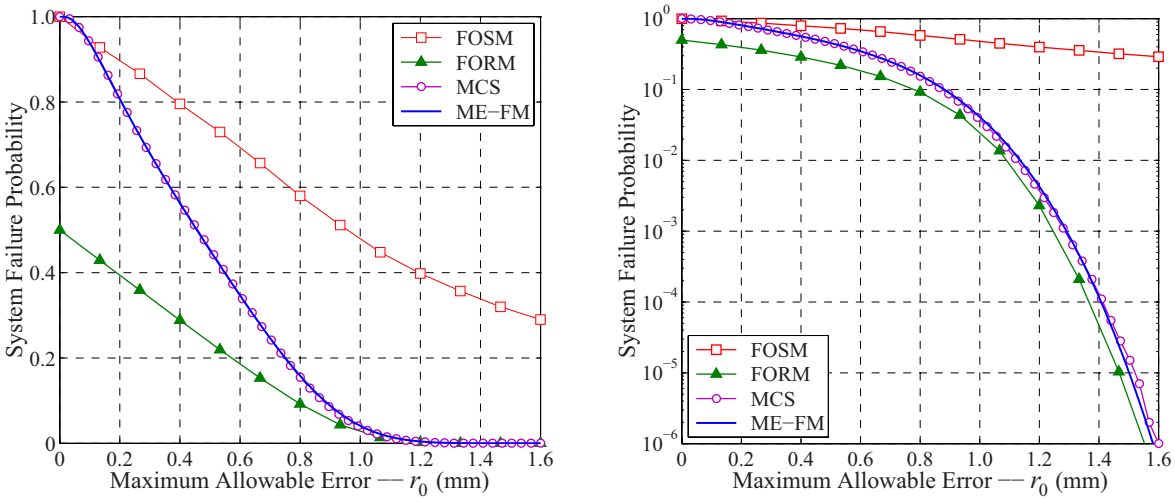

(a) Linear Scale

(b) Semi-log Scale

Figure 4.23: System failure probability of the four-bar mechanism with various methods

analysis. Given the semi-log scale of POEs in Figure 4.23(b), one can easily determine the mechanism system reliability. Taken the error threshold $r_0 = 1.2$ deg as an example, the probability of exceeding this value can be obtained as 3.891×10^{-3} by ME-FM, whereas the MCS method provides a close estimate of 3.834×10^{-3}.

4.6 Conclusion

The Chapter focuses on developing an efficient and accurate computation of system reliability of robotic manipulators with randomness in joint clearances and dimensions of links. Here, reliability is defined as the probability that the positional error of the end effector remains less than a specified design limit in an entire trajectory of interest. In the literature, this problem is also known as cumulative reliability analysis of the manipulator (or function generator).

The study shows that this problem is analogous to reliability of a series system that can be conveniently formulated in terms of an extreme event distribution of the positional error. Based on the principle of maximum entropy (MaxEnt), the Chapter presents an innovative method for the evaluation of the distribution of maximum positional error. Firstly, input variables, viz, random joint clearances and link dimensions, are simulated from their known distributions. For each set of simulated input, trajectories of the manipulator are computed using an appropriate

kinematic model. Finally, the maximum positional error of the effector is calculated as maximum difference between the simulated trajectory and that required by the design (without randomness).This simulated sample of positional error is a starting point of the proposed method, referred to as ME-FM method.

Realizing limitations of the use of integer order moments with MaxEnt, the study uses fractional moments that are computed from a small, simulated sample of maximum error. A novel aspect of this method is that the fractions for these moments need not be fixed a priori. Rather, the fractions as well as the Lagrangian parameters of the MaxEnt distribution are derived by the minimization of a divergence measure. This approach has proved to be extremely efficient in extracting information from a small sample of random observations.

The first example studied the system reliability analysis of a space elbow manipulator. A benchmark estimate of reliability is computed from Monte Carlo simulations with 10^6 samples. The reliability estimated from ME-FM method, based on 500 simulated samples and 3 fractional moments, is almost identical to the benchmark result. In addition to accuracy, the most remarkable point of ME-FM method is extremely high computational efficiency. The CPU time taken by this method is less than 1% of that required to calculate the benchmark result. Assessment of bias also confirms high accuracy of ME-FM method.

Two additional planar mechanisms of slider-crank and four-bar linkage were employed to confirm the accuracy of the ME-FM as comparing the first-order reliability method (FORM) and the first-order second moment (FOSM) method. With the benchmark provided by Monte Carlo simulation, the proposed approach can accurately estimate a system failure probability in the orders of 10^{-3} or less. The inaccuracy associated with FOSM and FORM is further confirmed the limitations of gradient-based methods in system reliability analysis.

In summary, the proposed entropy-based approach is generic and it provides an alternate and efficient way to analyze a wider class of system reliability problems that are computationally intensive due to large dimensions and implicit performance functions.

Chapter 5

Multiplicative Dimensional Reduction Method

5.1 Introduction

5.1.1 Background

The reliability analysis of an engineering system, structure or component is typically based on a model that describes system's response, such as deformation, as a function of applied loads, operating environment, material properties and geometry or configuration. For sake of simplicity, the response is denoted by a scaler random variable $Y = \eta(\mathbf{X})$, and $\mathbf{X}$ denotes a vector of random variables used to model uncertain variables that influence system's response. The probability of failure, P_F, is defined as the probability of response being in a domain of unacceptable operation, such as response (e.g. deformation) exceeding a critical threshold, y_c. It is typically defined in terms of a limit state function,

$$g(\mathbf{X}) = y_c - \eta(\mathbf{X}) \tag{5.1}$$

such that $P_F = \Pr\left[g(\mathbf{X}) \leqslant 0\right]$. In principle, this problem can be solved if the cumulative probability distribution of the response, $F_Y(y)$, can be evaluated either analytically, empirically or numerically. Once the distribution is available, $P_F = 1 - F_Y(y_c)$.

Analytical derivation of the distribution of a function of random variables is feasible only in very simplified cases and it is intractable in a general setting. An empirical approach based on actual failure data is not possible for highly reliable systems. Numerical approach based on

the Monte Carlo simulations (MCS) or its optimized versions, such as importance sampling, provides a viable alternative for reliability computation. It is however a well known fact that the simulation-based approach becomes tedious if the time and efforts required to compute the response function is large. For this reason, approximate methods like the First-Order Reliability Method (FORM) are widely used in engineering risk and reliability analysis (Breitung, 1984; Der Kiureghian et al., 1987; Hasofer and Lind, 1974). However, FORM lacks generality especially when the response is a complex and implicit function of many random variables (Koutsourelakis et al., 2004; Schuëller, 2001; Schuëller and Pradlwarter, 2007, 2009). In summary, two key issues in the reliability evaluation are to:

- minimize the number of function evaluations; and
- fit the most appropriate probability distribution to the response function.

The method of moment has been the most popular semi-analytical method to find an approximate solution of this problem. The idea is to calculate the first four moments of the response $Y = \eta(\mathbf{X})$ or the limit state function $g(\mathbf{X})$, which are mean, variance, skewness and kurtosis. Given the moments, back calculate the parameters of the distribution that is assumed to represent the response. For example, Pearson and Johnson system (Hong, 1996; Zhao and Ono, 2001)or generalized Lambda distribution (Ramberg and Schmeiser, 1974) can be used.

Since the inverse problem of deriving the probability distribution of a random variable from a finite number of moments has no unique solution (Stuart and Ord, 1994), researchers have resorted to heuristics to assume a parametric distribution for the response. The assumption of the distribution type is a rather contentious one from both philosophical and practical points of view. The reasons are that the tail probabilities tend to be very sensitive to parametric form and assigning a parametric form implies adding spurious information to the inference.

Moment computation of a function about multiple random variables is not an easy task. For example, to evaluate an n-dimensional integration with N-point scheme, N^n evaluations of $Y = \eta(\mathbf{X})$ are required, which is a prohibitively expensive task for a complex function. Many researchers focussed on efficient evaluation of moments. The point estimate method (Hong, 1998; Rosenblueth, 1981; Seo and Kwak, 2002; Taguchi, 1978) the Taylor series approximation and non-classical orthogonal polynomial (Kennedy and Lennox, 2000) are examples of some the methods.

The most notable and recent effort is the use of high dimensional model representation (HDMR), in which a function is decomposed in terms of functions increasing dimensions (Li

et al., 2001; Rabitz and Aliş, 1999). It is generally truncated to the one dimensional functions and the evaluation is further simplified by using the cut-point HDMR method (Rahman and Xu, 2004). In this formulation, the number of function evaluations are significantly reduced to nN from N^n. Based on these ideas, two steps approach can be formulated, i.e., the HDMR was used to compute economically the moments at first, and then employed MaxEnt to derive the distribution and carry out subsequent reliability analysis (Li and Zhang, 2011).

5.1.2 Objective

Objective of the Chapter is to:

- propose an efficient method to compute fractional moments of a generic structural response function;
- compute probability distribution of a system response for structural reliability analysis.

A natural extension of fractional moments to estimate the distribution of response function is a key motivation for this study. Recognizing that the computation of fractional moments is not possible using the conventional HDMR, a new multiplicative form of dimensional reduction method has been developed.

5.1.3 Organization

Organization of the Chapter is as follows. Section 5.2.1 reviews the development of high-dimensional model representation with an additive form of a series lower hieratical functions, which is referred to as the conventional dimensional reduction method (C-MDR). Then, a novel multiplicative dimensional reduction method (M-DRM) is derived to approximate the original complex input-output relation. The development of M-DRM is based on the formulation of the conventional high-dimensional model representation. However, its unique properties on the definition of cut-component functions is discussed in Section 5.2.3. One of merits of use M-DRM over C-DRM is in moment calculation. A numerical method is presented in Section 5.3 to calculate the moment (integer and fraction) of a generic function with multiple input variables. With the principle of maximum entropy (MaxEnt), output distribution of the system function can be derived with the fractional moment constraints. To demonstrate the applications of the proposed method for moment calculation, estimation of output distribution, and reliability analysis

of structural systems, three mathematics examples in Section 5.4, three structural examples in Section 5.5 are illustrated and verified by Monte Carlo simulation with 10^6 samples. Section 5.6 summarizes the Conclusions.

5.2 Modeling of System Response Function

The analysis of input uncertainty propagating through a physical system, the dealing with a complex and implicit function of several random variables is always a challenging problem that has received considerable attention from the research community. Numerical approach based on Monte Carlo simulations (MCS) or its optimized versions, such as importance sampling (Bucher, 1988; Harbitz, 1983; Helton and Davis, 2003; Melchers, 1990), provides a viable alternative for reliability computation. It is however a well known fact that the simulation-based approach becomes tedious if the time and efforts required to compute the response function is large. Another approach to deal with this problem is to approximate the actual input-output relation by a simple surrogate model (Montgomery and Myers, 2002). Although there is vast literature in statistics related to response surface modeling, here the attention is focussed on one recent development called the high-dimensional model representation (Li et al., 2001; Rabitz and Aliş, 1999) or dimensional reduction method (Rahman and Xu, 2004; Xu and Rahman, 2004) in literature.

5.2.1 Conventional Dimensional Reduction Method

The key idea is to express a high-dimensional function as a sum of functions of lower order in an increasing hierarchy as

$$\eta(\mathbf{x}) = \eta_0 + \sum_{i=1}^{n} \eta_i(x_i) + \sum_{1 \leqslant i < j \leqslant n} \eta_{ij}(x_i, x_j) + \cdots \tag{5.2}$$

Two routines of HDMR were developed according to the definition of lower dimensional functions, i.e., random sampling HDMR (RS-HDMR) and Cut-HDMR. One can refer to literature (Li et al., 2001; Rabitz and Aliş, 1999) for details.

In RS-HDMR, the component functions in Eq.(5.2) are defined in general by the following conditional expectations

$$\eta_0 = E[\eta(\mathbf{x})], \quad \eta_i(x_i) = E_{-i}[\eta(\mathbf{x})] - \eta_0, \quad \cdots \tag{5.3}$$

where the notation E_{-i} means the expectation operation over all the variables except the random variable X_i, one can refer to Chapter 6 (i.e., on global sensitivity analysis) for details on the formulations of conditional expectation. It is clear that the evaluation of the univariate (variance) component functions requires integration over $n-1$ dimensions, which can be a fairly involved task in case of a complex function.

The study develops an approximation of original input-output relation based on the method of Cut-HDRM. The cut-component functions in Cut-HDRM are evaluated about a specific reference point, named as the cut-point or anchor point in literature, $\boldsymbol{c} = [c_1, c_2, \cdots, c_n]^{\mathrm{T}}$:

$$\begin{cases} \eta_0 = \eta(\boldsymbol{c}) \\ \eta_i(x_i) = \eta(c_1, \cdots, c_{i-1}, x_i, c_{i+1}, \cdots, c_n) - \eta_0 \\ \eta_{ij}(x_i, x_j) = \eta(c_1, \cdots, c_{i-1}, x_i, c_{i+1}, \cdots, c_{j-1}, x_j, c_{j+1}, \cdots, c_n) - \eta_i(x_i) - \eta_i(x_j) - \eta_0 \\ \quad \cdots \end{cases} \tag{5.4}$$

One should note that:

$$\begin{cases} \eta_i(x_i) \neq \eta(c_1, \cdots, c_{i-1}, x_i, c_{i+1}, \cdots, c_n) \\ \eta_{ij}(x_i, x_j) \neq \eta(c_1, \cdots, c_{i-1}, x_i, c_{i+1}, \cdots, c_{j-1}, x_j, c_{j+1}, \cdots, c_n) \\ \quad \cdots \end{cases} \tag{5.5}$$

To distinguish the univariate function, $\eta(c_1, \cdots, c_{i-1}, x_i, c_{i+1}, \cdots, c_n)$, from the univariate cut-component function, $\eta_i(x_i)$, we denote:

$$\begin{cases} \eta(x_i, \boldsymbol{c}_{-i}) = \eta(c_1, \cdots, c_{i-1}, x_i, c_{i+1}, \cdots, c_n) \\ \eta(x_i, x_j, \boldsymbol{c}_{-ij}) = \eta(c_1, \cdots, c_{i-1}, x_i, c_{i+1}, \cdots, c_{j-1}, x_j, c_{j+1}, \cdots, c_n) \\ \eta(x_i, x_j, x_k, \boldsymbol{c}_{-ijk}) = \eta(c_1, \cdots, c_{i-1}, x_i, c_{i+1}, \cdots, c_{j-1}, x_j, c_{j+1}, \cdots, c_{k-1}, x_k, c_{k+1}, \cdots, c_n) \\ \quad \cdots \end{cases} \tag{5.6}$$

The properties of the cut-component function defined in Eq(5.4) can be summarized as follows:

Property 5.1. *A cut-component function of Cut-HDMR vanishes when any of its own variables takes the value of the corresponding element in cut-point* $\boldsymbol{c}$*, i.e.,*

$$\eta_{i_1 i_2 \cdots i_s}(x_{i_1}, x_{i_2}, \cdots, x_{i_s})\big|_{\boldsymbol{x}=\boldsymbol{c}} = 0 \quad \{i_1, i_2, \cdots, i_s\} \subset \{1, 2, \cdots, n\} \tag{5.7}$$

Property 5.2. *Orthogonality between the arbitrary two different cut-component functions can be derived by:*

$$\eta_{i_1\cdots i_p}(x_{i_1},\cdots,x_{i_p})\eta_{j_1\cdots j_p}(x_{j_1},\cdots,x_{j_q})\big|_{\boldsymbol{x}=\boldsymbol{c}} = 0 \quad \{i_1,\cdots,i_p\} \neq \{j_1,\cdots,j_q\} \tag{5.8}$$

Therefore, the cut-component functions in Eq.(5.4) are an orthogonal basis of $\mathbb{R}^n$, which the exact decomposition of a physical model, $y = \eta(\mathbf{x})$, with the form of Eq.(5.2) can be attained.

According to the principle of sparsity (Montgomery and Myers, 2002), for a sufficiently smooth function, the influence of higher-order terms in Eq.(5.2) is much smaller than the univariate terms, $\eta_i(x_i)$. This results in a simple representation of response function by retaining only up to the univariate functions (Rahman and Xu, 2004):

$$\eta(\mathbf{x}) \approx \sum_{i=1}^{n} \eta(c_1,\cdots,c_{i-1},x_i,c_{i+1},c_n) - (n-1)\eta(\boldsymbol{c}) \tag{5.9}$$

This approach is also referred to as the conventional DRM (C-DRM) in this Chapter. As the high-order terms make the significant contribution in the response function, $y = \eta(\mathbf{x})$, the bivariate C-DRM, then, can be used:

$$\eta(\mathbf{x}) \approx \sum_{1\leqslant i<j\leqslant n} \eta(x_i,x_j,\boldsymbol{c}_{-ij}) - (n-2)\sum_{i=1}^{n}\eta(x_i,\boldsymbol{c}_{-i}) + \frac{(n-1)(n-2)}{2}\eta(\boldsymbol{c}) \tag{5.10}$$

In general, approximation about the original input-output relation with an s-variate DRM was determined as (Xu and Rahman, 2004)

$$\eta(\mathbf{x}) \approx \sum_{k=0}^{s}(-1)^{s-k}\binom{n-k-1}{s-k} \sum_{1\leqslant i_1<\cdots<i_k\leqslant n} \eta(x_{i_1},x_{i_2},\cdots,x_{i_k},\boldsymbol{c}_{-i_1i_2\cdots i_k}) \tag{5.11}$$

Regarding the approximation errors of C-DRM, the zeroth-order function, $\eta(\boldsymbol{c})$, is a constant representing the system response evaluated at the cut-point. The univariate model in Eq.(5.9) gives the approximation of response function with the residual error of two and higher component functions. Therefore, the reminding error of a general s-variate model contains the terms of $s+1$ dimensions and higher. All terms of s- and lower-variate component functions are included in the approximation, which generally provides a more accurate approximation of $y = \eta(\mathbf{x})$ than the truncated models derived from the first- or second-order Taylor series in literature.

One best advantages of C-DRM is seen in the calculation of integer moments of a response function, because the high-dimensional moment integration can be accurately approximated by using the low-dimensional integrals (Xu and Rahman, 2004).

Taken a k^{th} moment calculation of $Y = \eta(\mathbf{X})$ as an example, using the univariate C-DRM, the moment can be approximated by

$$E\left[Y^k\right] = E\left\{\left[\eta(\mathbf{X})\right]^k\right\} \approx E\left\{\left[\sum_{i=1}^{n}\eta(X_i, \boldsymbol{c}_{-i}) - (n-1)\eta(\boldsymbol{c})\right]^k\right\} \tag{5.12}$$

which has shown that the original n-dimensional tedious multi-dimensional integration can be efficiently approximated by using n univariate integrals.

5.2.2 Proposed Multiplicative Dimensional Reduction Method (M-DRM)

In C-DRM, the dimensional reduction of a response function is carried out in the original space. In this section, it is proposed to apply the logarithmic transform of the response function, i.e., $\log[\eta(\mathbf{x})]$, which drives a multiplicative form approximate model of the original function.

Univariate M-DRM

Consider a general response function, $y = \eta(\mathbf{x})$. By using the logarithmic transformation, one can obtain:

$$\varphi(\mathbf{x}) = \log(y) = \log\left[\eta(\mathbf{x})\right] \tag{5.13}$$

Following the univariate C-DRM in Eq.(5.9), an approximation of $\varphi(\mathbf{x})$ can be written as

$$\varphi(\mathbf{x}) \approx \sum_{i=1}^{n}\varphi(x_i, \boldsymbol{c}) - (n-1)\varphi_0 \tag{5.14}$$

where the functions can be related to those in the original space as follows:

$$\begin{cases} \varphi_0 = \log(\eta_0) \\ \varphi(x_i, \boldsymbol{c}_{-i}) = \log\left[\eta(c_1, \cdots, c_{i-1}, x_i, c_{i+1}, c_n)\right] \\ \varphi(x_i, x_j, \boldsymbol{c}_{-ij}) = \log\left[\eta(c_1, \cdots, c_{i-1}, x_i, c_{i+1}, \cdots, c_{j-1}, x_j, c_{j+1}, \cdots c_n)\right] \\ \quad \cdots \end{cases} \tag{5.15}$$

By inverting the transformation, the original function can be written as:

$$\begin{aligned} \exp\left[\varphi(\mathbf{x})\right] &\approx \exp\left(\sum_{i=1}^{n}\varphi(c_1, \cdots, c_{i-1}, x_i, c_{i+1}, c_n) - (n-1)\varphi_0\right) \\ &= \exp\left[(1-n)\varphi_0\right] \times \exp\left(\sum_{i=1}^{n}\varphi(c_1, \cdots, c_{i-1}, x_i, c_{i+1}, c_n)\right) \end{aligned} \tag{5.16}$$

Substituting for the expressions from Eq.(5.15) into Eq.(5.16) leads to a multiplicative approximate of the response function:

$$\eta(\mathbf{x}) \approx [(\eta(\boldsymbol{c})]^{1-n} \prod_{i=1}^{n} \eta(c_1, \cdots, c_{i-1}, x_i, c_{i+1}, \cdots, c_n) \tag{5.17}$$

This approximate model of original input-output relation is referred to as the univariate multiplicative dimensional reduction method (M-DRM) in this document.

General M-DRM

As discussed in previous section, the univariate M-DRM, in some cases, might be not enough to represent the original input-output relation precisely. In this scenario, bivariate M-DRM can be developed.

Given the procedures in Eqs.(5.13) to (5.17), uses the bivariate C-DRM to approximate $\phi(\mathbf{x})$ instead of the univariate model in Eq.(5.14). One can easily derive the approximate model of bivariate M-DRM:

$$\eta(\mathbf{x}) \approx \frac{\left[\eta(\boldsymbol{c})\right]^{\frac{(n-1)(n-2)}{2}} \times \prod_{i=1}^{n-1} \prod_{j=i+1}^{n} \eta(c_1, \cdots, c_{i-1}, x_i, c_{i+1}, \cdots, c_{j-1}, x_j, c_{j+1}, \cdots, c_n)}{\left[\prod_{i=1}^{n} \eta(c_1, \cdots, c_{i-1}, x_i, c_{i+1}, \cdots, c_n)\right]^{n-2}} \tag{5.18}$$

In general, applying the s-variate C-DMR, the corresponding s-variate M-DRM can be obtained as

$$\eta(\mathbf{x}) \approx \frac{\prod\limits_{k_1=s,s-2,s-4,\cdots} \left[\prod\limits_{i_1=1}^{n-k_1+1} \cdots \prod\limits_{i_{k_1}=i_{k_1-1}+1}^{n} \eta(x_{i_1}, x_{i_2}, \cdots, x_{i_{k_1}}, \boldsymbol{c})\right]^{\binom{n-k_1-1}{s-k_1}}}{\prod\limits_{k_2=s-1,s-3,s-5,\cdots} \left[\prod\limits_{j_1=1}^{n-k_2+1} \cdots \prod\limits_{j_{k_2}=j_{k_2-1}+1}^{n} \eta(x_{j_1}, x_{j_2}, \cdots, x_{j_{k_2}}, \boldsymbol{c})\right]^{\binom{n-k_2-1}{s-k_2}}} \tag{5.19}$$

When $s = 1$, the method degenerates to the univariate M-DRM in Section 5.2.2. When $s = 2$, the method becomes the bivariate M-DRM. Similarly, trivariate, quadrivariate, and other higher-variate M-DRMs can be derived by appropriately selecting the value of s. In the limit, when $s = n$, there is no approximation and the proposed method converges to the exact solution.

Note that the limit state function in system reliability analysis is not smooth due to the multi-fold maximum and/or minimize operators. The study proposes that using the bivariate M-DRM to approximate the nonlinear response function. A general probability distribution using the fractional moments and MaxEnt is derived to calculate the system failure probability as shown in later section.

5.2.3 Remarks on Cut-Component Function

M-DRM is proposed in the Chapter to decompose a physical model in the logarithmic space. Corresponding to the original space, $\varphi(\mathbf{x}) = \log[\eta(\mathbf{x})]$ (assume that $\eta(\mathbf{x})$ is always positively defined, or else one should use the absolute operator), now, is considered to be exactly decomposed.

To distinguish the cut-component functions of M-DRM with the low-variate functions in Eq.(5.15), we use $h(\cdot)$ to expression the cut-component functions:

$$\begin{cases} h_0 = \log[\eta(\boldsymbol{c})] \\ h_i(x_i) = \log\left(\dfrac{\eta(c_1,\cdots,c_{i-1},x_i,c_{i+1},\cdots,c_n)}{\eta(\boldsymbol{c})}\right) \\ h_{ij}(x_i,x_j) = \log\left(\dfrac{\eta(\boldsymbol{c})\times\eta(c_1,\cdots,c_{i-1},x_i,c_{i+1},\cdots,c_{j-1},x_j,c_{j+1},\cdots,c_n)}{\eta(c_1,\cdots,c_{i-1},x_i,c_{i+1},\cdots,c_n)\times\eta(c_1,\cdots,c_{j-1},x_j,c_{j+1},\cdots,c_n)}\right) \\ \quad\cdots \end{cases} \tag{5.20}$$

It is seen that, $h_0 = \varphi_0$, $h_i(x_i) = \varphi(x_i,\boldsymbol{c}) - h_0$, $h_{ij}(x_{ij}) = \varphi(x_i,x_j,\boldsymbol{c}) - \varphi(x_i,\boldsymbol{c}) - \varphi_j(x_j,\boldsymbol{c}) - h_0$, etc. Therefore, except the constant, h_0, the cut-component functions do not directly apply for the logarithmic operator with respect to the counterpart in C-DRM. Take the univariate cut-component function as an example. In C-DRM, it is shown in Eq.(5.4) as:

$$\eta_i(x_i) = \eta(c_1,\cdots,c_{i-1},x_i,c_{i+1},\cdots,c_n) - \eta(\boldsymbol{c}) \quad (i = 1,2,\cdots,n) \tag{5.21}$$

If use the logarithmic transformation, one can obtain:

$$\log[\eta_i(x_i)] = \log[\eta(c_1,\cdots,c_{i-1},x_i,c_{i+1},\cdots,c_n) - \eta(\boldsymbol{c})] \tag{5.22}$$

The function is undefined with the limited boundaries at the cut-point, $x_i = c_i$, since that $\eta_i(x_i)\big|_{x_i=c_i} = 0 \Longrightarrow \lim\limits_{x_i\to c_i}\left\{\log[\eta_i(x_i)]\right\} = \infty$. More importantly, it is easy to prove that the

orthogonal properties in Eq.(5.7) and Eq.(5.8) are no long satisfied after applying the logarithmic transformation of the cut-component functions of C-DRM.

The study proposes the cut-component functions of M-DRM as shown in Eq.(5.20). It can be seen that:

Property 5.3. *The cut-component functions of M-DRM are zero-valued at the cut-point* $\boldsymbol{c}$*:*

$$h_{12\cdots s}(x_1, x_2, \cdots, x_s)\big|_{\boldsymbol{x}=\boldsymbol{c}} = \log(1) = 0 \quad \{1, 2, \cdots, s\} \subset \{1, 2, \cdots, n\} \tag{5.23}$$

Property 5.4. *Any two different cut-component functions are orthogonal to each other:*

$$\left[h_{i_1\cdots i_p}(x_{i_1}, \cdots, x_{i_p}) \cdot h_{i_1\cdots i_s}(x_{j_1}, \cdots, x_{j_q})\right]\big|_{\boldsymbol{x}=\boldsymbol{c}} = \log(1)\cdot\log(1) = 0 \quad \{x_{i_1}, \cdots, x_{i_p}\} \neq \{x_{j_1}, \cdots, x_{j_q}\} \tag{5.24}$$

Therefore, the function $\varphi(\mathbf{x}) = \log[\eta(\mathbf{x})]$ can be exactly decomposed by the orthogonal basis of $h_{1\cdots s}(x_1, \cdots, x_s)$ in the form of

$$\varphi(\mathbf{x}) = h_0 + \sum_{i=1}^{n} h_i(x_i) + \sum_{1 \leqslant i < j \leqslant n} h_{ij}(x_i, x_j) + \cdots \tag{5.25}$$

where the cut-component functions are given in Eq.(5.20). Simplify the expression through the logarithmic identities:

$$\log(ab) = \log(a) + \log(b), \quad \text{and} \quad \log(a/b) = \log(a) - \log(b) \tag{5.26}$$

One can obtain the s-variate M-DRM approximation of original model, $y = \eta(\mathbf{x})$, as shown in Eq.(5.19).

In summary, definitions of two cut-component functions in C-DRM and M-DRM are different as shown in Eq.(5.4) and Eq.(5.20), respectively, together with the corresponding objective functions $\eta(\mathbf{x})$ and $\log\{\text{abs}[\eta(\mathbf{x})]\}$. However, one should note that the two s-variate cut-component functions are commonly defined using the corresponding s-variate function, $\eta(\mathbf{x}_s)$, and the lower dimensional functions. Therefore, given the s-variate approximation models by C-DRM and M-DRM, the number of functional calls in later moment calculation is identical.

5.3 Calculation of Fractional Moment

Given a input-output relation, $y = \eta(\mathbf{x})$, an α^{th} order fractional moment of the response function can be obtained from a multi-dimensional integration as

$$M_Y^{\alpha} = \int_{\mathbf{X}} \left[\eta(\mathbf{x})\right]^{\alpha} f_{\mathbf{X}}(\mathbf{x}) \mathrm{d}\mathbf{x} \tag{5.27}$$

where, $f_{\mathbf{X}}(\mathbf{x})$ is the joint PDF of n random variables $\mathbf{X}$.

5.3.1 M-DRM for Computing Fractional Moments

Using the univariate M-DRM model to approximate the original input-output relation, an α^{th} order fractional moment of the response function can be accordingly approximated by

$$\begin{aligned} M_Y^{\alpha} = \int_{\mathbf{X}} [\eta(\mathbf{x})]^{\alpha} f_{\mathbf{X}}(\mathbf{x}) \mathrm{d}\mathbf{x} &\approx \int_{\mathbf{X}} \left\{ \left[\eta(\boldsymbol{c})\right]^{1-n} \prod_{i=1}^{n} \eta(c_1, \cdots, c_{i-1}, x_i, c_{i+1}, \cdots, c_n) \right\}^{\alpha} f_{\mathbf{X}}(\mathbf{x}) \mathrm{d}\mathbf{x} \\ &= \left[\eta(\boldsymbol{c})\right]^{\alpha - \alpha n} \prod_{i=1}^{n} \left\{ \int_{X_i} \left[\eta(c_1, \cdots, c_{i-1}, x_i, c_{i+1}, \cdots, c_n)\right]^{\alpha} f_i(x_i) \mathrm{d}x_i \right\} \end{aligned} \tag{5.28}$$

Thus, the original n-dimensional moment integration has been approximated by a product of n one-dimensional integrations. This is reason of the high efficiency of the M-DRM in the fractional (integer) moments calculation.

As the univariate M-DRM model is not enough to represent the original input-output relation, $y = \eta(\mathbf{x})$, a bivariate approximation can be used. Then, numerical integration procedure for the α^{th} order fractional moment can be given as

$$M_Y^{\alpha} \approx \frac{\left[\eta(\boldsymbol{c})\right]^{\frac{\alpha(n-1)(n-2)}{2}} \times \prod_{i=1}^{n-1} \prod_{j=i+1}^{n} \left[\int_{X_i} \int_{X_j} \eta(x_i, x_j, \boldsymbol{c}_{-ij}) f_i(x_i) f_j(x_i) \mathrm{d}x_i \mathrm{d}x_j \right]^{\alpha}}{\prod_{i=1}^{n} \left[\int_{X_i} \eta(x_i, \boldsymbol{c}_{-i}) f_i(x_i) \mathrm{d}x_i \right]^{\alpha(n-2)}} \tag{5.29}$$

Following this procedure, the calculation of fractional moments of original response function can be approximated by using the s-variate M-DRM. One can see that the M-DRM method for moment calculation entails evaluating at most s-dimensional integrals, which is substantially simpler and more efficient than performing one n-dimensional integration when $s \ll n$. Furthermore, M-DRM does not require calculation of any partial derivatives of response and inversion of random matrices as compared to other methods in literature. Needless to say that this approach can also be used to calculate integer moments by setting $\alpha = 1, 2, 3$, etc.

5.3.2 Remarks on Moment Computation

In this Section, an example is presented to elaborate the fact that the conventional method (C-DRM) is inadequate to evaluate the fractional moments of the response function.

Consider a bivariate function $Y = \eta(X_1, X_2)$, where X_1 and X_2 are mutually independent random variables. Using C-DRM and M-DRM, the function can be approximated as

$$\begin{cases} \text{C-DRM:} & \eta(x_1, x_2) \approx \eta(x_1, c_2) + \eta(c_1, x_2) - \eta(c_1, c_2) \\ \text{M-DRM:} & \eta(x_1, x_2) \approx [\eta(x_1, c_2) \times \eta(c_1, x_2)]/\eta(c_1, c_2) \end{cases} \tag{5.30}$$

A k^{th} integer moment of Y can be computed using these approximations as

$$\begin{cases} \text{C-DRM:} & E[Y^k] \approx E\left\{\left[\eta(X_1, c_2) + \eta(c_1, X_2) - \eta(c_1, c_2)\right]^k\right\} \\ \text{M-DRM:} & E[Y^k] \approx E\left\{\left[\eta(X_1, c_2) \times \eta(c_1, X_2)\right]/\eta(c_1, c_2)\right]^k\right\} \end{cases} \tag{5.31}$$

In case of C-DRM approximation, the integer moment can be evaluated using the following binomial expansion:

$$E\left[(A + B - C)^k\right] = \sum_{i=0}^{k} \binom{k}{i} E\left[A^{k-i}\right] E\left[(B - C)^i\right] \tag{5.32}$$

where $\binom{k}{i} = \frac{k!}{i!(k-i)!}$; and $A = \eta(X_1, c_2)$, $B = \eta(c_1, X_2)$, and $C = \eta(c_1, c_2)$.

However, to compute an α^{th} order fractional moment, the following fractional binomial expansion is required (Gzyl and Tagliani, 2010):

$$E\left[(A + B - C)^\alpha\right] = \sum_{i=0}^{\infty} \binom{\alpha}{i} E\left[A^{\alpha-i}\right] E\left[(B - C)^i\right] \tag{5.33}$$

Since Eq.(5.33) involves an infinite order moments of univariate functions, it is not practical to use C-DRM for the computation of fractional moment. One should note that the fractional binomial coefficient, $\binom{\alpha}{i}$, is defined as shown in literature (Graham et al., 1988)

$$\binom{\alpha}{i} = \frac{\alpha(\alpha - 1)\cdots(\alpha - i + 1)}{i(i - 1)\cdots 1} \tag{5.34}$$

In contrast, M-DRM leads to a much simpler algebraic structure of the (fractional) moment equation:

$$E[Y^\alpha] \approx \frac{E\left\{[\eta(X_1, c_2)]^\alpha\right\} \times E\left\{[\eta(c_1, X_2)]^\alpha\right\}}{E\left\{[\eta(c_1, c_2)]^\alpha\right\}}$$

Even in case of evaluation of integer moments (e.g., $\alpha = 1, 2, \cdots$), M-DRM does not require a binomial expansion of Eq.(5.32), which simplifies the overall computational procedure.

5.3.3 Low Dimensional Integration

Numerical integration of a low dimensional function in M-DRM can be highly optimized by using the scheme of Gauss quadrature. For example, in case of Normal variable, Gauss-Hermite integration scheme provides an excellent result.

Table 5.1 has summarized Gauss-points and Gauss weighs of the five-order rules of Gauss-Legendre, Gauss-Hermite and Gauss-Laguerre quadratures. More orders of Gauss points and

Table 5.1: Some frequently used Gauss-weight and Gauss-point (Order $N = 5$)

Gaussian Rule	k	1	2	3	4	5
Gauss-Legendre	w_k	0.2369	0.47863	0.5689	0.4786	0.2369
	x_k	−0.9062	−0.5385	0	0.5385	0.9062
Gauss-Hermite	w_k	1.13×10^{-2}	0.2221	0.5333	0.2221	1.13×10^{-2}
	x_k	−2.8570	−1.3556	0	1.3556	2.8570
Gauss-Laguerre	w_k	0.5218	0.39867	7.59×10^{-2}	3.61×10^{-3}	2.34×10^{-5}
	x_k	0.2636	1.4134	3.5964	7.0858	12.641

weights according to other orthogonal polynomials can be found in the textbook (Davis and Rabinowitz, 1975). Once the standard integration points are available, the procedure summarized as shown in literature (Zhang et al., 2011b) can be applied to generate the general integration grids for the low dimensional integration.

5.3.4 Computational Effort

The Gauss quadrature can be used directly to compute the moments of a response function. If each random variable uses N Gauss point, the required number of functional evaluations by direct numerical integration is $N_{\text{DNI}} = N^n$. This implies that the total number of functional calls is exponentially increasing with the dimensionality of $\mathbf{X}$.

When adopts the general s-variate M-DRM (or C-DRM), the number of functional evaluations is

$$N_{\text{DRM}} = \sum_{i=0}^{s} \binom{n}{s-i} N^{s-i} = 1 + nN + \frac{n(n-1)}{2} N^2 + \cdots \tag{5.35}$$

Therefore, if using the univariate M-DRM to approximate the original input-output relation, the

number of functional evaluations in the moment calculation is rather small:

$$N_{\mathrm{DRM}} = 1 + \sum_{i=1}^{k} \left(N_i - 1\right) + \sum_{i=k+1}^{n} N_i \tag{5.36}$$

where k ($\leqslant n$) denotes the number of variables with the symmetric distribution (say the Normal variate), and N_i is the adopted number of Gauss nodes for random variable X_i.

Consider an example of $n = 6$ and $N_i = 5$, in which the ratio of $\frac{N_{\mathrm{DRM}}}{N_{\mathrm{DNI}}} \leqslant 31/5^6 \approx 0.2\%$. This illustrates the high computational efficiency of M-DRM in the fractional (integer) moments calculation of the response function.

5.4 Examples of Genz's Function

Object of the section is using three mathematic testing functions to calculate the moment and probability distribution of the output quantity, $Y = \eta(\mathbf{X})$. The proposed methodology (M-DRM and ME-FM) for the object can be summarized as follows:

(i) Considering a general input-output relation, $y = \eta(\mathbf{x})$, employs the proposed M-DRM to approximate the function as the multiplicative form of low-dimensional functions.

(ii) Use the M-DRM model and the rules of Gauss quadrature to calculate fractional (integer) moment.

(iii) With the fractional moments as the constraints, run the MaxEnt optimization procedure describe as shown in Chapter 3 and record the determined Lagrange multipliers and fractional exponents.

(iv) Obtain the MaxEnt distribution of the system output. One should note that the fractional moments used during the iteration process are calculated only based on the integration grid determined in step 2.

Genz's functions (Genz, 1987) are defined as

$$\begin{cases} \text{Corner Peak Function:} & \eta(\mathbf{X}) = \left(1 + \sum_{i=1}^{n} a_i X_i\right)^{-(n+1)} \\ \text{Product Peak Function:} & \eta(\mathbf{X}) = \prod_{i=1}^{n} \left[a_i^2 + (X_i - b_i)^2\right]^{-1} \\ \text{Gaussian Function:} & \eta(\mathbf{X}) = \exp\left[-\sum_{i=1}^{n} a_i^2 (X_i - b_i)^2\right] \end{cases} \tag{5.37}$$

where X_i $(i = 1, 2, \cdots, n)$ are i.i.d standard Uniform random variables. The constant, a_i and b_i, are assumed as shown in Table 5.2.

Table 5.2: The dimensionality and constant of test functions

Corner Peak Function		Product Peak Function			Gaussian Function		
n	a_i	n	a_i	b_i	n	a_i	b_i
10	0.01	10	0.9	0.1	10	0.9	0.1

5.4.1 Integer Moment

The first-four moments of $Y = \eta(\mathbf{X})$ are calculated by M-DRM method using the five-order $(N = 5)$ Gaussian-Legendre quadrature. Therefore, the number of functional evaluations of M-DRM is $51 = (10 \times 5 + 1)$. The method of C-DRM is also used. Compared with the benchmarks provided by Monte Carlo simulation with 10^6 samples, the results are reported in Table 5.3.

It is clear to see that the M-DRM provides very close moment estimates compared to the benchmarks of crude Monte Carlo simulation. All relative errors determined by M-DRM are less than 1.0% for three Genz's functions. In the context of employing C-DRM in the moments computation, moment errors associated with test examples have revealed its inaccuracy in moment computation of Genz's functions.

5.4.2 Output Distribution

Distributions of the test function, $Y = \eta(\mathbf{X})$, are determined using ME-FM method. Empirical distributions of the Genz's functions are estimated by Monte Carlo simulation with 10^6 samples.

Parameters of MaxEnt distributions are determined as shown in Table 5.4, together with the plots of PDF and CDF in Figures 5.1 to 5.3. According to the MaxEnt distribution of the Genz's examples, it is clearly to see that the proposed method of ME-FM can obtain reliably estimates of an output distribution. Using M-DRM method and five-order Gauss-Legendre quadrature to calculate the fractional moments, the full distribution can be exactly determined with only 51 functional evaluations. Compared with the benchmarks provided by Monte Carlo simulation, the method of ME-FM is highlighted its efficiency and accuracy in the calculation of moment and probability distribution.

Table 5.3: Integer moments of the Genz's functions

Function	Corner Peak Function				Product Peak Function				Gaussian Function			
Moment	1^{st}	2^{nd}	3^{rd}	4^{th}	1^{st}	2^{nd}	3^{rd}	4^{th}	1^{st}	2^{nd}	3^{rd}	4^{th}
MCS	0.588	0.349	0.209	0.126	0.958	1.385	2.816	7.491	0.167	3.8×10^{-2}	1.2×10^{-2}	4.3×10^{-3}
C-DRM	0.471	0.231	0.117	0.062	−6.082	51.78	−501	5429	−0.525	0.475	−0.475	0.555
RE(%)	20.0	34.0	44.0	55.0	740.0	3600	1.8×10^{4}	7.2×10^{4}	4.1×10^{2}	1.1×10^{3}	4.2×10^{3}	1.3×10^{4}
M-DRM	0.581	0.341	0.202	0.121	0.957	1.381	2.790	7.356	0.167	3.9×10^{-2}	1.2×10^{-2}	4.3×10^{-3}
RE(%)	0.02	0.06	0.09	0.09	0.05	0.33	0.93	1.80	0.01	0.00	0.02	0.05

C-DRM: Conventional dimensional reduction method;

M-DRM: The proposed multiplicative dimensional reduction method;

MCS: Crude Monte Carlo simulation with 10^6 samples.

RE: Relative Error: = abs(DRM−MCS)/MCS×100%.

Table 5.4: MaxEnt distribution of the ten-dimensional Genz's functions

Function	Entropy	k	0	1	2	3
Corner Peak Function	-1.4649	λ_k	-8.2353	-0.6902	0.9806	27.581
		α_k	$--$	-3.4598	-3.7504	3.9183
		$M_Y^{\alpha_k}$	$--$	6.7536	7.9682	0.1312
Product Peak Function	0.7745	λ_k	102.71	-526.76	-142.78	567.42
		α_k	$--$	0.1198	0.1530	0.1523
		$M_Y^{\alpha_k}$	$--$	0.9712	0.9645	0.9647
Gauss Function	-1.0329	λ_k	50.608	1388.5	802.47	-2234.9
		α_k	$--$	0.1979	0.2195	0.1980
		$M_Y^{\alpha_k}$	$--$	0.6822	0.6548	0.6820

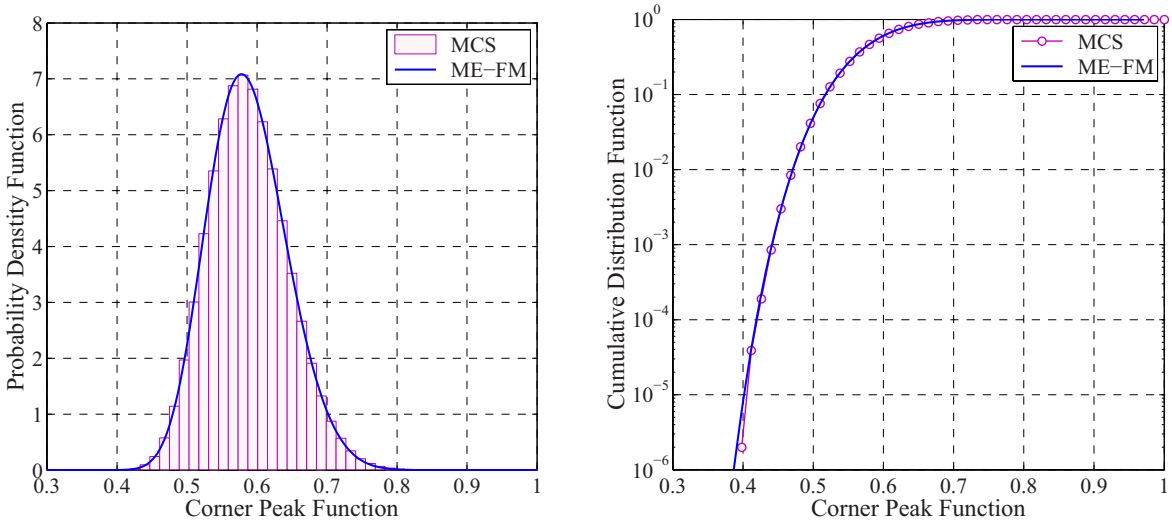

(a) Probability Density Function

(b) Cumulative Distribution Function

Figure 5.1: MaxEnt Distribution of the Corner Peak function

5.5 Structural Reliability Analysis

In this section, three structural reliability examples are analyzed using the proposed method. The first-four integer moments of response function is computed using the additive (or conventional) DRM method (C-DRM) and the proposed multiplicative DRM method (M-DRM), respectively.

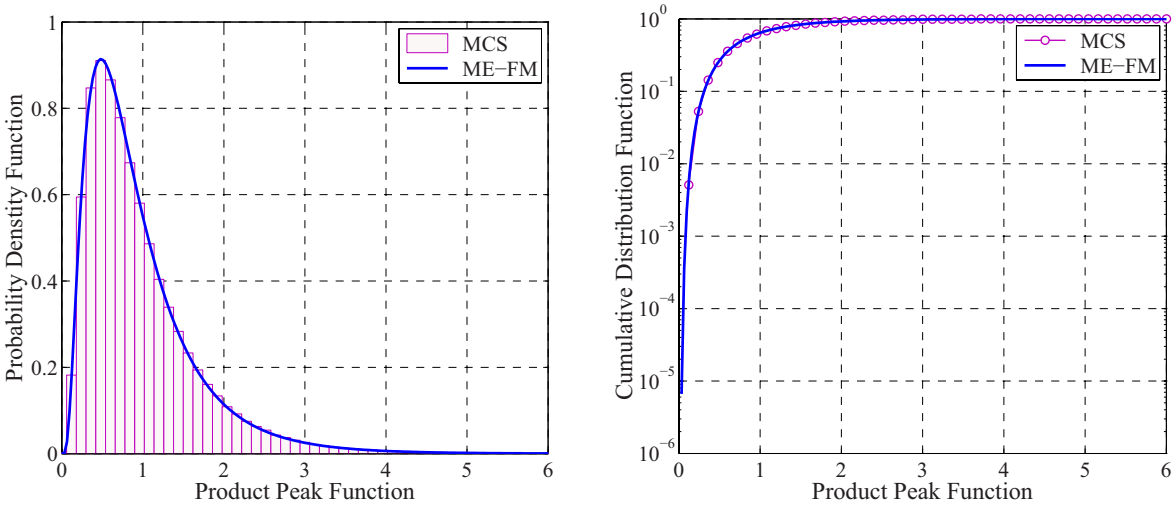

(a) Probability Density Function (b) Cumulative Distribution Function

Figure 5.2: MaxEnt Distribution of the Product Peak function

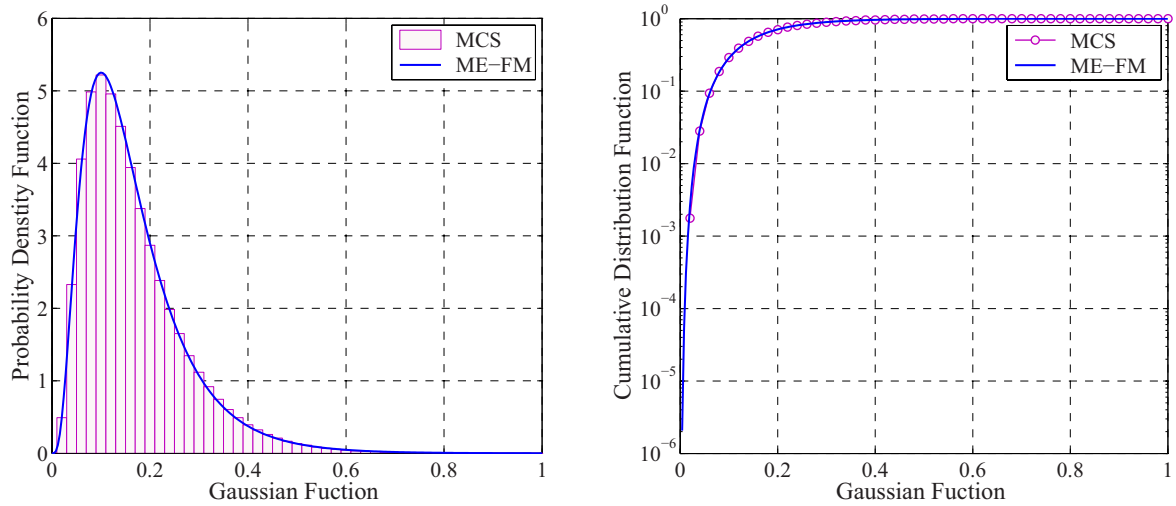

(a) Probability Density Function (b) Cumulative Distribution Function

Figure 5.3: MaxEnt Distribution of the Gauss function

MaxEnt with three orders of fractional moments is subsequently employed to determine the distribution of response function. Monte Carlo simulation with 10^6 samples is used to determine the benchmarks of statistical moment and probability distribution of a structural output, which allows the verify the accuracy of the proposed methods of M-DRM and ME-FM.

5.5.1 Reliability of a Reinforced Concrete Beam

The ultimate bending moment of resistance or capacity of a reinforced concrete beam is given by an explicit function (Breitung and Faravelli, 1994; Zhou and Nowak, 1988):

$$M_U(\mathbf{X}) = X_1 X_2 X_3 - X_4 \frac{X_1^2 X_2^2}{X_5 X_6} \tag{5.38}$$

Distributions of random variables are listed in Table 5.5.

Table 5.5: Random variables in the reinforced concrete beam example

Variable	Description	Distribution	Units	Mean	Std.D	COV
X_1	Area of reinforcement	Lognormal	mm^2	1260	252	0.20
X_2	Yield stress of reinforcement	Lognormal	N/mm^2	300	60	0.20
X_3	Effective depth of reinforcement	Lognormal	mm^2	770	154	0.20
X_4	Stress-strain factor of concrete	Lognormal	—	0.35	0.035	0.10
X_5	Compressive strength of concrete	Weibull	N/mm^2	25	5.0	0.20
X_6	Width of beam	Normal	mm	200	40	0.20
M_B	Applied bending moment	Lognormal	kN·m	100	30	0.30

Moments and Distribution of the Structural Capacity

Firstly, four integer product moments of the moment resistance are computed using C-DRM and the proposed M-DRM methods. Numerical integration grid to compute the moment integrations in both versions of DRM method is given in Table 5.6. One can notice that the moment calculations are based on 30 function evaluations. This grid is provided to assist the reader in the verification of numerical results.

Numerical accuracy is compared against the benchmark results obtained from simulation. Results summarized in Table 5.7 show that M-DRM estimates have less than 1% error for all the four moments, whereas C-DRM results in about 9% error in the estimate of the fourth moment. The next task is to determine the distribution of the response function.

Table 5.6: Numerical integration grid of the RC beam example

		Numerical Integration Grid						Output
Variable	No.	X_1	X_2	X_3	X_4	X_5	X_6	$M_U(\mathbf{X})$
X_1	1	**1235.5**	300.0	770.0	0.35	25.0	200.0	275.79
	2	**701.66**	300.0	770.0	0.35	25.0	200.0	158.98
	3	**2175.6**	300.0	770.0	0.35	25.0	200.0	472.74
	4	**944.62**	300.0	770.0	0.35	25.0	200.0	212.59
	5	**1616.0**	300.0	770.0	0.35	25.0	200.0	356.85
X_2	6	1260.0	**294.17**	770.0	0.35	25.0	200.0	275.79
	7	1260.0	**167.06**	770.0	0.35	25.0	200.0	158.98
	8	1260.0	**518.00**	770.0	0.35	25.0	200.0	472.74
	9	1260.0	**224.91**	770.0	0.35	25.0	200.0	212.59
	10	1260.0	**384.77**	770.0	0.35	25.0	200.0	356.85
X_3	11	1260.0	300.0	**755.05**	0.35	25.0	200.0	275.41
	12	1260.0	300.0	**428.80**	0.35	25.0	200.0	152.08
	13	1260.0	300.0	**1329.5**	0.35	25.0	200.0	492.56
	14	1260.0	300.0	**577.27**	0.35	25.0	200.0	208.21
	15	1260.0	300.0	**987.57**	0.35	25.0	200.0	363.30
X_4	16	1260.0	300.0	770.0	**0.34826**	25.0	200.0	281.11
	17	1260.0	300.0	770.0	**0.26190**	25.0	200.0	283.58
	18	1260.0	300.0	770.0	**0.46310**	25.0	200.0	277.83
	19	1260.0	300.0	770.0	**0.30421**	25.0	200.0	282.37
	20	1260.0	300.0	770.0	**0.39869**	25.0	200.0	279.67
X_5	21	1260.0	300.0	770.0	0.35	**41.822**	200.0	285.08
	22	1260.0	300.0	770.0	0.35	**37.848**	200.0	284.45
	23	1260.0	300.0	770.0	0.35	**33.669**	200.0	283.63
	24	1260.0	300.0	770.0	0.35	**28.660**	200.0	282.34
	25	1260.0	300.0	770.0	0.35	**21.452**	200.0	279.40
X_6	26	1260.0	300.0	770.0	0.35	25.0	**85.721**	267.72
	27	1260.0	300.0	770.0	0.35	25.0	**314.28**	284.70
	28	1260.0	300.0	770.0	0.35	25.0	**145.77**	277.34
	29	1260.0	300.0	770.0	0.35	25.0	**254.23**	283.19
Cut-Point	30	1260.0	300.0	770.0	0.35	25.0	200.0	281.06

Table 5.7: Integer moments estimated using C-DRM and M-DRM

Moments	1^{st}	2^{nd}	3^{rd}	4^{th}
C-DRM	279.65	8.7428×10^4	2.9904×10^7	1.1046×10^{10}
Relative Error (%)	0.17	0.012	−2.6	−8.9
M-DRM	279.65	8.7715×10^4	3.0842×10^7	1.2150×10^{10}
Relative Error (%)	0.17	0.34	0.43	0.22
Simulation	279.17	8.7418×10^4	3.0689×10^7	1.2177×10^{10}

C-DRM: Conventional dimensional reduction method;

M-DRM: The proposed multiplicative dimensional reduction method;

MCS: Crude Monte Carlo simulation with 10^6 samples.

As shown in Figure 5.4, PDF of the bending moment capacity obtained from the proposed method is in close agreement with that obtained from the simulation method.

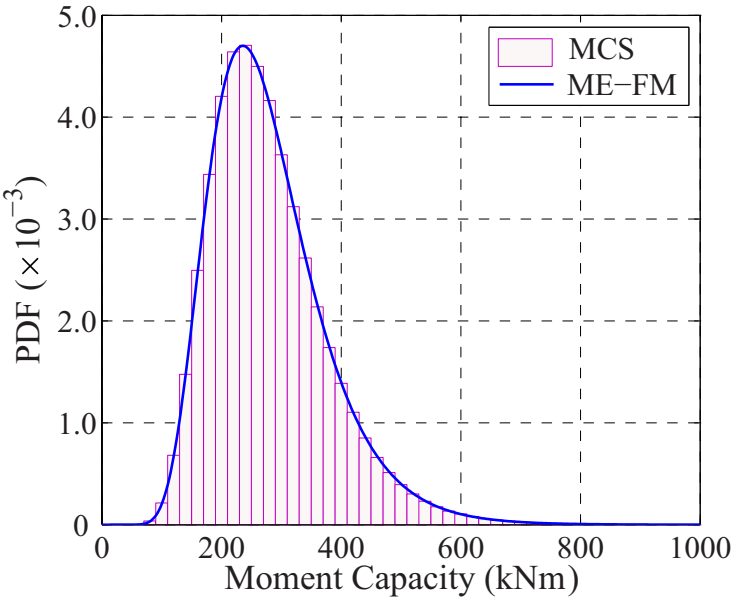

Figure 5.4: Probability distribution of the bending moment capacity (ME-FM: Principle of maximum entropy (MaxEnt) with fractional moment; MCS: Crude Monte Carlo simulation with 10^6 samples.)

Reliability Analysis

The limit state function for the reliability analysis is defined as

$$g(\mathbf{X}) = M_U(\mathbf{X}) - M_B \tag{5.39}$$

Since the use of fractional moment works with a positive random quantity only, the above limit state function is revised as

$$\hat{g}(\mathbf{X}) = \frac{M_U(\mathbf{X})}{M_B} = \frac{X_1 X_2 X_3}{M_B} - \frac{X_4 X_1^2 X_2^2}{M_B X_5 X_6} \tag{5.40}$$

such that the probability of failure is defined as $P_F = \Pr[\hat{g}(\mathbf{X}) \leqslant 1.0] = F_{\hat{G}}(1.0)$.

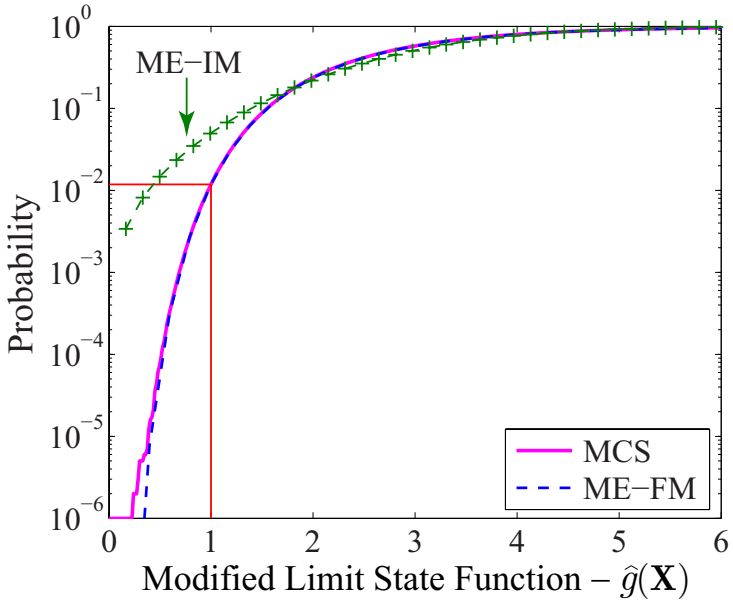

Figure 5.5: Cumulative distribution function of the modified limit state function (ME-FM: Principle of maximum entropy (MaxEnt) with fractional moments; ME-IM: Principle of maximum entropy (MaxEnt) with integer moments; MCS: Crude Monte Carlo simulation with 10^6 samples.)

Parameters of the MaxEnt distribution of $\hat{g}(\mathbf{X})$ are reported in Table 5.8 and a comparison of its CDF obtained from the three methods is illustrated in Figure 5.5. It is clear that the proposed M-DRM method provides highly accurate approximation in the entire range of the response distribution. The probability of failure calculated from the proposed method, 1.20×10^{-2}, is fairly close to that obtained from simulation (1.18×10^{-2}). The conventional DRM method estimates it as 5.01×10^{-2}.

Table 5.8: MaxEnt distribution of the modified limit state function

Entropy	k	0	1	2	3
1.6294	λ_k	708.37	79.136	622.59	−1407.4
	α_k		0.0686	−0.1109	−0.0422
	$M_Y^{\alpha_k}$		1.0725	0.8948	0.9583

5.5.2 Reliability Analysis of a Truss Structure

A ten-bar truss structure shown in Figure 5.6 is taken from a pervious study (Doltsinis and Kang, 2004).

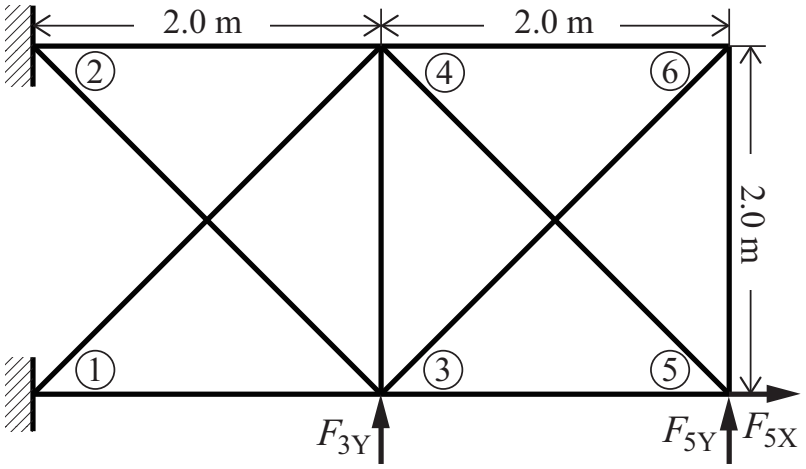

Figure 5.6: A ten-bar planar truss structure

Table 5.9: Random variables in the truss example

Variable	Description	Distribution	Units	Mean	Std.D	COV
E	Young's Modulus	Normal	GPa	210	21	0.1
A	Cross-sectional Area	Lognormal	mm^2	100	10	0.1
F_{3Y}	External Load	Lognormal	N	1000	100	0.1
F_{5X}	External Load	Lognormal	N	1000	100	0.1
F_{5Y}	External Load	Lognormal	N	1000	100	0.1

Random variables associated with this problem are listed in Table 5.9. Linear structural

analysis was performed to calculate the maximum joint displacement of the truss, defined as

$$\eta(\mathbf{X}) = \max_{3 \leqslant i \leqslant 6} \left\{ \sqrt{U_{\mathrm{X}_i}^2 + U_{\mathrm{Y}_i}^2} \right\}$$

where $U_{\mathrm{x}i}$ and $U_{\mathrm{y}i}$ are the horizontal and vertical components of displacement at an i^{th} node.

Integer Moments

The first-four integer moments of the maximum truss displacement are presented in Table 5.10. It is interesting that both DRM methods provide highly accurate estimates with absolute error less than 1%.

Table 5.10: Integer moments of the maximum displacement of the truss structure

Moments	1^{st}	2^{nd}	3^{rd}	4^{th}
C-DRM	1.3342	1.8238	2.5523	3.6543
Relative Error (%)	−0.01	−0.096	−0.36	−0.91
M-DRM	1.3344	1.8256	2.5618	3.6887
Relative Error (%)	-8.6×10^{-5}	8.2×10^{-4}	6.1×10^{-3}	0.02
Simulation	1.3344	1.8256	2.5616	3.6880

C-DRM: Conventional dimensional reduction method;
M-DRM: The proposed multiplicative dimensional reduction method;
MCS: Crude Monte Carlo simulation with 10^6 samples.

In this example, five Gauss points were used for the integration of each component function. The entire numerical integration grid is given in Table 5.11.

Reliability Analysis

The estimated MaxEnt PDF of the maximum displacement is compared with the simulation result in Figures 5.7. Parameters of the MaxEnt distribution are determined as shown in Table 5.12.

Figure 5.8 shows that the probability of exceedance (POE) curve obtained from M-DRM method is in fairly close agreement with the simulation result. For the sake of comparison, POE curve obtained from C-DRM using integer moment is also plotted in the figure. The POE curve for C-DRM has thinner tail and it underestimates the exceedance probability, i.e., it leads to non-conservative results.

Table 5.11: Numerical integration grid for the Truss example

Variable	No.	Numerical Integration Grid					Output
		E (GPa)	A (mm^2)	F_{3Y} (N)	F_{5X} (N)	F_{5Y} (N)	$\eta(\mathbf{X})$ (mm)
E	1	**150.00**	100.00	1000.0	1000.0	1000.0	1.8306
	2	**270.00**	100.00	1000.0	1000.0	1000.0	1.0170
	3	**181.53**	100.00	1000.0	1000.0	1000.0	1.5127
	4	**238.47**	100.00	1000.0	1000.0	1000.0	1.1515
A	5	210	**99.504**	1000.0	1000.0	1000.0	1.3141
	6	210	**74.829**	1000.0	1000.0	1000.0	1.7475
	7	210	**132.31**	1000.0	1000.0	1000.0	0.9883
	8	210	**86.918**	1000.0	1000.0	1000.0	1.5044
	9	210	**113.91**	1000.0	1000.0	1000.0	1.1479
F_{3Y}	10	210	100.00	**995.04**	1000.0	1000.0	1.3064
	11	210	100.00	**748.29**	1000.0	1000.0	1.2475
	12	210	100.00	**1323.1**	1000.0	1000.0	1.3855
	13	210	100.00	**869.18**	1000.0	1000.0	1.2763
	14	210	100.00	**1139.1**	1000.0	1000.0	1.3411
F_{5X}	15	210	100.00	1000.0	**995.04**	1000.0	1.3037
	16	210	100.00	1000.0	**748.29**	1000.0	1.1092
	17	210	100.00	1000.0	**1323.1**	1000.0	1.5626
	18	210	100.00	1000.0	**869.18**	1000.0	1.2045
	19	210	100.00	1000.0	**1139.1**	1000.0	1.4174
F_{5Y}	20	210	100.00	1000.0	1000.0	**995.04**	1.3062
	21	210	100.00	1000.0	1000.0	**748.29**	1.2374
	22	210	100.00	1000.0	1000.0	**1323.1**	1.3978
	23	210	100.00	1000.0	1000.0	**869.18**	1.2711
	24	210	100.00	1000.0	1000.0	**1139.1**	1.3464
Mean-Value	25	210	100.00	1000.0	1000.0	1000.0	1.3076

For example, if maximum allowable displacement is 2.5 mm, the associated POE or probability of failure can be obtained from Figure 5.8 as 5.67×10^{-5} from the M-DRM and 5.87×10^{-5} from simulation curve. The C-DRM estimates the failure probability as 4.79×10^{-6}, which is an

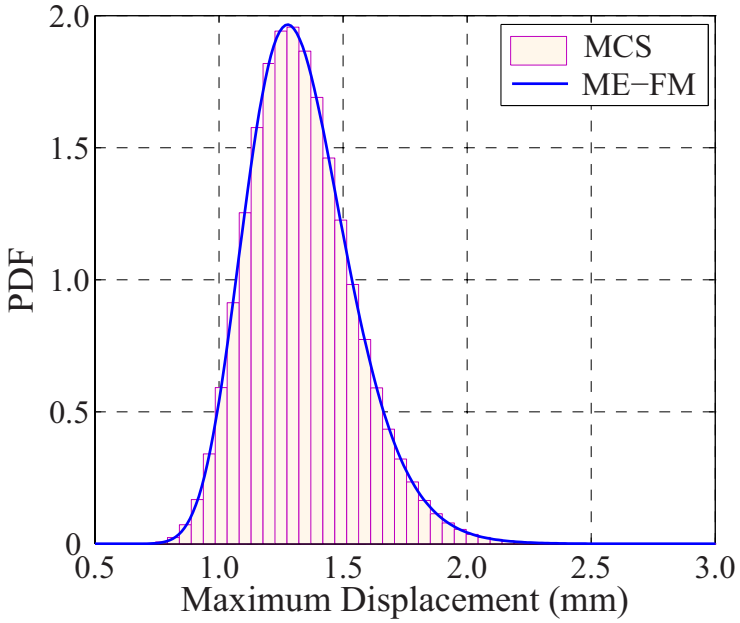

Figure 5.7: Distribution of the maximum displacement of the ten-bar truss (ME-FM: Principle of maximum entropy (MaxEnt) with fractional moments; MCS: Crude Monte Carlo simulation with 10^6 samples.)

Table 5.12: MaxEnt PDF of the structural maximal displacement

Entropy	k	0	1	2	3
−0.1581	λ_k	−165.21	50.014	54.412	61.404
	α_k		−0.8786	0.2748	0.2948
	$M_Y^{\alpha_k}$		0.7921	1.0798	1.0860

order of magnitude smaller than the simulation-based estimate.

5.5.3 Reliability of a Steel Frame Structure

The linear elastic analysis of a three-bay four-storey steel frame, shown in Figure 5.9, was carried out to compute the interstory drift or relative displacement at each of the 16 unsupported joints of the structure. This example is taken from a reference (Liu, 2007).

External loads include dead loads due to the gravity of members and slabs, short and long term live loads, snow load on the roof, and the lateral wind load. The distributed loads applied to each member are described in Table 5.13. Random variables and their distribution parameters

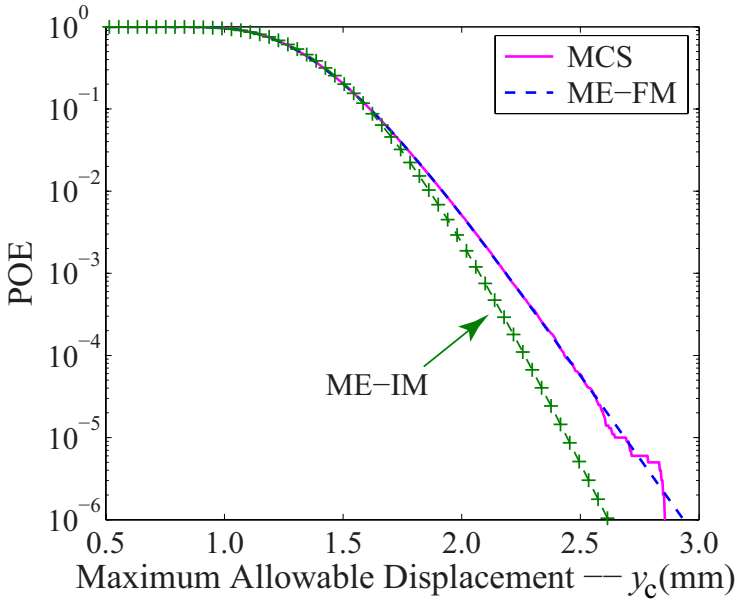

Figure 5.8: Probability of exceedance versus the maximum truss displacement (ME-FM: Principle of maximum entropy (MaxEnt) with fractional moments; ME-IM: Principle of maximum entropy (MaxEnt) with integer moments; MCS: Crude Monte Carlo simulation with 10^6 samples.)

Table 5.13: Description of load applied to each member

Member Load	Load Combination
$Q_{17}, Q_{19}, Q_{20}, Q_{22}, Q_{23}, Q_{25}$	$D_L + S_1 + L_1$
Q_{18}, Q_{21}, Q_{24}	$D_L + S_2 + L_2$
Q_{26}, Q_{27}, Q_{28}	$D_L + S_L$

are listed in Table 5.14. Note that the structural members, denoted as IPE and HEB sections, are the European standard wide flange H-beams.

The probability failure of the structure is defined as the probability of the interstorey drift at any joint, $D_{ij}(\mathbf{X})$, exceeding a code specified limit, y_c, which is analogous to a series system problem:

$$P_F = \Pr\left[\bigcup_{i=1}^{4}\bigcup_{j=1}^{4}\left(D_{ij}(\mathbf{X}) \geq y_c\right)\right] = 1 - F_Y(y_c) \tag{5.41}$$

where

$$\eta(\mathbf{X}) = \max_{1\leqslant i,j\leqslant 4}\left\{D_{ij}(\mathbf{X})\right\}$$

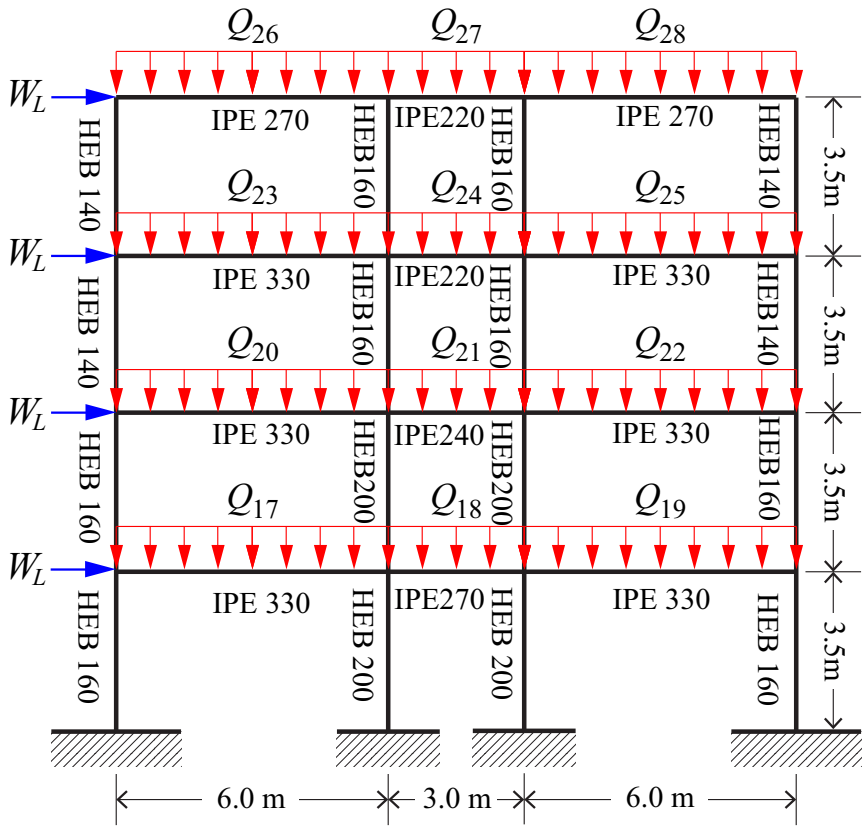

Figure 5.9: A three-bay four-storey steel frame structure

Table 5.14: Random variables in the steel frame example

Variable	Description	Distribution	Mean-Value	Std.D	COV
D_L	Dead load	Lognormal	20 kN	6.0 kN	0.30
S_1	Short term live load 1	Lognormal	10 kN	3.0 kN	0.30
S_2	Short term live load 2	Lognormal	5.0 kN	1.5 kN	0.30
L_1	Long term live load 1	Lognormal	10 kN	3.0 kN	0.30
L_2	Long term live load 2	Lognormal	5.0 kN	1.5 kN	0.30
S_L	Snow load	Lognormal	5.0 kN	1.5 kN	0.30
W_L	Wind load	Lognormal	8.0 kN	2.4 kN	0.30
E	Young's modulus	Lognormal	210 GPa	10.5 GPa	0.05

is the maximum interstory drift of the structure. Thus the probability of failure can be estimated from the extreme event distribution, $F_Y(y)$, about the structural interstory drifts.

Integer Moments

The first four integer moments calculated from both versions of DRM provide highly accurate estimates with error less than 1%. The parameters of the MaxEnt PDF and fractional moments are given in Table 5.15. These parameters were computed using 41 evaluations of maximum interstory drift of the frame.

Table 5.15: Moments of the maximum interstorey drift of the steel frame

Moments	1^{st}	2^{nd}	3^{rd}	4^{th}
C-DRM	5.0225	27.511	164.21	1067.3
Relative Error (%)	-1.7×10^{-3}	-6.6×10^{-2}	-0.29	-0.74
M-DRM	5.0225	27.528	164.68	1075.3
Relative Error (%)	-1.7×10^{-3}	-5.0×10^{-3}	-5.0×10^{-3}	-5.8×10^{-4}
Simulation	5.0226	27.529	164.69	1075.3

C-DRM: Conventional dimensional reduction method;

M-DRM: The proposed multiplicative dimensional reduction method;

MCS: Crude Monte Carlo simulation with 10^6 samples.

Table 5.16: MaxEnt distribution of the system maximum interstory drift

Entropy	k	0	1	2	3
1.7693	λ_k	-291.46	82.684	139.70	83.212
	α_k		-0.0095	-0.2506	0.2171
	$M_Y^{\alpha_k}$		0.9852	0.6765	1.4092

Reliability Analysis

Parameters on the MaxEnt distribution of maximum interstory drift are summarized in Table 5.16. Its PDF obtained from M-DRM compares well with the simulation results as shown in Figures 5.10. The POE versus maximum interstory drift is plotted in Figure 5.11. A close agreement between M-DRM and simulation results in the entire range of the distribution confirms the validity of the proposed approach. In contrast, C-DRM method has a fairly short tail, which underestimates the failure probability for POE $\leqslant 10^{-2}$.

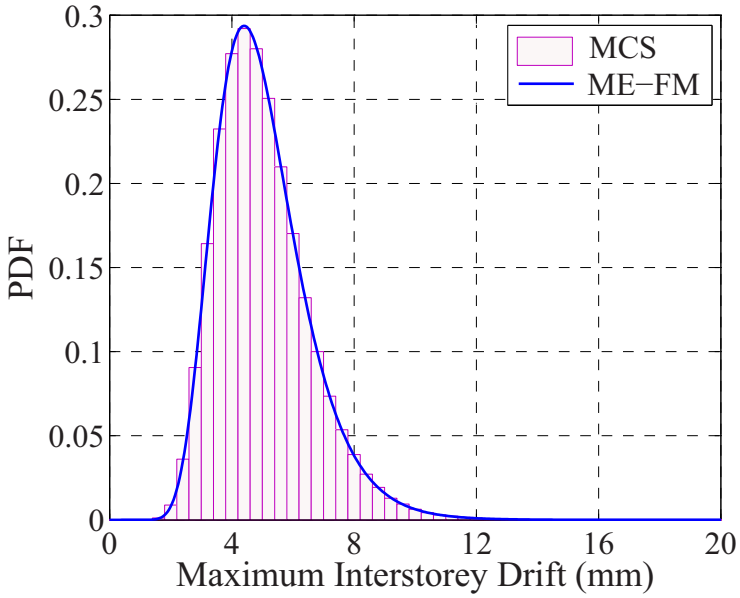

Figure 5.10: Distribution of the maximum interstory drift of the steel frame structure(ME-FM: Principle of maximum entropy (MaxEnt) with fractional moments; MCS: Crude Monte Carlo simulation with 10^6 samples.)

Table 5.17: System failure probability of the steel frame structure

Drift (mm)	5.83 ($h/600$)	7.00 ($h/500$)	8.75 ($h/400$)	11.67 ($h/300$)	17.50 ($h/200$)
ME-IM	2.5184×10^{-1}	9.8176×10^{-2}	2.2403×10^{-2}	1.1099×10^{-3}	7.7851×10^{-15}
ME-FM	2.5624×10^{-1}	1.0185×10^{-1}	2.1456×10^{-2}	1.3675×10^{-3}	6.2773×10^{-6}
Simulation	2.5639×10^{-1}	1.0187×10^{-1}	2.1442×10^{-2}	1.3507×10^{-3}	5.0×10^{-6}

The storey height $h = 3500$ mm in the example;
ME-IM: Principle of maximum entropy (MaxEnt) with integer moments;
ME-FM: Principle of maximum entropy (MaxEnt) with fractional moments;
MCS: Crude Monte Carlo simulation with 10^6 samples.

AISC steel design code (AISC, 2005) states that, *"typical drift limits in common usage vary from $h/200$ to $h/600$ for interstory drift, depending on building type and the type of cladding or partition materials used"*. Based on this consideration, failure probabilities of the steel frame were estimated from the threes methods (see Table 5.17). It is again clear that for higher drift values, such as 17.5 mm, ME-IM method underestimates the failure probability quite significantly. Results of ME-FM method are always in close agreement with the simulation results.

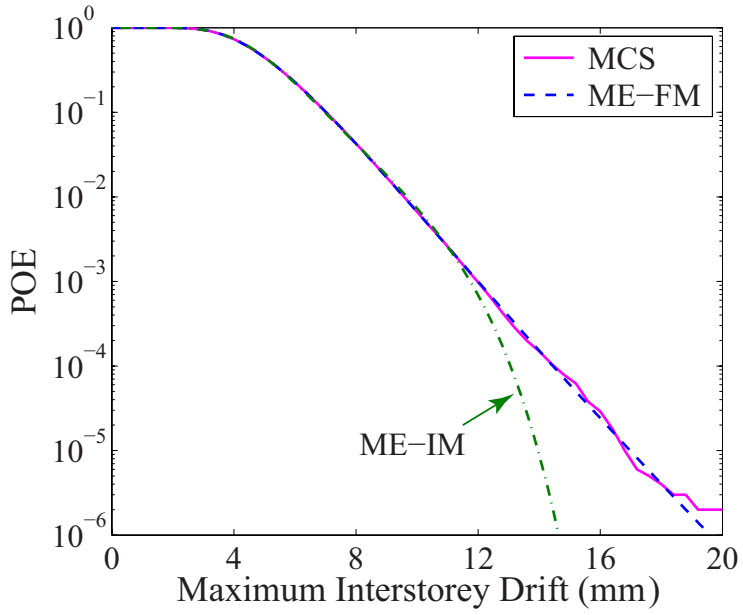

Figure 5.11: System failure probability of the steel frame structure (ME-FM: Principle of maximum entropy (MaxEnt) with fractional moments; ME-IM: Principle of maximum entropy (MaxEnt) with integer moments; MCS: Crude Monte Carlo simulation with 10^6 samples.)

5.6 Conclusion

The Chapter presents a general method for deriving the probability distribution of a function with multiple random variables representing the response of a structural system. The derivation is based on the principle of maximum entropy (MaxEnt) in which constraints are specified in terms of fractional moments (ME-FM). It is a further extension of ME-FM developed in Chapter 3 to compute the output distribution of an input-output relation instead of a random variable.

A multiplicative dimensional reduction method (M-DRM) was proposed to approximate a general high-dimensional function representing mechanistic model of a system. The primary advantage of M-DRM is to simplify a high-dimensional moment integration as the product of a series low-dimensional integrals. Together with the rules of Gauss quadrature, an efficient method for fractional moment computation was proposed.

Application of the method has been illustrated by several examples, i.e., math examples of Genz's function, examples on structural reliability analyses. Monte Carlo simulations were carried out to assess the accuracy of the proposed method. It is observed that moment computation of M-DRM has very small relative error ($\leqslant 1\%$). Final product of the proposed method is the

complete output distribution of a model function, which provides all information needed in probabilistic analysis.

Chapter 6

Global Sensitivity Analysis with M-DRM

6.1 Introduction

6.1.1 Literature Review

Sensitivity analysis has been widely used in engineering design to understand a complex model behavior and help designers make informed decisions regarding where to spend the effort (Grierson, 1983). In deterministic scenario, sensitivity analysis is conducted to find the rate of change in the model output by varying one input parameter at a time near a given reference point, which involves partial derivatives and thus is referred to as the local sensitivity analysis (Saltelli, 2002). For design under uncertainty, the probabilistic sensitivity analysis is a study to quantify the impact of uncertainty in input variables on the uncertainty in the model output (Liu et al., 2004). Among existing probabilistic sensitivity analysis methods, a popular category is the so-called variance-based method for global sensitivity analysis (Saltelli et al., 2000; Sobol', 2001). It is to study how variance in system output can be apportioned to different sources of uncertainty in model inputs (Saltelli, 2002). Application of variance to quantify the uncertainty and the associated sensitivity is based on the fact that the output variance is a unified summary of uncertainty regardless of the involved system model. Therefore, the global sensitivity analysis is on studying the impact of variations over the entire range of model inputs, as opposed to the local sensitivity on the variation near a reference point (Saltelli et al., 2000).

Method for variance-based sensitivity analysis is related to the concept of analysis of variance (ANOVA) in linear regression analysis, which is developed as a statistical tool to test the significance of each representative factor. The corresponding regression coefficient, hence, can be

employed to measure the sensitivity of model behavior with respect to the input variable. However, the standard (or classical) ANOVA is only limited to provide the effects of linear and/or second-order interaction of input variables, but it is seldom used to evaluate the highly nonlinear effects, such as the total linear effect, nonlinear main effect, and an arbitrary interaction effect, etc., that are critical for ranking the importance of input variables in a product development (Chen et al., 2005).

To extend the standard ANOVA for global sensitivity analysis, a number of variance-based methods have been developed, including the Fourier amplitude sensitivity test (McRae et al., 1982; Saltelli and Bolado, 1998), various importance measures (Homma and Saltelli, 1996), and the Sobol' total effect index (Saltelli and Sobol', 1995; Sobol', 2003), etc. Reviews on the methods of variance-based global sensitivity analysis can be found in literature (Saltelli et al., 2000, 2008). Similar to the concept in standard ANOVA, many of these methods decompose the total output variance to the items contributed by variations of input variables, and then derive the global sensitivity index as the ratio of a partial variance contributed by an effect of interest over the total output variance. The Chapter is proposed to conduct a the global sensitivity analysis by computing the Sobol' index, since it has been widely used in various areas of industry, such as nuclear engineering (Tarantola et al., 2006) and mechanical engineering design (Chen et al., 2005; Liu et al., 2006), etc.

Obviously, the variance-based sensitivity analysis can be applied directly to improve the quality of a product by reducing the output variance through controlling the variances of sensitive input random variables. Furthermore, the measurement is capable to capture the influential effect of each input variable and the interactions among a subset of inputs. In brief, the variance-based sensitivity analysis can be used in a prior-design stage to screen out variables that are probabilistically insignificant and to understand the interactions between design and noise variables, or applied in a post-design stage to determine where the effort should be made to reduce the variability so that the quality of a design can be improved (Chen et al., 2005).

To compute the Sobol' index for global sensitivity analysis, Ishigami and Homma (1990) presented the Monte Carlo simulation method. A mechanistic model with n input random variables, an N samples simulation needs $N(2^n-1)$ model evaluations for Sobol' index estimation (Saltelli and Sobol', 1995). To reduce computational cost of the crude Monte Carlo simulation, Tarantola et al. (2006) proposed random balance design (RBD) to conduct the global sensitivity analysis of a nuclear waste disposal system. Polynomial chaos expansion (PCE) developed in literature

(Ghanem and Spanos, 1991; Wiener, 1938) is another choice to compute the Sobol' index. The method decomposes an original input-output relation as a summation form of a serial orthogonal polynomial chaos, in which the associated coefficient of each polynomial chaos was estimated by using Monte Carlo simulation (Li and Ghanem, 1998) or the rules of Gauss quadrature (Blatman and Sudret, 2010a). Sudret (2008b) reviewed the PCE meta-model construction, in which the computation of Sobol' index was directly related to the coefficients of the PCE meta-model.

Nevertheless, most of methods for the variance-based global sensitivity analysis are without consideration that acquiring samples of model outputs is resource, i.e., demanding computationally cost involved in mechanistic model evaluations. The large number of functional calls related to the crude Monte Carlo simulation (Sobol', 2003) and the direct tensor Gauss quadrature (Blatman and Sudret, 2010b) is the motivation of developing an efficient computational technique for the variance-based global sensitivity analysis in this Chapter.

Rahman (2011) combined the functional polynomial decomposition with the dimensional reduction method (DRM) for the objective. The primary benefit of using DRM is that a series low-dimensional function (based on univariate DRM or bivariate DRM) are employed to approximate an original input-output relation, which reduces the high-dimensional integration as the summation of series of one- or two-dimensional integrals. Combined with the rules of Gaussian quadrature, the using of DRM can be trusted to remarkably reduce the number of mechanic model evaluations from $N(2^n - 1)$ (the crude Monte Carlo simulation) or N^n (the direct tensor Gaussian quadrature) to the magnitude of nN by using the univariate DRM or nN^2 by bivariate DRM, respectively.

6.1.2 Objective

The proposed study is a development of computational method for the Sobol' index computation by using the dimensional reduction method (DRM) in literature (Li et al., 2006; Rahman and Xu, 2004). The conventional DRM (C-DRM) was derived as a summation of a series low-dimensional function with increasing dimensionality. A novel dimensional reduction method given as a multiplicative form of low-dimensional functions is proposed to approximate a general input-output relation. The primary benefit of M-DRM entails a high-dimensional moment integration as the product of a series of one-dimensional integrals. The separative property of M-DRM will be employed to handle with the involved high-dimensional integrations infolded in the variance-based global sensitivity analysis.

6.1.3 Organization

Organization of the Chapter is as follows. Section 6.2 provides background on the variance-based global sensitivity analysis, which consists of mathematical definitions on output variance decomposition and Sobol' sensitivity index. Section 6.3 illustrates crucial challenge on the Sobol' index computation, i.e., one has to evaluate a series of high-dimensional integrals in terms of the second-order moment of the conditional expectation. To overcome the involved intensive computational cost, a multiplicative dimensional reduction method (M-DRM) is proposed to approximate the original high-dimensional integration as the product of a series of one-dimensional integrations. Six examples from literature are employed in Sections 6.4 to examine the accuracy and efficiency of M-DRM on the Sobol index computation. Section 6.5 summarizes the conclusions, and computational details are given in Appendices.

6.2 Background

6.2.1 The Variance Decomposition

We write $\mathbf{X} = [X_1, X_2, \cdots, X_n]^{\mathrm{T}}$ as the input parameters of a general model $Y = \eta(\mathbf{X})$, and refer to X_i as an i^{th} element of $\mathbf{X}$ or an i^{th} model input. We shall denote the sub-vector $[X_i, X_j]^{\mathrm{T}}$ by $\mathbf{X}_{ij}$, and in general if $\mathbf{p}$ is a set of indices then $\mathbf{X}_{\mathbf{p}}$ is the sub-vector of $\mathbf{X}$ whose elements have those indices. Finally, $\mathbf{X}_{-\mathbf{p}}$ is the sub-vector of $\mathbf{X}$ containing all elements except $\mathbf{X}_{\mathbf{p}}$.

Variance decomposition can be seen to express the general input-output relation as a series of component functions with increase dimensionality (Cox, 1982; Efron and Stein, 1981; Li et al., 2006; Rabitz and Aliş, 1999):

$$\eta(\mathbf{X}) = E[Y] + \sum_{k=1}^{n} \eta_i(X_i) + \sum_{i<j} \eta_{ij}(\mathbf{x}_{ij}) + \sum_{i<j<k} \eta_{ijk}(\mathbf{X}_{ijk}) + \cdots + \eta_{12\cdots n}(\mathbf{X}) \tag{6.1}$$

in which the total terms in the decomposition is 2^n. Generally, each component function in the

equation can be defined by using conditional exsection as

$$\begin{cases} \eta_i(X_i) = E[Y|X_i] - E[Y] \\ \eta_{ij}(\mathbf{X}_{ij}) = E[Y|\mathbf{X}_{ij}] - \eta_i(X_i) - \eta_j(X_j) - E[Y] \\ \eta_{ijk}(\mathbf{X}_{ijk}) = E[Y|\mathbf{X}_{ijk}] - \eta_{ij}(X_{ij}) - \eta_{ik}(X_{ik}) - \eta_{jk}(X_{jk}) - \eta_i(X_i) - \eta_j(X_j) - \eta_k(X_k) - E[Y] \\ \quad \cdots \end{cases} \tag{6.2}$$

in which, the function $E[Y|X_i]$ would be an one-dimensional function only with respect to input variable X_i, and in general, $E[Y|\mathbf{X}_\mathbf{p}]$ will be an s-dimensional function with respect to input variables $\mathbf{X}_\mathbf{p}$ with sub-index vector $\mathbf{p} = \{i_1, i_2, \cdots, i_s\}$.

More importantly, it has been shown that all terms in Eq.(6.1) have following properties, when input random variables are independent (Rabitz and Aliş, 1999; Rahman, 2011)

Property 6.1. *Mean-value of each variance component function is zero, i.e.,*

$$E\big[\eta_p(X_p)\big] = \int_{X_p} \eta_p(\boldsymbol{x}_p)\, f_{X_p}(\boldsymbol{x}_p) d\boldsymbol{x}_p = 0 \quad \forall \boldsymbol{p} = \{i_1, i_2, \cdots, i_s\}, \text{and } \boldsymbol{p} \subseteq \{1, 2, \cdots, n\} \tag{6.3}$$

Property 6.2. *Each two variance component functions are orthogonal to each other:*

$$\big\langle \eta_{p_1}(\boldsymbol{X}_{p_1}), \eta_{p_2}(\boldsymbol{X}_{p_2}) \big\rangle = \int_{X_p} \eta_{p_1}(\boldsymbol{x}_{p_1}) \eta_{p_2}(\boldsymbol{x}_{p_2})\, f_{X_p}(\boldsymbol{x}_p) d\boldsymbol{x}_p = 0 \tag{6.4}$$

for at least one index differing in $\boldsymbol{p}_1 = \{i_1, i_2, \cdots, i_s\}$ *and* $\boldsymbol{p}_2 = \{j_1, j_2, \cdots, j_q\}$*; and* $\boldsymbol{p} = \boldsymbol{p}_1 \cup \boldsymbol{p}_2$.

Due to the two properties, the total output variance, $\mathrm{Var}[Y]$, can be decomposed into terms relating to the main effect of each input random and various interactions of an arbitrary sub-group input variables. A general decomposition like the analysis of variance, therefore, has been formulated in literature (Li et al., 2006; Oakley and O'Hagan, 2004; Saltelli, 2002) as

$$\mathrm{Var}[Y] = \sum_{k=1}^{n} V_i + \sum_{i<j} V_{ij} + \sum_{i<j<k} V_{ijk} + \cdots + V_{12\cdots n} \tag{6.5}$$

where $V_\mathbf{p} = E\big[\eta_\mathbf{p}^2(\mathbf{X}_\mathbf{p})\big]$ is the interaction effect of variables with sub-index $\mathbf{p} = \{i_1, i_2, \cdots, i_s\}$.

In the decomposition of output variance, V_i is the main effect on the reduction in $\mathrm{Var}[Y]$ that is obtained by learning the true value of X_i. V_{ij} is the component of $\mathrm{Var}[Y]$ due solely to uncertainty about the interaction between inputs X_i and X_j. Following the concept, if only

tow input variables are considered in the input-output relation, i.e., $Y = \eta(X_1, X_2)$, one has $\mathrm{Var}[Y] = V_1 + V_2 + V_{12}$, where V_{12} is an extra amount of variance removed when we learn both X_1 and X_2 over the main effect variances V_1 and V_2. Hence, the variance decomposition procedure gives us a partition of the output variance into the variances of each random variable (i.e., the main effects) and the variances of a sub-group of random variables (i.e., the interaction effects).

6.2.2 Global Sensitivity Coefficients

A measure on the influence of input random X_i with respect to model output can be evaluated by the conditional variance, $\mathrm{Var}\{E[Y|X_i]\}$, as shown in literature (Castillo et al., 2008; Oakley and O'Hagan, 2004; Saltelli and Sobol', 1995)

$$S_i = \frac{\mathrm{Var}\{E[Y|X_i]\}}{\mathrm{Var}[Y]} = \frac{E\left[\eta_i^2(X_i)\right]}{\mathrm{Var}[Y]} \tag{6.6}$$

which is referred to as the main effect index of model input X_i, and has been scaled in $[0, 1]$.

Following this notation, a general expression on an arbitrary interaction effect can be defined as

$$S_{\mathbf{p}} = \frac{\mathrm{Var}\{E[Y|\mathbf{X}_{\mathbf{p}}]\} - \sum_{\mathbf{q}\subset\mathbf{p}} V_{\mathbf{q}}}{\mathrm{Var}[Y]} = \frac{E\left[\eta_{\mathbf{p}}^2(\mathbf{X}_{\mathbf{p}})\right]}{\mathrm{Var}[Y]} \tag{6.7}$$

Each index $S_{\mathbf{p}}$ is an importance measure describing the corresponding percentage of output variance contributed by joint-group input variables with sub-index $\mathbf{p} = \{i_1, i_2, \cdots, i_s\}$. And summation of the normalized sensitivity indices are one:

$$\sum_{k=1}^{n} S_i + \sum_{i<j} S_{ij} + \sum_{i<j<k} S_{ijk} + \cdots + S_{12\cdots n} = 1 \tag{6.8}$$

in which, the first order index S_i give the influence of each variable taken along, whereas the higher orders indices account for possible mixed influence of various input random variables.

6.3 Computation of Sensitivity Coefficients

6.3.1 Problem Formulation

Computation of the Sobol' sensitivity index needs to calculate a series of n-dimensional integrals. Taken the main effect of X_i as an example, its variance contribution is defined as

$$V_i = E\big[\eta_i^2(X_i)\big] = \int_{X_i} \big[\psi_i(x_i) - E(Y)\big]^2 f_i(x_i)\mathrm{d}x_i \tag{6.9}$$

where $\psi_i(X_i)$ is the conditional expectation:

$$\psi_i(X_i) = E\big[Y|X_i\big] = \int_{\mathbf{X}_{-i}} \eta(\mathbf{x}) f_{\mathbf{X}_{-i}}(\mathbf{x}_{-i})\mathrm{d}\mathbf{x}_{-i} \tag{6.10}$$

Substituting for the equation, the variance, V_i, on main effect can be rewritten as

$$\begin{aligned} V_i &= \int_{X_i} \big[\psi_i(x_i) - E(Y)\big]^2 f_i(x_i)\mathrm{d}x_i \\ &= \int_{X_i} \left[\int_{\mathbf{X}_{-i}} \eta(\mathbf{x}) f_{\mathbf{X}_{-i}}(\mathbf{x}_{-i})\mathrm{d}\mathbf{x}_{-i}\right]^2 f_i(x_i)\mathrm{d}x_i - \big[E(Y)\big]^2 \end{aligned} \tag{6.11}$$

which can be expressed as a compact form by using the conditional expectation as

$$S_i = \frac{\mathrm{Var}\big\{E[Y|X_i]\big\}}{\mathrm{Var}[Y]} = \frac{E\big[\psi_i^2(X_i)\big] - \big[E(Y)\big]^2}{\mathrm{Var}[Y]} \tag{6.12}$$

in which one can see that computation of S_i requires the second-order moment of the univariate conditional expectation $\psi_i(X_i) = E[Y|X_i]$.

To compute the joint variance of X_i and X_j $(i < j)$, one needs the bivariate variance component function:

$$\eta_{ij}(\mathbf{X}_{ij}) = \psi_{ij}(\mathbf{X}_{ij}) - \eta_i(X_i) - \eta_j(X_j) - E[Y] \tag{6.13}$$

in which, the bivariate conditional expectation function, $\psi_{ij}(X_i, X_j)$, is defined as

$$\psi_{ij}(\mathbf{X}_{ij}) = E\big[Y|\mathbf{X}_{ij}\big] = \int_{\mathbf{X}_{-ij}} \eta(\mathbf{x}) f_{\mathbf{X}_{-ij}}(\mathbf{x}_{-ij})\mathrm{d}\mathbf{x}_{-ij} \tag{6.14}$$

Given the zero mean-value, the joint variance contribution V_{ij} will be

$$\begin{aligned} V_{ij} &= E\big[\eta_{ij}^2(X_i, X_j)\big] = E\Big\{\big[\psi_{ij}(\mathbf{X}_{ij}) - \eta_i(X_i) - \eta_j(X_j) - E(Y)\big]^2\Big\} \\ &= \int_{\mathbf{X}_{ij}} \left[\int_{\mathbf{X}_{-ij}} \eta(\mathbf{x}) f_{\mathbf{X}_{-ij}}(\mathbf{x}_{-ij})\mathrm{d}\mathbf{x}_{-ij}\right]^2 f_{\mathbf{X}_{ij}}(\mathbf{x}_{ij})\mathrm{d}\mathbf{x}_{ij} - V_i - V_j - \big[E(Y)\big]^2 \end{aligned} \tag{6.15}$$

The corresponding Sobol' sensitivity index to measure the joint effect of X_i and X_j is determined as

$$S_{ij} = \frac{\mathrm{Var}\{E[Y|\mathbf{X}_{ij}]\} - V_i - V_j}{\mathrm{Var}[Y]} = \frac{E\left[\psi_{ij}^2(\mathbf{X}_{ij})\right] - V_i - V_j - \left[E(Y)\right]^2}{\mathrm{Var}[Y]} \tag{6.16}$$

Generally, one can derive an arbitrary multi-variate sensitivity index, $S_{\mathbf{p}}$, to calibrate the joint effect of input random variables $\mathbf{X}_{\mathbf{p}}$ acted together (Saltelli and Sobol', 1995; Sobol', 2003). Also, one will notice that the general Sobol' index, $S_{\mathbf{p}}$, is also defined as the second moment of the s-variate conditional expectation, i.e., $\psi_{\mathbf{p}}(\mathbf{X}_{\mathbf{p}}) = E[Y|\mathbf{X}_{\mathbf{p}}]$, as well as all lower variance components. Therefore, a general expression on an s-variate Sobol' index can be derived as

$$S_{\mathbf{p}} = \frac{\mathrm{Var}\{E[Y|\mathbf{X}_{\mathbf{p}}]\} - \sum_{\mathbf{q}\subset\mathbf{p}} V_{\mathbf{q}}}{\mathrm{Var}[Y]} = \frac{E\left[\psi_{\mathbf{p}}^2(\mathbf{X}_{\mathbf{p}})\right] - \sum_{\mathbf{q}\subset\mathbf{p}} V_{\mathbf{q}} - [E(Y)]^2}{\mathrm{Var}[Y]} \tag{6.17}$$

where the subscript index vectors $\mathbf{p} = \{i_1, i_2, \cdots, i_s\}$ and $\mathbf{q} = \{j_1, j_2, \cdots, j_k\}$. The expression implies that, to computation of an s-variate sensitivity index, one has to evaluate $2^s - 1$ n-dimensional integrals:

$$E\left\{\left[E(Y|\mathbf{X}_{\mathbf{q}})^2\right]\right\} = \int_{\mathbf{X}_{\mathbf{q}}} \left[\int_{\mathbf{X}_{-\mathbf{q}}} \eta(\mathbf{x}) f_{\mathbf{X}_{-\mathbf{q}}}(\mathbf{x}_{-\mathbf{q}}) \mathrm{d}\mathbf{x}_{-\mathbf{q}}\right]^2 f_{\mathbf{X}_{\mathbf{q}}}(\mathbf{x}_{\mathbf{q}}) \mathrm{d}\mathbf{x}_{\mathbf{q}} \qquad \text{where } \mathbf{q} \subseteq \mathbf{p} \tag{6.18}$$

The high-dimensional integrals are difficult to be evaluated analytically, and thus, the sample-based method, say crude Monte Carlo simulation and its variants are recommended in literature (Ishigami and Homma, 1990; Sobol', 2001). The simulation methods are easy to be implemented, the variance reduction of the estimates, however, is very expensive due to the intensive computational cost. This motivates the development of M-DRM for the Sobol' index computation in the study.

6.3.2 Proposed Computational Method

On the development of multiplicative dimensional reduction method (M-DMR), one can refer to Section 5.2.2 in Chapter 5 for details. Here is the primary result on the univariate M-DRM.

Considering a general input-output relation, $y = \eta(\mathbf{x})$, through M-DRM, the multi-variate model can be approximated as an multiplicative form of n one-dimensional functions:

$$\eta(\mathbf{x}) \approx \left[\eta(\boldsymbol{c})\right]^{1-n} \prod_{k=1}^{n} \eta(c_1, \cdots, c_{k-1}, x_k, c_{k+1}, \cdots, c_n) \tag{6.19}$$

where $\boldsymbol{c} = [c_1, c_2, \cdots, c_n]^{\mathrm{T}}$ is referred to as the cut-point of the approximation. In the univariate M-DRM approximation, one should note that the function $\eta(c_1, \cdots, c_{k-1}, x_k, c_{k+1}, \cdots, c_n)$ is an one-dimensional function only with respect to x_k by fixing other input variables with the corresponding cut points. The Chapter is proposed to develop an efficient computational method to conduct global sensitivity analysis by using the M-DRM method.

To demonstrate the proposed M-DRM for Sobol' index computation, we first consider the main effect of an i^{th} random variable, X_i. Through the formulation in Section 6.3.1, one needs to calculate the second-order moment of the univariate conditional expectation $\psi_i(X_i) = E[Y|X_i]$:

$$E\left[\psi_i^2(X_i)\right] = E\left\{\left[E(Y|X_i)\right]^2\right\} = \int_{X_i}\left[\int_{\mathbf{X}_{-i}} \eta(\mathbf{x}) f_{\mathbf{X}_{-i}}(\mathbf{x}_{-i})\mathrm{d}\mathbf{x}_{-i}\right]^2 f_i(x_i)\mathrm{d}x_i \tag{6.20}$$

Substituting for the M-DRM approximation of $\eta(\mathbf{x})$, the integral can be rewritten as

$$E\left[\psi_i^2(X_i)\right] \approx \int_{X_i}\left\{\int_{\mathbf{X}_{-i}}\left[\eta(\boldsymbol{c}) \times \prod_{k=1}^{n}\frac{\eta(x_k, \boldsymbol{c}_{-k})}{\eta(\boldsymbol{c})}\right] f_{\mathbf{X}_{-i}}(\mathbf{x}_{-i})\mathrm{d}\mathbf{x}_{-i}\right\}^2 f_i(x_i)\mathrm{d}x_i \tag{6.21}$$

in which, each one-dimensional function has be rewritten in a compact form:

$$\eta(x_k, \boldsymbol{c}_{-k}) = \eta(c_1, \cdots, c_{k-1}, x_k, c_{k+1}, \cdots, c_n)$$

Therefore, given mutually independent input random variables, the original n-dimensional integration in terms of $E\left[\psi_i^2(X_i)\right]$ has been further simplified as a series of one-dimensional integrations:

$$E\left[\psi_i^2(X_i)\right] \approx [\eta(\boldsymbol{c})]^{2-2n} \times \prod_{k=1, k\neq i}^{n}\left[\int_{X_k}\eta(x_k, \boldsymbol{c}_{-k}) f_k(x_k)\mathrm{d}x_k\right]^2 \times \int_{X_i}[\eta(x_i, \boldsymbol{c}_{-k})]^2 f_i(x_i)\mathrm{d}x_i \tag{6.22}$$

in which, $\eta(\boldsymbol{c})$ is a constant as model $Y = \eta(\mathbf{X})$ deterministically evaluated at the cut-point $\boldsymbol{c}_{-k}$; the second term is the product of $n-1$ squared mean-values of one-dimensional function $\eta(X_k, \boldsymbol{c}_{-k})$ as $k = 1, \cdots, i-1, i+1, \cdots, n$; and the third term is the second-order moment of $\eta(X_k, \boldsymbol{c}_{-k})$.

In general, to compute an s-variate Sobol' index, $S_{\mathbf{p}}$, the corresponding second-order moment of the conditional expectation function $E[Y|\mathbf{X}_{\mathbf{p}}]$ has been defined as follows:

$$E\left\{\left[E\left(Y|\mathbf{X}_{\mathbf{p}}\right)\right]^2\right\} = E\left[\psi_{\mathbf{p}}^2(\mathbf{X}_{\mathbf{p}})\right] = \int_{\mathbf{X}_{\mathbf{p}}}\left[\int_{\mathbf{X}_{-\mathbf{p}}}\eta(\mathbf{x}) f_{\mathbf{X}_{-\mathbf{p}}}(\mathbf{x}_{-\mathbf{p}})\mathrm{d}\mathbf{x}_{-\mathbf{p}}\right]^2 f_{\mathbf{X}_{\mathbf{p}}}(\mathbf{x}_{\mathbf{p}})\mathrm{d}\mathbf{x}_{\mathbf{p}} \tag{6.23}$$

where the s-variate multiple index vector is defined as $\mathbf{p} = \{i_1, i_2, \cdots, i_s\}$.

Substituting for the M-DRM approximation in Eq.(6.19), one can simplify the high-dimensional integration as

$$E\left[\psi_{\mathbf{p}}^2(\mathbf{X}_{\mathbf{p}})\right] \approx \left[\eta(\boldsymbol{c})\right]^{2-2n} \times \prod_{\substack{k=1 \\ k\neq i_1\cdots i_s}}^{n} \left\{E\left[\eta(X_k, \boldsymbol{c}_{-k})\right]\right\}^2 \times \prod_{k=i_1\cdots i_s} E\left\{\left[\eta(X_k, \boldsymbol{c}_{-k})\right]^2\right\} \tag{6.24}$$

in which, one can make a general conclusion that the proposed M-DRM can approximate the second-order moment integration with respect to an s-variate conditional expectation as the product of $n-s$ mean-values and s second-order moments of $\eta(X_k, \boldsymbol{c}_{-k})$:

$$\begin{cases} E\left[\eta(X_k, \boldsymbol{c}_{-k})\right] = \displaystyle\int_{X_k} \eta(c_1, \cdots, c_{k-1}, x_k, c_{k+1}, \cdots, c_n)\, f_k(x_k)\mathrm{d}x_k \\ E\left\{[\eta(X_k, \boldsymbol{c}_{-k})]^2\right\} = \displaystyle\int_{X_k} [\eta(c_1, \cdots, c_{k-1}, x_k, c_{k+1}, \cdots, c_n)]^2\, f_k(x_k)\mathrm{d}x_k \end{cases} \tag{6.25}$$

The proposed M-DRM can also be employed to compute statistical moments of model output. In the variance-based global sensitivity analysis, for instance, the overall mean-value and second order moment of output are approximated as

$$\begin{cases} E\left[\eta(\mathbf{X})\right] \approx \left[\eta(\boldsymbol{c}_{-k})\right]^{1-n} \times \displaystyle\prod_{k=1}^{n} \left[\int_{X_k} \eta(c_1, \cdots, c_{k-1}, x_k, c_{k+1}, \cdots, c_n)\, f_k(x_k)\mathrm{d}x_k \right] \\ E\left\{\left[\eta(\mathbf{X})\right]^2\right\} \approx \left[\eta(\boldsymbol{c}_{-k})\right]^{2-2n} \displaystyle\prod_{k=1}^{n} \left\{ \int_{X_k} \left[\eta(c_1, \cdots, c_{k-1}, x_k, c_{k+1}, \cdots, c_n)\right]^2 f_k(x_k)\mathrm{d}x_k \right\} \end{cases} \tag{6.26}$$

as well as the estimate of total output variance: $\mathrm{Var}[Y] = E[Y^2] - [E(Y)]^2$.

The one-dimensional integrals derived by M-DRM can be efficiently calculated by using the rules of Gaussian quadrature as shown in Chapter 5:

$$\begin{cases} \displaystyle\int_{X_k} \eta(x_k, \boldsymbol{c}_{-k})\, f_k(x_k)\mathrm{d}x_k \approx \sum_{l=1}^{N} w_{kl}\, \eta(c_1, \cdots, c_{k-1}, x_{kl}, c_{k+1}, \cdots, c_n) \\ \displaystyle\int_{X_k} \left[\eta(x_k, \boldsymbol{c}_{-k})\right]^2 f_k(x_k)\mathrm{d}x_k \approx \sum_{l=1}^{N} w_{kl} \left[\eta(c_1, \cdots, c_{k-1}, x_{kl}, c_{k+1}, \cdots, c_n)\right]^2 \end{cases} \tag{6.27}$$

in which, an l^{th} Gaussian point, x_{kl}, and weight, w_{kl}, can be determined according to the probability measure of random variable X_k.

6.3.3 Efficiency Analysis

With an N^{th} order Gauss-type integration scheme, computational cost associated with M-DRM for Sobol' index computation can be assessed by

$$\text{Total Number of Functional Evaluations: } = 1 + nN \tag{6.28}$$

which is believed to reduce the number of functional evaluation from N^n by employing the direct tensor Gauss quadrature method.

The primary superiority of use the proposed M-DRM on Sobol' index computation is due to that one can approximate a high-dimensional integration as the product of a series of one-dimensional integrals, which would be trusted to dramatically reduce the total number of functional evaluations as compared to available methods in literature.

6.4 Numerical Examples

6.4.1 General

Six examples in literature are employed in the section to illustrate the applications of M-DRM for Sobol' sensitivity index computation. A flow chart on numerical implementation of the proposed method is summarized as shown in Figure 6.1. Benchmarks determined by analytic integration (for low dimensional example, i.e., $n \leqslant 3$) or crude Monte Carlo simulation with 10^6 samples (for high dimensional example, i.e., $n \geqslant 4$) are also provided to examine the accuracy and efficiency of M-DRM on Sobol' index computation.

6.4.2 Polynomial Function

The first example considers a polynomial function:

$$\eta(\mathbf{X}) = \frac{1}{2^n} \prod_{k=1}^{n} \left(3X_k^2 + 1\right) \tag{6.29}$$

which is proposed by Sobol' (2003), and later studied by Sudret (2008b) to examine the polynomial chaos expansion (PCE) method on global sensitivity analysis.

In the polynomial function, each input variable X_i is independently and identically distributed (i.i.d.) as a Uniform random variable over $[0, 1]$. Exact mean-value and variance are determined

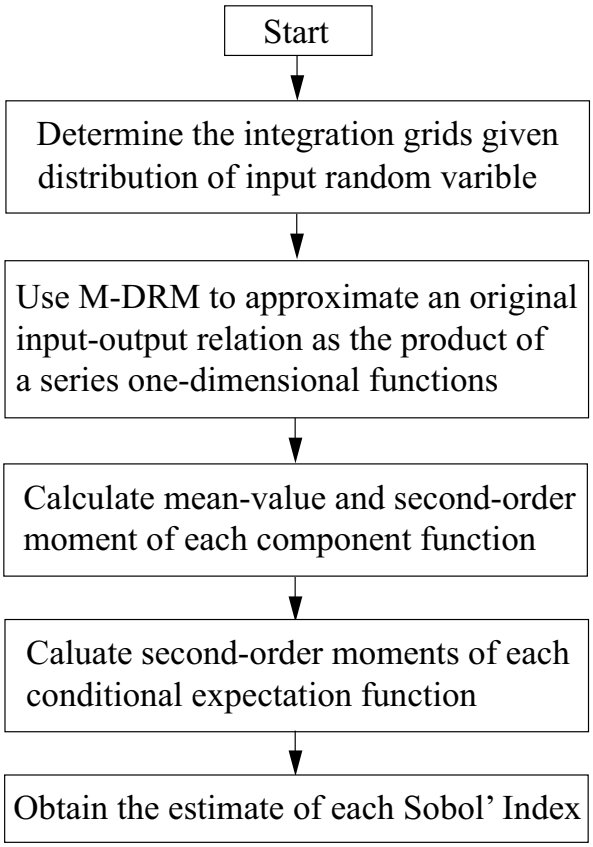

Figure 6.1: Steps of M-DRM for Sobol' sensitivity index computation

as

$$E[\eta(\mathbf{X})] = 1; \qquad \mathrm{Var}[Y] = (6/5)^n - 1$$

And the analytic expressions of Sobol' sensitivity index are:

$$S_{i_1 i_2 \cdots i_s} = \frac{5^{-s}}{(6/5)^n - 1} \qquad (1 \leqslant i_1 < \cdots < i_s \leqslant n)$$

Table 6.1 reported the results on global sensitivity analysis by using the methods of polynomial chaos expansion (PCE), polynomial dimensional decomposition (PDD) and the proposed multiplicative dimensional reduction method (M-DRM), respectively.

Assumed that $n = 3$, the polynomial function in Eq.(6.29) is defined as the tensor product of three quadratic functions. The proposed M-DRM with three-order Gauss-Legendre quadrature ($N = 3$) is able to provide exact result of each Sobol' sensitivity index.

Sudret (2008b) approximated the polynomial function with three- and six-order truncated PCE meta-model, i.e., $p = 3$ and $p = 6$, respectively, which needs 29 and 116 function e-

Table 6.1: Global sensitivity analysis of polynomial function with various methods

Sensitivity Index	M-DRM		PCE		PDD		Exact
	$N=2$	$N=3$	$p=3$	$p=6$	$m=1$	$m=2$	
S_1	0.2780	0.2747	0.2879	0.2747	0.2780	0.2747	0.2747
S_2	0.2780	0.2747	0.2773	0.2747	0.2780	0.2747	0.2747
S_3	0.2780	0.2747	0.2773	0.2747	0.2780	0.2747	0.2747
S_{12}	0.0521	0.0549	0.0506	0.0549	0.0521	0.0549	0.0549
S_{13}	0.0521	0.0549	0.0506	0.0549	0.0521	0.0549	0.0549
S_{23}	0.0521	0.0549	0.0481	0.0549	0.0521	0.0549	0.0549
S_{123}	0.0098	0.0110	0.0081	0.0110	0.0098	0.0110	0.0110
Number of FEs	7	10	29	116	8	27	––

PCE: Polynomial chaos expansion (Sudret, 2008b); PDD: Polynomial dimensional decomposition (Rahman, 2011); M-DRM: The proposed multiplicative dimensional reduction method.

valuations, respectively, to compute the corresponding Sobol' sensitivity index. Rahman (2011) integrated the additive (or conventional) dimensional reduction method in PCE to simplify the high-dimensional integration with respect to the expansion coefficients. The method reduced the number of functional evaluations as 8 and 27, respectively, by using the univariate C-DRM ($m=1$) and bivariate C-DRM ($m=2$), respectively. Compared to the methods in literature, the proposed M-DRM is more efficient and accurate, since it needs only 10 ($=3\times 3+1$) functional evaluations to obtain the estimates as exact as analytic integration.

6.4.3 Ishigami Function

The example considers a triangle function proposed by Ishigami and Homma (1990):

$$\eta(\mathbf{X}) = \sin(X_1) + a[\sin(X_2)]^2 + b\sin(X_1)X_3^2 \tag{6.30}$$

where X_i are i.d.d. Uniform random variables over $[-\pi,\pi]$.

The total output variance is analytically determined as

$$\mathrm{Var}[Y] = \frac{1}{2} + \frac{a^2}{8} + \frac{b\pi^4}{5} + \frac{b^2\pi^8}{18}$$

as well as the corresponding Sobol' sensitivity indices:

$$S_1 = \frac{b^2\pi^8 + 10b\pi^4/5 + 25}{50\text{Var}[Y]}; \qquad S_2 = \frac{a^2/8}{\text{Var}[Y]}; \qquad S_{13} = \frac{8b^2\pi^8/225}{\text{Var}[Y]} \tag{6.31}$$

which implying other indices are almost zero.

We assume that $a = 0.1$ and $b = 0.7$, respectively. The various orders of Gauss-Legnedre quadrature are employed to estimate of the Sobol' indices as summarized in Table 6.2.

Table 6.2: Global sensitivity analysis of the Ishigami function

Sensitivity	M-DRM				Exact
	$N = 3$	$N = 4$	$N = 5$	$N = 6$	
S_1	0.5912	0.4147	0.3942	0.3942	0.3932
RE (%)	50	5.5	0.26	0.26	−−
S_{13}	0.4088	0.5853	0.6058	0.6058	0.5992
RE (%)	−33	−3.5	−0.17	−0.17	−−
Var$[Y]$	732.41	293.44	269.62	274.56	272.25
RE (%)	69	7.7	−1.04	0.78	−−
No. FEs	7	10	13	16	−−

M-DRM: The proposed multiplicative dimensional reduction method;
RE: Relative Error: = (M-DRM − Exact)/Exact×100%.

The example examines the proposed M-DRM on global sensitivity analysis with varied orders (N) of Gauss quadrature. Compared to benchmarks, one can see that the corresponding relative errors (REs) by M-DRM decrease with the increase of order of Gauss quadrature. Using three-point ($N = 3$) Gauss-Legendre quadrature, the estimates of Sobol' index have a large relative error ($\approx 50\%$), whereas M-DRM can remarkably improve the accuracy of the estimates with five-order ($N = 5$) Gauss quadrature. The small REs (0.26% and 0.17%) associated with S_1 and S_{13} highlight the accuracy of M-DRM for Sobol' index computation. In addition, it is interesting to see that M-DRM was companied a rather small increase in terms of the total number of mechanistic model evaluations, i.e., 16 $(= 5 \times 3 + 1)$ by five-order Gauss quadrature versus 7 $(= 2 \times 3 + 1)$ by three-order Gauss quadrature, which has further confirmed the efficiency of M-DRM for Sobol' index computation.

6.4.4 Non-Smooth Function

The third example examines of the performance of M-DRM on Sobol' index computation by considering a non-smooth function (Sobol', 2001):

$$\eta(\mathbf{X}) = \prod_{k=1}^{n} \frac{|4X_k - 2 + a_k|}{a_k + 1} \tag{6.32}$$

in which, n-dimensional input random variables X_k $(k = 1, \cdots, n)$ are uniformly distributed over $[0, 1]$. Analytic results of output variance and sensitivity indices are given as

$$\begin{cases} \text{Output Variance :} & \text{Var}[Y] = -1 + \prod_{k=1}^{n} \left[\frac{1}{3(a_k + 1)^2} + 1 \right] \\ \text{Sobol' Index :} & S_{i_1 \cdots i_s} = \frac{1}{\text{Var}[Y]} \prod_{k=1}^{s} \frac{1}{3(a_{i_k} + 1)^2} \qquad (1 \leqslant i_1 < \cdots i_s \leqslant n) \end{cases}$$

Assume that the dimensionality parameter $n = 8$, and the constants $a_1 = 0.001$, $a_2 = 1$, $a_3 = 4.5$, $a_4 = 9$ and $a_5 = \cdots = a_8 = 99$, respectively (Sobol', 2003). Main effects of input variables determined by M-DRM are summarized in Table 6.3, together with the results in literature provided by methods trivariate polynomial dimensional decomposition (T-PDD), random balance design (RBD) and state-dependent parameter modelling (SDP), respectively.

According to the results in Table 6.3, one can see that the primary contribution (71.62%) of output variance comes from X_1 due to $a_1 = 0.001$, and variables $X_{5\sim9}$ almost make the null contributions due to large values of $a_5 \sim a_8$. Compared to the benchmarks, M-DRM associated with ten order (i.e., $N = 10$) Gauss-Legendre quadrature obtains fairly accurate estimates of S_k $(k = 1, \cdots, 8)$. Together with the smaller numbers of functional evaluations, i.e., 81 $(= 1 + 8 \times 10)$, compared to other methods in literature, one can conclude that M-DRM can achieve accurate estimates of Sobol' index with small number of functional evaluations. Since the function is defined as a product form in terms of each random variable, the trivariate PDD needs 30529 functional evaluations, as well as a similar number of mechanistic model evaluations d by using large size RBD and SDP methods.

Table 6.3: Results of global sensitivity analysis of the non-smooth function

Sensitivity	M-DRM		PDD		RBD		SDP		Exact
	$N = 5$	$N = 10$	$m = 4$	$m = 8$	Small Size	Large Size	Small Size	Large Size	
S_1	0.7049	0.7172	0.7140	0.7218	0.704	0.714	0.717	0.716	0.7162
S_2	0.1664	0.1803	0.1642	0.1723	0.173	0.181	0.179	0.179	0.1791
S_3	0.0212	0.0239	0.0193	0.0207	0.0314	0.0278	0.0235	0.0236	0.0237
S_4	0.0064	0.0072	0.0053	0.0057	0.0084	0.0073	0.0070	0.0071	0.0072
S_5	6.3×10^{-5}	7.2×10^{-5}	4.8×10^{-5}	5.2×10^{-5}	4.4×10^{-3}	3.0×10^{-4}	2.1×10^{-5}	6.1×10^{-5}	7.2×10^{-5}
S_6	6.3×10^{-5}	7.2×10^{-5}	4.8×10^{-5}	5.2×10^{-5}	3.8×10^{-3}	3.0×10^{-4}	2.3×10^{-5}	5.8×10^{-5}	7.2×10^{-5}
S_7	6.3×10^{-5}	7.2×10^{-5}	4.8×10^{-5}	5.2×10^{-5}	2.2×10^{-3}	4.0×10^{-4}	2.2×10^{-5}	5.8×10^{-5}	7.2×10^{-5}
S_8	6.3×10^{-5}	7.2×10^{-5}	4.8×10^{-5}	5.2×10^{-5}	1.7×10^{-3}	3.0×10^{-4}	2.0×10^{-5}	5.9×10^{-5}	7.2×10^{-5}
No. FEs	41	81	4065	30529	4096	32768	4096	32768	––

M-DRM: The proposed multiplicative dimensional reduction method; RBD: Random balance design (Gatelli et al., 2009);
PDD: Polynomial dimensional decomposition (Rahman, 2011); SDP: State-dependent parameter model (Gatelli et al., 2009).

6.4.5 Corner Peak Function

The example examines the performance of M-DRM by considering the corner peak function (Genz, 1987):

$$\eta(\mathbf{X}) = \left(1 + \sum_{k=1}^{n} a_k X_k\right)^{-(n+1)} \tag{6.33}$$

in which, the independent input variables X_i are uniformly distributed over $[0, 1]$.

Two cases in terms of various dimensionality of input vector $\mathbf{X}$ are considered. The first case assumed that $n = 3$, and two combinations (uniform and non-uniform) of constants $\boldsymbol{a}$ are considered. Benchmarks of main effects are determined through analytical integration as shown in Table 6.4. M-DRM with three-order ($N = 3$) Gauss quadrature can obtain very accurate estimates of Sobol' index compared to the benchmarks.

Table 6.4: Main effect of Sobol' index of the corner peak function ($n = 3$)

Sensitivity	$a_1 = a_2 = a_3 = 0.01$		$a_1 = 0.02,\ a_2 = 0.05,\ a_3 = 0.08$	
	M-DRM	Exact	M-DRM	Exact
S_1	0.3333	0.3333	0.0430	0.0429
S_2	0.3333	0.3333	0.2685	0.2681
S_3	0.3333	0.3333	0.6860	0.6851
No. FEs	10	––	10	––

M-DRM: The proposed multiplicative dimensional reduction method;

Benchmark: Result determined by analytic integration.

The second case assumes that $n = 10$ (i.e., ten input random variables), and the weighting constants are equally spaced as $a_1 = 0.01, a_2 = 0.02, \cdots, a_{10} = 0.1$. Since the analytic integrations on the Sobol' index are impossible due to the high dimensionality of $\mathbf{X}$, Monte Carlo simulation is conducted to estimate each main effect and and the associated variation.

After 10 rounds simulation with 10^5 samples in each, 95^{th} confidence intervals (CIs) of each main effect are determined as shown in Figure 6.2. The close estimates provided by M-DRM has verified the accuracy of proposed method on Sobol' sensitivity index computation. In addition, the small number of functional evaluations ($31 = 3 \times 10 + 1$) has further highlighted its superiority on handling with the involved high-dimensional integrations.

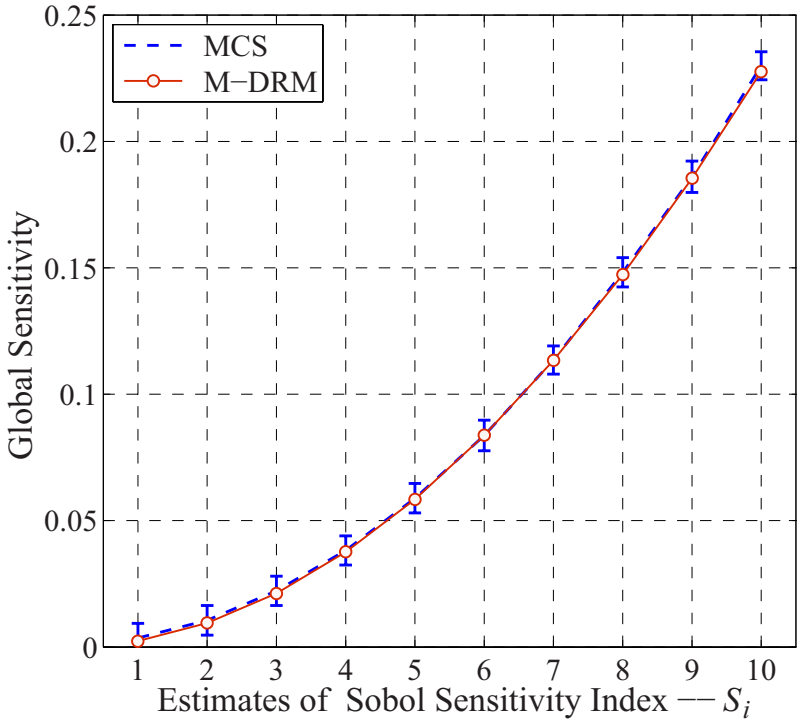

Figure 6.2: Estimates of Sobol' sensitivity index for the example of corner-peak function (M-DRM: The proposed multiplicative dimensional reduction method; MCS: Ten rounds of Monte Carlo simulation with 10^5 samples in each).

6.4.6 Thermal Stress Intensity Factor

A crack has been observed in a metal membrane due to the variation of temperature in a heating system. During functioning, the system is heated with a permanent uniform temperature field, T_0. During maintenance, the system is stopped, and consequently the temperature is reduced to ambient temperature, T. The heat drop implies tension and the crack opening according to mode I. Mathematic model of the corresponding stress intensity factor (SIF) is given as (Tada et al., 2000)

$$K_{\mathrm{IC}}(\mathbf{X}) = -\alpha E(T - T_0)\sqrt{\frac{\pi a}{\cos(\pi a/4B)}}\left[1 - 0.025\left(\frac{a}{2B}\right)^2 + 0.06\left(\frac{a}{2B}\right)^4\right] \tag{6.34}$$

where the properties of input random variables, $\mathbf{X}$, are listed in Table 6.5.

With the proposed method of M-DRM, main effect of each random variable is estimated by two ($N = 2$) and four ($N = 4$) orders of Gauss quadrature, respectively. Together with benchmarks provided by Monte Carlo simulation (10 rounds simulation and 10^5 samples in each), the

Table 6.5: Random variables in the example of thermal stress intensity factor

Variable	Description	Distribution	Mean	Std.D	COV
T_0	Initial Temperature	Lognormal	100 °C	20.0 °C	0.20
T	Amphibian Temperature	Lognormal	20 °C	4.0 °C	0.20
a	Crack Size	Lognormal	10 mm	2.0 mm	0.20
B	Width of Plate	Lognormal	200 mm	40 mm	0.20
E	Young's Module	Lognormal	210 GPa	42 GPa	0.20
α	Expansion Cof.	Deterministic	12.5×10^{-6} °C^{-1}	—	—

Table 6.6: Global sensitivity analysis of the thermal stress intensity factor

Variable	M-DRM		Monte Carlo Simulation	
	$N = 2$	$N = 4$	Mean-Value	95^{th} CI
T_0	0.5256	0.5265	0.5263	[0.5236, 0.5291]
T	0.0210	0.0211	0.0212	[0.0195, 0.0228]
a	0.0860	0.0833	0.0836	[0.0811, 0.0860]
B	2.2×10^{-7}	2.5×10^{-7}	2.0×10^{-4}	[−0.0016, 0.0021]
E	0.3364	0.3369	0.3388	[0.3363, 0.3413]
Mean	37.05	37.06	37.05	[37.03, 37.08]
Variance	155.9	163.0	162.9	[162.3, 163.6]
No. FEs	11	21	$10^5 \times 10 \times 6$	

M-DRM: The proposed multiplicative dimensional reduction method.

determined Sobol' indices are summarized and verified as shown in Table 6.6. According to the estimates, one can see that the M-DRM with four-order Gauss-Hermite quadrature (due to the lognormally distributed input random variables) is believed to provide accurate results on the global sensitivity analysis of the probabilistic thermal SIF example.

6.4.7 Eigenvalue Analysis of a Spring-Mass System

The last example examine the accuracy of M-DRM for global sensitivity analysis by considering eigenvalue analysis of a linear spring-mass system (Rahman, 2006). The eigenvalue problem can be formulated as

$$\mathbf{K}\boldsymbol{\Phi} = \lambda \mathbf{M}\boldsymbol{\Phi} \tag{6.35}$$

Table 6.7: Global sensitivity analysis: a 3-DOF spring-mass system

Eigenvalue	$\lambda_1(\mathbf{X})$ (rad/s)		$\lambda_2(\mathbf{X})$ (rad/s)		$\lambda_3(\mathbf{X})$ (rad/s)	
Sensitivity	M-DRM	MCS 95$^{\text{th}}$ CI	M-DRM	MCS 95$^{\text{th}}$ CI	M-DRM	MCS 95$^{\text{th}}$ CI
S_{M_1}	0.1644	[0.1572, 0.1755]	0.0325	[0.0264, 0.0447]	0.2356	[0.2246, 0.2393]
S_{M_2}	0.1648	[0.1511, 0.1756]	0.5547	[0.5360, 0.5604]	0	[−0.0057, 0.0064]
S_{M_3}	0.1644	[0.1525, 0.1813]	0.0325	[0.0205, 0.0492]	0.2356	[0.2263, 0.2429]
S_{K_1}	0.1672	[0.1471, 0.1759]	0.0021	[−0.0125, 0.0162]	0.0036	[−0.0019, 0.0102]
S_{K_2}	0.1659	[0.1509, 0.1787]	0.0343	[0.0202, 0.0480]	0	[−0.0053, 0.0067]
S_{K_3}	0.1672	[0.1523, 0.1787]	0.0021	[−0.0095, 0.0169]	0.0038	[−0.0022, 0.0111]
S_{K_4}	0	[−0.0102 , 0.0156]	0.1680	[0.1556, 0.1814]	0.0038	[−0.0014, 0.0112]
S_{K_5}	0	[−0.0105, 0.0157]	0.1680	[0.1561, 0.1823]	0.0038	[−0.0011, 0.0111]
S_{K_6}	0	[−0.0103, 0.0156]	0	[−0.0127, 0.0132]	0.5063	[0.5047, 0.5215]
Mean	1.0	[1.0, 1.001]	4.063	[4.062, 4.063]	8.231	[8.230, 8.232]
Variance	0.0148	[0.0147, 0.0153]	0.3051	[0.3005, 0.3060]	1.693	[1.639, 1.653]
No. FEs	46	$10^5 \times 10 \times 10$	46	$10^5 \times 10 \times 10$	46	$10^5 \times 10 \times 10$

where $\mathbf{M}$ and $\mathbf{K}$ are the mass matrix and stiffness matrix; and λ_k is a kth order eigenvalues of the system.

In deterministic scenario, each eigenvalue can be determined via the system characteristic equation:

$$\det[\mathbf{K} - \lambda\mathbf{M}] = 0 \tag{6.36}$$

Structural mass matrix is:

$$\mathbf{M} = \begin{bmatrix} M_1 & 0 & 0 \\ 0 & M_2 & 0 \\ 0 & 0 & M_3 \end{bmatrix}$$

as well as the stiffness matrix:

$$\mathbf{K} = \begin{bmatrix} K_1 + K_4 + K_6 & -K_4 & -K_6 \\ -K_4 & K_2 + K_4 + K_5 & -K_5 \\ -K_6 & -K_5 & K_3 + K_5 + K_6 \end{bmatrix}$$

Mean-values of mass and stiffness are assumed as $\mu_{M_i} = 1\text{kg}$ $(i = 1, 2, 3)$, $\mu_{K_i} = 1\text{N/m}$ $(i = 1, \cdots, 5)$, and $\mu_{K_6} = 3\text{N/m}$. All input random variables are Lognormally distributed with COV $= 15\%$.

With five-order Gauss-Hermite quadrature, the sensitivity indices are computed for each eigenvalue. According to in Table 6.7, it is clear to see that the proposed method is fairly efficient, i.e., the number of functional evaluations is only $46\,(= 5 \times 9 + 1)$. Compared to the confidence intervals provided by Monte Carlo simulation (10 rounds of simulation with 10^5 samples in each), it is verified the accuracy of the prosed method.

6.5 Conclusion

Objective of the Chapter is designed to propose a computationally efficient method for variance-based global sensitivity analysis. Through the concept of general analysis of variance (ANOVA), the variance of a system output was decomposed as the summation of a series second-order moments of the conditional expectation. The ANOVA is an extension of the classical ANOVA developed in linear regression or design of experiment.

Applications of the M-DRM for global sensitivity analysis were examined by six examples selected from literature, which includes four mathematic problems and two engineering applica-

tions. Compared to benchmarks, the results indicate that the proposed M-DRM method provides fairly accurate estimates about the global sensitivity coefficients.

Chapter 7

Polynomial Chaos Expansion with M-DRM

7.1 Introduction

7.1.1 Literature Review

The term polynomial chaos was coined by Norbert Wiener in 1938 in his work studying the decomposition of Gaussian stochastic process (Wiener, 1938). This was long before the phenomenon of chaos in dynamic systems was known. In Wiener's work, Hermite polynomials serve as an orthogonal base, and the validity of the approach was proved by Cameron and Martin (1947).

The original polynomial chaos work was started by Ghanem and Spanos (1991) for the probabilistic mechanics computation. Inspired by the theory of Wiener-Hermite polynomial chaos, Ghanem employed Hermite polynomials as an complete base to represent a random process and applied the technique to many practical engineering problems with success.

The use of Hermite polynomials, albeit mathematically sound, presents difficulties in some applications, particularly in terms of convergence and probability approximation for non-Gauss problems (Orszag and Bissonnette, 1967). Consequently, the generalized polynomial chaos was proposed in literature (Xiu and Karniadakis, 2002b, 2003) to alleviate the difficulty. In generalized polynomial chaos, it depends on the probability distribution of an input variable to select the representative orthogonal polynomial. Optimal convergence can be achieved by choosing a proper basis, and strength of use the generalized polynomial chaos was demonstrated for a variety of partial differential equations (Xiu and Karniadakis, 2002a).

The work on generalized polynomial chaos expansion was further extended by not requiring

the basis polynomials to be globally smooth. In fact, in principle any set of complete bases can be a viable choice. Such generalization includes the piecewise polynomial basis, the wavelet basis (Maître et al., 2004), and multi-element polynomial chaos (Doostan et al., 2007).

Upon choosing a proper basis, a numerical technique is needed to conduct the polynomial chaos expansion. The early works were mostly based on the Galerkin method, which minimizes the error of a finite-order expansion by an orthogonal projection (Ghanem and Spanos, 1991). This is the stochastic Galerkin approach (Li and Ghanem, 1998). The Galerkin procedure usually results in a set of coupled deterministic equations and requires additional effort to evaluate. Also, derivation of the extended set of equations is also a challenging task when the mechanistic model takes a complicated form.

Another approach for the objective can be realized by repetitively executing an established deterministic code on a prescribed node in the random space. Upon completing the simulations, a postprocessing procedure is followed to obtain the desired output properties. This is the stochastic collocation method (Babuška et al., 2007). The idea, primarily based on the classical simulation method, the crude Monte Carlo simulation. Other works in the field mostly employ the method of tensor Gasss quadrature. Although the tensor product construction makes mathematical analysis more accessible, the total number of functional evaluations grows exponentially fast with respect to the number of input variables, which is known as the curse of dimensionality. Since each node requires a fully scale deterministic model evaluation, the tensor product approach is practically only for a problem with the low dimensionality input variables.

To alleviate the computational burden due to a large number of input variables, the adaptive sparse grid collocation method was developed in literature (Blatman and Sudret, 2010a,b). Even though the number of functional evaluations can be reduced to some extents, the involved computational cost needs to explore an efficient method for PCE meta-model construction (Blatman, 2009).

7.1.2 Objective

The Chapter is designed to propose a computationally efficient method on a meta-model construction with polynomial chaos expansion. Since coefficients of the surrogate model are defined as a series high-dimensional integrations, compared to the methods in literature, the proposed method is ideally sought to be:

- easy to implement. The method is desired to reserve the simplicity of Monte Carlo simula-

tion, i.e., uncertainty quantification is only based on a couple of "predefined" deterministic model evaluations. This is a stochastic collocation method in nature; and

- not only efficient, i.e., the required number of mechanistic model analyses is very small, but also accurate, i.e., it is capable to precisely determine the complete output distribution and a small failure probability associated with a predefined failure threshold.

The method is developed by using the multiplication dimensional reduction method (M-DRM) as proposed in Chapter 5. First of all, M-DRM is employed to approximate a general response function with multiple input variables as the product of a series low-dimensional functions. It helps to reduce the computational effort involved in the high-dimensional integrations. Together with the optimized Gauss grid, an efficient method for polynomial chaos expansion is proposed. The associated uncertainty quantification of a system will be implemented from the following aspects: (a) Moment computation; (b) The variance-based global sensitivity analysis; and (c) The complete output distribution estimation.

7.1.3 Organization

The Chapter is organized as follows. Section 7.2 collects the basic elements of polynomial chaos expansion (PCE), which include the orthogonality of the polynomial chaos, the construction of multi-dimensional polynomial chaos, the general expression of a PCE meta-model, and a brief review on the related computational methods in literature. Section 7.3 proposes the using of multiplicative dimensional reduction method for polynomial chaos expansion of a system. With the determined PCE meta-model, Section 7.4 summarizes a generic postprocessing procedure on uncertainty quantification. In numerical sections, examples form literature are employed to illustrate the proposed method for system uncertainty quantification. Section 7.8 summarizes the conclusion.

7.2 Polynomial Chaos Expansion (PCE)

7.2.1 Background

Polynomial chaos expansions have been introduced on stochastic mechanics in the early 90's by Ghanem and Spanos (1991). In the original setting, a boundary valued problem is considered in

which some parameters are modelled as random fields. The quantities of interest are the resulting stochastic displacement and stress fields. Thus the use of polynomial chaos expansion has been intimately associated with spatial variability and considered as a separate topic with respect to structural reliability for a while.

In the present study, the spectral expansion of an output quantity onto a bases made of orthogonal polynomials, commonly referred to as the polynomial chaos expansion are of interest. In this setup, characterizing a model response is equivalent to computing the corresponding coefficients of the PCE surrogate model. To achieve this, the stochastic collocation method allows to compute the multi-dimensional integration with respect to expansion coefficient with deterministic model evaluations. However, the methods in literature need demanding computational resources. Therefore, the study is proposed to reduce the computational burden in PCE by using the multiplicative dimensional reduction method (M-DRM). Together with the rules of Gauss quadrature, a non-intrusive method for system uncertainty propagation is proposed to construct the PCE meta-model based on a small number of "well chosen" deterministic analyses.

7.2.2 Polynomial Chaos Basis

One simple fashion of constructing an n-dimensional polynomial chaos is to follow the partial tensorization of one-dimensional polynomials. Thus, we first focus on the polynomials of a single standard Normal variable, X, with the probability density function of

$$f_X(x) = \frac{1}{\sqrt{2\pi}} \exp(-x^2/2) \tag{7.1}$$

By $\psi_k(X)$, we denote a k^{th} order polynomial. And following the same convention, the zeroth degree polynomial is defined as $\psi_0(X) = 1$. Recall that the polynomial basis are orthogonal to each other, which can be expressed as

$$\begin{aligned} E\big[\psi_i(X)\psi_j(X)\big] &= \big\langle \psi_i(X), \psi_j(X) \big\rangle \\ &= \int_X \psi_i(x)\psi_j(x) f_X(x) \mathrm{d}x = \delta_{ij} E\big[\psi_i^2(X)\big] \end{aligned} \tag{7.2}$$

where δ_{ij} is the Kronecker symbol, and it is equal to 1 if $i = j$ and 0 otherwise.

The one-dimensional polynomials thus defined, which are mutually orthogonal with respect to the standard Normal distribution, constitute a well-known family, the Hermite orthogonal

polynomials. In addition, the normalized polynomials can be determined as

$$\widehat{\psi}_k(X) = \frac{\psi_k(X)}{\sqrt{\langle \psi_k(X), \psi_k(X) \rangle}} = \frac{1}{\sqrt{k!}} \psi_k(X) \qquad (k = 0, 1, \cdots) \tag{7.3}$$

The normalized (Hermite) orthogonal polynomials have the following properties:

$$\begin{cases} E\big[\widehat{\psi}_k(X)\big] = E\big[\widehat{\psi}_0(X) \cdot \widehat{\psi}_k(X)\big] = 0 \quad (k = 1, 2, \cdots) \\ E\Big\{\big[\widehat{\psi}_k(X)\big]^2\Big\} = \int_X \big[\widehat{\psi}_k(x)\big]^2 f_X(x) \mathrm{d}x = 1 \quad (k = 0, 1, \cdots) \end{cases} \tag{7.4}$$

in which, one can see that the normalized orthogonal polynomials have the mean-value of zero only except $E\big[\widehat{\psi}_0(X)\big] = 1.0$, and the unit variance only except $\mathrm{Var}\big[\widehat{\psi}_0(X)\big] = 0$.

An n-dimensional polynomial chaos can be set up by tensorizing one-dimensional polynomials as follows. We will denote the multi-dimensional input variables as $\mathbf{X} = [X_1, X_2, \cdots, X_n]^{\mathrm{T}}$. Since these random variables are independent, the joint probability density of $\mathbf{X}$, then, can be defined using each marginal PDF:

$$f_{\mathbf{X}}(\mathbf{x}) = \prod_{k=1}^{n} f_k(x_k) \tag{7.5}$$

The chaos polynomial was originally formulated with standard Normal variables and Hermite polynomials as the finite-dimensional Wiener polynomial chaos (Wiener, 1938). It was later extended to other classical random variables from the Askey-scheme of polynomials (Xiu and Karniadakis, 2002b). The scheme classifies the hypergeometric orthogonal polynomials that satisfy some type of differential equations and indicates that the limit relations between them. Hermite polynomials are a subset of the Askey-scheme. And each subset of the orthogonal polynomials has different weighting function as defining the orthogonality relationship. It has been realized that some of these weighting functions are identical (or similar) to the probability density functions of certain random variables as shown in Table 7.1.

If the involved random variable does not listed in Table 7.1, it is possible to employ a nonlinear mapping such that the generalized polynomial chaos expansion can be applied to represent the new variable (Der Kiureghian and Liu, 1986; Rosenblatt, 1952). For instance, a Lognormal variable can be recast as a function of a standard Normal variable, which will be used in conjunction with the Hermit polynomial. As an alternative, ad hoc orthogonal polynomial can be generated for a random variable with an arbitrary probability measure (Wan and Karniadakis, 2006).

Table 7.1: Relation between orthogonal polynomial and random variable distribution

Polynomial	Weight Function	Support	Orthogonality	Distribution
Hermite	$\exp(-x^2/2)$	$(-\infty, +\infty)$	$\langle \psi_i, \psi_j \rangle = \sqrt{2\pi} i! \delta_{ij}$	Normal
Legendre	1	$[-1, 1]$	$\langle \psi_i, \psi_j \rangle = \frac{1}{2i+1} \delta_{ij}$	Uniform
Jacobi	$(1-x)^a (1+x)^b$	$[-1, 1]$	$\langle \psi_i, \psi_j \rangle = C_{\text{Jacobi}} \delta_{ij}$	Beta
Laguerre	$\exp(-x)$	$[0, +\infty)$	$\langle \psi_i, \psi_j \rangle = \frac{\Gamma(i+1)}{i!} \delta_{ij}$	Exponential
General Laguerre	$\Gamma(x, a+1, 1)$	$[0, +\infty)$	$\langle \psi_i, \psi_j \rangle = \binom{i+a}{i} \delta_{ij}$	Gamma

where the normalization constant of Jacobi polynomial is $C_{\text{Jacobi}} = \frac{2^{a+b+1}}{2i+a+b+1} \frac{\Gamma(i+a+1)\Gamma(i+b+1)}{\Gamma(i+a+b+1)i!}$.

Let $\boldsymbol{\pi}$ denote the multiple-index of an n-dimensional polynomial, $\boldsymbol{\pi} = \{\pi_1, \pi_2, \cdots, \pi_n\}$, and let $L(p)$ denote the following set of multi-indices:

$$L(p) = \arg \left\{ \boldsymbol{\pi} : \sum_{k=1}^{n} \pi_k = p \right\} \tag{7.6}$$

which implies the summation (or the length) of the index vector $\boldsymbol{\pi}$ is p.

Following the definition, one can construct the p^{th} order polynomial chaos with the form of

$$\left[\boldsymbol{\Psi}_p(\mathbf{X}) \right] = \left\{ \bigcup_{\boldsymbol{\pi} \in L(p)} \left(\prod_{k=1}^{n} \psi_{\pi_k}(x_k) \right) \right\} \tag{7.7}$$

The definition on chaos polynomial is illustrated by approximating a two dimensional function $Y = \eta(X_1, X_2)$ as follows. We assume that $\mathbf{X}$ are the standard Normal variables. A meta-model with the corresponding Hermit polynomial chaos can be conducted as

$$\begin{aligned} \eta(X_1, X_2) = {} & a_{00}\psi_0(X_1)\psi_0(X_2) + a_{10}\psi_1(X_1)\psi_0(X_2) + a_{01}\psi_0(X_1)\psi_1(X_2) + \\ & a_{20}\psi_2(X_1)\psi_0(X_2) + a_{11}\psi_1(X_1)\psi_1(X_2) + a_{02}\psi_0(X_1)\psi_2(X_2) + \\ & a_{30}\psi_3(X_1)\psi_0(X_2) + a_{21}\psi_2(X_1)\psi_1(X_2) + a_{12}\psi_1(X_1)\psi_2(X_2) + \\ & a_{03}\psi_0(X_1)\psi_3(X_2) + a_{40}\psi_4(X_1)\psi_0(X_2) + \cdots \end{aligned} \tag{7.8}$$

in which one can see a multiple superscript is employed to represent the corresponding one-dimensional polynomials associated with an expansion coefficient. For the sake of simplicity in notation, the expression can be recast as the following compact form:

$$\eta(X_1, X_2) = \sum_{k=0}^{\infty} a_k \Psi_k(X_1, X_2) \tag{7.9}$$

where the two-dimensional polynomial chaos $\Psi_k(X_1, X_2)$ can be determined as

$$\begin{aligned}
&\Psi_0(X_1, X_2) = 1 && \Psi_1(X_1, X_2) = X_1 && \Psi_2(X_1, X_2) = X_2 \\
&\Psi_3(X_1, X_2) = X_1^2 - 1 && \Psi_4(X_1, X_2) = X_1 X_2 && \Psi_5(X_1, X_2) = X_2^2 - 1 \\
&\Psi_6(X_1, X_2) = 3X_1^2 - 3X_1 && \Psi_7(X_1, X_2) = (X_1^2 - 1)X_2 && \cdots
\end{aligned} \tag{7.10}$$

In view of the expression of the two-dimensional polynomial chaos, it becomes clear that except for a different indexing convention, the meta-model in Eq.(7.8) and Eq.(7.9) are identical. For example, the term $a_{21}\psi_2(X_1)\psi_1(X_2)$ in Eq.(7.8) is identified as the term $a_7\Psi_7(X_1, X_2)$ in Eq.(7.9).

In the following discussion, we will employ the condensed notation of a polynomial chaos expansion:

$$\eta(\mathbf{X}) = \sum_{k=0}^{\infty} a_k \Psi_k(X_1, X_2, \cdots, X_n) \tag{7.11}$$

In addition, as mentioned earlier, it is necessary to truncate the expansion up to order p, so that the expansion will be finite and result in a truncation error. The total number of terms (d) retained in the expansion can be determined with the dimensionality (n) of input variables, $\mathbf{X}$, and the truncation order (p) of the expansion:

$$d = \frac{(n + p)!}{n!\ p!} \tag{7.12}$$

The dependence of d on n and p is illustrated in Table 7.2, which provides the total number of expansion terms, d, for $1 \leqslant p, n \leqslant 6$.

Table 7.2: The number of terms (d) with n input variables and p truncation order

p/n	1	2	3	4	5	6	p/n	1	2	3	4	5	6
1	2	3	4	5	6	7	4	5	15	35	70	126	210
2	3	6	10	15	21	28	5	6	21	56	126	252	462
3	4	10	20	35	56	84	6	7	28	84	210	462	924

Therefore, an expression for the truncated PCE meta-model can be generally expressed as

$$\eta(\mathbf{X}) = \sum_{k=0}^{d-1} a_k \Psi_k(\mathbf{X}) + \epsilon(n, p) \tag{7.13}$$

in which one can see that the truncation error depends on both of n and p. This error is itself a random variable. The truncated meta-model converges to the original input-output relation in the mean square sense as n and p to go to infinity (Ghanem and Spanos, 1991):

$$\lim_{n,p\to\infty} E\left\{\left[\epsilon(n,p)\right]^2\right\} = 0 \tag{7.14}$$

7.2.3 Coefficient Computation of a PCE Meta-Model

With polynomial chaos expansion, one can approximate an input-output relation with a surrogate model contains d terms of multi-dimensional orthogonal polynomials:

$$\eta(\mathbf{X}) \approx \sum_{k=0}^{d-1} a_k \Psi_k(X_1, X_2, \cdots, X_n) \tag{7.15}$$

As reviewed in forging section, the primary task in PCE is to calculate the corresponding expansion coefficients, which are generally defined as

$$a_k = \left\langle \Psi_k(\mathbf{x}), \eta(\mathbf{x}) \right\rangle = \int_{\mathbf{X}} \Psi_k(\mathbf{x}) \cdot \eta(\mathbf{x}) \cdot f_{\mathbf{X}}(\mathbf{x}) \mathrm{d}\mathbf{x} \quad (k = 0, 1, \cdots, d-1) \tag{7.16}$$

Therefore, one should note that calculation of a_k needs to evaluate an n-dimensional integration. In practice, it is necessary to estimate the high-dimensional integration by using the methods of Monte Carlo simulation and Gauss quadrature as suggested in literature.

The concept of Monte Carlo simulation relies upon a large number of functional evaluations (e.g., $N = 10^6$) to compute the integration. Given N samples of input variables, an estimate on the coefficient can be obtained as

$$a_k \approx \hat{a}_k = \frac{1}{N} \sum_{i=1}^{N} \left[\eta\left(\mathbf{x}^{(i)}\right) \cdot \Psi_k\left(\mathbf{x}^{(i)}\right)\right] \tag{7.17}$$

Mean-value and variance of the estimate can be assessed by (Blatman and Sudret, 2010a)

$$\begin{cases} E[\hat{a}_k] = a_k \\ \mathrm{Var}[\hat{a}_k] = \dfrac{\sigma^2}{N}, \quad \text{where } \sigma^2 = \mathrm{Var}\left[\eta(\mathbf{X})\Psi_k(\mathbf{X})\right] \end{cases} \tag{7.18}$$

in which one can see that standard variance (i.e., $\sqrt{\mathrm{Var}[\hat{a}_k]}$) of the estimate is decreasing with $N^{-1/2}$. This induces a particularly low convergence rate, which is the well-known drawback of simulation-based method for high-dimensional integration (Dubourg, 2011).

An alternative to the simulation method is the scheme of tensor Gauss quadrature, in which the multi-dimensional integration defining each expansion coefficient can be approximated as

$$a_k \approx \sum_{i_1=1}^{N} \cdots \sum_{i_n=1}^{N} \left[\left(\prod_{j=1}^{n} w_{i_j} \right) \cdot \Psi_k\left(x_{i_1}, \cdots, x_{i_n}\right) \cdot \eta\left(x_{i_1}, \cdots, x_{i_n}\right) \right] \tag{7.19}$$

where w_{i_l} and x_{i_l} are an l^{th} Gauss weight and point of variable X_i, respectively. One should note that the total number of terms in the n-fold summation is N^n. The curse of dimensionality causes the total number of mechanistic model evaluations exponentially increases with respect to the dimensionality of $\mathbf{X}$. This leads to intractable computational cost for the PCE surrogate model construction.

7.3 Proposed Approximation Method

7.3.1 PCE Model with Univariate M-DRM

Considering an input-output relation, $y = \eta(\mathbf{x})$, the univariate M-DRM can approximated the mechanistic model as

$$\eta(\mathbf{x}) \approx \left[\eta(\boldsymbol{c})\right]^{1-n} \times \prod_{i=1}^{n} \eta(c_1, \cdots, c_{i-1}, x_i, c_{i+1}, \cdots, c_n) \tag{7.20}$$

where $\boldsymbol{c} = [c_1, c_2, \cdots, c_n]^{\mathrm{T}}$ is the cut-point, and $\eta(x_i, \boldsymbol{c}_{-i}) = \eta(c_1, \cdots, c_{i-1}, x_i, c_{i+1}, \cdots, c_n)$ is a univariate function only with respect to x_i. One can refer to Chapter 5 for the detailed derivations of the proposed multiplicative dimensional reduction method.

Substituting the univariate M-DRM approximation for the integration with respect to the expansion coefficient a_k, Eq.(7.16) can can be approximated as

$$\begin{aligned} a_k &\approx \int_{\mathbf{X}} \left(\left[\eta(\boldsymbol{c})\right]^{1-n} \prod_{i=1}^{n} \eta(x_i, \boldsymbol{c}_{-i}) \right) \times \Psi_k(\mathbf{x}) \times f_{\mathbf{X}}(\mathbf{x}) \mathrm{d}\mathbf{x} \\ &= \eta(\boldsymbol{c}) \times \int_{\mathbf{X}} \left(\prod_{i=1}^{n} \frac{\eta(x_i, \boldsymbol{c}_{-i})}{\eta(\boldsymbol{c})} \right) \times \Psi_k(\mathbf{x}) \times f_{\mathbf{X}}(\mathbf{x}) \mathrm{d}\mathbf{x} \end{aligned} \tag{7.21}$$

Recall that a k^{th} order polynomial chaos, $\Psi_k(\mathbf{X})$, is defined as a tensor product of each margin polynomial, i.e., $\Psi_k(\mathbf{X}) = \prod_{i=1}^{n} \psi_{\pi_i}(X_i)$. Therefore, the above equation can be further rewritten as

$$a_k \approx \eta(\boldsymbol{c})^{1-n} \times \prod_{i=1}^{n} \left(\int_{X_i} \eta(x_i, \boldsymbol{c}_{-i}) \psi_{\pi_i}(x_i) f_i(x_i) \mathrm{d}x_i \right) \tag{7.22}$$

In the context of calculating another coefficient (e.g., a_q for example), one only needs to update the responses of $\Psi_k(\mathbf{X})$ as $\Psi_q(\mathbf{X})$ with respect to the integration grids. This implies that the proposed univariate M-DRM can reduce the total number of mechanistic model evaluations as $1 + nN$.

7.3.2 PCE Model with Bivariate M-DRM

As discussed in forgoing section, in the context of a univariate M-DRM approximation, in some cases, might be not enough to mimic the original input-output relation, the corresponding procedure by considering the bivariate M-DRM can be developed to improve the computational accuracy.

Given an input-output relation, $y = \eta(\mathbf{x})$, recall that the model can be approximated by the bivariate M-DRM as

$$\eta(\mathbf{x}) \approx \frac{\big[\eta(\boldsymbol{c})\big]^{\frac{(n-1)(n-2)}{2}} \times \prod_{i=1}^{n-1}\prod_{j=i+1}^{n} \eta(c_1,\cdots,c_{i-1},x_i,c_{i+1},\cdots,c_{j-1},x_j,c_{j+1},\cdots,c_n)}{\left(\prod_{i=1}^{n}\eta(c_1,\cdots,c_{i-1},x_i,c_{i+1},\cdots c_n)\right)^{n-2}} \tag{7.23}$$

Substituting for the bivariate approximation, the corresponding integration with respect to PCE coefficients in Eq.(7.16) can be realized as

$$\begin{aligned} a_k &\approx \big[\eta(\boldsymbol{c})\big]^{\frac{(n-1)(n-2)}{2}} \times \int_{\mathbf{X}} \left(\frac{\prod_{i=1}^{n-1}\prod_{j=i+1}^{n}\eta(x_i,x_j,\boldsymbol{c}_{-ij})}{\prod_{i=1}^{n}\big[\eta(x_i,\boldsymbol{c}_{-i})\big]^{n-2}}\right) \times \left(\prod_{i=1}^{n}\psi_{\pi_i}(x_i)\right) \times f_{\mathbf{X}}(\mathbf{x})\,\mathrm{d}\mathbf{x} \\ &= \big[\eta(\boldsymbol{c})\big]^{\frac{(n-1)(n-2)}{2}} \times \frac{\prod_{i=1}^{n-1}\prod_{j=i+1}^{n}\int_{X_i}\int_{X_j}\eta(x_i,x_j,\boldsymbol{c}_{-ij})\,f_i(x_i)\,f_j(x_j)\,\mathrm{d}x_i\mathrm{d}x_j}{\prod_{i=1}^{n}\int_{X_i}\Big\{\big[\eta(x_i,\boldsymbol{c}_{-i})\big]^{n-2}\big/\psi_{\pi_i}(x_i)\Big\}f_i(x_i)\mathrm{d}x_i} \end{aligned} \tag{7.24}$$

One should note that the dimensionality of the integrand has reduced from n to 2, which guarantees the computational efficiency of the proposed M-DRM method. The corresponding number of functional evaluations is:

$$\text{Number of FEs by Bivariate M-DRM: } = \frac{n(n-1)}{2} \times N^2 + n \times N + 1 \tag{7.25}$$

in which, n is the total number of input variables; and N is the order of Gauss quadrature.

In the context of bivariate M-DRM is still not enough to determine the coefficients of a PCE meta-model precisely, one can refer to Chapter 5 for a general s-variate M-DRM approximation. However, numerical examples will show that the bivariate M-DRM method is able to provide fairly accurate results on a surrogate model construction.

7.4 Postprocessing of a PCE Meta-Model

After determined the coefficients of a PCE meta-model, uncertainty propagation of the original input-output relation can be extensively conducted based on the polynomial chaos expansion. The section is designed to illustrate the corresponding postprocessing procedures for moment computation, global sensitivity analysis and output probability distribution estimation based on the PCE meta-model.

7.4.1 Moment and Global Sensitivity Coefficient

We start the discussion by using a two-variate model, $Y = \eta(X_1, X_2)$, in which $\mathbf{X} = [X_1, X_2]^{\mathrm{T}}$ are assumed to follow the standard Normal distribution. Therefore, a general expression of the corresponding PCE meta-model can be given as

$$\eta(X_1, X_2) = \sum_{k=0}^{\infty} a_k \Psi_k(X_1, X_2) \tag{7.26}$$

Truncation of the PCE meta-model with $p = 4$, one can determine the corresponding surrogate model as

$$\eta(X_1, X_2) \approx \sum_{k=0}^{d-1} a_k \Psi_k(X_1, X_2) \tag{7.27}$$

where $d = \frac{(4+2)!}{4!2!} = 15$; and the involved two-dimensional Hermite polynomials (normalized), $\Psi_k(X_1, X_2)$, are listed in Table 7.3.

Therefore, with the two-dimensional joint standard Normal PDF, $f_{\mathbf{X}}(\mathbf{x})$, as the weighting function, one can test the zero mean-value of the polynomials:

$$E\big[\Psi_i(\mathbf{X})\big] = \int_{\mathbf{X}} \Psi_i(\mathbf{x})\, f_{\mathbf{X}}(\mathbf{x}) \mathrm{d}\mathbf{x} = \begin{cases} 1 & \text{if } i = 0 \\ 0 & \text{if } i \geqslant 1 \end{cases} \tag{7.28}$$

Table 7.3: Two-dimensional Hermite polynomials with truncation order $p = 4$

k	Multiple Indices	$p = \sum_{i=1}^{2} \pi_i$	Chaos Polynomials – $\Psi_k(\mathbf{X})$
0	$\boldsymbol{\pi} = \{0, 0\}$	0	$\Psi_0(\mathbf{X}) = \psi_0(X_1)\psi_0(X_2) = 1$
1	$\boldsymbol{\pi} = \{0, 1\}$	1	$\Psi_1(\mathbf{X}) = \psi_0(X_1)\psi_1(X_2) = X_2$
2	$\boldsymbol{\pi} = \{1, 0\}$	1	$\Psi_2(\mathbf{X}) = \psi_1(X_1)\psi_0(X_2) = X_1$
3	$\boldsymbol{\pi} = \{0, 2\}$	2	$\Psi_3(\mathbf{X}) = \psi_0(X_1)\psi_2(X_2) = \frac{1}{\sqrt{2}}(X_2^2 - 1)$
4	$\boldsymbol{\pi} = \{1, 1\}$	2	$\Psi_4(\mathbf{X}) = \psi_1(X_1)\psi_1(X_2) = X_1 X_2$
5	$\boldsymbol{\pi} = \{2, 0\}$	2	$\Psi_5(\mathbf{X}) = \psi_2(X_1)\psi_0(X_2) = \frac{1}{\sqrt{2}}(X_1^2 - 1)$
6	$\boldsymbol{\pi} = \{0, 3\}$	3	$\Psi_6(\mathbf{X}) = \psi_0(X_1)\psi_3(X_2) = \frac{1}{\sqrt{3!}}(X_2^3 - 3X_2)$
7	$\boldsymbol{\pi} = \{1, 2\}$	3	$\Psi_7(\mathbf{X}) = \psi_1(X_1)\psi_2(X_2) = \frac{1}{\sqrt{2}} X_1(X_2^2 - 1)$
8	$\boldsymbol{\pi} = \{2, 1\}$	3	$\Psi_8(\mathbf{X}) = \psi_2(X_1)\psi_1(X_2) = \frac{1}{\sqrt{2}} X_2(X_1^2 - 1)$
9	$\boldsymbol{\pi} = \{3, 0\}$	3	$\Psi_9(\mathbf{X}) = \psi_3(X_1)\psi_0(X_2) = \frac{1}{\sqrt{3!}}(X_1^3 - 3X_1)$
10	$\boldsymbol{\pi} = \{0, 4\}$	4	$\Psi_{10}(\mathbf{X}) = \psi_0(X_1)\psi_4(X_2) = \frac{1}{\sqrt{4!}}(X_2^4 - 6X_2^2 + 3)$
11	$\boldsymbol{\pi} = \{1, 3\}$	4	$\Psi_{11}(\mathbf{X}) = \psi_1(X_1)\psi_3(X_2) = \frac{1}{\sqrt{3!}} X_1(X_2^3 - 3X_2)$
12	$\boldsymbol{\pi} = \{2, 2\}$	4	$\Psi_{12}(\mathbf{X}) = \psi_2(X_1)\psi_2(X_2) = \frac{1}{2}(X_1^2 - 1)(X_2^2 - 1)$
13	$\boldsymbol{\pi} = \{3, 1\}$	4	$\Psi_{13}(\mathbf{X}) = \psi_3(X_1)\psi_1(X_2) = \frac{1}{\sqrt{3!}} X_2(X_1^3 - 3X_1)$
14	$\boldsymbol{\pi} = \{4, 0\}$	4	$\Psi_{14}(\mathbf{X}) = \psi_4(X_1)\psi_0(X_2) = \frac{1}{\sqrt{4!}}(X_1^4 - 6X_1^2 + 3)$

and the unit variance (order $\geqslant 1$):

$$\left\langle \Psi_i, \Psi_j \right\rangle = E\left[\Psi_i(\mathbf{X})\Psi_j(\mathbf{X})\right] = \delta_{ij} \quad (\text{for } i, j \geqslant 1) \tag{7.29}$$

which implies $\text{Var}[\Psi_i(\mathbf{X})] = 1$ as $i \geqslant 1$ and 0 otherwise.

Given the 15 orders two-dimensional Hermite polynomials, the PCE meta-model with respect to $Y = \eta(X_1, X_2)$ can be realized as

$$\eta(X_1, X_2) \approx a_0 + a_1\Psi_1(\mathbf{X}) + a_2\Psi_2(\mathbf{X}) + \cdots + a_{14}\Psi_{14}(\mathbf{X}) \tag{7.30}$$

in which one should note that the zeroth order polynomial chaos $\Psi_0(\mathbf{X}) = 1$.

To estimate moments of model output, one can perform the operators of mean-value and variance on both sides of the equation. It is interesting to note that the determined mean-value

and variance are directly related to the coefficients of PCE meta-model due to the orthogonality of the polynomial chaos:

$$\begin{cases} E[Y] \approx E\big[a_0 + a_1\Psi_1(\mathbf{X}) + \cdots + a_{14}\Psi_{14}(\mathbf{X})\big] = a_0 \\ \mathrm{Var}[Y] \approx \mathrm{Var}\big[a_0 + a_1\Psi_1(\mathbf{X}) + \cdots + a_{14}\Psi_{14}(\mathbf{X})\big] = \sum_{k=1}^{14} a_k^2 \mathrm{Var}\big[\Psi_k(\mathbf{X})\big] \end{cases} \tag{7.31}$$

in which one should note that $\mathrm{Var}\big[\Psi_k(\mathbf{X})\big] = 1$ as derived in Eq.(7.29).

Therefore, for a mechanistic model $Y = \eta(\mathbf{X})$ with n-dimensional input variables, mean-value and output variance can be calculated from the expansion coefficients as

$$E[Y] = a_0; \qquad \mathrm{Var}[Y] = \sum_{k=1}^{d-1} a_k^2 \tag{7.32}$$

To conduct the variance-based global sensitivity analysis, one needs to decompose the total output variance into three components:

$$V_{\mathrm{Tol}} = V_1 + V_2 + V_{12} \tag{7.33}$$

in which V_1 and V_2 denote the output variance purely relate to X_1 and X_2, respectively, and V_{12} is the joint variance of due to X_1 and X_2 taking effect together.

Given an arbitrary polynomial chaos, $\Psi_k(\mathbf{X})$, in Table 7.3, one should note that $\mathrm{Var}\big[\Psi_k(\mathbf{X})\big] = 1$ ($\forall k \geqslant 1$). Then, the output variance contributed by a term $a_k\Psi_k(\mathbf{X})$ in the PCE meta-model is directly determined by a_k^2. Therefore, if $\Psi_k(\mathbf{X})$ is a pure function with respect to X_i, the corresponding variance, a_k^2, would be one of sources of component variance V_i. However, if the expression of $\Psi_k(\mathbf{X})$ contains both X_1 and X_2, the associated a_k^2 will contribute to the joint variance V_{12}. Follow this convention, the variance component associated with $a_k\Psi_k(\mathbf{X})$ can be directly identified from its corresponding multiple-index $\boldsymbol{\pi}$ of the k^{th} order polynomial chaos.

The multiple-index, $\boldsymbol{\pi}$, of each polynomial chaos associated with the two-variate function $Y = \eta(\mathbf{X})$ is summarized as shown in Table 7.3. And Table 7.4 has been developed to summarize the component variance related to the index of each orthogonal polynomial.

As summarized in Table 7.4, the total output variance can be directly partitioned to each PCE coefficient as

$$\begin{aligned} V_1 &\approx a_2^2 + a_5^2 + a_9^2 + a_{14}^2; \qquad V_2 \approx a_1^2 + a_3^2 + a_6^2 + a_{10}^2 \\ V_{12} &\approx a_4^2 + a_7^2 + a_8^2 + a_{11}^2 + a_{12}^2 + a_{13}^2 \end{aligned} \tag{7.34}$$

Table 7.4: Variance decomposition with polynomial chaos expansion

Source of Variance	Multiple-Index: $\{\boldsymbol{\pi}\}$	Orthogonal Polynomial: $\Psi_k(\mathbf{X})$
V_1	$\{1,0\};\{2,0\};\{3,0\};\{4,0\}$	$k=\{2,5,9,14\}$
V_2	$\{0,1\};\{0,2\};\{0,3\};\{0,4\}$	$k=\{1,3,6,10\}$
V_{12}	$\{1,1\};\{1,2\};\{2,1\};\{1,2\};\{2,2\};\{3,1\}$	$k=\{4,7,8,11,12,13\}$

And the corresponding estimates of Sobol' index are

$$\begin{aligned} S_1 &\approx \frac{a_2^2+a_5^2+a_9^2+a_{14}^2)}{\sum_{k=1}^{14} a_k^2}; \qquad S_2 \approx \frac{a_1^2+a_3^2+a_6^2+a_{10}^2}{\sum_{k=1}^{14} a_k^2} \\ S_{12} &\approx \frac{a_4^2+a_7^2+a_8^2+a_{11}^2+a_{12}^2+a_{13}^2}{\sum_{k=1}^{14} a_k^2} \end{aligned} \tag{7.35}$$

Therefore, with the multiple-indies $\boldsymbol{\pi} = \{\pi_1\pi_2\cdots\pi_n\}$ of a general PCE meta-model, one can define an indicator for the variance sources of V_{i_1} as

$$\mathbf{1}_{i_1}(\boldsymbol{\pi}) = \arg\left\{\boldsymbol{\pi} : [\pi_{i_1} \neq 0] \cup [\pi_{i_k} = 0]_{k=2}^{d-1}\right\} \quad (i_1 = 1,2,\cdots,n) \tag{7.36}$$

And the corresponding main effect of the input random variable is:

$$S_{i_1} = \frac{\sum_{k\in\mathbf{1}_{i_1}(\boldsymbol{\pi})} a_k^2}{\sum_{k=1}^{d-1} a_k^2} \qquad (i_1 = 1,2,\cdots,n) \tag{7.37}$$

In addition, a general indicator to evaluate a s-variate joint variance is defined as

$$\mathbf{1}_{i_1 i_2\cdots i_s}(\boldsymbol{\pi}) = \arg\left\{\boldsymbol{\pi} := \left[\pi_{i_1},\pi_{i_2},\cdots,\pi_{i_s} \neq 0\right] \cup \left[\pi_{i_k} = 0\right]_{k=s+1}^{d-1}\right\} \tag{7.38}$$

which determines the s-variate Sobol' index as

$$S_{i_1 i_2\cdots i_s} = \frac{\sum_{k\in\mathbf{1}_{i_1 i_2\cdots i_s}(\boldsymbol{\pi})} a_k^2}{\sum_{k=1}^{d-1} a_k^2} \quad (1 \leqslant i_1,\cdots,i_s \leqslant n) \tag{7.39}$$

7.4.2 Output Distribution

A key problem in system uncertainty quantification is to determine the complete probability distribution of a model output. With the proposed method of polynomial chaos expansion, the surrogate model allows to use the crude Monte Carlo simulation to estimate the probability distribution of the model response.

7.4.3 Implementation Procedure

Figure 7.1 describes a general frame work on polynomial chaos expansion, in which one can note that the method for uncertainty quantification includes two sections, i.e., construction of a PCE meta-model to mimic the original input-output relation, and a postprocessing procedure based on the PCE meta-model for system uncertainty quantification. Details of the method can be summarized as follows:

(i) Determine the truncation order (p) of a PCE meta-model. Given the distributions of input variables, generate the corresponding polynomial chaos basis of the expansion.

(ii) Since that the expansion coefficients are defined as a series high-dimensional integrations, a numerical method employed in the step features a procedure of polynomial chaos expansion, such as the simulation-based method uses Monte Carlo simulation or its variance (e.g., Latin hypercube sampling) to calculate the integration, whereas a quadrature-based method employs the tensor Gauss quadrature or its sparsity version for the objective.

(iii) With the determined expansion coefficients, the postprocessing schemes for moment and Sobol' index derived in Section 7.4.1 can be employed to conduct uncertainty analysis of the problem.

In the study, the M-DRM method proposed in Chapter 5 is employed to approximate the high-dimensional integrations involved in PCE. Flow chart of the proposed method is developed as shown in Figure 7.2.

Compared to the classical methods in Figure 7.1, the second block in Figure 7.2 is proposed to handle with the demanding integrations. Therefore, the first and third blocks of the proposed flow chart are designed as identical with the classical procedure. On the development of M-DRM, one can refer to Chapter 5 for details, as well as the computational issue for the low dimensional (one or two) integrations.

7.4.4 Error Analysis

Regarding potential errors of the method, one can conduct the error analysis from the following three aspects:

$$\text{Total Error } (\varepsilon_{\text{Tol}}) := \varepsilon_{\text{Trun}} + \varepsilon_{\text{M-DRM}} + \varepsilon_{\text{GQ}} \tag{7.40}$$

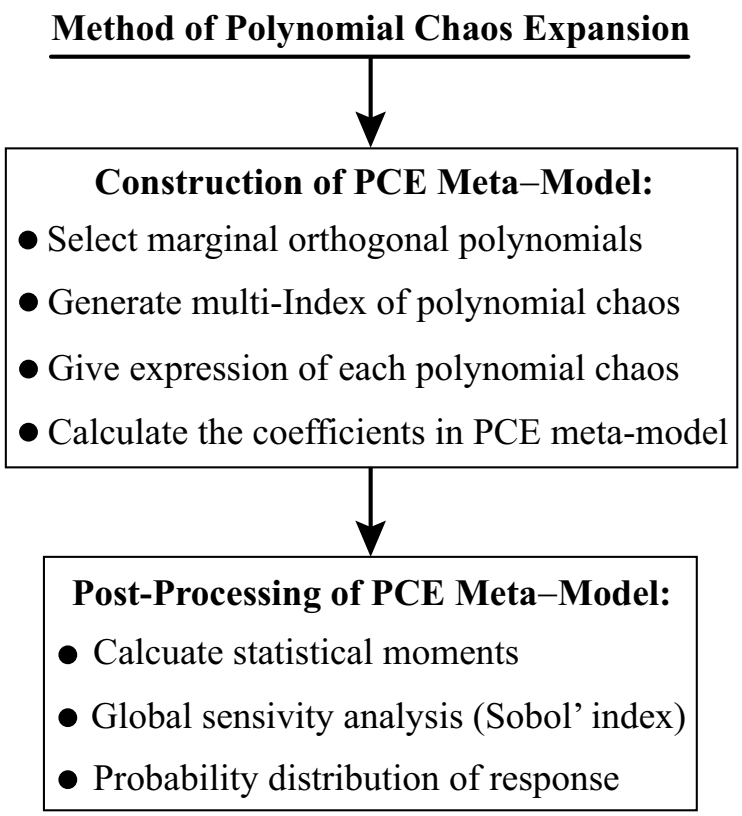

Figure 7.1: Overview of polynomial chaos expansion for uncertainty analysis

in which one can see that the total error ε_{Tol} can be expressed as the errors contributed by $\varepsilon_{\text{Trun}}$, which arises from a low truncation order (p) in the PCE model development, $\varepsilon_{\text{M-DRM}}$, which is due to the use of M-DRM to approximate the mechanistic function, and ε_{GQ}, which is due to the errors associated with a numerical Gauss quadrature for the low dimensional integrations.

On the first error term, $\varepsilon_{\text{Trun}}$, one can reduce the error by considering a high expansion order (i.e., a larger value of p). It is important to note that the proposed method for PCE model development does not need additional functional evaluations with respect to the increase of p. The second error, $\varepsilon_{\text{M-DRM}}$, arises from a poor approximation of the mechanistic function by using a low-variate M-DRM. A higher variate M-DRM is an alternative to reduce the error. The third term, ε_{GQ}, is the result of using a low number of Gauss points to evaluate the involved low-dimensional integrations. Therefore, a higher order Gauss quadrature will help to reduce the error term.

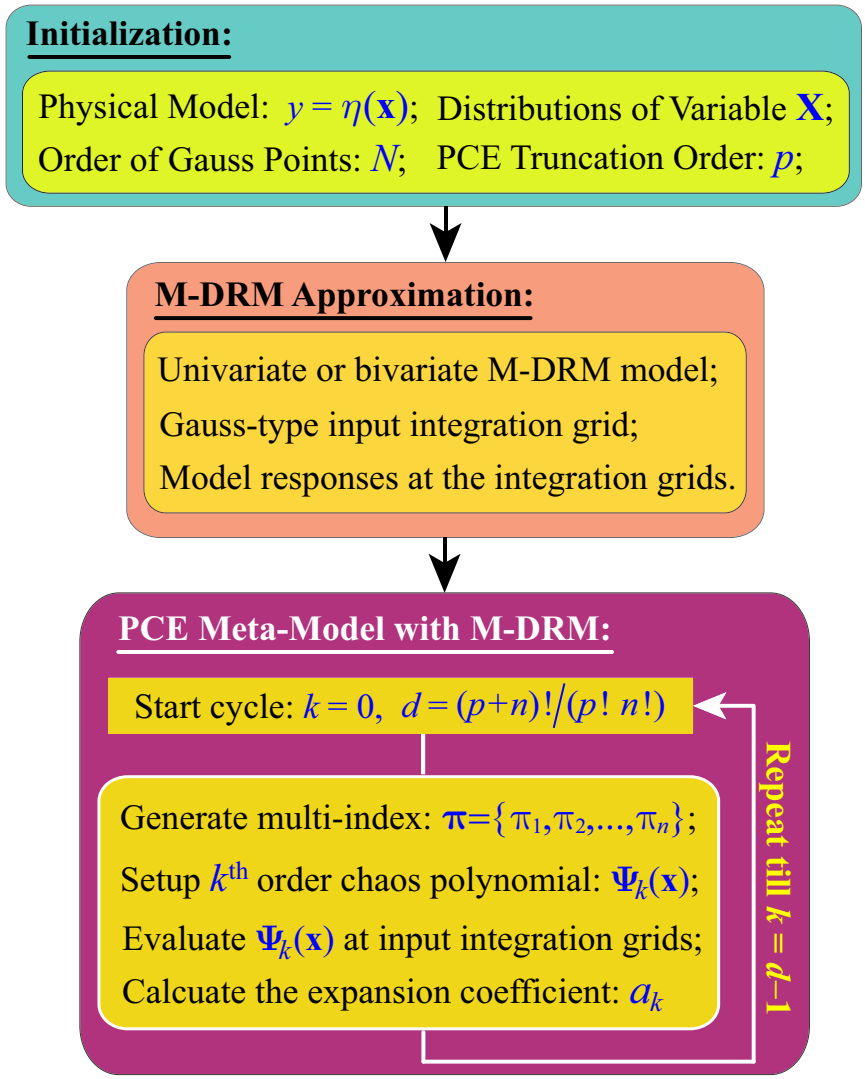

Figure 7.2: The proposed flow chart for polynomial chaos expansion with M-DRM

7.4.5 Verification Procedure

To verify the proposed method for uncertainty quantification of a system, the following three proceduress are employed to check the associated accuracy and efficiency:

- Regression Test: First of all, N_0 samples of input variables are randomly generated ($N_0 = 500$). Based on the mechanistic model and PCE meta-model, the corresponding responses are simulated, respectively. If the meta-model can exactly mimic the original input-output relation (i.e., mechanistic model), a plot on the predicted outputs versus the simulated counterparts would fall on a straight line. However, due to the inadequateness of a surro-

gate model, a general coefficient of determination, R^2, can be employed to calibrate the corresponding model fitness.

- Moment and Sobol' sensitivity index: At first, accuracy of the proposed PCE meta-model is checked by comparing the output moment to its benchmark. Secondly, Chapter 6 derived that the output variance can be completely decomposed as a series component variances due to the uncertain input variables. The corresponding Sobol' sensitivity index will be further employed check the accuracy of the proposed method.

- Output probability distribution: Based on the PCE meta-model, output distribution can be economically estimated based on a large number samples of input vector. Also, by substituting for the mechanistic model, a comparison to the empirical distribution will be employed to examine the accuracy of the proposed method for output distribution estimation.

A generic relative error to check the fitness of PCE surrogate model is defined as

$$\mathcal{L}^2 \text{ Error} := \frac{\sum_{i=1}^{N_0} \left[\eta(\mathbf{x}^{(i)}) - \widehat{\eta}(\mathbf{x}^{(i)})\right]^2}{\sum_{i=1}^{N_0} \left[\eta(\mathbf{x}^{(i)}) - \overline{y}\right]^2} \qquad \text{where} \quad N_0 = 500 \tag{7.41}$$

Given N_0 samples of input variables, $\widehat{y} = \widehat{\eta}(\mathbf{x})$ denotes the predicted response using the PCE meta-model. And $y = \eta(\mathbf{x})$ is the simulated counterpart. The population mean-value, $\overline{y}$, can be estimated by

$$\overline{y} = \frac{1}{N_0} \sum_{i=1}^{N_0} \eta\big(\mathbf{x}^{(i)}\big) \tag{7.42}$$

Therefore, numerator of the relative error is the total residual error due to unfitness of the PCE meta-model. The denominator is the total variance of model responses. According to the theory of regression analysis (Montgomery and Myers, 2002), the total output variance (denominator) can be decomposed independently as the total residual error (numerator) and the output variance estimated by the PCE meta-model (the explained error). Therefore, if the residual error is a fairly small quantity, the predicted output variance based on the PCE meta-model should be very close to the total output variance. With the idea, one can define a general coefficient of determination using the $\mathcal{L}^2$ Error as

$$R^2 = 1 - \mathcal{L}^2 \text{ Error} = 1 - \frac{\sum_{i=1}^{N_0} \left[\eta(\mathbf{x}^{(i)}) - \widehat{\eta}(\mathbf{x}^{(i)})\right]^2}{\sum_{i=1}^{N_0} \left[\eta(\mathbf{x}^{(i)}) - \overline{y}\right]^2} \tag{7.43}$$

in which, a value of R^2 closed to 1.0 (i.e., $\mathcal{L}^2$ Error ≈ 0) indicates the good fitness of the PCE meta-model in modelling the original input-output relation.

7.5 Math Examples

In the section, two examples from literature are employed to examine the proposed multiplicative dimensional reduction method for PCE meta-model construction of a math function.

7.5.1 Ishigami Function

The example considers the Ishigami function (Ishigami and Homma, 1990) as given in Section 6.4.3. In the study, assume that constants are $a = 0.1$ and $b = 0.7$, respectively. To construct the PCE meta-model, let the truncation order $p = 10$. One can determined that total terms of the PCE meta-model is:

$$d = \frac{(n+p)!}{n!p!} = \frac{(3+10)!}{3!10!} = 286$$

According to the flow chart depicted in Figure 7.2, the univariate M-DRM and bivariate M-DRM are employed to approximate the Ishigami function at first. Then, 286 coefficients of the corresponding surrogate models are determined with integration schemes in Eq.(**??**) and Eq.(**??**), respectively.

Given $N_0(= 500)$ samples of input random variables, the simulated model outputs and the predicted counterparts by using PCE meta-models are plotted as shown in Figure 7.3. Since the corresponding R^2s are very close to 1.0, the $\mathcal{L}^2$ Errors are used in the study to check the goodness of fit. Together with the number of functional evaluations, one can refer to Table 7.5 for details.

Table 7.5: $\mathcal{L}^2$ Error and computational cost for the Ishigami example

PCE Meta-Model	$\mathcal{L}^2$ Error $(1 - R^2)$	Number of Functional Evaluations
Univariate M-DRM	2.60×10^{-5}	$31 = 1 + 3 \times 10$
Bivariate M-DRM	2.09×10^{-6}	$331 = 1 + 3 \times 10 + 3 \times (3-1)/2 \times 10^2$

Figure 7.3 depicts the simulated and the predicted responses based on the mechanistic model and PCE meta-model, respectively. If a PCE meta-model could represent the Ishigami function very well, all the points of simulated versus predicted would fall on a straight line. The small

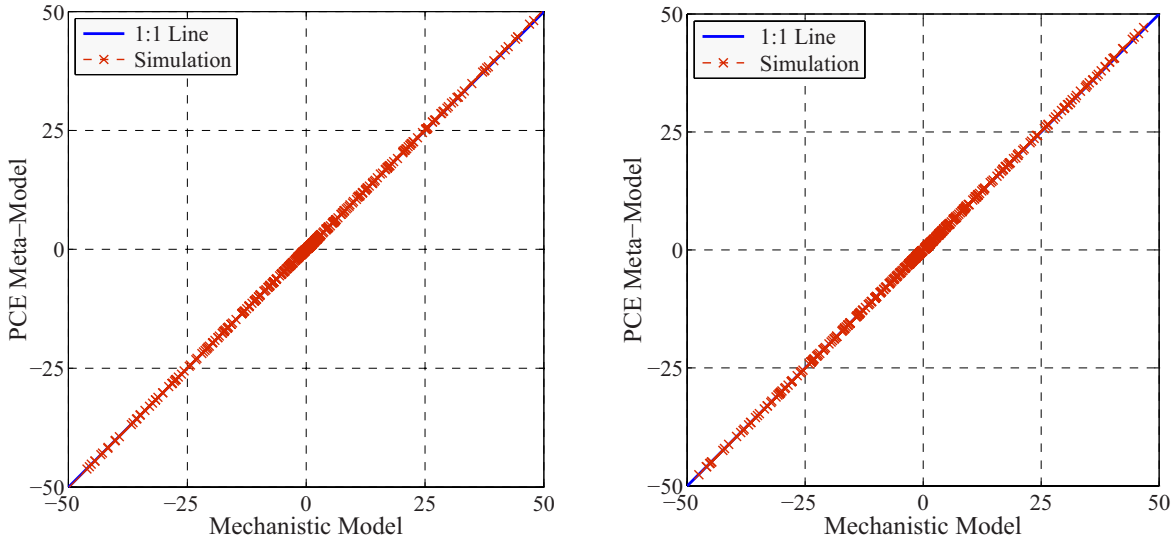

(a) Univariate M-DRM

(b) Bivariate M-DRM

Figure 7.3: Simulated versus predicted model responses of Ishigami example (Mechanistic Model: Simulated responses based on the original Ishigami function with 500 samples; PCE Meta-model: Predicted responses based on the PCE meta-model with M-DRM; M-DRM: The proposed multiplicative dimensional reduction method.)

values of $\mathcal{L}^2$ Error in Table 7.5 have indicated the accuracy of the proposed method for PCE meta-model construction. Given the number of functional evaluations as listed in Table 7.5, one can further confirm the efficiency and accuracy of the proposed method for polynomial chaos expansion the Ishigami function.

Statistical moment and Sobol' sensitivity index of the Ishigami function are calculated with the coefficients of PCE meta-model as shown in Table 7.6. Compared to the analytic results, it is clear to confirm that the estimates on moment and Sobol' sensitivity index are very accurate (the relative error $\leqslant 2\%$).

Once determined the expansion coefficients of the PCE meta-model, the crude Monte Carlo simulation can be followed based the surrogate model for the complete output distribution. Based on the mechanistic function, an empirical distribution can be determined as the benchmark result. Figure 7.4 compared the PCE estimate with the benchmark distribution of the Ishigami function. It is clear to see that the function with an extremely abnormal distribution compared to the frequently ones encountered in probabilistic analysis. The proposed method can accurately determine output distribution at its entire definition domain. Only differences between univari-

Table 7.6: Moment and global sensitivity index of the Ishigami example

Method	Mean-Value	Variance	Sobol' Index – S_1	Sobol' Index – S_{13}
Exact	5.00×10^{-2}	272.25	0.3932	0.5992
Univariate M-DRM	4.494×10^{-2}	273.84	0.3906	0.6093
Relative Error (%)	-10.37	0.583	-0.639	1.685
Bivariate M-DRM	5.001×10^{-2}	272.27	0.3936	0.6064
Relative Error (%)	2.03×10^{-2}	8.35×10^{-3}	0.104	1.199

Relative Error: = (PCE Meta-Model − Exact)/Exact ×100%.

M-DRM: The univariate or bivariate multiplicative dimensional reduction method.

ate M-DRM and bivariate M-DRM can been identified for the peak regions of the two PDFs. Together with a very small number of mechanistic model evaluations (31 by univariate M-DRM versus 331 by bivariate M-DRM), the proposed method is believed to accurately and efficiently set up a PCE meta-model.

7.5.2 Corner Peak Function

The example examines the proposed method by considering the corner peak function as shown in Section 6.4.5. With a truncation order $p = 4$, the corresponding PCE meta-model will contain $210 = (4 + 6)!/(4!6!)$ terms. Four-order Gauss-Legendre quadrature is employed to calculate the low-dimensional integrations. Compared to the classical tensor product quadrature method, the proposed univariate and bivariate M-DRMs can reduce the number of functional evaluations from $4^6 (= 4096)$ to 25 and 265, respectively.

Given 500 samples of input variables, the accuracy of PCE meta-model is examined by using the quality plot as shown in Figure 7.5, together with the relative error and computational effort by using M-DRM as shown in Table 7.7. One can see that the univariate M-DRM approximation determines relative error of the corresponding PCE meta-model as 3.24×10^{-3}. It implies that the coefficient of determination is $R^2 = 1 - \mathcal{L}^2$ Error $= 0.9968$.

Figure 7.5(a) describes the plot of simulated and the predicted responses. It is clear to see that PCE meta-model determined by the univariate M-DRM underestimates of the upper quantiles of the corner peak function. Figure 7.5(b) has shown a good agreement of the PCE meta-model with the bivariate M-DRM for the entire range of responses, which is confirmed by the fairly small relative error of $\mathcal{L}^2$ Error $\leqslant 1 \times 10^{-6}$.

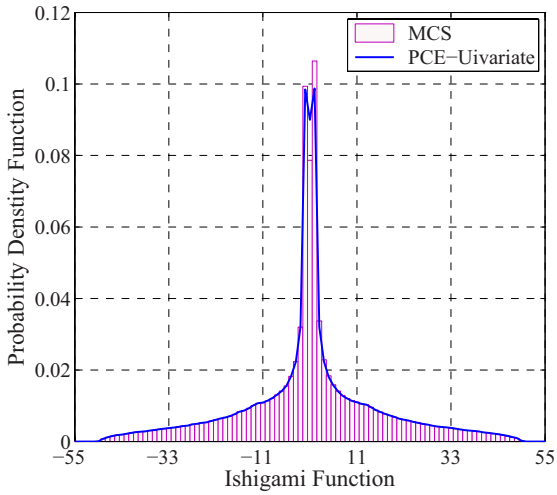

(a) PDF with Univariate M-DRM

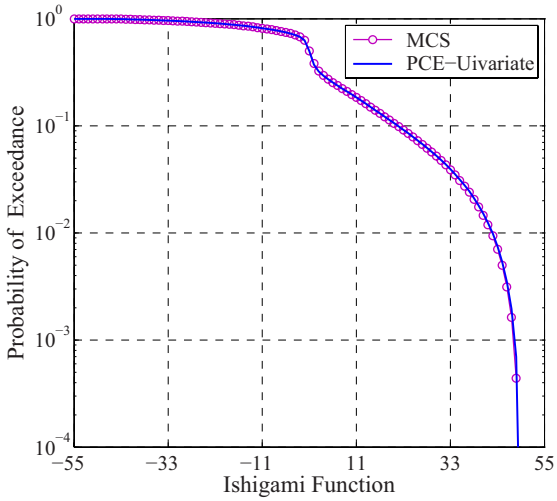

(b) Distribution Tails with Univariate M-DRM

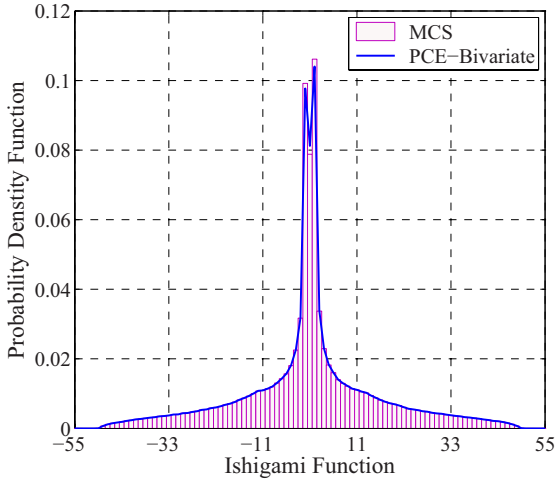

(c) PDF with Bivariate M-DRM

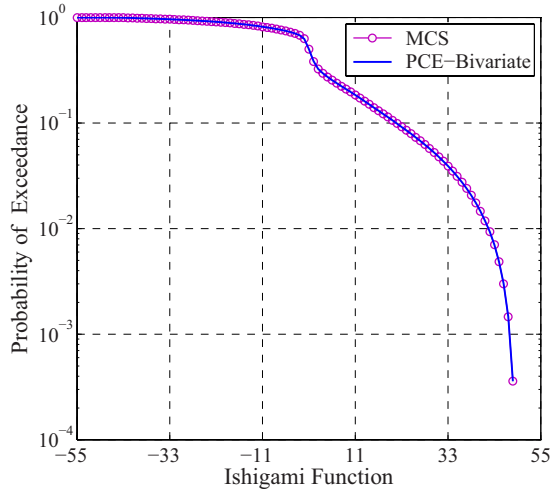

(d) Distribution Tails with Bivariate M-DRM

Figure 7.4: Probability distribution of the Ishigami function estimated by PCE with univariate and bivariate M-DRM (PCE: Polynomial chaos expansion; M-DRM: The univariate or bivariate multiplicative dimensional reduction method; MCS: Crude Monte Carlo simulation with 10^6 samples.)

Global sensitivity analysis of the corner peak function needs to evaluate a series six-dimensional integrations, which are impossible to be analytically evaluated. Crude Monte Carlo simulation with 10^6 samples, hence, is assume to provide benchmark results for the corresponding Sobol' sensitivity indices. PCE meta-model allows one to compute the output moment and sensitivi-

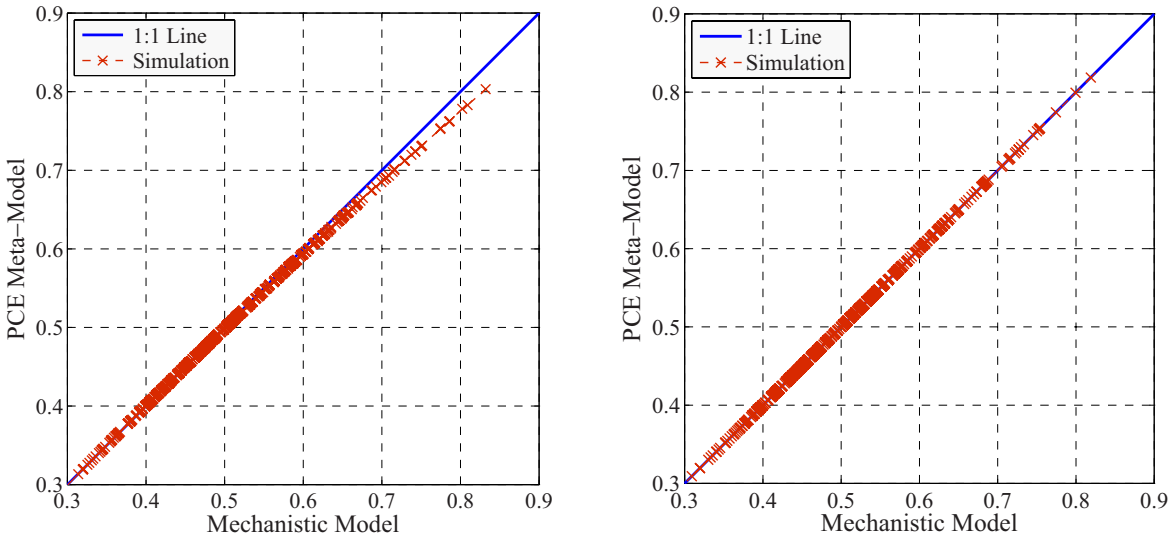

(a) Univariate M-DRM

(b) Bivariate M-DRM

Figure 7.5: Simulated versus predicted model responses of the corner peak function (Mechanistic Model: Simulated responses based on the original physical model; PCE: Predicted responses by the PCE meta-model; M-DRM: The univariate or bivariate multiplicative dimensional reduction method.)

Table 7.7: $\mathcal{L}^2$ Error and computational cost for the corner peak function

PCE Meta-Model	$\mathcal{L}^2$ Error	Number of Functional Evaluations
Univariate M-DRM	3.24×10^{-3}	$25 = 1 + 4 \times 6$
Bivariate M-DRM	9.20×10^{-7}	$265 = 1 + 4 \times 6 + 6 \times (6-1)/2 \times 4^2$

ty index directly by using the expansion coefficients. Compared to the benchmarks, Table 7.8 indicates that the proposed method can be believed to provide accurate results on the global sensitivity analysis.

Output distribution of the corner peak function is also estimated as shown in Figure 7.6. According to the result provided by the univariate M-DRM, one can see that it underestimates the upper quantiles given the predefined probabilities of exceedance (e.g., POEs $\leqslant 10^{-2}$). Comparatively, the bivariate M-DRM model can be believed to describe the complete output distribution exactly. Therefore, in the context of an output distribution (instead of the moment and Sobol' sensitivity index) is of interest, the bivariate M-DRM can be employed to compute the corresponding PCE meta-model.

Table 7.8: Moment and global sensitivity index of the corner peak function

Method	S_1	S_2	S_3	S_4	S_5	S_6	$\sum_i S_i$
MCS	1.091×10^{-2}	4.365×10^{-2}	9.734×10^{-2}	0.1733	0.2712	0.3892	0.9857
U-M-DRM	1.072×10^{-2}	4.303×10^{-2}	9.719×10^{-2}	0.1734	0.2721	0.3933	0.9897
RE (%)	−1.82	−1.43	−0.151	0.058	0.30	1.06	0.412
B-M-DRM	1.085×10^{-2}	4.340×10^{-2}	9.762×10^{-2}	0.1734	0.2708	0.3895	0.9856
RE (%)	−0.574	−0.579	0.288	0.054	−0.172	0.087	−0.007

U-M-DRM: PCE Meta-Model constructed by using the univariate M-DRM.

B-M-DRM: PCE Meta-Model constructed by using the bivariate M-DRM.

Relative Error: = (PCE Meta-Model − MCS)/Exact ×100%.

7.6 Structural Examples

In the section, three examples for probabilistic structural analysis are employed to examine the accuracy and efficiency of the proposed method on polynomial chaos expansion.

7.6.1 Burst Margin of a Rotation Disk

The first example studies the burst margin of a rotation disk (Wei and Rahman, 2007). Consider an annular disk with the outer radius R_o, inner radius R_i, and a constant thickness $t \ll R_i$ (plane stress). The disk subjects to an angular velocity ω about the axis perpendicular to its plane at the center. Therefore, the maximum angular velocity, $\omega_{\max}(\mathbf{X})$, can be calculated by

$$\omega_{\max}(\mathbf{X}) = \sqrt{\frac{3\alpha_m S_u (R_o - R_i)}{\rho(R_o^3 - R_i^3)}} \tag{7.44}$$

where ρ is the mass density of the material; S_u is the material ultimate strength and α_m is the material utilization factor.

According to the design provision, the satisfactory performance of the disk can be defined by using its burst margin, $M_b(\mathbf{X})$:

$$M_b(\mathbf{X}) = \frac{\omega_{\max}(\mathbf{X})}{\omega} = \sqrt{\frac{3\alpha_m S_{\mathrm{u}} (R_o - R_i)}{\rho\omega^2(R_o^3 - R_i^3)}} \tag{7.45}$$

in which, the random variables of the problem are listed in Table 7.9.

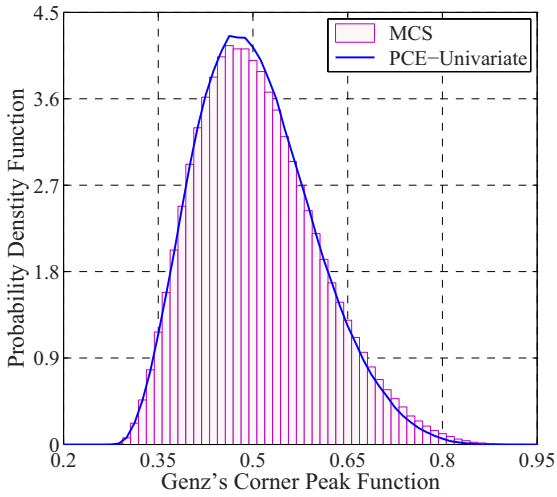

(a) PDF with Univariate M-DRM

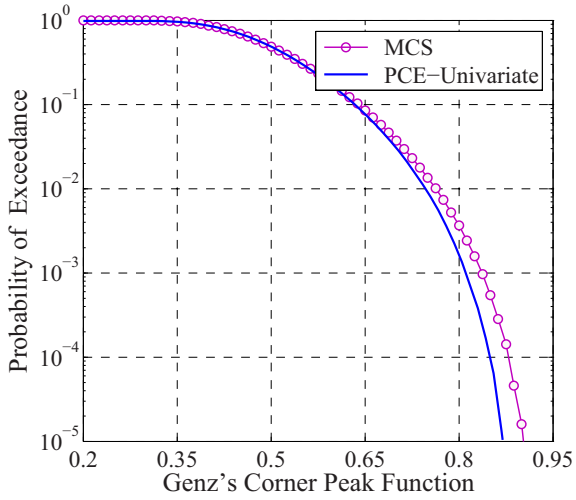

(b) Distribution Tails with Univariate M-DRM

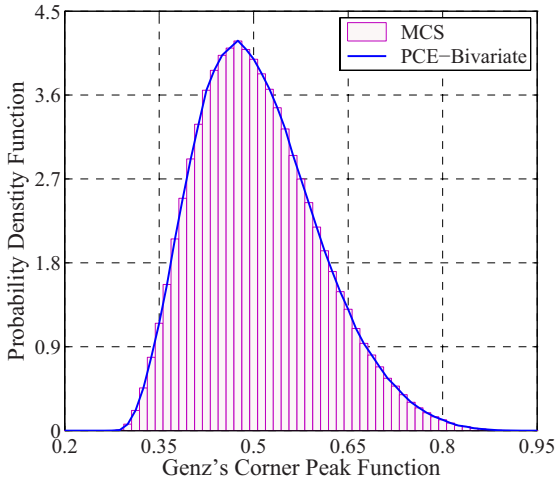

(c) PDF with Bivariate M-DRM

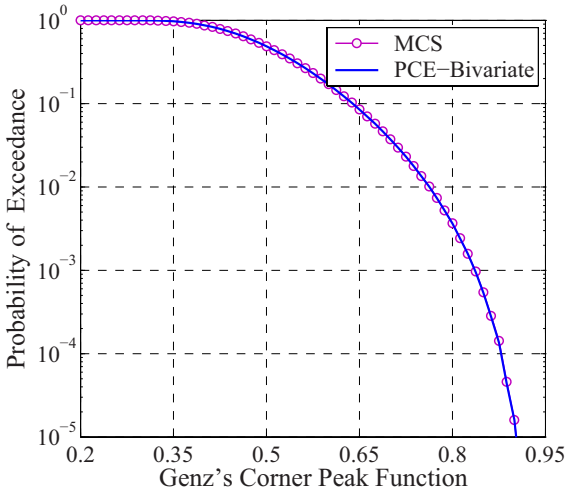

(d) Distribution Tails with Bivariate M-DRM

Figure 7.6: Output distribution of the corner peak function estimated by PCE meta-models with univariate and bivariate M-DRM (PCE: Polynomial chaos expansion; M-DRM: The proposed multiplicative dimensional reduction method; MCS: Crude Monte Carlo simulation with 10^6 samples.)

Use the univariate M-DRM to approximate the physical model, $M_b(\mathbf{X})$, whereas the corresponding number of functional evaluations are summarized in Table 7.10.

Two expansion orders, i.e., $p = 3$ and $p = 6$, are considered to study the corresponding truncation errors in a PCE meta-model development. The increase of value p (i.e., a higher

Table 7.9: Properties of input random variable of the rotation disk example

Variable	Description	Unit	Distribution	Mean	Std.D
S_u	Material strength	ksi	Lognormal	240	5
ω	Angular velocity	rmp	Lognormal	22000	500
ρ	Material density	lbs^2/in^4	Uniform	$0.29/g_0$	$0.0058/g_0$
R_o	Outer radius	inch	Normal	24	0.5
R_i	Inner radius	inch	Normal	8.0	0.3
α_{m}	Material factor	$--$	Lognormal	0.95	0.05

$g_0 = 385.82\text{in}/\text{s}^2$ and ρ is uniformly distributed over $[0.28, 0.30]\,\text{lbs}^2/\text{in}^4$.

Table 7.10: $\mathcal{L}^2$ Error and computational cost of the disk example

Univariate M-DRM	$\mathcal{L}^2$ Error	Number of Functional Evaluations
$p = 3,\ N = 3$	5.30×10^{-3}	$19 = 1 + 3 \times 6$
$p = 6,\ N = 8$	3.74×10^{-6}	$49 = 1 + 8 \times 6$

truncation order) implies the increase of nonlinearity involved in coefficient integration due to the involved high-order polynomials. This is the motivation of increasing the order of Gauss quadrature from $N = 3$ to $N = 8$ for the two cases. With the dimensionality $n = 6$ (i.e., six input variables), the total terms of PCE mete-models are 84 and 924, respectively, given $p = 3$ and $p = 6$.

Figure 7.7 depicts the quality plots on the simulated and predicted values of the burst margin. It is clear to see that the PCE meta-model associated with three expansion orders ($p = 3$) has underestimated the upper quantiles of the burst margin. However, after increasing the truncation order p to 6, a good agreement between the simulated and predicted outputs has verified the accuracy the proposed method in a model representation. The small numbers of functional evaluations (49 as $p = 6$) also indicates the high efficiency of the proposed method.

The global sensitivity analysis of the burst rotation margin are determined as shown in Table 7.11, which are verified with the benchmarks provided by crude Monte Carlo simulation. It is clear to see that the Sobol' indices estimated with three truncation orders ($p = 3$) are fairly close to the benchmarks. Given the values of the sensitivity analysis, the material density, ρ, is the most influential parameter and followed by the angular rotation speed, ω, which are the two primary sources of output variance compared to the other input variables.

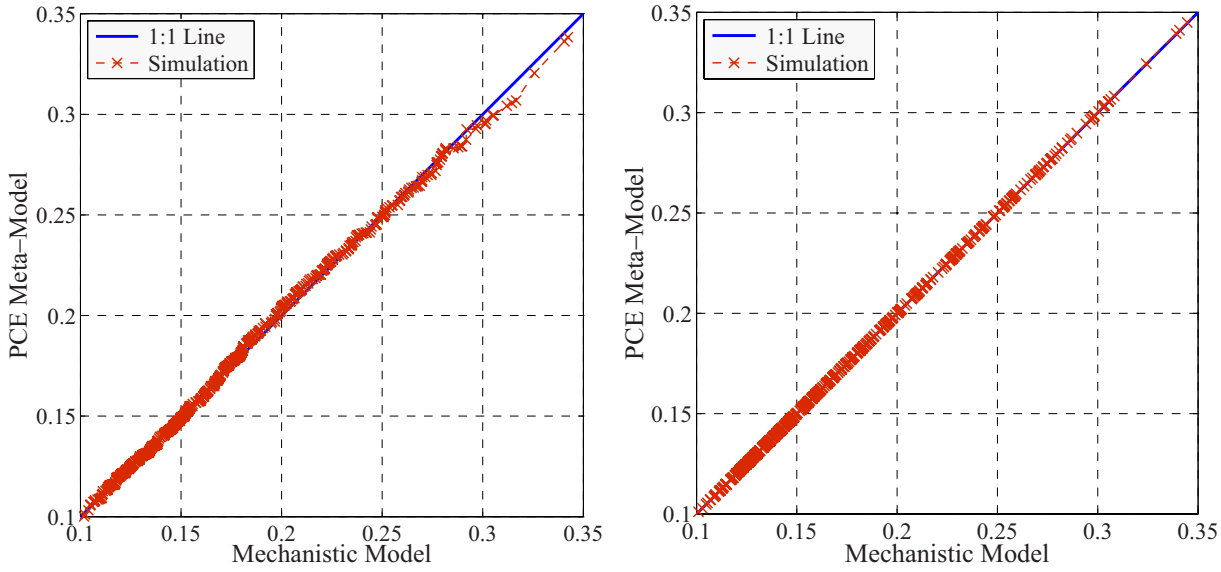

(a) Univariate M-DRM: $p = 3, N = 3$ (b) Univariate M-DRM: $p = 6, N = 8$

Figure 7.7: Simulated versus predicted burst margins of the rotation disk example (Univariate M-DRM: The univariate multiplicative dimensional reduction method.)

Table 7.11: Global sensitivity analysis of the rotation disk example

Variable	S_u	ω	ρ	R_o	R_i	α_m	$\sum_i S_i$
MCS	4.676×10^{-3}	0.1652	0.8024	2.629×10^{-3}	-3.40×10^{-4}	7.959×10^{-3}	0.9825
M-DRM[a]	5.983×10^{-3}	0.1746	0.7937	3.928×10^{-3}	7.315×10^{-4}	9.536×10^{-3}	0.9885
M-DRM[b]	5.704×10^{-3}	0.1665	0.8026	3.745×10^{-3}	6.973×10^{-4}	9.091×10^{-3}	0.9884

M-DRM[a]: The univariate M-DRM with truncation order $p = 3$ and Gauss points $N = 3$.

M-DRM[b]: The univariate M-DRM with truncation order $p = 6$ and Gauss points $N = 8$.

Output distribution of the burst margin, $M_b(\mathbf{X})$, based on the two PCE meta-models are generated as shown in Figure 7.8. Compared with the empirical distribution, one can see that the three order ($p = 3$) PCE meta-model has underestimated the upper quantile of the output distribution, which results in the dangerous estimates on the estimates of failure probability. In the context of using the six-order truncation, the corresponding PCE meta-model can precisely describe the complete probability distribution of $M_b(\mathbf{X})$. Therefore, with 49 functional evaluations of the mechanistic model, the proposed method can be believed to determine the reliable estimates on output moment, Sobol' sensitivity index and output distribution of the burst margin.

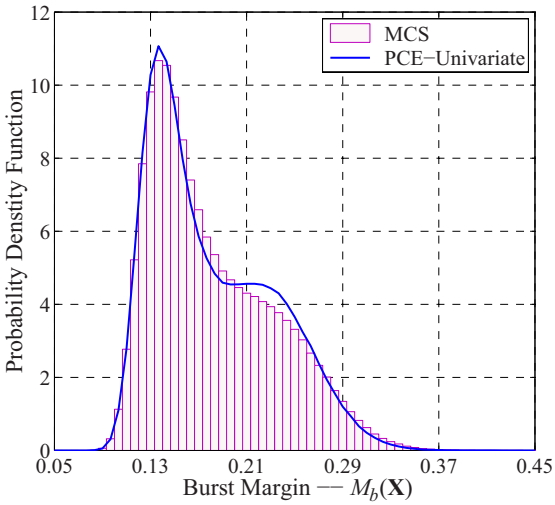

(a) PDF with Univariate M-DRM: $p = 3, N = 3$

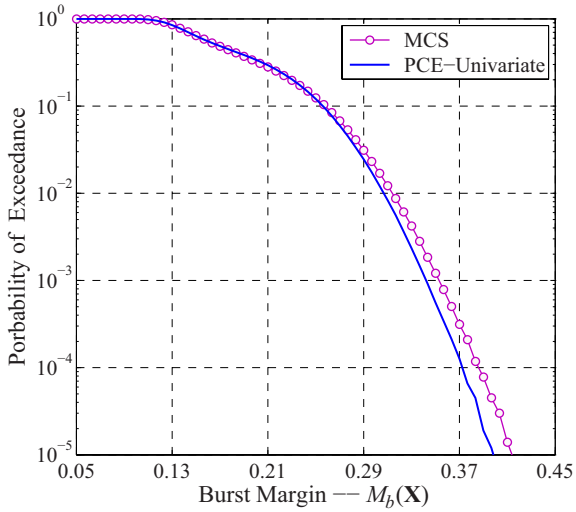

(b) Distribution with Univariate M-DRM: $p = 3, N = 3$

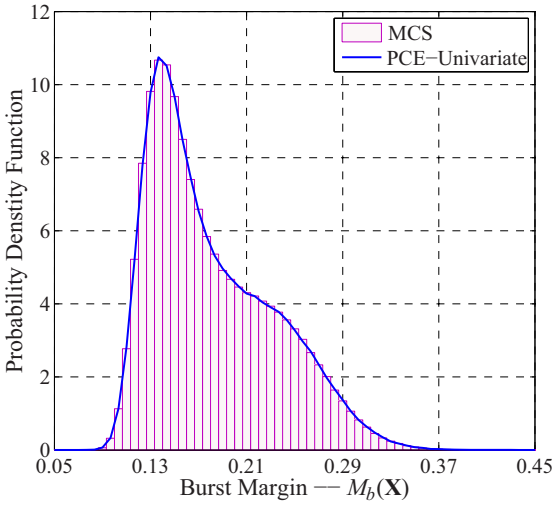

(c) PDF with Univariate M-DRM: $p = 6, N = 8$

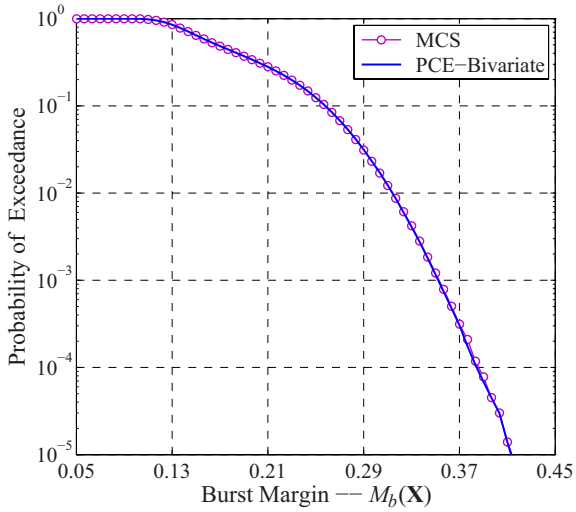

(d) Distribution with Univariate M-DRM: $p = 6, N = 8$

Figure 7.8: Output distribution of burst margin of a rotating disk estimated by PCE meta-model(PCE: Polynomial chaos expansion; M-DRM: The proposed multiplicative dimensional reduction method; MCS: Crude Monte Carlo simulation with 10^6 samples.)

7.6.2 A Ten-Bar Truss Structure

The example has been employed in Chapter 5 to examine the performance of ME-FM (the principle of maximum entropy with fractional moment) in estimating the probability distribution of a maximal structural response. In the section, the proposed method for polynomial chaos expan-

sion is further studied.

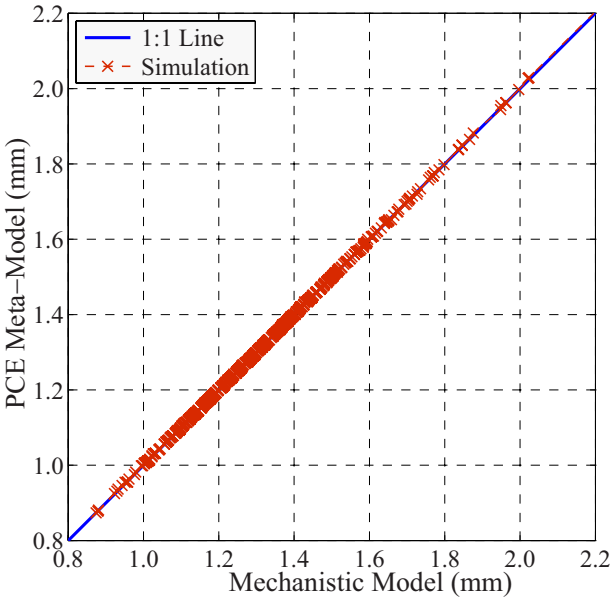

Figure 7.9: Simulated versus predicted maximum displacement of the ten-bar truss example (Univariate M-DRM: The univariate multiplicative dimensional reduction method; Truncation order $p = 4$; Order of Gauss quadrature $N = 4$; The number of orthogonal polynomials in the PCE meta-model is $d = 126$.)

Truncation order of the PCE meta-model is assumed to $p = 4$. With 500 samples of input variables, Figure 7.9 depicts the simulated and the predicted maximal displacements of the truss structure. The regression test obtained a fairly small relative error ($\mathcal{L}^2$ Error$= 1.11 \times 10^{-4}$) for the PCE meta-model.

With four-order Gauss-Hermite quadratures, the total number of functional evaluations is $26 = (1 + 5 \times 5)$, which implies the high efficiency of the proposed method. Global sensitivity analysis of the problem has been conducted, and Figure 7.10 describes the corresponding results. The variable of A (area of each truss member) and the material Young's module E are the most two sensitive variables for the uncertainty of structural maximal displacement, both of which are almost identical to 41%.

Compared to the benchmark distribution provided by the mechanistic model, probability distribution of the structural maximum displacement is estimated by using the PCE meta-model as shown in Figure 7.11, in which one can see the exact estimates lower quantiles can be guaranteed by the proposed polynomial chaos expansion method.

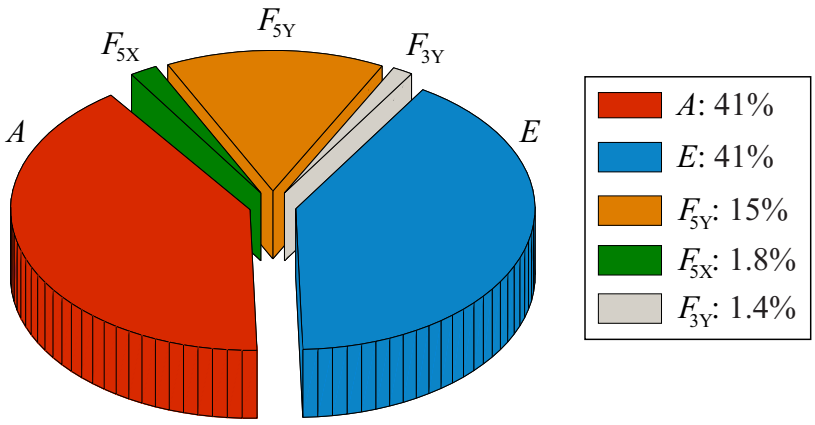

Figure 7.10: Sobol' global sensitivity index of the ten-bar truss example

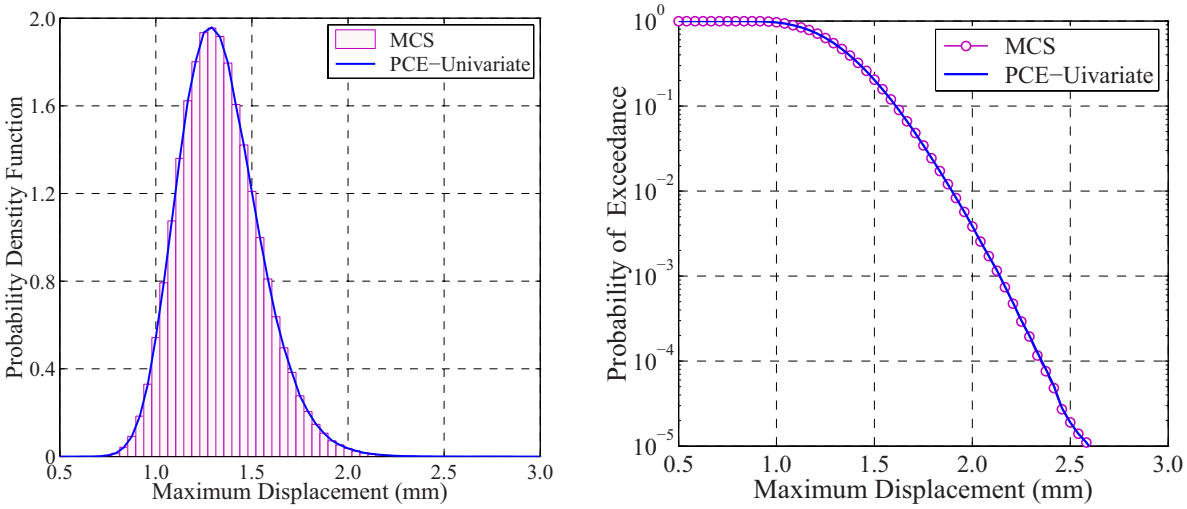

(a) Probability Density Function

(b) Distribution Tails of the Maximum Displacement

Figure 7.11: Probability distribution of the maximum structural displacement (PCE: Polynomial chaos expansion; Univariate M-DRM: The univariate multiplicative dimensional reduction method; MCS: Crude Monte Carlo simulation with 10^6 samples.)

7.7 Kinematic Analysis of Mechanisms

This section evaluates accuracy and efficiency of the proposed method by considering the examples of mechanism kinematic analysis. Since the mechanism kinematic analysis needs to evaluates the positioning errors incurred at a large number of points on the whole output trajectory of a mechanism (Pandey and Zhang, 2012; Zhang and Pandey, 2013), the study is proposed

to approximate the extreme-value distribution by using the multiplicative dimensional reduction method.

7.7.1 A Planar Four-Bar Linkage

Figure 7.12 describes a four-bar linkage, in which the model parameters are defined as $\mathbf{z} = [L_1, L_2, L_3, L_4, L_5, \theta_2, \theta_5]^{\mathrm{T}}$. The output angles of links L_3 and L_4 can be expressed as

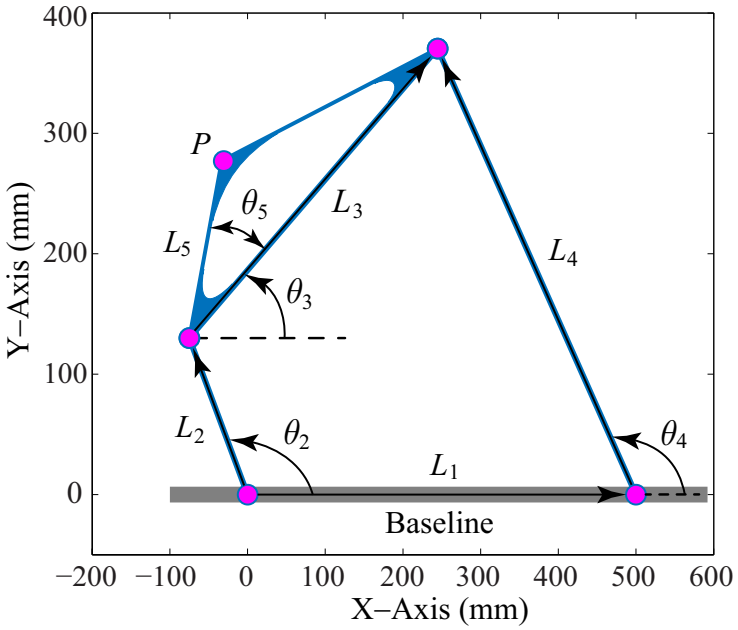

Figure 7.12: A four-bar linkage mechanism (Huang and Zhang, 2010): Model parameters of the four-bar linkage are $L_1 = 500\,\mathrm{mm}$, $L_2 = 150\,\mathrm{mm}$, $L_3 = 400\,\mathrm{mm}$, $L_4 = 450\,\mathrm{mm}$, $L_5 = 150\,\mathrm{mm}$, $\theta_5 = \pi/9$ rad, and operating angle $\theta_2 = 2\pi/3$ rad.

$$\begin{cases} \theta_3(\mathbf{z}) = \psi(\mathbf{z}) - \beta(\mathbf{z}), \quad \theta_4(\mathbf{z}) = \pi - \phi(\mathbf{z}) - \beta(\mathbf{z}); & \text{if } 0 \leqslant \theta_2 \leqslant \pi \\ \theta_3(\mathbf{z}) = \psi(\mathbf{z}) + \beta(\mathbf{z}), \quad \theta_4(\mathbf{z}) = \pi - \phi(\mathbf{z}) + \beta(\mathbf{z}); & \text{if } \pi \leqslant \theta_2 \leqslant 2\pi \end{cases} \tag{7.46}$$

where $L_0 = \sqrt{L_1^2 + L_2^2 - 2L_1L_2\cos(\theta_2)}$; $\psi(\mathbf{z}) = \cos^{-1}\left(\frac{L_3^2+L_0^2-L_4^2}{2L_3L_0}\right)$; $\beta(\mathbf{z}) = \cos^{-1}\left(\frac{L_1^2+L_0^2-L_2^2}{2L_1L_0}\right)$, and $\phi(\mathbf{z}) = \cos^{-1}\left(\frac{L_4^2+L_0^2-L_3^2}{2L_4L_0}\right)$. Therefore, a closed function governing the coordinates of output position P can be determined as

$$\begin{cases} p_{\mathrm{x}}(\theta_2) = L_2\cos(\theta_2) + L_5\cos(\theta_3 + \theta_5) \\ p_{\mathrm{y}}(\theta_2) = L_2\sin(\theta_2) + L_5\sin(\theta_3 + \theta_5) \end{cases} \tag{7.47}$$

Using a general variable θ to represent the operating angle of a mechanism, the whole range of $\theta \in [\theta_L, \theta_H]$, then, can be equally discretized as a number of "time" instants by an increment of $\Delta\theta$. The corresponding number of output positions will be $b = (\theta_H - \theta_L)/\Delta\theta + 1$, whereas a k^{th} instant operating anlage is $\tau_k = \theta_L + (k-1)\Delta\theta$.

Define the maximal output error in the entire trajectory of the mechanism:

$$\eta(\mathbf{X}) = \max\left\{\left[r(\mathbf{X}, \tau_k)\right]_{k=1}^{b}\right\} \tag{7.48}$$

The study employs the method of M-DRM to develop a PCE surrogate model to mimic the maximal error function. And the corresponding results on the moment, sensitivity analysis and the complete probability distribution of the extreme-valued positional error will be determined based on the PCE meta-model.

In the example of four-bar linkage, operating angle θ_2 is discreted as $\theta_2 = [0 : \pi/50 : 2\pi]$ rad, which implies the system reliability analysis contains 101 limit state functions (i.e., $b = 101$). Random variables about errors $\boldsymbol{\varepsilon} = [\varepsilon_{L_1}, \varepsilon_{L_2}, \varepsilon_{L_3}, \varepsilon_{L_3}, \varepsilon_{L_4}, \varepsilon_{L_5}, \varepsilon_{\theta_1}, \varepsilon_{\theta_2}]^{\mathrm{T}}$ of model parameters $\mathbf{z}$ are listed in Table 7.12.

Table 7.12: Random variables of the four-bar linkage example

Variable	Description	Distribution	Units	Mean	COV
ε_{L_1}	Error in length L_1	Lognormal	mm	1.0	0.2
ε_{L_2}	Error in length L_2	Lognormal	mm	1.0	0.2
ε_{L_3}	Error in length L_3	Lognormal	mm	1.0	0.2
ε_{L_4}	Error in length L_4	Lognormal	mm	1.0	0.2
ε_{L_5}	Error in length L_5	Lognormal	mm	1.0	0.2
ε_{θ_2}	Error in angle θ_2	Lognormal	deg	$1.8/\pi$	0.2
ε_{θ_5}	Error in angle θ_5	Lognormal	deg	$1.8/\pi$	0.2

PCE Meta-Model

PCE meta-model of the maximal positioning error of the four-bar linkage was determined with the methods of univariate and bivariate M-DRM. Given the truncation order $p = 4$, each PCE meta-model contains 330 $\left(= \frac{(7+4)!}{7!4!}\right)$ terms in total. With $N_0 = 500$ random numbers of input variables, plots on the responses determined by mechanistic model and PCE meta-model are

depicted in Figure 7.13, The four-point Gauss quadrature is employed. The corresponding $\mathcal{L}^2$ Error and computational cost are summarized in Table 7.13.

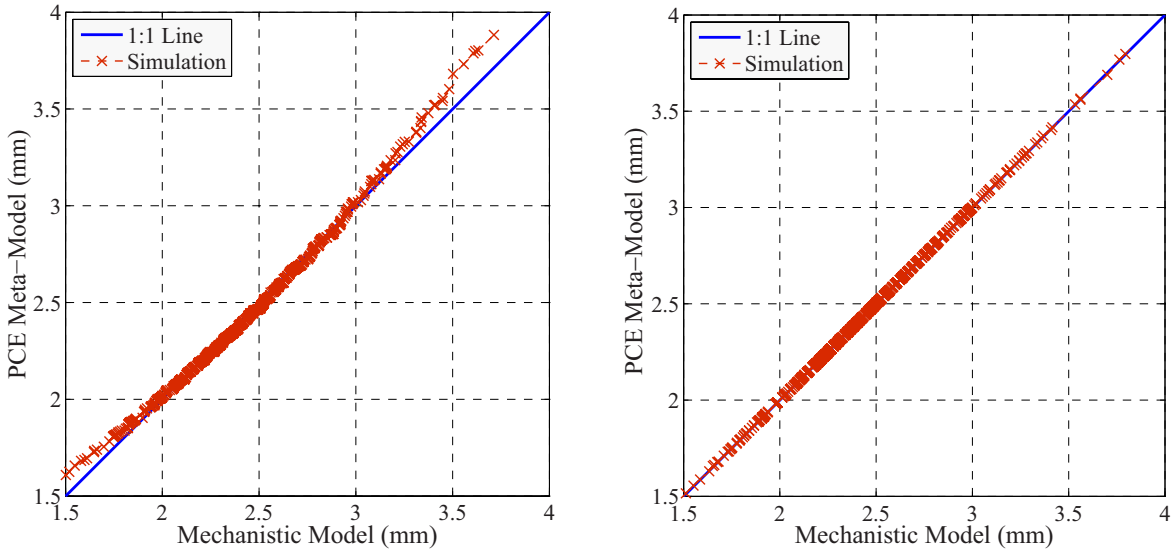

(a) Univariate M-DRM (b) Bivariate M-DRM

Figure 7.13: Simulated versus predicted maximum output error of the four-bar mechanism (Mechanistic Model: Simulated responses based on the original physical model; PCE: Predicted response based on the PCE meta-model; M-DRM: The univariate or bivariate multiplicative dimensional reduction method.)

Table 7.13: $\mathcal{L}^2$ Error and computational cost for the four-bar linkage example

Method	$\mathcal{L}^2$ Error	Number of Functional Evaluations
Univariate M-DRM	1.01×10^{-2}	$29 = 1 + 4 \times 7$
Bivariate M-DRM	2.76×10^{-5}	$365 = 1 + 4 \times 7 + 4^2 \times 7 \times (7-1)/2$

Based on the quality test of the PCE meta-models, one can see that the univariate M-DRM underestimated the true output distribution at the tail region. The bivariate M-DRM can precisely determine the output distribution (see Figure 7.14) with a fairly small regression error ($\mathcal{L}^2$ Error $= 2.76 \times 10^{-5}$).

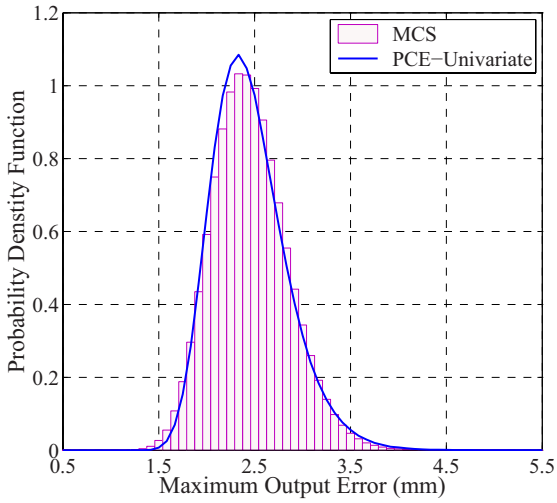

(a) PDF with Univariate M-DRM

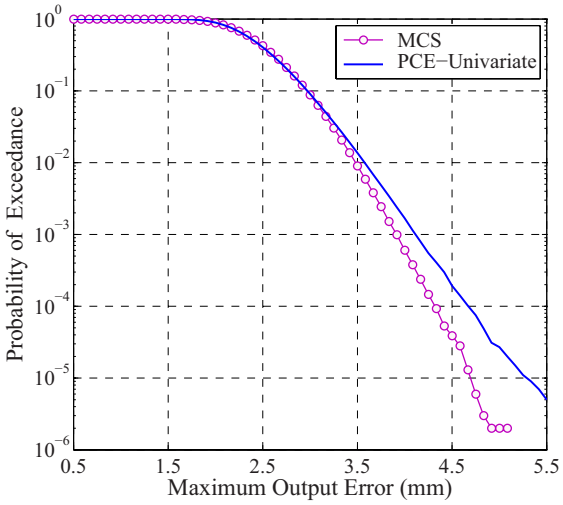

(b) Distribution Tails with Univariate M-DRM

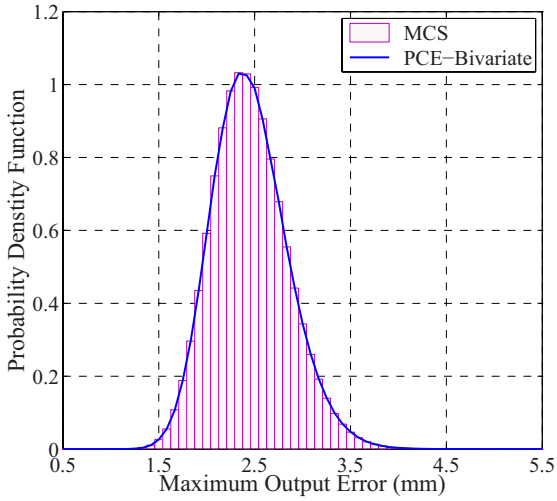

(c) PDF with Bivariate M-DRM

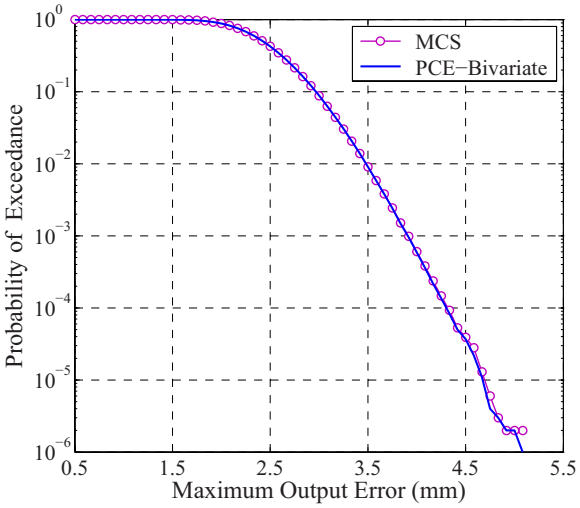

(d) Distribution Tails with Bivariate M-DRM

Figure 7.14: Distribution of the system maximum positioning error estimated by PCE (PCE: Polynomial chaos expansion; M-DRM: The proposed multiplicative dimensional reduction method; MCS: Crude Monte Carlo simulation with 10^6 samples.)

Sensitivity Analysis

Global sensitivity analysis of the maximal positioning error with respect to input variables $\mathbf{X}$ are conducted as shown in Table 7.14, which was verified by the crude Monte Carlo simulation with 10^6 samples.

Table 7.14: Global sensitivity analysis of the four-bar linkage mechanism

Variable	ε_{L_1}	ε_{L_2}	ε_{L_3}	ε_{L_4}	ε_{L_5}	ε_{θ_2}	ε_{θ_5}
MCS	7.43×10^{-3}	2.91×10^{-2}	2.95×10^{-3}	3.54×10^{-2}	8.89×10^{-6}	0.4035	0.5257
U-M-DRM	6.46×10^{-3}	2.86×10^{-2}	2.03×10^{-3}	3.52×10^{-2}	0	0.3955	0.5251
B-M-DRM	6.29×10^{-3}	2.76×10^{-2}	1.95×10^{-3}	3.45×10^{-2}	0	0.4035	0.5254

U-M-DRM: The meta-model of polynomial chaos expansion with univariate M-DRM;
B-M-DRM: The meta-model of polynomial chaos expansion with bivariate M-DRM;
MCS: Crude Monte Carlo simulation with 10^6 samples.

The importance analysis revealed that the input errors associated with angles θ_2 and θ_5 were the primary sources of output variability due to the large Sobol' sensitivity indices (i.e., 40.35% and 52.54%, respectively). However, the errors of links have a very small contributions (less than 8%). Especially for the link 5, it almost makes a null contribution for the total output variance. In addition, compared to benchmarks provided by Monte Carlo simulation, both univariate and bivariate M-DRM can provide accurate estimates on the Sobol' sensitivity index for the global sensitivity analysis.

7.7.2 A Six-DOF Elbow Manipulator

The last example to further examine the proposed method on system uncertainty propagation by considering a space elbow robotic manipulator. Detailed descriptions of the example please refer to Chapter 4 for system reliability analysis of the mechanism. Random variables of errors in the manipulator's parameters are listed in Table 7.15.

The proposed method of M-DRM will be employed to conduct the polynomial chaos expansion of the extreme-valued positioning error.

Verification of PCE Meta-Model

With PCE meta-models of the system maximum error function have been constructed by using the univariate M-DRM the bivariate M-DRM, respectively, in which the truncation order $p = 4$, and four-order Gauss quadrature has been employed to compute the model coefficients. With 500 samples of input random variables,

Table 7.16 summarized the corresponding relative errors and the involved computational cost

related to the meta-models by using the univariate and bivariate methods, respectively. The small $\mathcal{L}^2$ Error determined by the bivariate M-DRM was confirmed its accuracy in modeling the maximal positioning error of the elbow manipulator.

Global sensitivity analysis has conducted as a byproduct of the PCE meta-model. The corresponding Sobol' sensitivity indices are summarized in Table 7.17, which were verified very well by crude Monte Carlo simulation.

Probability distribution of the system maximal positioning error was estimated based on the PCE meta-models. Compared to the empirical distribution provided by the mechanistic mod-

Table 7.15: Random variables in the six-DOF elbow robotic manipulator

Variable	Description	Distribution	Units	Mean-Value	COV
ε_{L_1}	Error in Length L_1	Lognormal	mm	1.0	0.1
ε_{L_2}	Error in Length L_2	Lognormal	mm	1.0	0.1
ε_{L_3}	Error in Length L_3	Lognormal	mm	1.0	0.1
ε_{L_4}	Error in Length L_4	Lognormal	mm	1.0	0.1
ε_{L_5}	Error in Length L_5	Lognormal	mm	1.0	0.1
ε_{θ_2}	Error in angle θ_2	Lognormal	deg	$1.8/\pi$	0.1
ε_{θ_5}	Error in angle θ_5	Lognormal	deg	$1.8/\pi$	0.1

Table 7.16: $\mathcal{L}^2$ Error and computational cost of the robotic manipulator

Method	$\mathcal{L}^2$ Error	Number of Functional Evaluations
Univariate M-DRM	3.44×10^{-3}	$29 = 1 + 4 \times 7$
Bivariate M-DRM	6.46×10^{-6}	$365 = 1 + 4 \times 7 + 4^2 \times 7 \times (7-1)/2$

Table 7.17: Global sensitivity analysis of the six-DOF elbow robotic manipulator

Variable	ε_{L_1}	ε_{L_2}	ε_{L_3}	ε_{L_4}	ε_{L_5}	ε_{θ_2}	ε_{θ_5}
MCS	1.375×10^{-2}	1.638×10^{-2}	1.202×10^{-3}	8.934×10^{-3}	9.190×10^{-3}	0.6835	0.2688
U-M-DRM	1.343×10^{-2}	1.343×10^{-2}	2.289×10^{-4}	8.825×10^{-3}	9.089×10^{-3}	0.6839	0.2701
B-M-DRM	1.336×10^{-2}	1.336×10^{-2}	2.290×10^{-4}	8.872×10^{-3}	9.038×10^{-3}	0.6839	0.2704

U-M-DRM: The meta-model of PCE computed by the univariate M-DRM;

B-M-DRM: The meta-model of PCE computed by the bivariate M-DRM;

Truncation order of meta-model $p = 4$, and the order of Gauss quadrature $N = 4$;

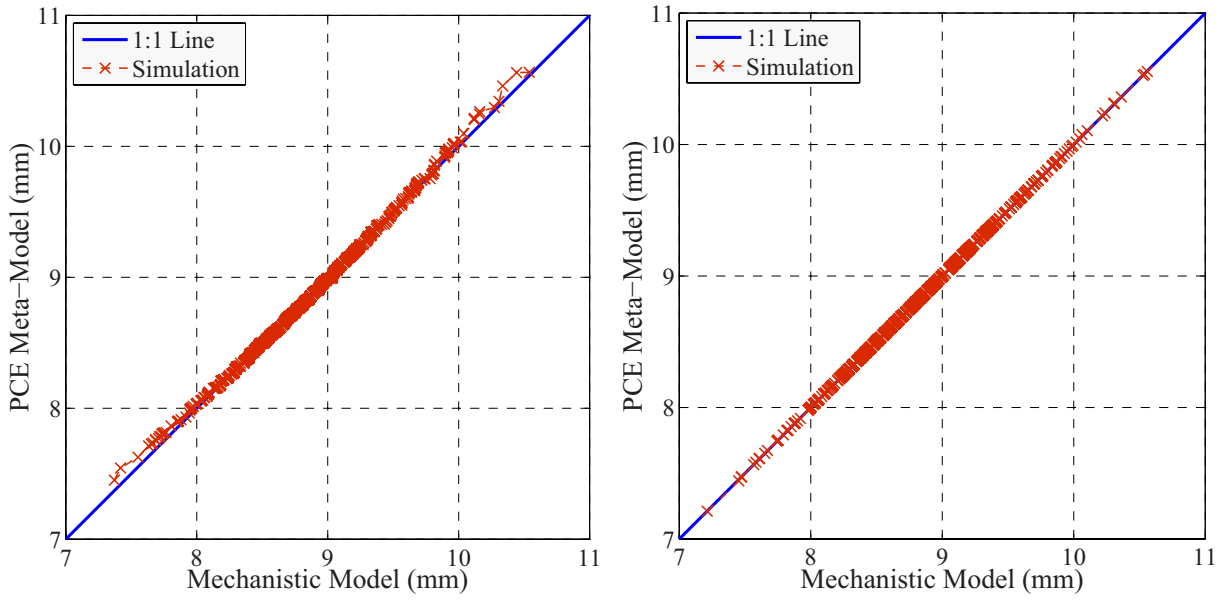

(a) Univariate M-DRM

(b) Bivariate M-DRM

Figure 7.15: Simulated versus predicted maximum output errors of the robotic manipulator (Mechanistic Model: Simulated responses based on the physical model; PCE: Predicted responses based on PCE meta-model.)

el as listed in Figure 7.16, one can see that univariate M-DRM has underestimated the quntial functions the maximal distribution as POE $\leqslant 10^{-2}$, which implies the conservative estimates on failure probabilities associated with an upper threshold. The bivariate M-DRM can provide precisely estimation on the output probability distribution at its entire definition domain. Together with the example of planar four-bar linkage, the proposed method has illustrate its superiority for system kinematic analysis of robotic manipulators.

7.8 Conclusion

The Chapter presents a computationally efficient method for polynomial chaos expansion of a complicated function. Classical methods in literature (simulation-based and Gauss quadrature-based) lead to intractable computational cost due to the involved high-dimension integrations with respect to expansion coefficients. The study proposes the use of multiplicative dimensional reduction method (M-DRM) for the objective.

Seven examples are employed in the Chapter to examine the accuracy and efficiency of the

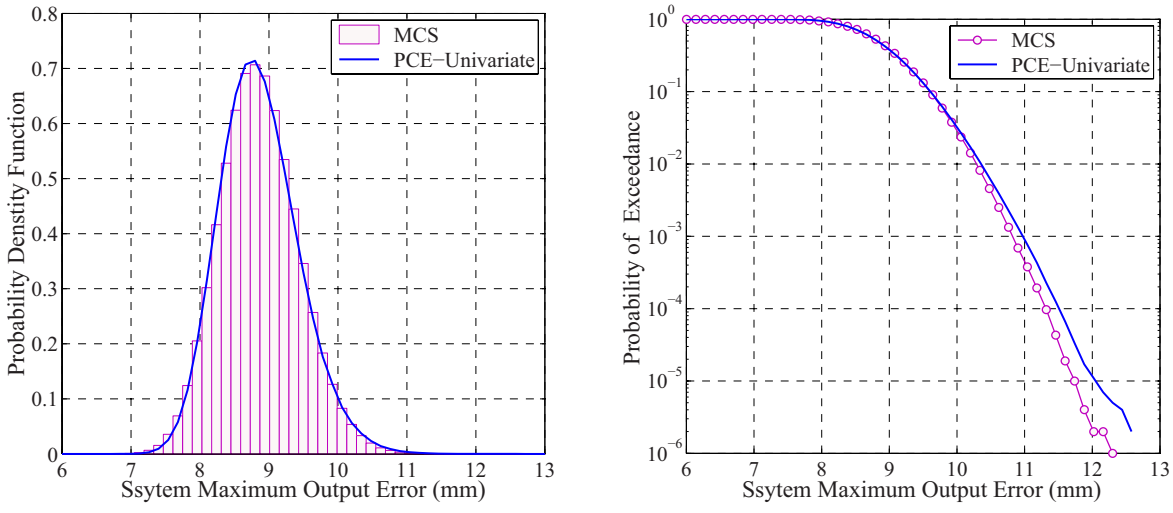

(a) PDF with Univariate M-DRM

(b) Distribution Tails with Univariate M-DRM

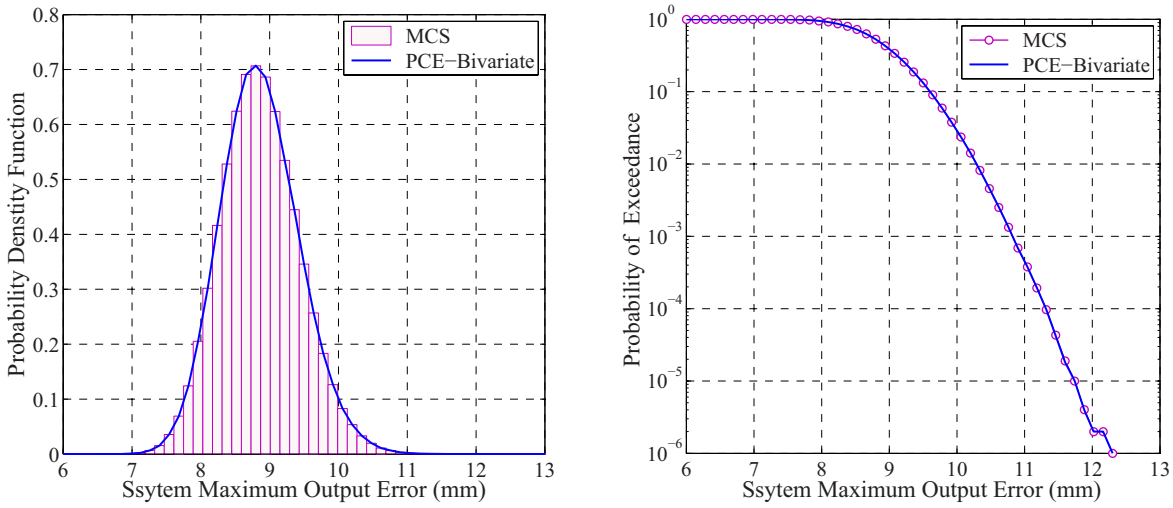

(c) PDF with Bivariate M-DRM

(d) Distribution Tails with Bivariate M-DRM

Figure 7.16: Distribution of the maximum positioning error of the robotic manipulator estimated by PCE meta-model with univariate and bivariate M-DRM (PCE: Polynomial chaos expansion; M-DRM: The proposed multiplicative dimensional reduction method; MCS: Crude Monte Carlo simulation with 10^6 samples.)

proposed method on a PCE surrogate model construction. A generic coefficient of determination (i.e., the relative $\mathcal{L}^2$ Error) is employed to evaluate the good-of-fitness of the proposed PCE model. All the examples have shown that the relative errors of PCE meta-model are fairly small (i.e., $\mathcal{L}^2$ Error $\leqslant 10^{-5}$). The determined moment, Sobol' sensitivity index, and output distribution

are verified very well by the benchmarks of Monte Carlo simulation.

Compared to the direct tensor quadrature method in literature, the proposed univariate and bivariate M-DRMs can reduce the number of functional evaluations from N^n to $1 + nN$ and $1 + nN + n(n-1)N^2/2$, respectively. In addition, the proposed method is a non-intrusive method in nature, since that the corresponding PCE meta-model construction is only based on a small number of deterministic model responses.

Chapter 8

Conclusions and Recommendations

The purpose of the work is to develop computationally efficient methods for reliability and global sensitivity analyses. The governing function related to the framword is an implicit or explicit physical function with multiple input variables. Several contributions for this purpose have been made in this study as summarized in the following.

8.1 Summary

Chapter 3 developed an innovative method for parent distribution estimation of a positive random variable. The principle of maximum entropy is applied to derive this distribution. A novel feature of the analysis is the use of fractional moments, instead of integer moments commonly used in the entropy literature. Compared to the benchmark results, examples of several heavy tail distributions have illustrated the accuracy and efficiency of the proposed method for quantile function estimation.

Chapter 4 was further extended the simulation-based distribution estimation method for system reliability analysis of mechanism, which needs to evaluate extreme event distribution of output positional errors along an entire trajectory. Fractional moments of the maximal positioning error were computed by Monte Carlo simulation (with 1000 to 5000 samples). Three examples were employed to show that this entropy-based approach can accurately estimated the probability of failures in the order of $P_F \leqslant 10^{-4}$.

Chapter 5 further optimized the entropy-based method for estimation of an output probability distribution by minimizing the computation effort associated with the fractional moments. A

novel multiplicative dimensional reduction method (M-DRM) was proposed to approximate a general model function. Combined with Gauss quadratures, it proposes a computationally efficient method for (fractional and integer) moment calculation. Several examples illustrated that the numerical accuracy and efficiency of the proposed method in comparison to the Monte Carlo simulation method.

Chapter 6 presented a computationally efficient method for global sensitivity analysis with M-DRM. The M-DRM approximates a high-dimensional function as the product of a series one-dimensional functions. The separative feature was employed to simplify the involved computational intensive integrations in global sensitivity analysis. Compared to the benchmarks provided by Monte Carlo simulation, the determined global sensitivity coefficients of several examples in literature confirmed the accuracy and efficiency of the proposed method

Chapter 7 presented an efficient method for polynomial chaos expansion (PCE) with M-DRM. The M-DRM was further employed to compute the expansion coefficients of a PCE metamodel.

8.2 Conclusions

This study has developed an effective tool for conducting uncertainty propagation of a system for moment computation, global sensitivity analysis and reliability analysis. A number of specific conclusions can be drawn from the investigation described in this thesis:

- The proposed multiplicative dimensional reduction method effectively models a high-dimensional complex input-output relation;
- The proposed use of fractional (integer) moment with the principle maximum entropy can accurately estimate probability distribution of the structural response.
- The multiplicative dimensional reduction method can provide reliable estimate of system global sensitivity coefficient efficiently; and
- The proposed M-DRM method for polynomial chaos expansion can produce accurate estimates of moment, global sensitivity coefficients and complete output distribution of a structural response.

8.3 Recommendations for Future Research

The thesis primary focuses on the uncertainty propagation with the multiplicative dimensional reduction method. Two approaches have been developed. One technique uses M-DRM to compute fractional moments and further estimate response distribution through the principle of maximum entropy (MaxEnt). Another routine is employing M-DRM to conduct the polynomial chaos expansion (PCE). With the corresponding PCE meta-model in hand, the fast evaluations of the surrogate model allows to perform the uncertainty quantification by using Monte Carlo simulations.

To better focus on the main objectives, some simplifications are made in the discussion. All the uncertainties related to model input random variables are characterized by the corresponding probability distribution function. However, the determination of these distribution models may vary with the knowledge of analyst. This variation due to the professional knowledge is known as the epistemic uncertainty. The methods discussed in the thesis do not consider the influence of epistemic uncertainty on model output uncertainty analysis. In addition, all input random variables are assumed mutually independent due to the simplicity, which may not be realistic in some cases. Generalization of the methods to account for epistemic uncertainties and the colored input probability measures should be investigated in future.

Bibliography

AISC, 2005. Specification for Structural Steel Buildings (ANSI/AISC 360–05). American Institute of Steel Construction Inc., Chicago.

Andrieu-Renaud, C., Sudret, B., Lemaire, M., 2004. The PHI2 method: A way to compute time-variant reliability. Reliability Engineering & System Safety 84 (1), 75 – 86.

Au, S., Beck, J., 1999. A new adaptive importance sampling scheme for reliability calculations. Structural Safety 21 (2), 135 – 158.

Babuška, I., Nobile, F., Tempone, R., 2007. A stochastic collocation method for elliptic partial differential equations with random input data. SIAM Journal on Numerical Analysis 45 (3), 1005 – 1034.

Bennett, R., Ang, A., 1983. Investigation of methods for structural system reliability. Tech. rep., University of Illinois at Urbana-Champaign.

Bjerager, P., 1988. Probability integration by directional simulation. ASCE Journal of Engineering Mechanics 114 (8), 1285 – 1302.

Blatman, G., 2009. Adaptive sparse polynomial chaos expansions for uncertainty propagation and sensitivity analysis. Ph.D. thesis, Universit Blaise Pascal, Clermont-Ferrand.

Blatman, G., Sudret, B., 2010a. An adaptive algorithm to build up sparse polynomial chaos expansions for stochastic finite element analysis. Probabilistic Engineering Mechanics 25 (2), 183 – 197.

Blatman, G., Sudret, B., 2010b. Efficient computation of global sensitivity indices using sparse polynomial chaos expansions. Reliability Engineering & System Safety 95 (11), 1216 – 1229.

Breitung, K., 1984. Asymptotic approximations for multinormal integrals. ASCE Journal of Engineering Mechanics 110 (3), 357 – 366.

Breitung, K., Faravelli, L., 1994. Log-likelihood maximization and response surface in reliability assessment. Nonlinear Dynamics 5 (3), 273 – 285.

Bucher, C., 1988. Adaptive samplingałan iterative fast monte carlo procedure. Structural Safety 5 (2), 119 – 126.

Cameron, R., Martin, W., 1947. The orthogonal development of non-linear functionals in series of fourier-hermite functionals. The Annals of Mathematics 48 (2), 385 – 392.

Castillo, E., Mínguez, R., Castillo, C., 2008. Sensitivity analysis in optimization and reliability problems. Reliability Engineering & System Safety 93 (12), 1788 – 1800.

Chao, M., Strawderman, W., 1972. Negative moments of positive random variables. Journal of the American Statistical Association 67 (338), 429 – 431.

Chen, W., Jin, R., Sudjianto, A., 2005. Analytical variance-based global sensitivity analysis in simulation-based design under uncertainty. ASME Journal of Mechanical Design 127 (5), 875 – 886.

Cheng, T., 2011. Stochastic renewal process models for maintenance cost analysis. Ph.D. thesis, University of Waterloo.

Choi, J., Lee, S., Choi, D., 1998. Stochastic linkage modeling for mechanical error analysis of planar mechanisms. Mechanics of Structures and Machines 26 (3), 257 – 276.

Cox, D., 1982. An analytic method for uncertainty analysis of nonlinear output functions, with applications to fault-tree analysis. IEEE Transactions on Reliability 31 (5), 465 – 468.

Cox, D., Isham, V., 1980. Point Processes. Chapman & Hall, New York.

Craig, J., 2005. Introduction to Robotics: Mechanics and Control, 3rd Edition. Pearson Prentice Hall, New Jersey.

Cressie, N., Davis, A., Folks, J., Policello, G., 1981. The moment-generating function and negative integer moments. The American Statistician 35 (3), 148 – 150.

Davis, P., Rabinowitz, P., 1975. Methods of Numerical Integration. Academic Press, New York.

Deng, J., Pandey, M., 2008. Estimation of the maximum entropy quantile function using fractional probability weighted moments. Structural Safety 30 (4), 307 – 319.

Deng, J., Pandey, M., 2009. Estimation of minimum cross-entropy quantile function using fractional probability weighted moments. Probabilistic Engineering Mechanics 24 (1), 43 – 50.

Der Kiureghian, A., Dakessian, T., 1998. Multiple design points in first and second-order reliability. Structural Safety 20 (1), 37 – 49.

Der Kiureghian, A., Lin, H., Hwang, S., 1987. Second-order reliability approximations. ASCE Journal of Engineering Mechanics 113 (8), 1208 – 1205.

Der Kiureghian, A., Liu, P., 1986. Structural reliability under incomplete probability information. ASCE Journal of Engineering Mechanics 112 (1), 85 – 104.

Dhande, S., Chakraborty, J., 1973. Analysis and synthesis of mechanical error in linkages – A stochastic approach. ASME Journal of Engineering for Industry 95 (3), 672 – 676.

Ditlevsen, O., Madsen, H., 1996. Structural Reliability Methods. John Wiley & Sons Inc., New York.

Doltsinis, I., Kang, Z., 2004. Robust design of structures using optimization methods. Computer Methods in Applied Mechanics and Engineering 193 (23-26), 2221 – 2237.

Doostan, A., Ghanem, R. G., Red-Horse, J., 2007. Stochastic model reduction for chaos representations. Computer Methods in Applied Mechanics and Engineering 196 (37 – 40), 3951 – 3966.

Dubourg, V., 2011. Adaptive surrogate models for reliability analysis and reliability-based design optimization. Ph.D. thesis, Université Blaise Pascal, Clermont-Ferrand, France.

Dubowsky, S., Maatuk, J., Perreira, N. D., 1975. A parameter identification study of kinematic errors in planar mechanisms. ASME Journal of Engineering for Industry 97 (2), 635 – 642.

Efron, B., Stein, C., 1981. The jackknife estimate of variance. The Annals of Statistics, 586 – 596.

Faik, S., Erdman, A. G., 1991. Sensitivity distribution in the synthesis solution space of four-bar linkages. ASME Journal of Mechanical Design 113 (1), 3 – 9.

Frangopol, D., 1985. Sensitivity of reliability-based optimum design. ASCE Journal of Structural Engineering 111 (8), 1703 – 1721.

Freudenstein, F., 1954. An analytical approach to the design of four-link mechanisms. Transactions of the ASME 76, 483 – 492.

Gatelli, D., Kucherenko, S., Ratto, M., Tarantola, S., 2009. Calculating first-order sensitivity measures: A benchmark of some recent methodologies. Reliability Engineering & System Safety 94 (7), 1212 – 1219.

Genz, A., 1987. A package for testing multiple integration subroutines. In: Numerical Integration: Recent Developments, Software and Applications. pp. 337 – 340.

Ghanem, R., Spanos, P., 1991. Stochastic Finite Elements: A Spectral Approach. Springer-Verlag, New York.

Graham, R. L., Knuth, D. E., Patashnik, O., 1988. Concrete Mathematics: A Foundation for Computer Science. Addison-Wesley Publishing Company, Menlo Park, In: Chapter 5, Page 154, Equaiton 5.1.

Grierson, D., 1983. The intelligent use of structural analysis. Perspectives in Computing 3 (4), 32 – 39.

Gzyl, H., Tagliani, A., 2010. Hausdorff moment problem and fractional moments. Applied Mathematics and Computation 216 (11), 3319 – 3328.

Harbitz, A., 1983. Efficient and accurate probability of failure calculation by the use of the importance sampling technique. In: Proceedings of Fourth International Conference on Applications of Statistics and Probability in Soil and Structural Engineering. pp. 825 – 836.

Hasofer, A., Lind, N., 1974. Exact and invariant second-moment code format. ASCE Journal of the Engineering Mechanics Division 100 (1), 111 – 121.

Helton, J., Davis, F., 2003. Latin hypercube sampling and the propagation of uncertainty in analyses of complex systems. Reliability Engineering & System Safety 81 (1), 23 – 69.

Heyde, C., 1963. On a property of the lognormal distribution. Journal of the Royal Statistical Society: Methodological Series 25 (2), 392 – 393.

Hirschhorn, J., 1962. Kinematics and Dynamics of Plane Mechanisms. McGraw-Hill Book Company, New York.

Hohenbichler, M., Rackwitz, R., 1988. Improvement of second-order reliability estimates by importance sampling. ASCE Journal of Engineering Mechanics 114 (12), 2195 – 2199.

Homma, T., Saltelli, A., 1996. Importance measures in global sensitivity analysis of nonlinear models. Reliability Engineering & System Safety 52 (1), 1 – 17.

Hong, H., 1998. An efficient point estimate method for probabilistic analysis. Reliability Engineering & System Safety 59 (3), 261 – 267.

Hong, H. P., 1996. Point estimate moment based reliability analysis. Civil Engineering Systems 13 (4), 281 – 294.

Huang, X., Zhang, Y., 2010. Robust tolerance design for function generation mechanisms with joint clearances. Mechanism and Machine Theory 45 (9), 1286 – 1297.

IAEA, 1997. Assessment and management of ageing of major nuclear power plant components important to safety: Steam generators. Tech. Rep. IAEA-TECDOC-981, International Atomic Energy Agency, Vienna, Austria.

IAEA, 1998. Assessment and management of ageing of major nuclear power plant components important to safety: CANDU pressure tubes. Tech. Rep. IAEA-TECDOC-1037, International Atomic Energy Agency, Vienna, Austria.

IAEA, 2005. Assessment and management of ageing of major nuclear power plant components important to safety: BWR pressure vessel internals. Tech. Rep. IAEA-TECDOC-1471, International Atomic Energy Agency, Vienna, Austria.

Inverardi, P., Tagliani, A., 2003. Maximum entropy density estimation from fractional moments. Communications in Statistics: Theory and Methods 32 (2), 327 – 345.

Inverardi, P. N., Pontuale, G., Petri, A., Tagliani, A., 2003. Hausdorff moment problem via fractional moments. Applied Mathematics and Computation 144 (1), 61 – 74.

Ishigami, T., Homma, T., 1990. An importance quantification technique in uncertainty analysis for computer models. In: IEEE Proceedings of First International Symposium on Uncertainty Modeling and Analysis. pp. 398 – 403.

Jaynes, E., 1957. Information theory and statistical mechanics. Physical Review 108 (2), 171 – 190.

Johnson, N., 1949. Systems of frequency curves generated by methods of translation. Biometrika 36 (1-2), 149 – 176.

Jones, D., 1979. Elementary Information Theory. Oxford University Press, New York.

Kapur, J., Kesavan, H., 1992. Entropy Optimization Principles with Applications. Academic Press Inc., New York.

Kennedy, C., Lennox, W., 2000. Solution to the practical problem of moments using non-classical orthogonal polynomials, with applications for probabilistic analysis. Probabilistic Engineering Mechanics 15 (4), 371 – 379.

Khuri, A., Casella, G., 2002. The existence of the first negative moment revisited. The American Statistician 56 (1), 44 – 47.

Kim, J., Song, W., Kang, B., 2010. Stochastic approach to kinematic reliability of open-loop mechanism with dimensional tolerance. Applied Mathematical Modelling 34 (5), 1225 – 1237.

Koutsourelakis, P., Pradlwarter, H., Schuëller, G., 2004. Reliability of structures in high dimensions, part I: algorithms and applications. Probabilistic Engineering Mechanics 19 (4), 409 – 417.

Lagarias, J., Reeds, J., Wright, M., Wright, P., 1998. Convergence properties of the Nelder-Mead simplex method in low dimensions. SIAM Journal on Optimization 9 (1), 112 – 147.

Lai, X., Duan, J., 2011. Probabilistic approach to mechanism reliability with multi-influencing factors. Proceedings of the Institution of Mechanical Engineers, Part C: Journal of Mechanical Engineering Science 225 (12), 2991 – 2996.

Lee, T. W., Freudenstein, F., 1976a. Heuristic combinatorial optimization in the kinematic design of mechanisms: Applications. ASME Journal of Engineering for Industry 98 (4), 1281 – 1284.

Lee, T. W., Freudenstein, F., 1976b. Heuristic combinatorial optimization in the kinematic design of mechanisms: Theory. ASME Journal of Engineering for Industry 98 (4), 1277 – 1280.

Li, G., Hu, J., Wang, S., Georgopoulos, P., Schoendorf, J., Rabitz, H., 2006. Random sampling-high dimensional model representation (RS-HDMR) and orthogonality of its different order component functions. The Journal of Physical Chemistry A 110 (7), 2474 – 2485.

Li, G., Rosenthal, C., Rabitz, H., 2001. High dimensional model representations. The Journal of Physical Chemistry A 105 (33), 7765 – 7777.

Li, G., Zhang, K., 2011. A combined reliability analysis approach with dimension reduction method and maximum entropy method. Structural and Multidisciplinary Optimization 43, 121 – 134.

Li, J., Chen, J., Fan, W., 2007. The equivalent extreme-value event and evaluation of the structural system reliability. Structural Safety 29 (2), 112 – 131.

Li, R., Ghanem, R., 1998. Adaptive polynomial chaos expansions applied to statistics of extremes in nonlinear random vibration. Probabilistic Engineering Mechanics 13 (2), 125 – 136.

Liu, H., Chen, W., Sudjianto, A., 2004. Relative entropy based method for global and regional sensitivity analysis in probabilistic design. In: Proceedings of DETC'04 ASME 2004 International Design Engineering Technical Conferences & Computers and Information in Engineering Conference. pp. 983 – 992.

Liu, H., Chen, W., Sudjianto, A., 2006. Relative entropy based method for probabilistic sensitivity analysis in engineering design. ASME Journal of Mechanical Design 128 (2), 326 – 336.

Liu, Y., 2007. Progressive failure analysis of steel building structures under abnormal loads. Ph.D. thesis, Canada: University of Waterloo.

Madsen, H., Krenk, S., Lind, N., 2006. Methods of Structural Safety. Dover publications Mineola, New York.

Maître, O. L., Najm, H., Ghanem, R., Knio, O., 2004. Multi-resolution analysis of wiener-type uncertainty propagation schemes. Journal of Computational Physics 197 (2), 502 – 531.

McRae, G., Tilden, J., Seinfeld, J., 1982. Global sensitivity analysis – A computational implementation of the fourier amplitude sensitivity test (FAST). Computers & Chemical Engineering 6 (1), 15 – 25.

Melchers, R., 1990. Radial importance sampling for structural reliability. ASCE Journal of Engineering Mechanics 116 (1), 189 – 203.

Montgomery, D., Myers, R., 2002. Response Surface Methodology: Process and Product Optimization Using Designed Experiments, 2nd Edition. John Wiley & Sons Ltd., New York.

Myszka, D., 2012. Machines and Mechanisms: Applied Kinematic Analysis, 4th Edition. Prentice Hall, New Jersey.

Neal, R., 2001. Annealed importance sampling. Statistics and Computing 11 (2), 125 – 139.

Novi Inverardi, P., Petri, A., Pontuale, G., Tagliani, A., 2005. Stieltjes moment problem via fractional moments. Applied Mathematics and Computation 166 (3), 664 – 677.

Oakley, J., O'Hagan, A., 2004. Probabilistic sensitivity analysis of complex models: a Bayesian approach. Journal of the Royal Statistical Society: Series B (Statistical Methodology) 66 (3), 751 – 769.

Orszag, S. A., Bissonnette, L. R., 1967. Dynamical properties of truncated wiener-hermite expansions. Physics of Fluids 10 (12), 2603 – 2613.

Pandey, M., 2000. Direct estimation of quantile functions using the maximum entropy principle. Structural Safety 22 (1), 61 – 79.

Pandey, M., 2001a. Extreme quantile estimation using order statistics with minimum cross-entropy principle. Probabilistic Engineering Mechanics 16 (1), 31 – 42.

Pandey, M., 2001b. Minimum cross-entropy method for extreme value estimation using peaks-over-threshold data. Structural Safety 23 (4), 345 – 363.

Pandey, M., Ariaratnam, S., 1996. Crossing rate analysis of non-gaussian response of linear systems. ASCE Journal of Engineering Mechanics 122 (6), 507 – 511.

Pandey, M., Van Gelder, P., Vrijling, J., 2001. Assessment of an l-kurtosis-based criterion for quantile estimation. Journal of Hydrologic Engineering 6 (4), 284 – 292.

Pandey, M., Zhang, X., 2012. System reliability analysis of the robotic manipulator with random joint clearances. Mechanism and Machine Theory 58 (0), 137 – 152.

Pearson, E., 1963. Some problems arising in approximating to probability distributions, using moments. Biometrika 50 (1-2), 95 – 112.

Piegorsch, W., Casella, G., 1985. The existence of the first negative moment. The American Statistician 31 (9), 60 – 62.

Pradlwarter, H., Schuëller, G., Koutsourelakis, P., Charmpis, D., 2007. Application of line sampling simulation method to reliability benchmark problems. Structural Safety 29 (3), 208 – 221.

Rabitz, H., Aliş, Ö., 1999. General foundations of high-dimensional model representations. Journal of Mathematical Chemistry 25 (2), 197 – 233.

Rackwitz, R., Flessler, B., 1978. Structural reliability under combined random load sequences. Computers & Structures 9 (5), 489 – 494.

Rahman, S., 2006. A solution of the random eigenvalue problem by a dimensional decomposition method. International Journal for Numerical Methods in Engineering 67 (9), 1318 – 1340.

Rahman, S., 2011. Global sensitivity analysis by polynomial dimensional decomposition. Reliability Engineering & System Safety 96 (7), 825 – 837.

Rahman, S., Xu, H., 2004. A univariate dimension-reduction method for multi-dimensional integration in stochastic mechanics. Probabilistic Engineering Mechanics 19 (4), 393 – 408.

Ramberg, J., Schmeiser, B., 1974. An approximate method for generating asymmetric random variables. Communications of the Association for Computing Machinery 17 (2), 78 – 82.

Ramberg, J., Tadikamalla, P., Dudewicz, E., Mykytka, E., 1979. A probability distribution and its uses in fitting data. Technometrics 21 (2), 201 – 214.

Ramírez, P., Carta, J., 2006. The use of wind probability distributions derived from the maximum entropy principle in the analysis of wind energy. Energy Conversion and Management 47 (15-16), 2564 – 2577.

Rao, A., Hamed, K., 2000. Flood Frequency Analysis. CRC Press, New York.

Rao, S., Bhatti, P., 2001. Probabilistic approach to manipulator kinematics and dynamics. Reliability Engineering & System Safety 72 (1), 47 – 58.

Rosenblatt, M., 1952. Remarks on a multivariate transformation. The Annals of Mathematical Statistics 23 (3), 470 – 472.

Rosenblueth, E., 1981. Two point estimates in probabilities. Applied Mathematical Modelling 5 (5), 329 – 335.

Sahoo, A., Pandey, M., 2010. A risk-informed approach to assessment of DHC initiation in pressure tubes of CANDU reactors. Nuclear Engineering and Design 240 (3), 630 – 638.

Saltelli, A., 2002. Making best use of model evaluations to compute sensitivity indices. Computer Physics Communications 145 (2), 280 – 297.

Saltelli, A., Bolado, R., 1998. An alternative way to compute fourier amplitude sensitivity test (FAST). Computational Statistics & Data Analysis 26 (4), 445 – 460.

Saltelli, A., Chan, K., Scott, E., 2000. Sensitivity Analysis. John Wiley & Sons Inc., New York.

Saltelli, A., Ratto, M., Andres, T., Campolongo, F., Cariboni, J., Gatelli, D., Saisana, M., Tarantola, S., 2008. Global Sensitivity Analysis: The Primer. John Wiley & Sons Ltd., Chichester.

Saltelli, A., Sobol', I., 1995. About the use of rank transformation in sensitivity analysis of model output. Reliability Engineering & System Safety 50 (3), 225 – 239.

Sandor, G., Erdman, A., 1984. Advanced Mechanism Design: Analysis and Synthesis. Vol. 1. Prentice Hall, New Jersey.

Schuëller, G., 2001. Computational stochastic mechanics: Recent advances. Computers & Structures 79 (22-25), 2225 – 2234.

Schuëller, G., Pradlwarter, H., 2007. Benchmark study on reliability estimation in higher dimensions of structural systems: An overview. Structural Safety 29 (3), 167 – 182.

Schuëller, G., Pradlwarter, H., 2009. Uncertainty analysis of complex structural systems. International Journal for Numerical Methods in Engineering 80 (6-7), 881 – 913.

Schuëller, G., Pradlwarter, H., Koutsourelakis, P., 2004. A critical appraisal of reliability estimation procedures for high dimensions. Probabilistic Engineering Mechanics 19 (4), 463 – 474.

Seo, H., Kwak, B., 2002. Efficient statistical tolerance analysis for general distributions using three-point information. International Journal of Production Research 40 (4), 931 – 944.

Shannon, C., 1949. The Mathematical Theory of Communication. University of Illinois Press, Urbana.

Shinozuka, M., 1983. Basic analysis of structural safety. ASCE Journal of Structural Engineering 109 (3), 721 – 740.

Shore, J., Johnson, R., 1980. Axiomatic derivation of the principle of maximum entropy and the principle of minimum cross-entropy. IEEE Transactions on Information Theory 26 (1), 26 – 37.

Snyder, D., 1975. Random Point Processes. John Wiley & Sons, New York.

Sobezyk, K., Trebicki, J., 1990. Maximum entropy principle in stochastic dynamics. Probabilistic Engineering Mechanics 5 (3), 102 – 110.

Sobol', I., 2001. Global sensitivity indices for nonlinear mathematical models and their monte carlo estimates. Mathematics and computers in simulation 55 (1-3), 271 – 280.

Sobol', I., 2003. Theorems and examples on high dimensional model representation. Reliability Engineering & System Safety 79 (2), 187 – 193.

Stuart, A., Ord, J., 1994. Kendall's Advanced Theory of Statistics: Distribution Theory, 6th Edition. Edward Arnold, London.

Sudret, B., 2007. Uncertainty propagation and sensitivity analysis in mechanical models – Contributions to structural reliability and stochastic spectral methods. Habilitation à diriger des recherches, Université Blaise Pascal, Clermont-Ferrand, France.

Sudret, B., 2008a. Analytical derivation of the outcrossing rate in time-variant reliability problems. Structure and Infrastructure Engineering 4 (5), 353 – 362.

Sudret, B., 2008b. Global sensitivity analysis using polynomial chaos expansions. Reliability Engineering & System Safety 93 (7), 964 – 979.

Tada, H., Paris, P., Irwin, G., 2000. The Stress Analysis of Cracks Handbook, 3rd Edition. ASME Press, New York.

Tagliani, A., 1994. Maximum entropy in the hamburger moments problem. Journal of Mathematical Physics 35 (9), 5087 – 5096.

Tagliani, A., 1999. Hausdorff moment problem and maximum entropy: A unified approach. Applied Mathematics and Computation 105 (2-3), 291 – 305.

Taguchi, G., 1978. Performance analysis design. International Journal of Production Research 16 (6), 521 – 530.

Tarantola, S., Gatelli, D., Mara, T., 2006. Random balance designs for the estimation of first order global sensitivity indices. Reliability Engineering & System Safety 91 (6), 717 – 727.

Taufer, E., Bose, S., Tagliani, A., 2009. Optimal predictive densities and fractional moments. Applied Stochastic Models in Business and Industry 25 (1), 57 – 71.

Wan, X., Karniadakis, G., 2006. Multi-element generalized polynomial chaos for arbitrary probability measures. SIAM Journal on Scientific Computing 28 (3), 901 – 928.

Wang, J., Zhang, J., Du, X., 2011. Hybrid dimension reduction for mechanism reliability analysis with random joint clearances. Mechanism and Machine Theory 46 (10), 1396 – 1410.

Wei, D., Rahman, S., 2007. Structural reliability analysis by univariate decomposition and numerical integration. Probabilistic Engineering Mechanics 22 (1), 27 – 38.

Wiener, N., 1938. The homogeneous chaos. American Journal of Mathematics 60 (4), 897 – 936.

Wikipedia, 2013. Qinshan Nuclear Power Plant. http://en.wikipedia.org/wiki/Qinshan_Nuclear_Power_Plant, Updated: 25 October 2010.

Wu, W., Rao, S., 2007. Uncertainty analysis and allocation of joint tolerances in robot manipulators based on interval analysis. Reliability Engineering & System Safety 92 (1), 54 – 64.

Xiu, D., Karniadakis, G., 2002a. Modeling uncertainty in steady state diffusion problems via generalized polynomial chaos. Computer Methods in Applied Mechanics and Engineering 191 (43), 4927 – 4948.

Xiu, D., Karniadakis, G., 2002b. The wiener–askey polynomial chaos for stochastic differential equations. SIAM Journal on Scientific Computing 24 (2), 619 – 644.

Xiu, D., Karniadakis, G., 2003. Modeling uncertainty in flow simulations via generalized polynomial chaos. Journal of Computational Physics 187 (1), 137 – 167.

Xu, H., Rahman, S., 2004. A generalized dimension-reduction method for multidimensional integration in stochastic mechanics. International Journal for Numerical Methods in Engineering 61 (12), 1992 – 2019.

Zhang, J., Du, X., 2011. Time-dependent reliability analysis for function generator mechanisms. ASME Journal of Mechanical Design 133 (3), 031005, 9 pages.

Zhang, J., Wang, J., Du, X., 2011a. Time-dependent probabilistic synthesis for function generator mechanisms. Mechanism and Machine Theory 46 (9), 1236 – 1250.

Zhang, X., Pandey, M., 2013. An efficient method for system reliability analysis of planar mechanisms. Proceedings of the Institution of Mechanical Engineers, Part C: Journal of Mechanical Engineering Science 227 (2), 373 – 386.

Zhang, X., Pandey, M., Zhang, Y., 2011b. A numerical method for structural uncertainty response computation. Science China Technological Sciences 54, 3347 – 3357.

Zhao, Y., Ono, T., 2001. Moment methods for structural reliability. Structural Safety 23 (1), 47 – 75.

Zhou, J., Nowak, A., 1988. Integration formulas to evaluate functions of random variables. Structural Safety 5 (4), 267 – 284.

Zio, E., Pedroni, N., 2009. Functional failure analysis of a thermal–hydraulic passive system by means of line sampling. Reliability Engineering & System Safety 94 (11), 1764 – 1781.